GEOLOGICAL SURVEY EXPLANATORY REPORT

SHEET 64

MACQUARIE HARBOUR

TASMANIA DEVELOPMENT AND RESOURCES

DIVISION OF MINES

COVER PHOTOGRAPH

Open folds in massively bedded calcareous sandstone of unit Ɛac, south of Birthday Bay (see page 72).

M. P. McClenaghan

TASMANIA DEVELOPMENT AND RESOURCES

DIVISION OF MINES 1993

GEOLOGICAL SURVEY EXPLANATORY REPORT

SHEET 64 (7913S)

MACQUARIE HARBOUR

by M. P. McClenaghan, B.Sc. (Hons), Ph.D.
and R. H. Findlay, B.A. (Hons) , Ph.D.

with an appendix on Economic Geology by J. Pemberton, B.Sc.(Hons), M.Sc.

TASMANIA • DEVELOPMENT AND RESOURCES • DIVISION OF MINES
GPO BOX 56, ROSNY PARK, TASMANIA 7018

ISBN 0 7246 4008 8

McCLENAGHAN, M. P.; FINDLAY, R. H. 1993. Geological atlas 1:50 000 series. Sheet 64 (7913S). Macquarie Harbour. *Explan. Rep. geol.Surv. Tasm.*

ISBN 0 7246 4008 8

TECHNICAL EDITOR: E. L. Martin

TEXT INPUT: Lisa Doran, M. P. McClenaghan
LINE ART / CAD: A. McGuinness, J. Ladaniwskyj, A. Hollick
PHOTOGRAPHS: M. P. McClenaghan, R. H. Findlay

CONTENTS

LIST OF PLATES

LIST OF FIGURES

LIST OF TABLES

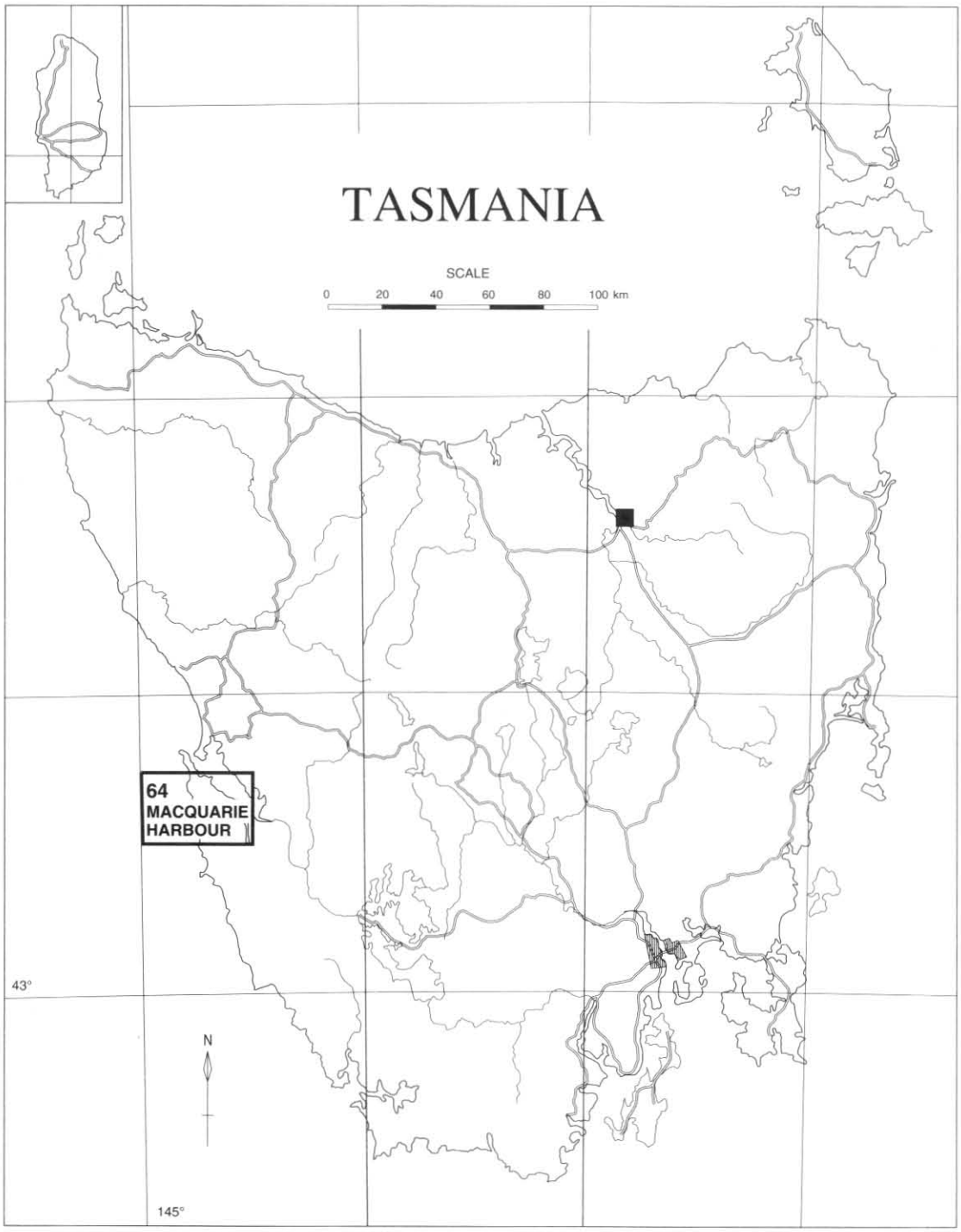

Figure 1. Location map

5 cm

INTRODUCTION

The Macquarie Harbour Quadrangle (fig. 1) is situated on the West Coast of Tasmania and is bounded by latitudes 42°15′ and 42°30′S. and longitudes 145°00′ and 145°30′E. It includes the Cape Sorell peninsula, except for its northern extremity which lies within the Strahan Quadrangle (Baillie *et al.*, 1985).

There are no permanent settlements on the Quadrangle and the nearest settlement is the township of Strahan, situated at the northern end of Macquarie Harbour. Strahan services the local tourism, fishing and forestry industries.

Vegetation is strongly controlled by rock type and ranges from dense rainforest dominated by myrtle beech (*Nothofagus cunninghami*) through to coastal heath and buttongrass plains. Minor stands of Huon pine (*Lagarostrobus franklinii*) occur on the forested coastline on the western side of Macquarie Harbour. The forested areas are largely confined to the Cambrian sedimentary and igneous rocks of the Cape Sorell peninsula and the northern part of the Tertiary sedimentary rocks on the eastern side of Macquarie Harbour. The quartz-rich Precambrian sequences of the peninsula support only peaty soil and here the country is open buttongrass plain except for incised river valleys which are thickly forested. Coastal heaths occur in a narrow zone along the western coast of the peninsula.

Precipitation occurs throughout the year with a maximum in late winter. Rainfall on the west coast is about 1600 mm and increases towards the eastern part of the Quadrangle.

Mapping was carried out between 1980 and 1988. Camps were established at various points along the coast of Macquarie Harbour using a fishing boat based at Strahan. Local travel along the coast from these camps was by a small boat with an outboard motor. Mapping of other areas of the Quadrangle was from camps established using a helicopter based at Queenstown. Field mapping was carried out at a scale of 1:20 000. The 1:50 000 map was published in 1989.

Previous geological work in the area consisted mainly of mineral exploration, particularly by BHP (Hall *et al.*, 1969*a*, *b*), which established the geology on a regional scale. Detailed mapping was carried out in the Timbertops area and on the Point Hibbs Mélange Belt in the upper Noddy Creek area (Langlands, 1971; McGregor, 1972; Close, 1972). A study of Cambrian volcanism and mineralisation by White (1975) included rocks from the Quadrangle. More recent mineral exploration was summarised by Jones (1986).

This report was written by M. P. McClenaghan and R. H. Findlay and the work was supervised by E. Williams.

PHYSIOGRAPHY

General

R. H. Findlay
M. P. McClenaghan

The Macquarie Harbour Quadrangle contains the southern two-thirds of Sorell Peninsula which is separated by the NW-trending graben or half-graben of Macquarie Harbour from relatively low ground to the north-west, underlain by Tertiary sedimentary beds flanking the 1200 m high West Coast Range (see McClenaghan and Findlay, 1989).

The topography of the Sorell Peninsula is characterised by steeply-sided peneplaned hills which are deeply incised by creeks, some of which meander markedly, thus indicating uplift and an antecedent drainage pattern.

The serpentinite belt (see McClenaghan and Findlay, 1989) in the southern part of the peninsula occupies the floor of a narrow, steep-sided valley which trends south-west, oblique to the regional dip of the adjacent land surface. The valley floor is everywhere about 50 m lower than the adjacent country, yet the valley walls are breached by W-flowing streams feeding the deeply incised Modder and Nielson Rivers. It is suggested that the valley represents an old drainage channel which once fed water south-west to the Point Hibbs Lagoon, but whose flow has since been captured by back-cutting of the headwaters of the Modder and Nielson Rivers.

Peneplanes

R. H. Findlay

Gregory (1903) identified as an important Tertiary peneplane the supposedly regionally developed Henty Surface. In the Strahan map sheet area, to the north of the present sheet, Baillie (1985) constructed a series of topographic profiles which he claimed demonstrated that the Henty Surface dipped shallowly west. This surface was held to be younger than the Cenozoic sediments he reported in the south-east of the Strahan Quadrangle. These sediments include both the Eocene unit (Tss), and the possibly Pliocene beds (Tsg) in the Macquarie Harbour Quadrangle.

To investigate further where the Henty Surface might extend into the Macquarie Quadrangle a contoured map of maximum heights per kilometre square was constructed for the Macquarie Quadrangle and adjacent areas (fig. 2). A series of E–W topographic sections with a vertical exaggeration of 10:1 was constructed from this map. These sections show a number of important features.

As seen in the field and as evident from Figure 2 the Henty Surface described by Baillie (1985) continues from the Strahan Quadrangle into the north-east corner of the Macquarie Harbour Quadrangle. Here it is defined in Section A–B with a dip of 5° to the west, extending across the Macquarie Harbour Graben (fig. 3). This surface terminates in the west at about the 160–180 m level, west of which the slope dips uniformly west at a dip of 10–12°; this hinge-point is evident in all the profiles (fig. 3). In both sections A–B and I–J, the 10–12° slope projects across the Macquarie Harbour Graben to the summit ridge of the West Coast Range.

All sections clearly show a surface with a dip of 5–7° extending from the western hinge-point across the Macquarie Harbour Graben; this surface is interpreted as the southern extension of the 5° slope of the Henty Surface in section A–B. It is reasonable to argue that as the 5–7° surface cuts across and down through the 10–12° surface and its projection across the Macquarie Harbour Graben, it must be the younger of the two surfaces. It is also reasonable to argue that as both surfaces cross Macquarie Harbour this graben or half-graben is younger than the peneplanation which formed the two surfaces. That is, as the Henty Surface is cut in beds to which a Pliocene age is attributed (see later discussion) the Macquarie Harbour Graben is a post-Pliocene feature.

Erosional terraces

R. H. Findlay

Sections C–D, E–F, and G–H (fig. 3) show marked benches at the 160 m level; these correspond to valley bottoms in sections C–D, E–F, and G–H. This may be interpreted as an old, but post-Henty Surface, erosional base level (glacier base?).

According to their estimated position on the 1:25 000 topographic map, in the Table Head–Liberty Bay region, terraces occur at about 180 m, 120 m, 80 m and 40 m a.s.l, and three lower terraces lie between 5 and 20 m a.s.l. The lower terraces are cut into rocks lithologically similar to the Eocene unit Tss on the eastern shore of the harbour, and the 80 m and 40 m terraces cut material interpreted either as a Tertiary lag deposit, or as a possible correlate of unit Tsg.

Along the western shore of the Sorell Peninsula, raised beaches are common and terminate in a cliff-line whose base lies at about 40 m a.s.l. and whose crest follows the 60–80 m level. McClenaghan has identified at CP549038 a raised

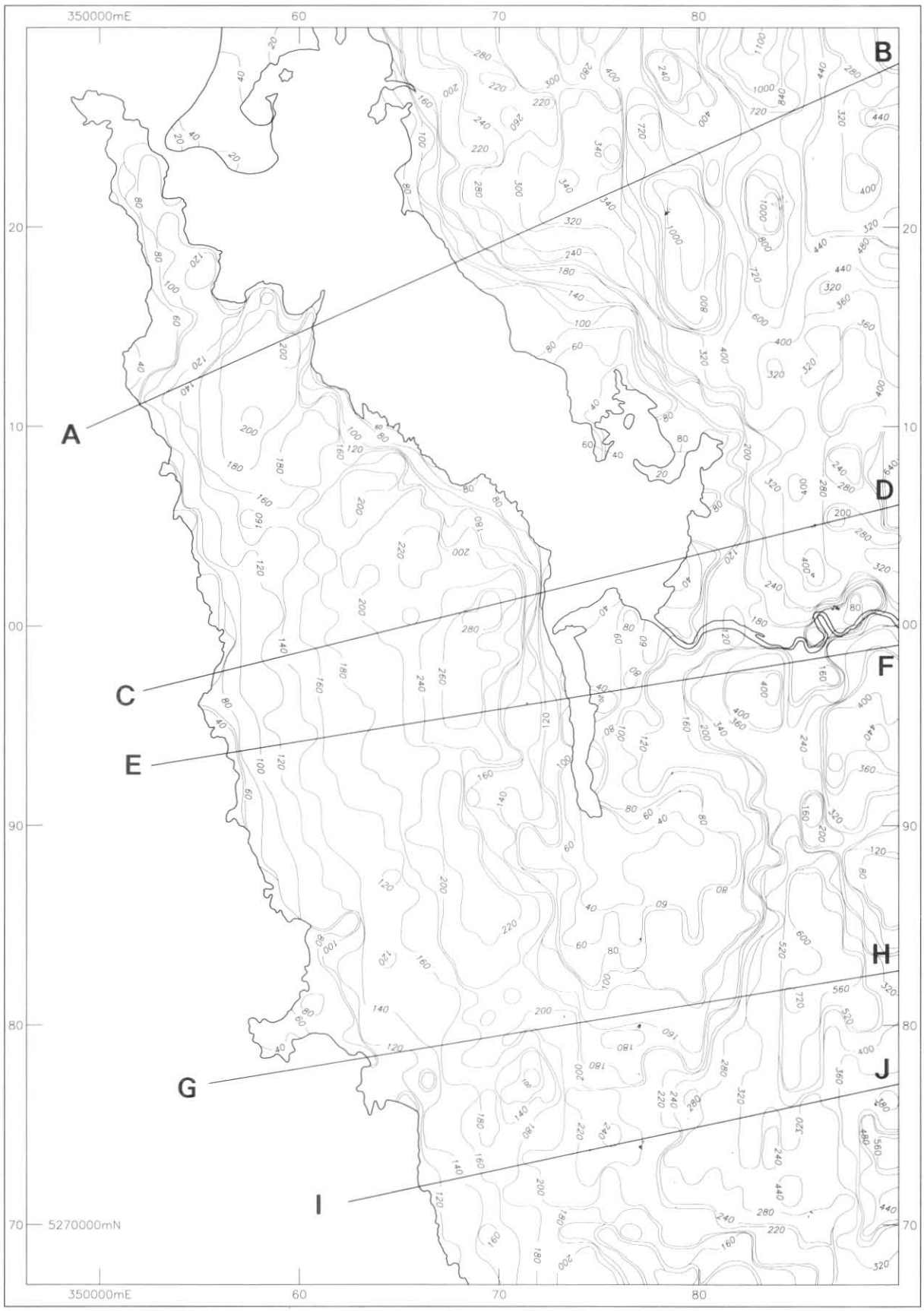

Figure 2. Sorell Peninsula area. Smoothed topographic contours and location of cross sections.

5 cm

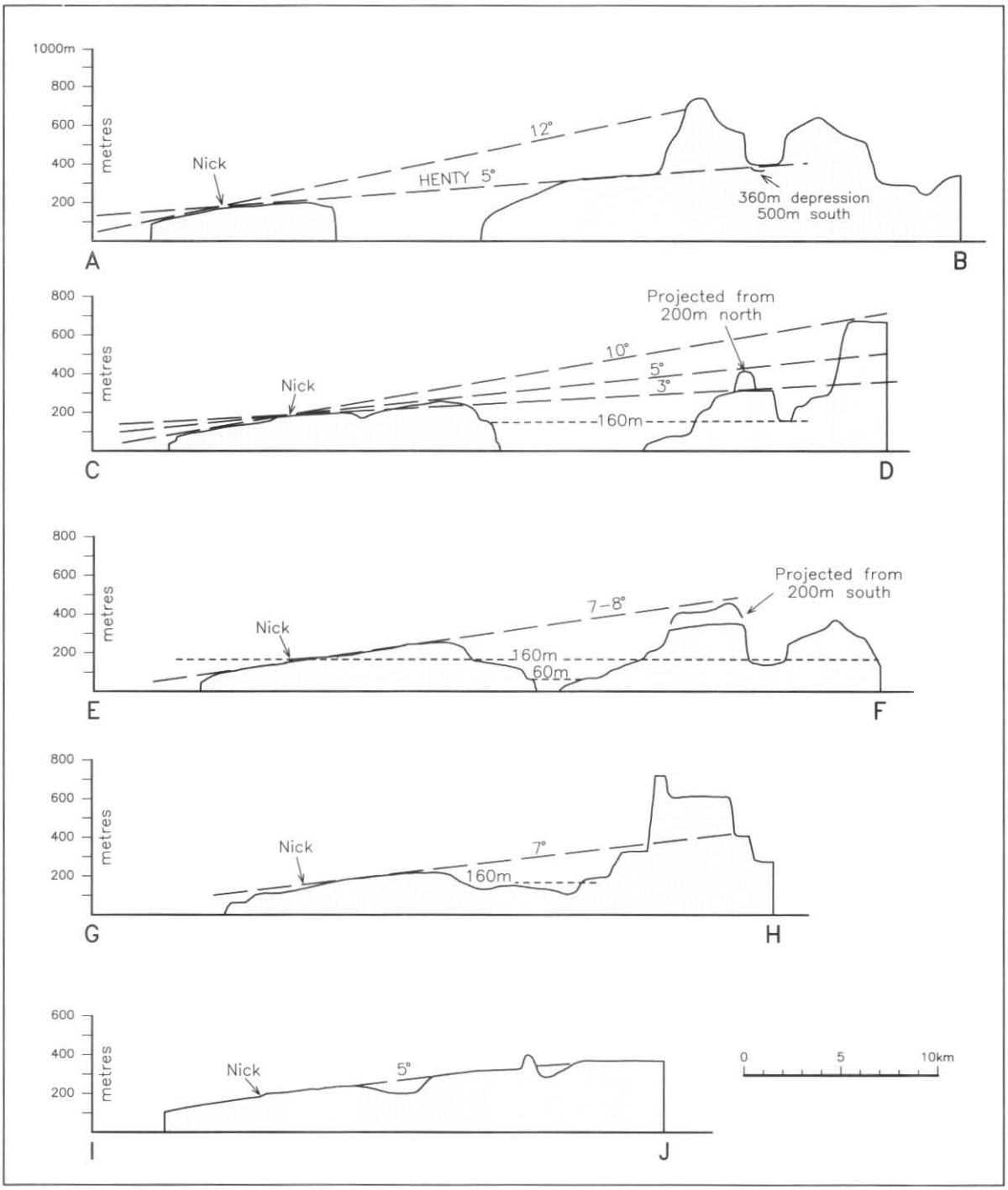

Figure 3. Sections across Sorell Peninsula area (see fig. 2). Note that the dips referred to here and in the text are exaggerated.

beach at the 20 m level, backed by a cliff whose base is between 30 and 40 m a.s.l. At this locality, an Aboriginal midden occurs at between 25–35 m, rather than along the present foreshore as is the common case. This may point to a very young age for the raised beaches and terraces at and below the 40 m level.

Topographic levels in the Birchs Inlet area

M. P. McClenaghan

Several approximately horizontal topographic levels were recognised in the buttongrass country east of Birchs Inlet and can be seen to extend further south. This area is underlain by poorly consolidated Tertiary sediments which can be eroded by the sea relatively quickly. The levels may have been produced by marine erosion at a time when the sea was at a higher level relative to the land in that area. As data on these levels may add to information on eustatic changes in sea level or provide information on recent faulting in the area the levels were investigated further. Seven main levels were recognised in the field though only the four highest levels had a marked separation in height and could be recognised over a wide area.

Areas were considered part of the same level on the basis of apparent continuity, when seen in the field and when viewed from aerial photographs. In order to establish the height of the levels more accurately than could be done with the map contours, traverses were made in three areas on the east side of Birchs Inlet and accurate spot heights were obtained by levelling. The spot heights obtained and the distribution of the main levels for the three areas are shown in Figure 4.

The levels recognised in the three areas are summarised in Table 1. There is a slight fall in Levels 5 and 6 from area 1

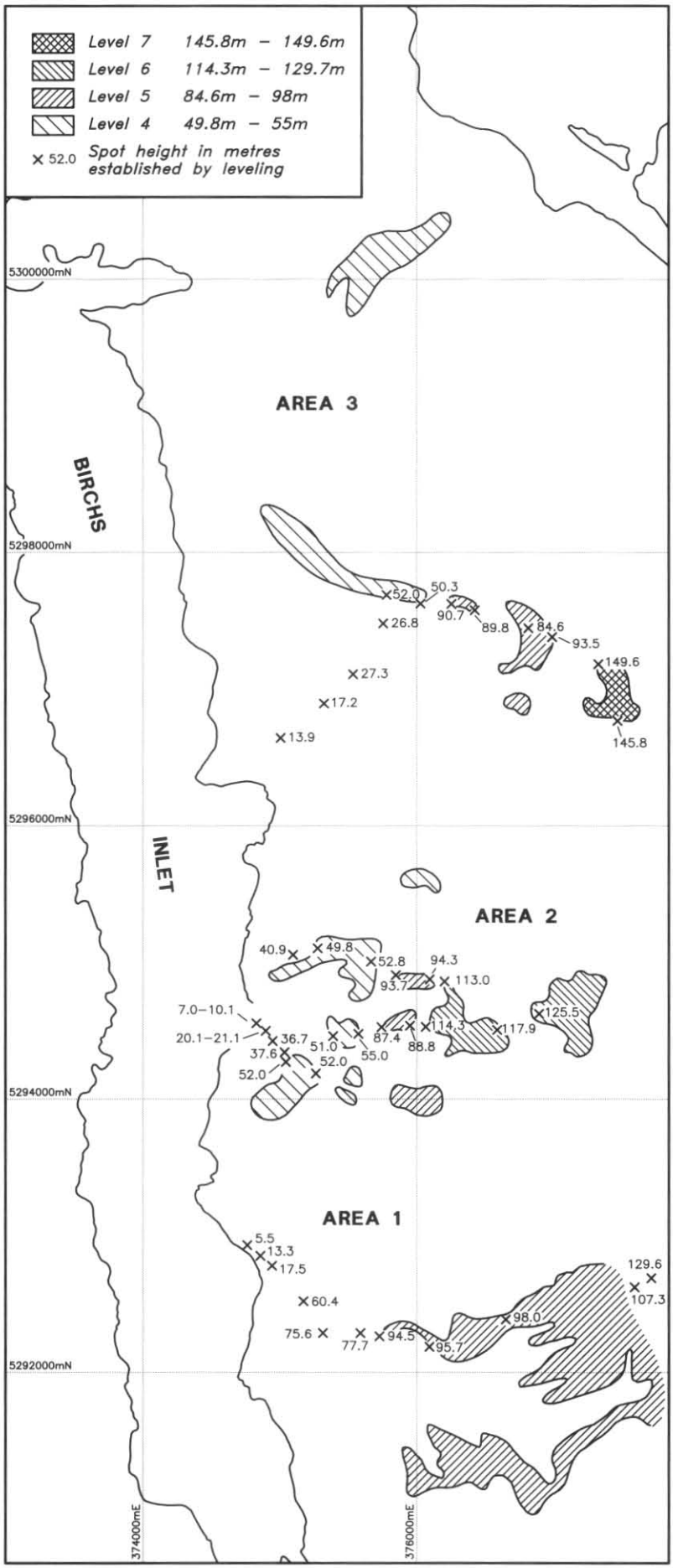

Figure 4. Levels cut in Tertiary beds, Birchs Inlet area.

to area 2, suggesting the levels fall slightly to the north. There is also a similar slope from east to west, as also seen in the erosional terraces of the Sorell Peninsula.

These levels may be correlated tentatively with the terraces in the Table Head–Liberty Bay region as follows:

Levels 1 and 2 lie between the 5–20 m interval seen in the Table Head–Liberty Bay region.

Levels 3 and possibly 4 may be equivalent to the terraces mapped at the 40 m a.s.l. interval.

Level 5 would probably correspond to the terrace mapped at 80 m a.s.l.

Levels 6 would correspond to the terrace at 120 m a.s.l.

Level 7 has no obvious equivalent in the Table Head–Liberty Bay area.

A number of strandline levels have been recognised elsewhere in Tasmania (Davies, 1960) and three of them at 50.3–54.9 m, 36.6–45.7 m and 18.3–22.9 m a.s.l. may correspond to Levels 4, 3 and 2 in Birchs Inlet. A strandline at 73.2–82.3 m a.s.l. is not recognised in Birchs Inlet and a strandline at Level 7 was not recorded by Davies (1960). The poorly defined Level 1 also does not appear to correspond to other strandlines in Tasmania.

Table 1. TOPOGRAPHIC LEVELS IN THE BIRCHS INLET AREA

	Area 1	Area 2	Area 3
Level 1		7.0–10.1 m	
Level 2		20.1–21.1 m	
Level 3		36.7–37.6 m	
Level 4		49.8–55.0 m	50.1–52.0 m
Level 5	94.5–98.0 m	87.4–94.3 m	84.6–93.5 m
Level 6	129.7 m	114.3–125.5 m	
Level 7			145.8–149.6 m

STRATIGRAPHY

Proterozoic rocks of the Liberty Point to Gorge Point area

R. H. Findlay

These rocks occupy the region between Liberty and Lagoon creeks and the northern end of the Sorell Peninsula. They consist of a complexly deformed, lower greenschist facies sequence of interbedded orthoquartzite, phyllite and less common siliceous conglomerate beds. The conglomeratic beds are known only in the southern part of the sequence, although Baillie *et al.* (1985) also report minor conglomeratic horizons in the peninsula to the north of the Macquarie sheet area.

The most common units are white-weathering, variably foliated to massive, orthoquartzite beds ranging in thickness between 10 mm and one metre. These units are very well sorted and contain fine- to medium-grained quartz grains which are well rounded. Coarse quartz grains occur in some of the cross-bedded units.

The quartzite beds are massive to laminated on a millimetre scale, and in the weathered units it is commonly difficult to distinguish between cross-bedding and cleavage refraction. In the region of Cosy Corner to Betsys Bay, cross-bedded quartzite horizons are easily recognised in the fresh coastal exposures, and similar cross-bedding can be identified inland. The cross-bedded units occur either singly or in groups and adjacent beds may show opposed flow directions; many beds show a concavity below a planar upper bedding contact, although some beds show tabular cross-bedding. No nested cross-bedded units were recognised; some cross-bedded units coarsened downwards whereas in others there was no change in grain size. One example of herring-bone cross- bedding was seen.

Orthoquartzite beds with rippled tops were noted in the Gorge Point region. Different ripple orientations occur through this sequence and indicate marked variations in current direction.

The conglomeratic beds appear to be lensoidal. These range from cobble to pebble conglomerates and they are commonly bimodal, containing generally either pebbles or cobbles in contact and with coarse- to fine-grained quartzite in the interstices. These rocks are associated with thin beds of fine-grained, finely laminated pink orthoquartzite, interbedded with finely laminated orthoquartzite.

The pelitic units contain siltstone intervals no thicker than 10 mm. Any sedimentary structures within these units have been destroyed by multiple deformation and the low greenschist facies (to biotite zone) metamorphism. The dominant mineral assemblage seen is chlorite-white mica-quartz; green-brown biotite occurs in one thin section.

The sequence north of Lagoon and Liberty creeks differs markedly from that of Nielson River area to the south. In contrast to those probably turbiditic units, the Lagoon Creek–Liberty Creek sequence is best regarded as a shallow marine to tidal sequence. In addition, the dolomite-rich beds of the southern sequence are not known in the northern sequence (see also Baillie *et al.*, 1985).

Proterozoic rocks of the Nielson River area

M. P. McClenaghan

Precambrian rocks crop out along the eastern coast of the Sorell Peninsula for about 2 km south-east of the mouth of Butler Creek and extend south-west in a gradually widening zone across the peninsula with the northern boundary reaching the western coast at the northern end of Varna Bay. Both the western and eastern boundaries with the flanking Cambrian (?) sequences are faulted. The area of Precambrian outcrop is generally covered by button grass, except for the heavily forested creek valleys which is in marked contrast to the thick forest in areas underlain by Cambrian (?) rocks. Two sequences form the Precambrian rocks and consist of metamorphosed impure dolomite (Pnd) and metamorphosed interbedded quartzwacke and mudstone/siltstone (Pnq). The boundary between the sequences is gradational. Multiple deformation has partly obliterated sedimentary features and the original stratigraphy is unclear.

METAMORPHOSED IMPURE DOLOMITE-RICH SEQUENCES (Pnd)

These rocks crop out in Varna Bay on the west coast and extend inland to near the Nielson River where they are exposed in Timms, Birthday, Iron and various other unnamed creeks. The sequence can best be seen in coastal outcrops in Varna Bay. The rocks have been recrystallised and show grain sizes ranging from fine to coarse. Fine-grained units range from pale green to red/grey, probably reflecting different degrees of oxidation since the boundaries between zones of different colour do not follow bedding. Other rocks show various shades of grey with coarser grain sizes being paler. Parallel bedding is generally the only sedimentary feature visible although thin (<50 mm) graded bedding units occur at CN562945. Quartz occurs with the carbonate in varying proportions and a small amounts of muscovite and opaques are generally present. Talc was identified by XRD from several samples (e.g. at CN563937) which suggests that a metamorphic temperature of between 400°C and 500°C was attained.

METAMORPHOSED INTERBEDDED QUARTZWACKE AND MUDSTONE/ SILTSTONE SEQUENCES (Pnq)

Rocks of these sequences are best exposed on the eastern coast south of Butler Creek. They are also well exposed in the Nielson River down-stream from the track-crossing at

Plate 1. Load casts in mudstone/siltstone from Pnq unit at CP673077.

CN613999, although outcrops are sparse in some of the lesser creeks. The rocks consist of pale grey massive sandstone units up to 3 m thick, interbedded with medium to dark grey siltstone and mudstone beds generally less than one metre thick. Due to the strong tectonism sedimentary structures have mainly been obliterated; grain-size graded units were recognised in siltstone beds at only a few localities [e.g. CP663087]. At CP673077 (plate 1) a load cast occurs together with graded units and at CP673078 flute casts (plate 2) are present on the base of a sandstone bed. A thin (<100 mm) unit of tabular current bedding was recognised in a siltstone bed at CP667082.

In thin section the sandstone and siltstone units consist of coarse, poorly sorted and strained quartz grains, set in a finer matrix of recrystallised quartz and colourless mica with varying amounts of fine opaques. Some specimens contain grains of feldspar rich in sericite. Sparse tourmaline and zircon grains are present in most specimens. A strongly developed crenulation cleavage is generally evident and is defined by the alignment of mica. In thin section the mudstone consists of very fine-grained, recrystallised quartz and colourless mica with abundant opaques.

The poor sorting of the sandstone and siltstone together with the occurrence of graded bedding units and flute casts, suggest that they were deposited by turbidity currents. The detrital material indicates derivation from a siliceous terrain. This depositional environment is clearly different from that of the Precambrian rocks in the Liberty Point to Gorge Point area and suggests that they belong to different sequences.

The recrystallisation of the rocks indicates that they have been subject to low grade metamorphism, but the lack of compositional variation has not allowed the development of minerals which would more exactly define the grade.

Eocambrian–Cambrian sequences

M. P. McClenaghan

ALBINA CREEK AREA

Mudstone/lithicwacke sequences (Ꞓaml)

Rocks from these sequences are best exposed along the coast adjacent to the mouth of the Albina Creek on the west coast of the peninsula and they underlie a broad zone of country stretching north-east to the Liberty Creek – Lucas Creek area. Another small zone of outcrop occurs bordering the Nielson River farther south. The rocks are interbedded at a number of places with basalt-rich sequences (Ꞓab). Boundaries with other units are considered to be faulted except in two areas [CP582075, CP563014] where they are adjacent to the calcareous mudstone/siltstone/sandstone sequences (Ꞓac); the nature of the boundary is unknown.

The rocks are generally medium- to dark-grey mudstone and siltstone with some sandstone units. They are tightly folded with a strongly developed cleavage which has largely obliterated sedimentary features. Fine-scale parallel bedding shown by thin more pale-coloured siltstone bands in darker-grey, finer-grained rock can be seen in some areas. Some of the bands show grain size-grading. Small flame structures of fine mudstone penetrating a coarser siltstone layer can also be seen in some places.

Plate 2. Flute casts on base of a quartzwacke bed from Pnq unit at CP673078.

Table 2. PYROXENE COMPOSITIONS FROM BASALT LAVAS (Cab)

	MH104_1/1	MH104_1/2	MH104_2/1	MH104_2/2	MH104_5/1	MH105_1/3	MH105_2/1	MH105_3/1	MH105_4/1
SiO_2	51.25	51.68	51.51	50.55	51.1	51.05	52.65	52.64	52.77
TiO_2	0.61	0.64	0.58	0.72	0.45	0.91	0.57	0.49	0.53
Al_2O_3	3.27	2.56	2.60	3.40	4.65	2.33	2.58	2.24	2.51
Cr_2O_3	0.22	<0.15	<0.15	0.29	0.63	0.23	0.45	0.42	0.48
Fe_2O_3	0.80	<0.15	0.80	1.72	0.26	0.68	<0.15	<0.15	<0.15
FeO	8.59	9.91	8.38	8.58	5.32	10.87	7.50	7.71	6.96
MnO	<0.15	0.29	0.22	<0.15	<0.15	0.28	<0.15	<0.15	<0.15
MgO	14.75	14.48	14.98	14.13	16.00	15.12	16.70	16.84	16.97
CaO	20.31	20.44	20.93	20.32	21.59	18.54	19.55	19.66	19.78
Na_2O	0.20	<0.15	<0.15	0.28	<0.15	<0.15	<0.15	<0.15	<0.15
K_2O	<0.15	<0.15	<0.15	<0.15	<0.15	<0.15	<0.15	<0.15	<0.15
H_2O	<0.15	<0.15	<0.15	<0.15	<0.15	<0.15	<0.15	<0.15	<0.15
Si	1.904	1.928	1.916	1.887	1.874	1.910	1.934	1.937	1.935
Al^4	0.096	0.072	0.084	0.113	0.126	0.090	0.066	0.063	0.065
Σ	2.000	2.000	2.000	2.000	2.000	2.000	2.000	2.000	2.000
Al^8	0.047	0.040	0.030	0.036	0.075	0.013	0.045	0.034	0.043
Ti	0.017	0.018	0.016	0.020	0.012	0.026	0.016	0.014	0.015
Fe^3	0.022	0	0.022	0.048	0.007	0.019	0	0	0
Cr	0.006	0	0	0.009	0.018	0.007	0.013	0.012	0.014
Mg	0.817	0.805	0.830	0.786	0.874	0.843	0.914	0.923	0.927
Fe^2	0.267	0.309	0.261	0.268	0.163	0.340	0.230	0.237	0.213
Mn	0	0.009	0.007	0	0	0.009	0	0	0
Ca	0.809	0.817	0.834	0.813	0.849	0.743	0.769	0.775	0.777
Na	0.014	0	0	0.020	0	0	0	0	0
K	0	0	0	0	0	0	0	0	0
Σ	2.000	1.998	2.000	2.000	2.000	2.000	1.988	1.995	1.989
Mg*	0.75	0.72	0.76	0.75	0.84	0.71	0.80	0.81	0.82

	MH101_1/1	MH101_2/1	MH101_2/2	MH101_3/1	MH101_3/2	MH106_1/1	MH106_2/1	MH106_4/1	MH106_5/1
SiO_2	50.91	50.70	51.02	52.00	50.79	51.25	51.48	51.31	50.21
TiO_2	0.54	0.68	0.49	0.52	0.69	1.10	1.05	0.95	1.48
Al_2O_3	4.16	3.57	4.44	3.38	4.81	2.69	2.80	2.23	3.80
Cr_2O_3	0.60	0.26	0.49	0.38	0.70	0.29	0.37	0.31	0.34
Fe_2O_3	0.54	1.25	1.11	<0.15	<0.15	<0.15	<0.15	2.92	<0.15
FeO	6.32	8.61	5.79	7.66	6.39	9.88	10.01	7.05	10.83
MnO	0.25	0.30	<0.15	<0.15	<0.15	0.24	0.23	0.22	0.27
MgO	15.55	14.42	15.12	15.38	15.33	15.58	16.12	15.70	15.30
CaO	21.13	20.01	21.21	20.68	21.29	18.97	17.94	18.65	17.77
Na_2O	<0.15	0.21	0.33	<0.15	<0.15	<0.15	<0.15	0.66	<0.15
K_2O	<0.15	<0.15	<0.15	<0.15	<0.15	<0.15	<0.15	<0.15	<0.15
H_2O	<0.15	<0.15	<0.15	<0.15	<0.15	<0.15	<0.15	<0.15	<0.15
Si	1.878	1.889	1.879	1.918	1.870	1.907	1.910	1.903	1.873
Al^4	0.122	0.111	0.121	0.082	0.130	0.093	0.090	0.097	0.127
Σ	2.000	2.000	2.000	2.000	2.000	2.000	2.000	2.000	2.000
Al^8	0.059	0.046	0.072	0.065	0.079	0.025	0.032	0.001	0.040
Ti	0.015	0.019	0.014	0.014	0.019	0.031	0.029	0.026	0.042
Fe^3	0.015	0.035	0.031	0	0	0	0	0.082	0
Cr	0.017	0.008	0.014	0.011	0.020	0.009	0.011	0.009	0.010
Mg	0.855	0.801	0.830	0.845	0.841	0.864	0.891	0.868	0.805
Fe^2	0.195	0.268	0.178	0.236	0.197	0.307	0.311	0.219	0.338
Mn	0.008	0.009	0	0	0	0.008	0.007	0.007	0.009
Ca	0.835	0.799	0.837	0.817	0.840	0.756	0.713	0.741	0.710
Na	0	0.015	0.024	0	0	0	0	0.047	0
K	0	0	0	0	0	0	0	0	0
Σ	2.000	2.000	2.000	1.989	1.996	1.999	1.994	1.999	1.997
Mg*	0.81	0.75	0.82	0.78	0.81	0.74	0.74	0.80	0.72

Plate 3. Basalt pillows in unit Cabp at CP554007.

In thin section the siltstone and sandstone beds consist of poorly sorted angular fragments generally of quartz, lithic fragments and less common plagioclase set in a finer grained matrix of recrystallised quartz, white mica, chlorite and opaques. The quartz grains are commonly strained with a small proportion being unstrained and embayed. The unstrained and embayed grains are interpreted to have been derived from volcanic rocks whereas the strained grains, some of which are composite, are probably derived from metamorphic rocks.

The lithic grains are of various types. Most common are fine grained, granular and consist of quartz and feldspar with thin needle-like crystals of sericite with or without chlorite. Some grains contain larger crystals of both plagioclase and quartz and resemble lava fragments of (intermediate or acid composition). Other lithic grains are of coarser rock consisting of intergrown quartz and feldspar some of which shows graphic texture. These are clearly derived from an igneous rock, probably of a similar chemical composition to the finer grained fragments.

Other grains in these rocks are white mica and chlorite.

The mudstone consist of very fine-grained quartz, white mica and opaque grains.

Thin beds (<1 m) of dolomite occur interbedded with siltstone units at CP550025, CP548033 and CP546045. Neighbouring beds are rich in secondary carbonate and have thin carbonate veining.

The poor sorting, immaturity of the grains and graded bedding in the siltstone and sandstones suggest that these sequences were mostly deposited by turbidity currents. It seems probable that they were derived from an intermediate to acid volcanic terrain with some contribution from a metamorphic area.

Basalt lavas (€ab)

Rocks of this unit crop out in a zone stretching south-west from the northern part of Double Cove and are interbedded with the mudstone/lithicwacke sequence (€aml). The best outcrops occur on the coast on the northern side of Double Cove and on the western coast at CP547023 opposite Albina Rock and farther south at CP553003 and CP554007. At these localities the rock consists of massive pale to medium-dark grey lava some of which has pillow structures (see plate 3). The lava is associated with units of basaltic tuff and breccia, and thin finely banded siltstone and mudstone units. The rocks near Double Cove were named the Lucas Creek Volcanics by White (1972).

In thin section the rocks from the Double Cove area are the least altered and generally consist of glomerophyric plagioclase and clinopyroxene set in a matrix of plagioclase, clinopyroxene and opaques. The plagioclase is cloudy with sericite alteration. Possible chlorite pseudomorphs of olivine occur as relics of probable olivine phenocrysts in a matrix of slightly finer grain-size. The pyroxene phenocrysts are augite (table 2) and the opaques are ilmenite (confirmed by microprobe) with minor associated sphene. Small granular patches of epidote are common in the matrix. Other sections demonstrate the presence of a more basic lava consisting of abundant skeletal clinopyroxene set in a mass of serpentine, chlorite and opaques; this may be a quench texture.

In thin section rocks from this unit from the western part of the peninsula are more highly altered and consist of albite, actinolite, chlorite, epidote, sphene, carbonate and leucoxene with little indication of the original igneous texture except for the shape of feldspar laths as phenocrysts and in the matrix.

Calcareous mudstone/siltstone/sandstone sequences (€ac)

Rocks from these sequences crop out in broad zones stretching south-west across the peninsula from the Double Cove – Hogan Cove area. They are best exposed on the eastern coast south of Double Cove and on the western coast south of Birthday Bay. Inland, the outcrops are generally sparse and confined to the creeks. The sequences have faulted boundaries with the Precambrian rocks (Pm, Pnd and Pnq). Boundaries with the mudstone/lithicwacke sequences (€am) and the associated basalt (€ab) are faulted except in the area north-west of the Nielson River at CP564014 where the nature of the boundary is unknown. Though some boundaries with the poorly bedded crystalline dolomite sequences (€ad) are faulted, elsewhere the boundaries are assumed to be stratigraphic.

Outcrops along the eastern coast consist of a sequence of pale grey sandstone, siltstone and mudstone which in most areas such as Double Cove and Hogan Cove consist of thin (7.5-30 mm) interbedded units of siltstone and mudstone (plate 4). The coarser units which may also consist of sandstone generally show tabular current bedding. In some areas massive units of sandstone up to one metre thick are interbedded with siltstone. At CP652095 several beds of very coarse-grained sandstone (€acc) occur containing rounded quartzite boulders of various sizes up to 230 mm in diameter (plate 5). At several places e.g. CP649097 and CP632113 slump folding (plate 6) is present in finely banded siltstone/mudstone.

Inland and south-west of Double Cove in Schofield Creek, a sequence of carbonate rich rocks occur which consist of massive pale grey carbonate with irregular thin (<70 mm) chert bands. Minor carbonate is also present in the coastal outcrops at CP657094 in the form of several thin (<300 mm) beds of fine-grained and finely banded pale buff rock. XRD determinations show that the carbonate in these rocks is dolomitic and that talc is present in some samples. In thin section the carbonate-bearing outcrops on the coast also contain plagioclase, quartz and white mica.

In thin section the sandstone and siltstone units generally consist of angular, poorly sorted strained quartz grains set in a more fine matrix of recrystallised quartz and white mica. Quartzite and chert grains are rare and plagioclase was identified in only one specimen. Rare zircon, tourmaline and opaque grains are also present together with larger white mica grains. The mudstone consists of quartz and white mica with opaque grains.

Plate 4. Interbedded siltstone and mudstone in unit €ac at CP627109.

Plate 5. Conglomerate horizon (unit Cacc) in unit Cac at CP652095.

Plate 6. Slump folds in unit Cac at CP632113.

Plate 7. Interbedded siltstone and mudstone in unit Cac at CN557950.

On the west coast north of Varna Bay at CN557950 the rocks are thinly bedded with light grey siltstone units up to 15 mm thick but usually about 5 mm thick alternating with medium dark grey mudstone units about 25 mm thick (plate 7). The thin siltstone beds have grain-size grading. More massive beds (25–150 mm thick) of sandstone showing tabular current bedding are also interbedded with the mudstone units in this area. In thin section the siltstone consists mostly of recrystallised carbonate with minor quartz and fine opaque grains. XRD determination indicates that the carbonate is dolomite and the sandstone beds are also rich in dolomite. Farther north along the coast as far as CN549960 similar rocks occur but have been strongly cleaved so that bedding has mainly been obscured. In the remaining stretch of coast south of Birthday Bay the beds are more massive with fine sandstone and siltstone beds up to 1.2 m thick; at some localities these show tabular current bedding. Near Birthday Creek at CN567983 thin (10–25 mm thick) graded medium dark grey siltstone units are interbedded with more massive light grey sandstone beds (up to 300 mm thick). Some of the siltstone beds have groove casts on their base (plate 8). In thin section the siltstone units consist of recrystallised quartz,

white mica and opaques and the sandstone beds are mainly recrystallised carbonate with minor quartz. Similar sequences of mudstone, siltstone and sandstone containing variable amounts of carbonate crop out in the creeks to the north-east.

Farther north, in the middle parts of the Albina and Waller Creeks near CP585055, CP578034 and CP598044, sequences of medium- to dark-grey mudstone and siltstone occur. In thin section they consist of angular poorly sorted strained quartz grains set in a fine-grained recrystallised matrix of quartz, white mica and fine opaque grains. Very minor amounts of zircon and tourmaline are also present. These rocks are very similar in thin section to the non-carbonate bearing rocks on the east coast.

Massive dolomite sequences (Ꞓad)

Sequences of this rock-type form good outcrops on the west coast at Discovery Beach, closely adjacent to Albina Rock and in Birthday Bay. Outcrops extend inland in north-west to south-east trending zones that are partly fault-bounded but are also considered to have stratigraphic contacts with variably calcareous mudstone/siltstone/ sandstone sequences (Ꞓac). The rocks are recrystallised and tectonised and thus sedimentary features are largely obliterated. They are generally massive, light grey- or pale buff-coloured depending on their weathered state and have characteristic irregular surfaces with many sharp protuberances on coastal outcrops. Poorly defined parallel bedding occurs in some places as shown by slight colour differences and variable resistance to weathering. Resistance to weathering reflects quartz content; thin irregular upstanding bands of chert are common. Probable intrafolial slump folds and conglomeratic bands composed of rounded carbonate and chert clasts occur at CP552016. In the Discovery Beach area there are massive beds composed of silicified ellipsoidal objects up to 40 mm in length showing concentric structures with intergranular coarse crystalline carbonate (plate 9). These are interpreted to be oncolites. Cleavage is generally poorly developed but in some areas it is very intense and has produced thin upstanding layers [e.g. at CP552013].

In thin section these rocks are entirely recrystallised and generally consist of carbonate with varying small amounts of quartz. Grain size is highly variable and enigmatic oval structures are often present. Chert bands consist of fine-grained recrystallised quartz. XRD determination indicates that the carbonate is dolomite and that some of samples contain talc. Magnesite and ankerite were also detected.

The recrystallisation and the presence of talc indicates that the rocks have been subject to low grade metamorphism probably between 400°C and 500°C.

Plate 8. Groove casts on the base of a siltstone bed in unit Ꞓac.

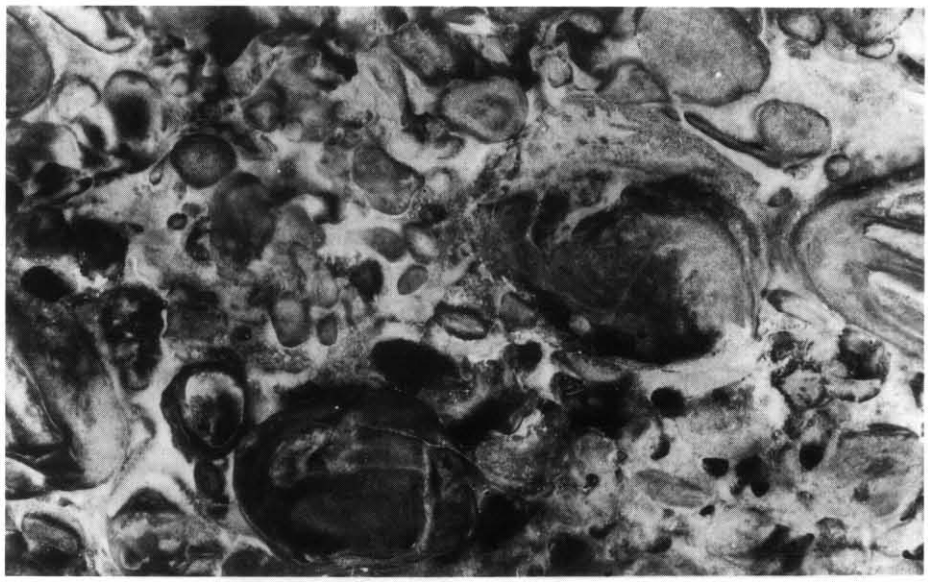

Plate 9. Possible oncolithic structures in unit Ꞓad at CP542054.

5 cm

Table 3. PYROXENE COMPOSITIONS FROM BASALT LAVA (Ctbc)

	MH47_1/1	MH47_2/1	MH47_3/1	MH47_5/1	MH57_1/3	MH57_2/1	MH57_3/1	MH57_4/1	MH57_4/2	MH57_5/1	MH59_1/1	MH59_1/2	MH57_5/1	MH57_5/3	MH200_5/1
SiO_2	51.63	51.32	52.28	52.40	50.40	51.11	53.29	51.27	50.76	50.84	51.34	51.11	51.46	51.2	52.67
TiO_2	0.31	0.38	0.22	0.22	0.92	0.39	0.21	0.35	0.69	0.23	<0.15	0.85	1.03	1.03	0.10
Al_2O_3	3.80	2.75	3.25	2.87	2.18	4.53	2.49	4.28	2.16	4.77	1.32	1.41	1.55	1.64	3.01
Cr_2O_3	0.21	0.48	0.52	0.55	<0.15	0.57	0.37	0.44	<0.15	0.67	<0.15	<0.15	<0.15	0.22	0.79
Fe_2O_3	0.65	1.66	<0.15	<0.15	<0.15	0.29	<0.15	0.53	<0.15	0.92	0.19	<0.15	<0.15	<0.15	<0.15
FeO	5.83	7.84	6.22	6.59	17.70	5.84	5.92	5.85	17.32	5.12	17.28	17.21	14.38	14.41	4.70
MnO	<0.15	0.25	<0.15	<0.15	0.47	<0.15	<0.15	<0.15	0.50	<0.15	0.53	0.36	0.35	0.32	<0.15
MgO	16.03	15.15	16.27	16.08	12.29	15.68	16.9	15.98	13.39	15.77	11.95	12.17	12.88	12.95	17.17
CaO	21.55	19.94	21.24	21.29	16.04	21.6	20.82	21.30	15.18	21.68	17.38	16.89	18.35	18.23	21.55
Na_2O	<0.15	0.23	<0.15	<0.15	<0.15	<0.15	<0.15	<0.15	<0.15	<0.15	<0.15	<0.15	<0.15	<0.15	<0.15
K_2O	<0.15	<0.15	<0.15	<0.15	<0.15	<0.15	<0.15	<0.15	<0.15	<0.15	<0.15	<0.15	<0.15	<0.15	<0.15
H_2O	<0.15	<0.15	<0.15	<0.15	<0.15	<0.15	<0.15	<0.15	<0.15	<0.15	<0.15	<0.15	<0.15	<0.15	<0.15
Si	1.897	1.907	1.919	1.927	1.929	1.879	1.947	1.884	1.933	1.868	1.967	1.954	1.949	1.941	1.923
Al^4	0.103	0.093	0.081	0.073	0.071	0.121	0.053	0.116	0.067	0.132	0.033	0.046	0.051	0.059	0.077
Σ	2.000	2.000	2.000	2.000	2.000	2.000	2.000	2.000	2.000	2.000	2.000	2.000	2.000	2.000	2.000
Al^8	0.062	0.027	0.059	0.052	0.028	0.075	0.055	0.069	0.031	0.074	0.027	0.018	0.019	0.014	0.052
Ti	0.009	0.011	0.006	0.006	0.026	0.011	0.006	0.010	0.020	0.006	0	0.024	0.029	0.029	0.003
Fe^3	0.018	0.047	0	0	0	0.008	0	0.015	0	0.026	0.005	0	0	0	0
Cr	0.006	0.014	0.015	0.016	0	0.017	0.011	0.013	0	0.019	0	0	0	0.007	0.023
Mg	0.878	0.839	0.890	0.881	0.701	0.859	0.921	0.875	0.760	0.863	0.682	0.693	0.727	0.732	0.934
Fe^2	0.179	0.244	0.191	0.203	0.567	0.179	0.181	0.180	0.552	0.157	0.554	0.550	0.456	0.457	0.144
Mn	0	0.008	0	0	0.015	0	0	0	0.016	0	0.017	0.012	0.011	0.010	0
Ca	0.848	0.794	0.835	0.839	0.658	0.851	0.815	0.839	0.620	0.853	0.714	0.692	0.745	0.741	0.843
Na	0	0.017	0	0	0	0	0	0	0	0	0	0	0	0	0
K	0	0	0	0	0	0	0	0	0	0	0	0	0	0	0
Σ	2.000	2.000	1.997	1.997	1.995	2.000	1.988	2.000	1.998	2.000	2.000	1.990	1.987	1.990	1.998
Mg*	0.83	0.77	0.82	0.81	0.55	0.83	0.84	0.83	0.58	0.85	0.55	0.56	0.61	0.62	0.87

	MH200_3/2	MH200_2/1	MH192_1/1	MH192_2/1	MH192_4/1	MH192_5/1	MH192_6/1	MH194A_1/1	MH194A_2/1	MH194A_3/1	MH194A_4/1	MH194A_5/1	MH194A_6/1	MH59_5/1	MH59_5/3
SiO_2	52.91	50.54	52.22	51.52	52.19	52.2	51.94	51.50	51.32	51.94	50.07	50.52	50.56	51.46	51.20
TiO_2	<0.15	0.18	0.51	0.44	0.34	0.48	0.58	0.29	0.28	0.22	0.53	0.39	0.39	1.03	1.03
Al_2O	2.72	5.38	2.42	3.40	3.01	2.82	2.77	3.86	4.22	3.08	5.22	5.11	5.05	1.55	1.64
Cr_2O_3	0.35	0.82	0.41	0.88	0.89	0.59	0.31	0.72	0.86	0.54	0.51	0.62	0.8	<0.15	0.22
Fe_2O_3	<0.15	0.96	0.23	0.51	0.13	<0.15	0.49	0.36	0.27	0.45	0.95	0.58	0.49	<0.15	<0.15
FeO	6.48	5.64	8.12	6.59	5.84	7.61	8.09	6.06	5.67	6.47	6.65	6.18	6.19	14.38	14.41
MnO	<0.15	<0.15	<0.15	0.12	<0.15	<0.15	0.13	<0.15	<0.15	<0.15	<0.15	<0.15	<0.15	0.35	0.32
MgO	17.14	16.35	17.03	16.89	17.35	17.39	17.06	16.17	16.09	16.07	14.97	15.34	15.62	12.88	12.95
CaO	20.40	20.14	19.07	19.66	20.25	18.91	18.55	21.05	21.27	21.22	21.09	21.25	20.89	18.35	18.23
Na_2O	<0.15	<0.15	<0.15	<0.15	<0.15	<0.15	<0.15	<0.15	<0.15	<0.15	<0.15	<0.15	<0.15	<0.15	<0.15
K_2O	<0.15	<0.15	<0.15	<0.15	<0.15	<0.15	<0.08	<0.15	<0.15	<0.15	<0.15	<0.15	<0.15	<0.15	<0.15
H_2O	<0.15	<0.15	<0.15	<0.15	<0.15	<0.15	<0.15	<0.15	<0.15	<0.15	<0.15	<0.15	<0.15	<0.15	<0.15
Si	1.937	1.854	1.924	1.894	1.911	1.917	1.914	1.893	1.885	1.913	1.851	1.861	1.861	1.949	1.941
Al^4	0.063	0.146	0.076	0.106	0.089	0.083	0.086	0.107	0.115	0.087	0.149	0.139	0.139	0.051	0.059
Σ	2.000	2.000	2.000	2.000	2.000	2.000	2.000	2.000	2.000	2.000	2.000	2.000	2.000	2.000	2.000
Al^8	0.055	0.086	0.029	0.042	0.041	0.039	0.035	0.060	0.067	0.047	0.078	0.083	0.080	0.019	0.014
Ti	0	0.005	0.014	0.012	0.009	0.013	0.016	0.008	0.008	0.006	0.015	0.011	0.011	0.029	0.029
Fe^3	0	0.026	0.006	0.014	0.004	0	0.014	0.010	0.008	0.012	0.026	0.016	0.014	0	0
Cr	0.010	0.024	0.012	0.026	0.026	0.017	0.009	0.021	0.025	0.016	0.015	0.018	0.023	0	0.007
Mg	0.935	0.894	0.935	0.926	0.947	0.952	0.937	0.886	0.881	0.882	0.825	0.842	0.857	0.727	0.732
Fe^2	0.198	0.173	0.250	0.203	0.179	0.234	0.249	0.186	0.174	0.199	0.206	0.191	0.191	0.456	0.457
Mn	0	0	0	0.004	0	0	0.004	0	0	0	0	0	0	0.011	0.010
Ca	0.800	0.792	0.753	0.775	0.794	0.744	0.732	0.829	0.837	0.837	0.835	0.839	0.824	0.745	0.741
Na	0	0	0	0	0	0	0	0	0	0	0	0	0	0	0
K	0	0	0	0	0	0	0.004	0	0	0	0	0	0	0	0
Σ	1.999	2.000	2.000	2.000	2.000	2.000	2.000	2.000	2.000	2.000	2.000	2.000	2.000	1.987	1.990
Mg*	0.83	0.84	0.79	0.82	0.84	0.80	0.79	0.83	0.84	0.82	0.80	0.82	0.82	0.61	0.62

SARAH ISLAND TO TIMBERTOPS AREA

Whole rock chemistry of the igneous rocks in this section is discussed in the geochemistry section and mineral analyses are presented in Tables 3–6.

Basalt lava (Ctbc)

Massive basalt lavas crop out on the western shore of Birchs Inlet and in the small creeks flowing into it from the west. They are faulted to the north-west against the siliceous mudstone/siltstone/sandstone/conglomerate sequences (Cts). The southern continuation of these rocks in the Point Hibbs map sheet area is overlain unconformably by Ordovician siliceous quartz sandstone (Otc). The basaltic rocks are generally poorly exposed and boundaries between flows were not seen. The lavas are generally fine grained but at CN731946 a coarse-grained variety occurs. Abundant green amygdales are generally present.

In thin section the basalts consist of unorientated plagioclase laths, subophitic augite (table 3, fig. 5) and intergranular opaque grains. The plagioclase is generally very cloudy and mainly replaced by sericite. The pyroxene is altered variably to chlorite and there are irregular patches of chlorite which probably represent altered pyroxene. Chlorite amygdales are

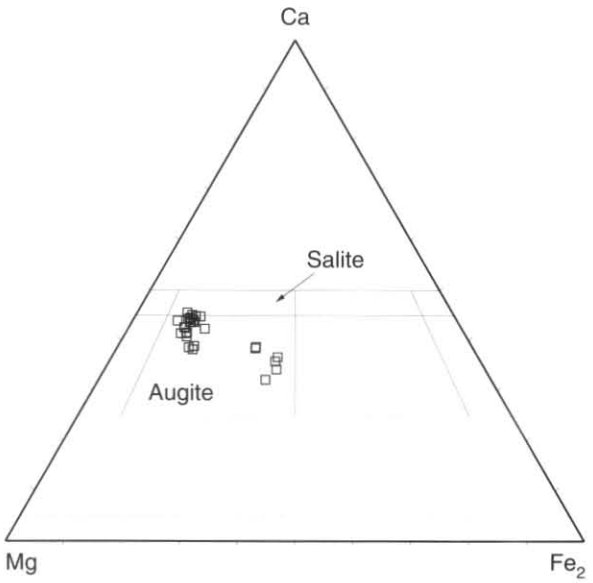

Figure 5. Pyroxene compositions from basalt lava (Cts).

Table 4. SPINEL COMPOSITIONS FROM MAFIC PROBABLE LAVAS (€tm)

	41546 _1/2	41546 _2/1	41546 _2/2	41546 _3/1	41546 _3/2	41546 _5/1	41546 _5/2	41546 _6/2	41546 _6/3	41546 _7/1	41546 _7/2	41543 _4/2	41543 _3/1
SiO_2	<0.15	<0.15	<0.15	<0.15	<0.15	<0.15	<0.15	<0.15	<0.15	<0.15	<0.15	<0.15	<0.15
TiO_2	0.21	0.23	0.19	<0.15	<0.15	<0.15	0.23	<0.15	<0.15	0.19	<0.15	<0.15	0.28
Al_2O_3	5.68	5.43	5.43	5.61	5.45	5.51	5.54	5.70	6.03	5.62	5.13	7.21	7.53
Cr_2O_3	62.36	63.48	63.88	63.33	63.24	63.38	63.02	62.95	62.07	63.34	64.13	60.89	54.09
Fe_2O_3	4.57	4.32	4.15	4.54	4.57	4.78	4.85	4.84	4.42	4.26	4.49	6.38	12.01
FeO	16.35	14.63	14.03	14.49	15.14	14.01	14.06	14.44	17.10	14.70	13.85	11.18	12.93
MnO	<0.15	<0.15	<0.15	<0.15	<0.15	<0.15	<0.15	<0.15	<0.15	<0.15	<0.15	<0.15	<0.15
MgO	10.82	11.92	12.32	12.03	11.59	12.33	12.30	12.07	10.37	11.90	12.4	14.34	13.17
CaO	<0.15	<0.15	<0.15	<0.15	<0.15	<0.15	<0.15	<0.15	<0.15	<0.15	<0.15	<0.15	<0.15
Na_2O	<0.15	<0.15	<0.15	<0.15	<0.15	<0.15	<0.15	<0.15	<0.15	<0.15	<0.15	<0.15	<0.15
K_2O	<0.15	<0.15	<0.15	<0.15	<0.15	<0.15	<0.15	<0.15	<0.15	<0.15	<0.15	<0.15	<0.15
H_2O	<0.15	<0.15	<0.15	<0.15	<0.15	<0.15	<0.15	<0.15	<0.15	<0.15	<0.15	<0.15	<0.15
Si	0	0	0	0	0	0	0	0	0	0	0	0	0
Ti	0.043	0.045	0.038	0	0	0	0.046	0	0	0.037	0	0	0.055
Al	1.799	1.706	1.704	1.760	1.719	1.725	1.736	1.787	1.912	1.766	1.610	2.215	2.332
Fe^3	0.923	0.867	0.830	0.910	0.919	0.956	0.971	0.970	0.895	0.854	0.898	1.250	2.375
Cr	13.23	13.38	13.42	13.33	13.36	13.31	13.24	13.24	13.19	13.34	13.49	12.53	11.23
Σ	16.000	16.000	16.000	16.000	16.000	16.000	16.000	16.000	16.000	16.000	16.000	16.000	16.000
Fe^2	3.670	3.264	3.119	3.226	3.385	3.114	3.127	3.214	3.845	3.275	3.083	2.435	2.841
Mn	0	0	0	0	0	0	0	0	0	0	0	0	0
Mg	4.330	4.736	4.881	4.774	4.615	4.886	4.873	4.786	4.155	4.725	4.917	5.565	5.159
Ca	0	0	0	0	0	0	0	0	0	0	0	0	0
NA	0	0	0	0	0	0	0	0	0	0	0	0	0
K	0	0	0	0	0	0	0	0	0	0	0	0	0
Σ	8.000	8.000	8.000	8.000	8.000	8.000	8.000	8.000	8.000	8.000	8.000	8.000	8.000
Cr*	0.88	0.88	0.88	0.88	0.88	0.88	0.88	0.88	0.87	0.88	0.89	0.84	0.82
Mg*	0.54	0.59	0.61	0.59	0.57	0.61	0.60	0.59	0.51	0.59	0.61	0.69	0.64

Table 5. PYROXENE COMPOSITIONS FROM INTERMEDIATE PROBABLE EXTRUSIVES AND INTRUSIVES OF ANDESITIC CHEMICAL COMPOSITION (€ta)

	MH561_2/1	MH561_2/3	MH561_2/4
SiO_2	53.73	54.54	54.22
TiO_2	<0.15	<0.15	<0.15
Al_2O_3	1.84	1.04	1.97
Cr_2O_3	1.21	0.76	0.44
Fe_2O_3	<0.15	<0.15	<0.15
FeO	3.26	3.22	3.77
MnO	<0.15	<0.15	<0.15
MgO	17.80	18.32	17.60
CaO	22.16	22.12	21.99
Na_2O	<0.15	<0.15	<0.15
K_2O	<0.15	<0.15	<0.15
H_2O	<0.15	<0.15	<0.15
Si	1.952	1.977	1.967
Al^4	0.048	0.023	0.033
Σ	2.000	2.000	2.000
Al^8	0.031	0.022	0.051
Ti	0	0	0
Fe^3	0	0	0
Cr	0.035	0.022	0.013
Mg	0.964	0.990	0.952
Fe^2	0.099	0.098	0.114
Mn	0	0	0
Ca	0.863	0.859	0.855
Na	0	0	0
K	0	0	0
Σ	1.991	1.990	1.985
Mg*	0.91	0.91	0.90

Table 6. AMPHIBOLE COMPOSITIONS FROM INTERMEDIATE PROBABLE EXTRUSIVES AND INTRUSIVES OF ANDESITIC CHEMICAL COMPOSITION (€ta)

	MH561_3/1	MH561_3/2	MH561_3/3
SiO_2	41.56	41.45	43.89
TiO_2	1.94	1.89	1.47
Al_2O_3	13.51	13.46	11.04
Cr_2O_3	<0.15	<0.15	<0.15
Fe_2O_3	9.20	7.74	8.36
FeO	2.48	4.25	4.26
MnO	<0.15	<0.15	<0.15
MgO	14.82	14.37	14.84
CaO	11.51	11.72	11.68
Na_2O	1.90	1.96	1.60
K_2O	1.01	1.09	0.79
H_2O	2.08	2.07	2.08
Si	6.001	6.019	6.341
Al^4	1.999	1.981	1.659
Σ	8.000	8.000	8.000
Al^8	0.300	0.323	0.221
Ti	0.210	0.206	0.159
Fe^3	0.999	0.846	0.909
Cr	0	0	0
Fe^2	0.300	0.517	0.514
Mn	0	0	0
Mg	3.190	3.109	3.196
Σ	5.000	5.000	5.000
EXM	0	0	0
Ca	1.781	1.823	1.808
NAM	0.219	0.177	0.192
Σ	2.000	2.000	2.000
NAA	0.312	0.376	0.257
K	0.186	0.202	0.146
Σ	0.499	0.578	0.403
OH	2.000	2.000	2.000
Mg*	0.91	0.85	0.86

common and some containing a small amount of carbonate in addition. A few samples show small, sparse intergranular patches of quartz. Glomerophyric plagioclase with sparse pyroxene phenocrysts are present in over half the samples examined. Small patches of chlorite associated with an unidentified orange mineral may be pseudomorphs after olivine. Patches and irregular veins of epidote occur in some samples and there are also less common patches of secondary albite with thin needle-shaped crystals of apatite.

Siliceous mudstone/siltstone/sandstone/conglomerate (€ts)

Rocks of this type form generally poor outcrops in the upper parts of small creeks south of Commandant Creek which flow east into Birchs Inlet. They have are faulted against the mudstone/lithicwacke (€tl) sequences to the north-west and with the basalt lava (€tbc) sequence to the south-east.

These rocks are dominantly pale grey to white sandstone with minor siltstone and mudstone interbeds. Bedding is not easy to distinguish in outcrop, although at several localities [e.g. CN732967, CN722751, CN727956], the sandstone is interbedded with conglomerate horizons of uncertain thickness. These contain well rounded quartzite pebbles up 50 mm in diameter. No other sedimentary features were observed.

In thin section the finer grained rocks consist dominantly of moderately well sorted, strained quartz grains with very minor white mica, opaques, tourmaline and zircon. Very minor amounts of intergranular chlorite is present in some specimens and is generally partly altered to brown iron rich material. The opaque grains are white in reflected light which may indicate leucoxene derived from ilmenite. In some specimens e.g. at CN722948 a small amount of carbonate is also present. The clasts in the conglomerate samples are well rounded and consist of coarse recrystallised and strained quartz crystals often elongated with a preferred optical orientation.

Shallow marine sedimentation with derivation from a siliceous metamorphic terrain seems most likely on the basis of the features described.

At CN718947 a thin unit of basalt (Ctbb) is present.

Basalt lava (Ctbb)

A thin unit of basalt occurs within the siliceous mudstone/siltstone/sandstone/conglomerate sequence (Cts) around CN719847. In outcrop it is dark grey-green massive fine-grained with no structural features.

Two specimens collected from the unit show a slightly different character in thin section. That from CN719947 consists of a mesh of cloudy, plagioclase with subophitic pyroxene and abundant intergranular opaque grains. Amygdales filled with chlorite are abundant. The sample collected at CN718947 consists of cloudy plagioclase laths with minor intergranular patches of dark green chlorite/actinolite and opaque grains. This sample is more altered than the other one and is lighter coloured.

Mafic lavas, breccias and tuff (Ctm)

Mafic rocks, presumed to be lavas, crop out at various localities in the Timbertops area in close association with other units. At CN683962, CN676963, CN675967 and CN672965 outcrops of Ctm occur within an area of andesite rocks (Cta). The limited amount of outcrop prevented the determination of stratigraphic relationships between Ctm and Cta.

The rocks of Ctm are generally massive. Grain size ranges from fine- to coarse-grained and they are grey-green when fresh. Some specimens show unorientated laths of black or dark green mineral set in a medium dark, fine-grained matrix.

In thin section some specimens consist almost entirely of pyroxene pseudomorphs (up to 6 mm long) consisting of talc and chlorite (plate 10) within a subordinate matrix of talc with, chlorite and chrome spinel grains (table 4). Some pyroxene pseudomorphs show parallel laminae which probably follow exsolution laminae of calcium-rich pyroxene in clinoenstatite. Other pseudomorphs are probably after orthopyroxene. Some pyroxene crystals are pseudomorphed by carbonate. These rocks resemble the basaltic pyroxenite described from the high-magnesian andesite suite occurring in the Heazlewood River area (Brown, 1986). In other samples the proportion of matrix is greater and there are abundant vesicles filled with chlorite and finely granular quartz.

Intermediate probable extrusives and intrusives of andesitic chemical composition (Cta)

Rocks of this type crop out in the Timbertops and adjacent area. Their exposure is generally poor being confined to the partly overgrown BHP tracks and the upper part of Commandant Creek. Variations in grain size suggest that intrusive and extrusive rocks are present. Minor mudstone units are present in the sequence [e.g. at CN673966]. At CN693959 in the Commandant Creek they appear to have a stratigraphic contact with the mudstone/lithicwacke sequence (Ctl) and on the western side of the outcrop area they pass into rhyolitic quartz and feldspar porphyries (Ctr). The relationship of the andesites with unit Ctm, which occurs in the same area, is unclear. At Timbertops the andesitic igneous rocks are unconformably overlain by siliceous quartz sandstone of Ordovician age (Otc). The contact between Cta and Ctm has been inferred to be overlain unconformably by the Ordovician rocks.

The andesites are generally massive fine- to medium- grained and pale to medium dark grey-green. Less common coarse-grained varieties are also present. In some outcrops amygdales with white (? zeolite) infill are common. At CN677962 a breccia may represent an intraflow breccia.

Plate 10. Talc/chlorite pyroxene phenocryst pseudomorphs in unit Ctm.

In thin section samples of Cta show variations in texture and mineral composition. One sample from CN693959 has sparse plagioclase and opaque mineral phenocrysts set in a very fine-grained matrix with perlitic structures. Most samples are fine to medium grained, but rare ones are coarse. They consist mainly of randomly orientated or occasionally flow-aligned plagioclase laths. Plagioclase is variably altered to sericite and, rarely, is also present as small phenocrysts and glomerophyric aggregates. Where intergranular clinopyroxene is present it is partly or wholly altered to chlorite, amphibole and sometimes a brown-red alteration mineral. In one sample (MH561) the pyroxene is augite (table 5). In some samples the amphibole shows a green/brown colour suggesting that it may have a hornblende component and in sample MH561 the composition is close to pargasite (table 6). Intergranular fine and less commonly coarse grains of opaque mineral occur. This is probably ilmenite as it is associated with leucoxene a common alteration product of ilmenite. Minor patches of intergranular quartz occur in some specimens.

Quartz and feldspar rhyolite porphyries (Ctr)

Rocks of this type occur in three areas; the Muddy Cove – Briggs Creek area [CP695035], the area farther south centred on CP685987 and in the northern Timbertops area near CP677975. In the first two areas, unit Ctr is separated by pyroxene and feldspar-phyric andesite (Cal) with which they form part of a fault bounded block. In the east they are thrust over the mudstone /lithicwacke sequence (Ctl); in the west unit Ctr is faulted against unit Ctl and gabbro (Cg). In the third area, unit Ctr appears to overlie stratigraphically the mudstone/lithicwacke sequence (Ctl). At CN669967 a minor mudstone unit is present in the sequence.

Most outcrops of Ctr occur along the partly overgrown BHP tracks and in small thickly vegetated creeks (e.g. upper parts of the Cuthbertson Creek, CN685975) and are extremely weathered. Outcrops of Ctr are generally fine grained, pale grey with a slight green tint and contain common small phenocrysts of feldspar and quartz.

In thin section Ctr generally consists of phenocrysts of plagioclase and quartz set in a fine-grained matrix of quartz,

Plate 11. Trough current bedded sandstone in unit €tl at CP724026.

feldspar, sericite, chlorite and fine opaque grains. The plagioclase phenocrysts are generally more abundant than the quartz and are sometimes present as glomerophyric patches. They are substantially altered to sericite. The quartz phenocrysts have rounded and embayed outlines and are not strained. Small pseudomorphs of chlorite and opaque grains are common and may have been derived from pyroxene phenocrysts. In some specimens small partly chloritised biotite phenocrysts occur.

At CN682982 a welded tuff crops out of very fine- grained, elongate and flattened shard-shaped fragments which contain embayed and corroded quartz phenocrysts. Fine-grained lithic fragments could be distinguished in the thin section.

Mudstone/lithicwacke sequences (€tl)

Rocks from these sequences crop out in the southern and eastern parts of the peninsula from Steadmans Point in the north to the southern margin of the map sheet. The western outcrops occur in the Point Hibbs Mélange Belt and are faulted against sheared serpentinite (€ss), gabbro (€g) and various other igneous and probably igneous rock types. The bulk of the remaining outcrops occur in a broad zone stretching south from Asbestos Point to near the Timbertops area. The western boundary of this zone is faulted against pyroxene and feldspar-phyric andesite (€al) and quartz and feldspar-phyric rhyolite (€tr). A short distance north of the Timbertops area the sequences are in apparent stratigraphic contact with, and young towards, quartz and feldspar-phyric rhyolite (€tr) and andesite (€ta). The south-east boundary of the zone is a faulted against a siliceous mudstone/ siltstone/sandstone/ conglomerate (€ts) sequence. In the Timbertops area unit €tl is unconformably overlain by Ordovician siliceous quartz sandstone and conglomerate (Otc).

Unit €tl is well exposed in coastal outcrops stretching from Bryans Bay to the mouth of Commandant Creek in Birchs Inlet; excellent exposures may be viewed on Sarah and Grummet Islands. The major east-draining creeks south of Asbestos Point also provide good outcrops. Exposure in the western area is poor and is confined mainly to old BHP tracks.

The rocks generally consist of dark grey mudstone and medium to pale grey siltstone and sandstone. At CP720056 on Sarah Island, parallel-bedded sandstone units 150–230 mm thick alternate with mudstone layers less than 20 mm thick. The sandstone beds have thin (<30 mm) tabular current bedding. Nearby graded bedded sandstone up to 1.5 m thick occur. On Grummet Island some of the sandstone beds are very coarse grained and are interbedded with very poorly sorted conglomerate (€tlc) with clasts ranging from coarse sand grade to rounded boulders with diameters as great as 0.9 m. Within these beds the pebbles and boulders consist of quartz and quartzite with minor red chert fragments. The conglomerate and coarse sandstone units are size graded and flame structures occur at their bases. Lenses of coarse-grained sandstone also occur in the bases of the finer beds: these are interpreted as washout structures. In Davis Bay pieces of banded siltstone up to 0.6 m long, present in conglomerate, appear to have been torn up from the underlying bed which has contorted structures.

The conglomeratic beds at Sarah Island and Grummet Island strike directly towards identical beds at Davis Bay and other coastal outcrops farther south [e.g. CP722018].

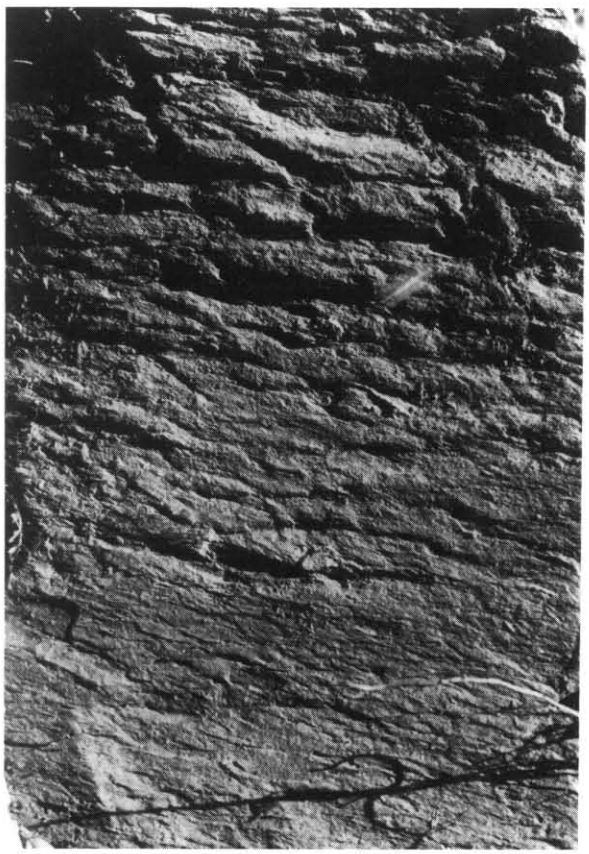

Plate 12. Flute casts on base of a sandstone bed in unit €tl at CN723972.

Conglomerate horizons also occur in one of the western fault-bounded blocks at CP679011, CP672000 and in the Fern Creek [CN662975] area. The clasts in these outcrops have a maximum length of about 30 mm.

Coarse sandstone beds occur throughout the area of outcrop but are more common in the region between Grummet Island and 3 km south of Rum Point. Size grading in the sandstone and siltstone is widespread; thin units of tabular and trough current bedded sandstone were also seen (plate 11). At CP708059 a 0.6 m thick units of sandstone with size grading pass up into tabular current bedding, and at CN723972 flute casts were seen on the base of a sandstone bed (plate 12).

The dark grey mudstones are commonly pyritic.

In thin section the sandstones and siltstones generally consist of angular, poorly sorted, strained quartz and quartzite grains set in a finer-grained recrystallised matrix of quartz, white mica, chlorite and opaques. Samples from Commandant, Cuthbertson, Henrietta and Muddy Cove Creeks commonly also contain lava clasts, plagioclase, embayed and unstrained quartz. The embayed and non-strained character of these quartz grains indicate that they were derived from volcanic rocks. The lava clasts are mostly very fine grained and variable in texture. Some consist of flow aligned plagioclase laths and others of granular quartz, feldspar and minor white mica with sparse small phenocrysts of quartz and plagioclase. Other volcanic fragments are very fine grained and are probably devitrified glass because perlitic structures are still visible. The volcanic clasts resemble intermediate and acid lavas. One sample from near Fern Creek at CN663971 contains rare grains of perthitic feldspar and altered biotite. These rocks are clearly mostly derived from a siliceous metamorphic and an intermediate to acid volcanic terrain though a minor granitic source is indicated by the perthitic feldspar grains described above. Volcanic quartz, plagioclase and lava clasts were not found in the rocks from the Sarah Island – Rum Point area. The mudstones consist of recrystallised quartz, white mica, chlorite and opaques and may be tuffaceous in part. At CN716966 in the middle part of Commandant Creek a minor amount of carbonate was detected in mudstone. Probable tuffaceous mudstone occurs at CP704065 near Asbestos Point. These rocks contain fine-grained recrystallised quartz and white mica with sparse unstrained subhedral quartz crystals. A probable vitric/crystal tuff is exposed in a nearby creek at CP706058 rock and consists of clasts of very fine-grained quartz and white mica together with unstrained quartz grains.

The presence of poorly sorted, graded siltstone, sandstone and conglomerate interbedded with mudstone together with the presence of flute casts indicates that the coarser-grained units were produced by turbidity currents.

The mineralogy and the recrystallised fine-grained matrix of the rocks indicates that they were metamorphosed to very low grade.

Basalt lava (€tba)

A small area of basalt occurs within the area of outcrop of the mudstone/lithicwacke sequence (€tl) and two samples were collected from a creek outcrop at CN712948. The relationship of the lava to the neighbouring sedimentary rocks is unknown. The basalt float occurs for at least 300 m east from the creek at that point, suggesting an extension of the basalt area. In outcrop the basalt is a fine-grained grey-green or purple-grey rock with no flow features evident.

In thin section one of the specimens consists of glomerophyric plagioclase crystals together with a lesser proportion of clinopyroxene phenocrysts set in a matrix of plagioclase laths, clinopyroxene grains, opaque grains and chlorite patches. The pyroxene is partly altered to chlorite and the plagioclase is extensively altered to sericite. The other specimen consists of thin plagioclase laths and subophitic clinopyroxene together with opaque grains. The pyroxene is partly altered to chlorite and the plagioclase is altered to sericite.

UPPER MODDER RIVER AREA

Mudstone/siltstone/sandstone sequence (€ms)

Rocks of this sequence crops out in a narrow (≈1 km wide) belt stretching SSW from Bryans Bay. The western boundary is in faulted contact with the Precambrian metamorphosed, interbedded quartzwacke and mudstone/ siltstone (Pnq) sequences. In the northern part of the belt the eastern boundary is in faulted contact with sheared serpentinite (€ss) but to the south it passes up with apparent conformity to siliceous quartz sandstone (Oms) of presumed Ordovician age. An Upper Cambrian fauna of agnostid trilobites, inarticulate brachiopods and broken dendroid graptolites occur in the BHP track at CN645982 (Clarke, 1968; Quilty, 1971; Jago, 1972).

The sequence generally consists of massive to poorly bedded reddish grey to grey mudstone and siltstone. Thin lenses and bands of sandstone are present in some areas. Sedimentary features are rare. Thin (<150 mm) siltstone graded units associated with sandstone filled washout structures occur at CP676073 and thin (<50 mm) tabular current bedding units occur at CP666031. Mudstone flakes up to 30 mm long can be seen in the siltstone at a number of localities. Conglomerate (€mc) with rounded pebbles up 10 mm in diameter occurs in the sequence at CP666030 and also in the southern part of the belt were it forms a larger unit.

In thin section the sediment consists generally of very poorly sorted angular grains of rock, unstrained quartz and less common plagioclase. The rock fragments are mostly very fine-grained quartz, feldspar and sericite. Rare euhedral quartz grains present in these clasts suggest that they are probably volcanic material of acid to intermediate composition. Some coarser-grained clasts consist of abundant chlorite with quartz and opaque mineral. The opaque mineral was probably originally ilmenite as it is white in reflected light which is assumed to be leucoxene altered from ilmenite. These clasts are also interpreted as being volcanic. The unstrained and rarely euhedral shaped quartz grains probably have a volcanic origin. Some samples have clasts of coarse-grained carbonate or of coarse-grained strained quartz and carbonate. Fine grains of probable ilmenite are common together with intergranular chlorite. Some samples have abundant secondary carbonate.

The poor sorting of the sediment, its immature composition and the presence of graded units suggest that it was deposited by turbidity currents. The nature of the clasts indicate that it was dominantly derived from an intermediate to acid volcanic terrain.

Ordovician Sequences

R. H. Findlay

TIMBERTOPS AREA

According to bedding and cleavage measurements near CN660933 an angular unconformity separates underlying Cambrian rocks from the overlying Ordovician sequence in the NW-trending Timbertops Syncline (McClenaghan and Findlay, 1989). The Ordovician rocks of the Timbertops Syncline consists of quartz sandstone with conglomeratic interbeds, siltstone with sandstone interbeds and quartz sandstone: these are correlated with the Denison Group of the Wurawina Supergroup. South of the map sheet area, carbonates correlated with the Gordon Group occur within the core of the syncline.

Siliceous sandstone and conglomerate sequence (Otc)

This basal unit of the Ordovician succession is reasonably well exposed in the BHP track along the eastern limb of the Timbertops Syncline and is less well exposed in creeks cutting through the west limb of the syncline. It consists in the main of beds of white-weathering finely laminated and massive, fine to coarse quartz sandstone with conglomeratic interbeds. Occasional tabular cross-beds have been noted within sandstone horizons. The bedding laminations are generally plane parallel and are spaced at 2–3 mm intervals; the cross-bedding occurs in units 100–500 mm thick. According to simple rotation of bedding to the horizontal, and taking into account also the plunge of the Timbertops Syncline, the four cross-bedded horizons observed were produced by flow from the east.

At CN670948 and CN67938 the basal beds of unit Otc are well-indurated, medium-grained quartzite bedded on the 0.3 m scale. At CN673961 the basal beds are of white quartzite, some of which contain disseminated pyrite, and include a 6–8 m thick, siliceous, matrix-supported conglomerate containing well-rounded pinkish quartzite pebbles with a maximum diameter of 25 mm. No pebble imbrication has been recognised.

Conglomeratic beds dominate the sequence in the BHP track in the region of CN686937. Here, the maximum thickness of this unit is inferred both from the distribution of loose pebbles on the track and also sporadic outcrops to be of the order of 170 m. The well-rounded pebbles of pink and white quartzite and vein quartz are framework-supported and neither imbrication nor size-grading has been recognised. According to observations in the BHP cross-track at CN702933, where a matrix-supported well-rounded quartzite and quartz pebble conglomerate forms the inferred continuation of the conglomeratic sequence, the sequence must thin southwards.

The fine- to medium-grained quartz sandstone beds at CN673962 contain a fauna of gastropods, orthocone nautiloids, and fragments of trilobites of both the asaphid type, offering comparison with *Basiliella*, as well dokimocephalid forms (Clarke, 1968). Clarke (1968) notes that the trilobite determinations must be treated with caution, and presents the conclusion that although the orthocone nautiloid indicates that the fauna are no older than Upper Cambrian, if the asaphid determination is correct the fauna is of Lower Ordovician age.

Siltstone sequence (Ott)

This unit is exposed in very limited outcrops in Timbertops Creek between grid references CN674934 and CN674949, and very small rare exposures in the well-overgrown BHP track just south of the map sheet. The sequence contains subordinate cleaved grey-green micaceous siltstone with interbeds of grey to dark grey fine-grained quartz sandstone. No sedimentary structures were observed in the sparsely-exposed sandstone beds; a plane parallel lamination occurs in some exposures of siltstone.

The siltstones are notable for the presence of deformed fragments of asaphid trilobites together with deformed internal and external moulds of Orthid brachiopods. Clarke (1968) reports several specimens of *Paurorthis* sp. nov. and *Tritoechia* (?) *careyi* Brown, and a crown and stem of a cystoid broadly similar to *Echinoencrinites*. Clarke (1968) notes that this faunal association indicates a Lower Ordovician age.

Siliceous sandstone sequence (Ots)

Siliceous sandstone beds with some conglomeratic layers crop out around CN683928 and are inferred to form the high ground about one kilometre north. An isolated outcrop of siliceous pebble conglomerate with a fine-grained quartzite matrix at CN683931 is followed apparently conformably by beds of white medium-grained quartz sandstone. Fine-pebble quartzitic conglomerate is inferred to be interbedded in this unit from float in the creek at CN684936. The quartzite beds contain a fine dark banding which forms a bedding lamination and is thought formed by trains of chromite grains.

UPPER MODDER RIVER

The Ordovician rocks here form a thin siliciclastic and carbonate sequence inferred to be repeated by steeply dipping faults.

Siliceous sandstone sequence (Oms)

This unit is inferred to overlie the Cambrian siltstone unit Oms conformably at grid reference CN647983 and CN642971 although a fault or possibly an angular unconformity is inferred from strike measurements at CN627927 immediately south of the map sheet boundary.

This unit contains white to light brown weathering sandstone beds and pebbly conglomerate horizons. The sandstone beds are typically medium to coarse grained, rich in rounded to sub-angular quartz grains and containing in addition clasts of white feldspar; the coarser beds contain also red chert grains. Cross-beds in four units yield a consistent north to north-westerly given simple rotation of palaeocurrent direction to horizontal about the strike of the bedding. The sandstone beds range between 70 mm and 450 mm in thickness, where reasonably well exposed.

Some sandstones display graded bedding. These contain granule-sized clasts floating in the sandstone matrix. These clasts are generally 5–10 mm across, are rounded to subangular and may be interspersed with less common pebbles as large as 10 mm which are rounded and sometimes tabular; the clasts are of white vein quartz, minor red and grey chert, and quartzite. No imbrication of clasts occurs in these beds, although some of the more tabular pebbles may lie parallel to bedding.

Clast-supported pebbly conglomerate beds are known south of the map sheet area at CN910930, where beds and loose blocks of conglomerate contain 25 to 30 mm sized clasts of rounded red chert, rounded mudflakes, quartzite and vein quartz in a grey-green, medium- to coarse-grained quartzo-feldspathic matrix. Rounded to sub-angular black chert pebbles as wide as 100 mm in diameter are known as float at this locality and are thought derived from the conglomerates. Also present here are quartz sandstone beds with cross-bedding picked out by probable chromite; when bedding is rotated about strike to the horizontal the cross-beds indicate a south-easterly source.

No fauna are known from this unit although Cambrian rocks at CN644985, which underlie the Ordovician sequence with apparent conformity, have yielded a probable upper Middle Cambrian age (Clarke 1968). As these Ordovician beds are overlain conformably by the inferred correlate of the Gordon Group limestones, and as chert clasts in the Ordovician siliciclastics of the West Coast Range are known only from the upper part of the Lower Ordovician Denison Group, then there may well be a major unconformity or fault between the Cambrian units Omc and Oms, and the Ordovician siliciclastic rocks described above.

Dolomite sequence (Omg)

This unit overlies unit Oms with apparent conformity. Exposures of the carbonate are known at CN649980, CN637954 (where it is visible in the creek only in very dry periods), and in the BHP track at CN633946; carbonate has been found also as float in tree roots at CN644969.

At all these localities the carbonate is micritic, weathers grey, and is mottled with interlinked brown-weathering dolomitic patches. The carbonate is bedded in units approximately

150–250 mm thick; in two horizons at CN633946 the dolomitic mottling increases towards the inferred bases of the beds.

No fauna have been found in this unit. However it is identical to the unfossiliferous carbonate which is exposed in the Timbertops Syncline and which overlies Denison Group correlates of Lower Ordovician age; in the Modder River region, unit Omg overlies, apparently conformably, siliciclastic rocks thought to be correlates of the upper part of the Lower Ordovician Denison Group and thus unit Omg is correlated with the lower units of the Gordon Group.

Tertiary

R. H. Findlay

Tertiary beds in the map sheet area occur in three well-separated regions – east of Macquarie Harbour between Sophia Point and Farm Cove; west of the harbour at Liberty Bay and Betsys Bay as well as immediately north of Liberty Creek; and, in the south, east of Birchs Inlet.

The Tertiary sequences underlying the northern and eastern part of Macquarie Harbour are known as the Macquarie Beds (Bradley, 1954) and according to gravity measurements are thought to be at least 450–500 m thick. North of the Macquarie Harbour sheet area, the Macquarie Beds were mapped by Baillie (in Baillie *et al.*, 1985) who on the basis of limited palynological data recognised Eocene and Plio-Pleistocene sequences. No faunal or floral evidence for Oligocene or Miocene rocks is known in the sequence, and this, the presence of a possible palaeosol, and the reported greater induration and jointing in the Eocene rocks (Baillie *et al.*, 1985) may indicate an unconformity within the Tertiary sequence in the Strahan – King River region.

SOPHIA POINT –FARM COVE AREA

In this region, the principal exposures are found along the sea-cliffs north of Farm Cove, along the Coal Creek track and the upper part of Braddon River and in the creeks draining west off Mt Sorell about 2–3 km east of the map sheet area.

In the northern part of the Sophia Point – Farm Cove area, Tertiary beds are exposed in creek beds but are concealed beneath dense forest and, in hill tops, below Quaternary gravels.

Within the Tertiary sequence there is an apparently gradational but abrupt change from the lower unit Tss, which is formed of quartz sandstone and carbonaceous sandstone and siltstone beds, to conglomeratic beds (Unit Tsg) which increase markedly in volume and grain size up the sequence. This change is thought indicative of increasingly rapid uplift of the quartz-rich rocks of the West Coast Range.

On the basis of lithological correlation of units Tss and Tsg with the palynologically dated Tertiary beds in the Strahan – King River region (Baillie *et al.*, 1985), unit Tss is assigned an Eocene age whereas Unit Tsg is thought to be of Plio-Pleistocene age.

Quartz sandstone and carbonaceous siltstone (Tss)

This unit consists of poorly indurated, yellow weathering, white, fine- to medium-grained quartz sandstone which where predominantly close to sea level is interbedded with carbonaceous siltstone with fine variably carbonaceous sandstone both of which commonly contain variably coalified plant stems, logs, roots and leaf impressions. Towards the upper part of the unit (~60 m above sea level), and principally in the west, outcrops of the white sandstone contain thin beds of rounded quartz pebbles; also present are horizons containing ellipsoidal ferricrete concretions.

In the quartz sandstone sequences the following sedimentary structures have been recognised: high-angle tabular cross-bedding in units as thick as 2 m, although such thick units appear to be the exception; low-angular and trough-cross-bedding; plane-parallel lamination; small-scale ripple lamination; apparently massive non-laminated bedding; at Coal Head large dunes occur with low-angle cross-bedding; at grid reference CP703156 a small sand diapir penetrates undulatory parallel-laminated bedding forming cuspate ripples; and load structures are known. No point bar gravel deposits, nor sequences of graded beds are known. These sedimentary structures are indicative of a variable high to low flow-regime in a probably tidal environment, and would suggest that the Macquarie Beds were deposited in a Cenozoic graben open to the sea.

In sequences where carbonaceous quartz siltstone and quartz sandstone are interbedded with quartz sandstone units, additional sedimentary structures include: burrowed

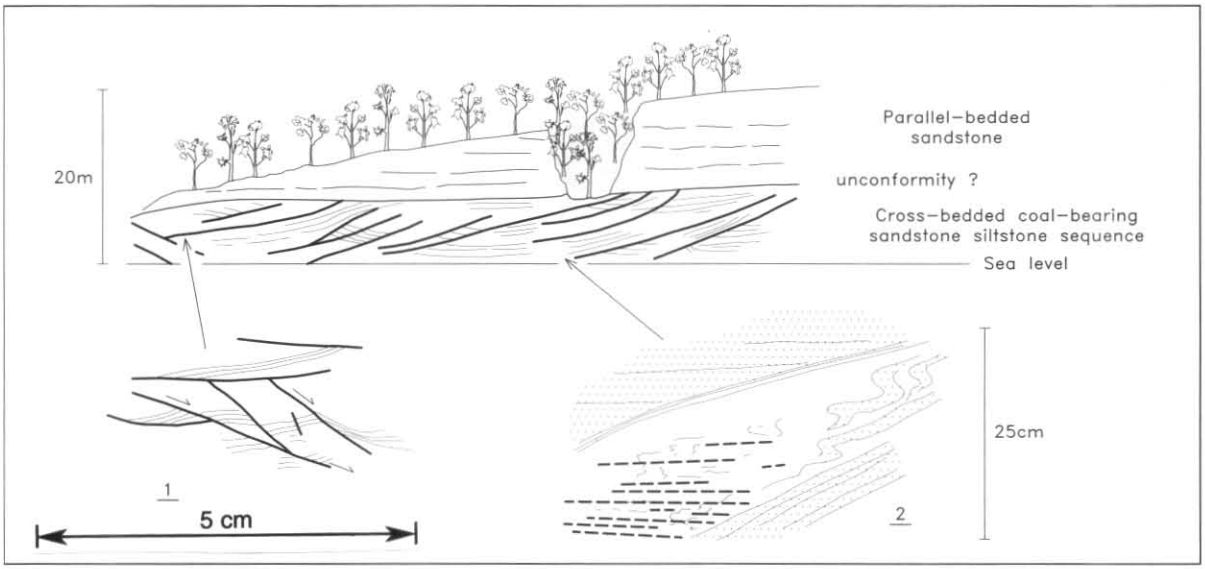

Figure 6. Low angle faults at CP735111 in Tertiary sandstone beds (Tss). The upper parallel-bedded sandstone sequence is typical of the upper part of the probable Eocene beds in ther Farm Cove area, and therefore faulting may be of intra-Eocene age. Inset 1 shows normal faulting geometry. Inset 2 shows small-scale folding and flat axial plane cleavage (heavy broken lines) in beds underlying a fault plane. The geometry of these rootless folds is suggestive of normal faulting; stipple indicates sandstone, clear indicates pelite.

horizons; herring-bone cross-beds; low-amplitude ripple trains; channelised horizons; and lensoidal beds. These carbonaceous units contain also carbonised leaf impressions and twigs; coalified allochthonous stems and branches and in situ coalified tree roots are also present, indicating the likelihood of lagoonal or shoreline conditions during deposition of the carbonaceous units.

Palaeocurrent indicators within Unit Tss give a dominant trend of water flow along a N-S axis rather than an E-W axis; however in detail both north-west to north-east and WSW to south-east current directions have been observed. Plant stem orientations at two localities [CP703156, CP720119] support these observations.

Apparent large-scale cross-bedding is exposed in the cliff faces [CP703156, CP731129, CP735113. Detailed inspection has confirmed that these structures are low-angle faults (fig. 6); at grid reference CP703156, offsets of bedding and on minor faults below the main fault plane (fig. 6) confirm normal faulting; at CP731129 the topology of bedding across other faults (1, fig. 6) is consistent with reverse movement; and at CP735113 the vergence of folding along the fault plane (2, fig. 6) indicates normal slip. No cataclastically deformed rocks, nor mylonites occur along such fault planes; at CP735113 finely laminated sandstone layers within the fault zone are disrupted and folded and a weak cleavage has been formed.

The geometry of those structures is consistent with their interpretation as lystric normal faults formed by gravitational collapse of the thickened sedimentary pile.

Siliceous conglomerates (Tsg)

This is a sequence of pebble to boulder conglomerates containing clasts of principally quartz, quartzite and siliceous quartz and quartzite pebble conglomerate, set in a poorly indurated quartz-rich coarse- to medium-grained sandstone matrix. Around CP710200 and CP740205 are exposed conglomerate beds 5% of whose clasts are rounded, partly weathered dolerite pebbles (Unit Tsgd). These beds commence at the 200 m level in the northern part of the area, but are unknown among the conglomerates in the west and south, flanking Mt Sorell. Baillie (in Baillie *et al.* 1985) has described dolerite-rich conglomerates to the south-east of Teepookana [CP713223] and further north in the vicinity of Tully River. In the latter region, the dolerite clasts may form boulders as large as 2 m in diameter and, in contrast to the present area, occur within a matrix derived principally from decomposed dolerite. Further south in the Teepookana region Baillie *et al.* (1985) note that about 15% of the clasts are dolerite and such clasts may be as large as boulders; by analogy with fossiliferous beds elsewhere these dolerite-bearing conglomerates are thought to be of Eocene age.

In the southern and western parts of the Sophia Point – Farm Cove region, unit Tsg is most clearly exposed in the low hills flanking Mt Sorell. Here, the rapid gradation from unit Tss is heralded by influxes of quartzite vein-quartz pebbles. At a small outcrop at grid reference CP761150 pebble beds overlie the carbonaceous siltstone and sandstones of unit Tss with a low-angle angular unconformity although just to the east of the map sheet boundary the creeks draining the western flanks of Mt Sorell contain exposures indicating an abrupt but gradational transition from Tss to Tsg. It may be that either there are local angular unconformities in the sequence, or that the pebbly beds at CP761150 formed by reworking of unit Tsg during Quaternary times; as yet, no palynological investigations have been carried out.

Unit Tsg coarsens upwards rapidly and in its upper reaches contains well rounded quartzite and quartz conglomerate boulders as large as 6 m. Within the unit, channelled beds have been recognised; conglomerates are both clast and framework supported; fining-up graded beds are known; many pebbly beds show a fair imbrication of pebbles; all pebbles are well-rounded; coarse to very coarse sandstone lenses are known; and very coarse disorganised conglomerates indicative of mass flow deposits are present.

The rapid influx of the conglomerates overlying unit Tss, and its overall coarsening upwards character, confirm rapid, and possibly increasingly so, uplift of the east side of the Macquarie Harbour region during Late Tertiary times. The very low angle normal faults in Unit Tss have been described previously; these may represent gravitational collapse of the uplifted Tertiary sequence in latest Tertiary or Quaternary times, and may have formed during the uplift of the West Coast Range.

Palaeocurrent measurements determined from pebble imbrication indicate no preferred current direction, although in general the nature of the unit is consistent with its derivation as a series of coalescing alluvial fans flanking the uprising West Coast Range, here formed of Mt Darwin and Mt Sorell. There is clear evidence for a northerly source for the dolerite-bearing conglomerates described here and in Baillie *et al.* (1985): these rocks represent a mass flow deposit in the Henty River area, which may have been reworked south through the Teepookana region into the present area, according to the southward-diminishing volume of dolerite detritus in the sequence.

LIBERTY AND BETSYS BAYS

Undivided Tertiary beds (Unit Tu) and silicified scree deposits (Unit Tsq) occur in these regions. In addition a gravelly lag deposit covers the north-facing hillside overlooking Liberty Bay.

Undivided beds (Tu)

These beds consist in the main of light-brown weathering siltstone and at CP607150 of cross-bedded coarse to medium sandstone. No palynological data are yet available, but lithologically these beds resemble beds with unit Tss.

Silicified breccia (Tsq)

Unit Tsq is formed of coarse silicified breccias containing framework and clast-supported angular pebbles and cobbles lying in a medium to coarse quartz-rich sandstone matrix, clearly derived from the adjacent Precambrian quartzite beds forming Table Head. As these breccias occupy hollows in the hillside, and their primary dip, as seen in the foreshore, follows that of the hillside, they are interpreted as scree deposits.

LIBERTY CREEK AREA

Rocks of probably Tertiary age are exposed in the low hills in the region of the vehicular track running south-west from near the mouth of Liberty Creek [CP606130 to CP590105]. These beds are represented principally by a pebbly lag deposit, and such exposures as exist occur only in shallow gutters and washouts in the track. Here, the beds resemble lithologically the lower beds of unit Tsg as they consist of chocolate to light brown weathering sandstone and siltstone interspersed with fine to coarse pebble conglomerates containing clasts of vein quartz and quartzite in a quartz-sandstone dominated matrix. The thickness of these beds is unknown.

Quaternary

R. H. Findlay

Quaternary deposits have been mapped along the west coast of Sorell peninsula, where they form principally beach and dune sands with subordinate lagoonal and stream deposits. In the north-east of the Macquarie Harbour quadrangle, Quaternary gravel beds (Qg) capping terraces at levels between 85 and 315 m a.s.l. are thought to represent fluvial

Table 7. PYROXENE COMPOSITIONS FROM PYROXENE AND FELDSPAR PHYRIC ANDESITE (Ꞓal)

	MH202 _1/1	MH202 _1/2	MH202 _3/1	MH202 _4/1	MH202 _6/1	MH202 _8/1	MH202 _9/1	MH202 _2/1	MH202 _/1A	MH202 _/1A	MH202 _/3A	MH203 _1/1	MH203 _2/1	MH203 _3/1	MH203 _4/1
SiO_2	52.37	51.96	52.11	51.73	51.03	52.66	52.28	52.93	53.98	51.99	51.94	52.49	51.53	52.02	52.66
TiO_2	0.25	0.20	0.20	0.31	0.29	0.19	0.20	0.21	<0.15	0.27	0.23	0.29	0.35	0.22	0.22
Al_2O_3	2.37	2.36	2.22	2.73	2.37	2.23	2.43	1.32	1.35	2.20	2.20	1.54	2.47	1.71	1.44
Cr_2O_3	0.32	0.39	0.40	0.32	0.49	0.27	0.19	0.21	0.79	0.33	0.26	0.22	0.32	0.26	0.15
Fe_2O_3	<0.15	0.71	0.63	0.11	1.72	0.23	<0.15	0.02	<0.15	1.09	1.13	0.64	1.46	1.08	0.19
FeO	8.80	8.23	8.33	9.75	8.37	7.50	9.15	9.06	3.58	7.55	8.24	7.97	7.26	8.17	8.79
MnO	<0.15	<0.15	<0.15	<0.15	0.16	<0.15	<0.15	0.16	<0.15	<0.15	<0.15	<0.15	0.18	0.23	0.15
MgO	15.71	15.53	15.71	14.96	14.33	16.65	15.33	15.99	18.54	15.92	15.84	15.63	15.55	14.89	15.15
CaO	20.19	20.61	20.41	20.09	21.24	20.26	20.41	20.09	21.77	20.66	20.17	21.22	20.89	21.43	21.25
Na_2O	<0.15	<0.15	<0.15	<0.15	<0.15	<0.15	<0.15	<0.15	<0.15	<0.15	<0.15	<0.15	<0.15	<0.15	<0.15
K_2O	<0.15	<0.15	<0.15	<0.15	<0.15	<0.15	<0.15	<0.15	<0.15	<0.15	<0.15	<0.15	<0.15	<0.15	<0.15
H_2O	<0.15	<0.15	<0.15	<0.15	<0.15	<0.15	<0.15	<0.15	<0.15	<0.15	<0.15	<0.15	<0.15	<0.15	<0.15
Si	1.939	1.927	1.931	1.925	1.908	1.939	1.939	1.962	1.960	1.925	1.926	1.946	1.911	1.937	1.957
Al^4	0.061	0.073	0.069	0.075	0.092	0.061	0.061	0.038	0.040	0.075	0.074	0.054	0.089	0.063	0.043
Σ	2.000	2.000	2.000	2.000	2.000	2.000	2.000	2.000	2.000	2.000	2.000	2.000	2.000	2.000	2.000
Al^8	0.042	0.030	0.028	0.045	0.013	0.036	0.046	0.020	0.018	0.021	0.022	0.014	0.019	0.013	0.020
Ti	0.007	0.006	0.006	0.009	0.008	0.005	0.006	0.006	0	0.007	0.006	0.008	0.010	0.006	0.006
Fe^3	0	0.020	0.017	0.003	0.048	0.006	0	0.001	0	0.030	0.031	0.018	0.041	0.030	0.005
Cr	0.009	0.012	0.012	0.009	0.014	0.008	0.006	0.006	0.0230	0.010	0.008	0.006	0.009	0.008	0.004
Mg	0.866	0.858	0.868	0.829	0.799	0.914	0.848	0.884	1.003	0.879	0.876	0.864	0.860	0.827	0.839
Fe^2	0.273	0.255	0.258	0.303	0.262	0.231	0.284	0.281	0.109	0.234	0.255	0.247	0.225	0.254	0.273
Mn	0	0	0	0	0.005	0	0	0.005	0	0	0	0	0.006	0.007	0.005
Ca	0.801	0.819	0.811	0.801	0.851	0.799	0.811	0.798	0.847	0.820	0.801	0.843	0.83	0.855	0.846
Na	0	0	0	0	0	0	0	0	0	0	0	0	0	0	0
K	0	0	0	0	0	0	0	0	0	0	0	0	0	0	0
Σ	1.998	2.000	2.000	2.000	2.000	2.000	1.999	2.000	2.000	2.000	2.000	2.000	2.000	2.000	2.000
Mg*	0.76	0.77	0.77	0.73	0.75	0.80	0.75	0.76	0.90	0.79	0.77	0.78	0.79	0.77	0.75

deposits; similar but eroded gravel beds flank the Tertiary conglomerates forming the high ground below Mt Sorell and may have once formed scree slopes derived from the Tertiary conglomerate unit, Tsg. Swamp-covered alluvium (Qra) floors the shallow valley of the Braddon River and tributaries, and terraces on the southern side of the Braddon River and in the region of Lignite Creek are interpreted as capped by undivided Quaternary deposits.

The Quaternary gravels at the 315 m level (between CP700200, CP700213, CP764200 and CP764204) cap the southern extension of the Henty Surface of Gregory (1903). At low altitudes (≈100 m) in the Braddon River region, Quaternary gravels cap small mesas formed of unit Tss. These latter gravels resemble the pebbly conglomerates of the Tertiary unit Tsg; the pebbles are of quartz and quartzite and are commonly framework-supported in an unconsolidated coarse sandy matrix. As they crop out at lower altitudes than the base of unit Tsg and lie on flat erosion surfaces and terraces adjacent to the present streams in the Braddon River region, they are thought to be of Quaternary–Recent age.

IGNEOUS ROCKS

M. P. McClenaghan

Cambrian (?) rocks

Pyroxene and feldspar phyric andesite and breccia (Ꞓal)

Unit Cal is found in the area centred on CP690010 where it is exposed best on the old BHP tracks and in the upper parts of Briggs and Henrietta Creeks. It is flanked to the north and south by quartz and feldspar rhyolite porphyries (Ꞓtr) and is faulted against mudstone / lithicwacke sequences (Ꞓtl) to the east and west.

In outcrop the rock is fine grained and purple-grey or green-grey depending on its weathering. It often contains small feldspar phenocrysts and in many areas consists of an angular breccia with fragments ranging up to 100 mm in length [e.g. at CN690996]. These may be autoclastic flow breccias; in other areas the rock is massively bedded. Cleavage is not evident.

In thin section the rocks are generally fine grained with phenocrysts of plagioclase and euhedral augite (table 7). The plagioclase is more abundant than the augite and is extensively altered to sericite. Some pyroxenes are altered to chlorite whereas others are entirely replaced by epidote, chlorite and actinolite. The matrix generally consists of thin laths of plagioclase, chlorite and fine opaque grains and often appears dark. The matrix feldspar is almost entirely altered to sericite. In some specimens pyroxene grains are also present in the matrix. Veins consisting of chlorite, carbonate and epidote are common. Some specimens contain lava lapilli (up to 20 mm) and plagioclase and quartz crystals. Others contain very fine-grained fragments which may be devitrified glass shards.

Gabbro intrusives (Ꞓg)

Gabbro occurs as various small bodies associated with different units throughout the map sheet and it is probable that they represent different phases of intrusion. They are all tentatively assumed to be of Cambrian age.

One probable phase of intrusion consists of elongated fault-bound blocks present in the Point Hibbs Mélange Belt, which trend south-west from the Asbestos Point area and are in faulted contact with bodies of serpentinised pyroxenite (Ꞓsp), mudstone/ lithicwacke (Ꞓtl) sequences and various minor igneous units. These gabbroic rocks are generally poorly exposed with the best outcrops occurring on the coast near Asbestos Point and on the old BHP tracks inland.

In outcrop the gabbro is massive, coarse grained, green-grey and is rarely fresh. Minor fractures are evident but cleavage is not developed.

In thin section the gabbro shows varying degrees of alteration. The least altered rocks (Ꞓgh) consist of coarse-grained plagioclase, orthopyroxene and clinopyroxene. The plagioclase ranges in composition from andesine to bytownite. The clinopyroxene ranges in composition from diopside to augite and the orthopyroxene is bronzite or hypersthene (table 8, fig. 7).

In the more altered rocks the plagioclase is generally cloudy and altered to sericite but in some cases it is altered to a fine-grained high relief, isotropic or almost isotropic mineral which gives it a dark appearance. This may be grossular garnet. The orthopyroxene is more prone to alteration than the clinopyroxene and is often completely altered although in association with mainly unaltered clinopyroxene. The orthopyroxene alteration is progressive. The first alteration product is talc followed by tremolite with a small cummingtonite component and then this is replaced by chlorite. In the more altered samples patches of fibrous tremolite partly altered to chlorite or patches entirely of chlorite indicate the former presence of orthopyroxene. Rocks with the orthopyroxene pseudomorphed in this way

Table 8. PYROXENE COMPOSITIONS FROM GABBRO BODIES (€g) IN THE POINT HIBBS MÉLANGE BELT

	MH520_2/1	MH520_7/1	MH520_1/1	MH520_3/1	MH520_4/1	MH205_1/1	MH205_1/2	MH205_2/1	MH205_3/1
SiO_2	54.54	54.88	53.78	53.69	54.73	55.00	55.09	54.58	54.30
TiO_2	<0.15	<0.15	<0.15	<0.15	<0.15	<0.15	<0.15	<0.15	<0.15
Al_2O_3	1.10	0.85	1.56	2.75	1.24	0.41	0.10	0.18	0.32
Cr_2O_3	<0.15	<0.15	0.33	0.32	0.45	0.34	0.84	0.40	0.33
Fe_2O_3	0.93	0.56	<0.15	<0.15	<0.15	<0.15	<0.15	<0.15	<0.15
FeO	14.25	14.43	6.25	7.75	6.70	1.93	1.47	1.80	3.45
MnO	0.35	0.32	<0.15	<0.15	<0.15	<0.15	<0.15	<0.15	<0.15
MgO	27.28	27.52	16.25	17.41	17.92	16.82	16.97	17.08	16.13
CaO	1.56	1.43	21.83	18.08	18.96	25.5	25.53	25.96	25.47
Na_2O	<0.15	<0.15	<0.15	<0.15	<0.15	<0.15	<0.15	<0.15	<0.15
K_2O	<0.15	<0.15	<0.15	<0.15	<0.15	<0.15	<0.15	<0.15	<0.15
H_2O	<0.15	<0.15	<0.15	<0.15	<0.15	<0.15	<0.15	<0.15	<0.15
Si	1.964	1.974	1.973	1.959	1.993	1.998	2.001	1.988	1.989
Al^4	0.036	0.026	0.027	0.041	0.007	0.002	0	0.008	0.011
Σ	2.000	2.000	2.000	2.000	2.000	2.000	2.001	1.996	2.000
Al^8	0.011	0.01	0.04	0.078	0.046	0.016	0.004	0	0.003
Ti	0	0	0	0	0	0	0	0	0
Fe^3	0.025	0.015	0	0	0	0	0	0	0
Cr	0	0	0.01	0.009	0.013	0.01	0.024	0.011	0.009
Mg	1.464	1.475	0.888	0.947	0.972	0.911	0.918	0.927	0.881
Fe^2	0.429	0.434	0.192	0.236	0.204	0.059	0.045	0.055	0.106
Mn	0.011	0.010	0	0	0	0	0	0	0
Ca	0.060	0.055	0.858	0.707	0.74	0.993	0.994	1.013	1.000
Na	0	0	0	0	0	0	0	0	0
K	0	0	0	0	0	0	0	0	0
Σ	2.000	2.000	1.988	1.977	1.974	1.988	1.985	2.007	1.999
Mg*	0.77	0.77	0.82	0.80	0.83	0.94	0.95	0.94	0.89

	MH205_4/1	MH204_3/1	MH204_4/1	MH204_5/1	MH204_1/1	MH40_2/1	MH40_3/1	MH40_3/2
SiO_2	54.23	51.94	52.65	52.10	51.68	52.9	52.74	53.26
TiO_2	<0.15	0.15	0.28	0.17	0.26	<0.15	<0.15	<0.15
Al_2O_3	0.76	2.01	1.66	1.90	2.10	1.67	2.03	1.86
Cr_2O_3	0.36	0.52	<0.15	0.53	0.58	0.36	0.29	0.35
Fe_2O_3	<0.15	0.74	0.28	1.40	1.12	0.05	0.24	<0.15
FeO	5.37	7.78	8.00	7.23	7.12	6.94	8.36	6.99
MnO	<0.15	<0.15	0.25	0.18	0.16	0.21	0.25	<0.15
MgO	15.73	14.43	15.35	15.45	14.70	15.11	16.40	15.66
CaO	23.56	22.43	21.54	20.89	22.28	22.77	19.68	21.88
Na_2O	<0.15	<0.15	<0.15	0.16	<0.15	<0.15	<0.15	<0.15
K_2O	<0.15	<0.15	<0.15	<0.15	<0.15	<0.15	<0.15	<0.15
H_2O	<0.15	<0.15	<0.15	<0.15	<0.15	<0.15	<0.15	<0.15
Si	1.991	1.934	1.952	1.932	1.923	1.958	1.948	1.962
Al^4	0.009	0.066	0.048	0.068	0.077	0.042	0.052	0.038
Σ	2.000	2.000	2.000	2.000	2.000	2.000	2.000	2.000
Al^8	0.024	0.022	0.025	0.015	0.014	0.031	0.037	0.043
Ti	0	0.004	0.008	0.005	0.007	0	0	0
Fe^3	0	0.021	0.008	0.039	0.031	0.001	0.007	0
Cr	0.010	0.015	0	0.016	0.017	0.011	0.008	0.010
Mg	0.861	0.801	0.848	0.854	0.815	0.833	0.903	0.860
Fe^2	0.165	0.242	0.248	0.224	0.222	0.215	0.258	0.215
Mn	0	0	0.008	0.006	0.005	0.007	0.008	0
Ca	0.927	0.895	0.856	0.83	0.888	0.903	0.779	0.864
Na	0	0	0	0.011	0	0	0	0
K	0	0	0	0	0	0	0	0
Σ	1.987	2.000	2.000	2.000	2.000	2.000	2.000	1.992

Mg*	0.84	0.77	0.77	0.79	0.79	0.79	0.78	0.80

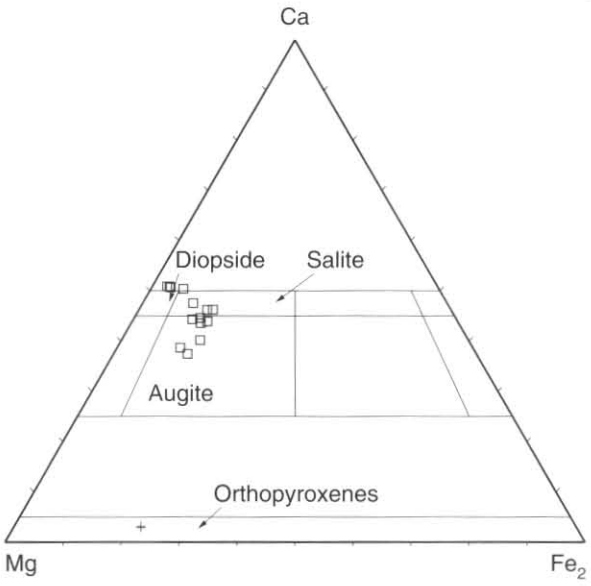

Figure 7. Pyroxene compositions from gabbro (€g) in the Point Hibbs Mélange Belt

are indicated on the map by the symbol €gp. The clinopyroxene shows alteration to actinolite.

Some samples contain actinolite without the chlorite patches and these may have been derived from rock with only clinopyroxene. Minor epidote is also present in some samples.

A number of small bodies of gabbro occur intruding the Precambrian rocks in the southern or Nielson River area and may be part of the same phase of intrusion as they have a similar petrographic character. Most of the intrusions are dyke shaped and are steep with a NNE trend. One body, however, exposed in the banks of the Nielson River at CP613007, is sill shaped. The intrusions are coarse-grained dark grey-green rock with the body at CP669081 on the eastern coast having a fine-grained, chilled contact with the country rock. They generally have a massive apparently unfoliated appearance in contrast with the highly tectonised country rock though the dyke at CP611010 had a poorly developed foliation.

In thin section they generally consist of plagioclase, clinopyroxene and opaque grains. The plagioclase is very cloudy and dark due to extreme alteration and the pyroxene is augite (see table 9, fig. 8) and is extensively altered to

Table 9. PYROXENE COMPOSITIONS FROM GABBRO (€g) SAMPLES MH314 AND MH333

	MH314_1/1	MH314_3/1	MH314_4/1	MH314_6/1	MH314_2/1	MH314_6/1	MH333_7/1	MH333_4/1
SiO_2	53.21	52.95	52.96	52.50	52.80	52.58	48.53	47.44
TiO_2	0.31	0.31	0.21	0.42	0.48	0.67	1.08	1.24
Al_2O_3	1.94	2.33	2.14	2.70	2.44	2.18	4.59	5.10
Cr_2O_3	0.48	1.01	0.82	0.60	0.27	<0.15	<0.15	<0.15
Fe_2O_3	<0.15	<0.15	<0.15	0.10	<0.15	<0.15	2.14	4.68
FeO	4.90	4.86	5.47	5.23	5.64	7.67	9.79	7.78
MnO	<0.15	<0.15	0.18	<0.15	<0.15	<0.15	<0.15	<0.15
MgO	17.21	16.96	16.59	17.31	16.89	16.40	11.55	11.05
CaO	21.94	21.59	21.62	21.13	21.49	20.50	22.34	22.34
Na_2O	<0.15	<0.15	<0.15	<0.15	<0.15	<0.15	<0.15	0.37
K_2O	<0.15	<0.15	<0.15	<0.15	<0.15	<0.15	<0.15	<0.15
H_2O	<0.15	<0.15	<0.15	<0.15	<0.15	<0.15	<0.15	<0.15
Si	1.945	1.935	1.942	1.920	1.933	1.937	1.837	1.798
Al^4	0.055	0.065	0.058	0.080	0.067	0.063	0.163	0.202
Σ	2.000	2.000	2.000	2.000	2.000	2.000	2.000	2.000
Al^8	0.029	0.036	0.035	0.037	0.039	0.032	0.041	0.026
Ti	0.009	0.009	0.006	0.012	0.013	0.018	0.031	0.035
Fe^3	0	0	0	0.003	0	0	0.061	0.133
Cr	0.014	0.029	0.024	0.017	0.008	0	0	0
Mg	0.937	0.924	0.907	0.943	0.922	0.900	0.651	0.624
Fe^2	0.150	0.148	0.168	0.160	0.173	0.236	0.310	0.247
Mn	0	0	0.006	0	0	0	0	0
Ca	0.859	0.845	0.849	0.828	0.843	0.809	0.906	0.907
Na	0	0	0	0	0	0	0	0.027
K	0	0	0	0	0	0	0	0
Σ	1.998	1.991	1.994	2.000	1.997	1.997	2.000	2.000
Mg*	0.87	0.86	0.84	0.85	0.84	0.79	0.68	0.72

chlorite and actinolite. The opaque grains are ilmenite partly altered to sphene and leucoxene. Minor amounts of pyrite are also present. The intrusion at CN564942 on the west coast also contains epidote as patches and veins.

A number of gabbro bodies occur in the Timbertops area and one at CN683970 forms an approximately oval stock like body and is contiguous with probable andesite extrusives and intrusives (€ta), and with quartz and feldspar rhyolite porphyries (€tr).

In thin section it is coarse grained and consists of plagioclase, subophitic clinopyroxene and opaque grains. The plagioclase is cloudy with alteration to sericite and the clinopyroxene is partly altered to actinolite and chlorite.

Additional small gabbro intrusions in the northern or Albina Creek area intrude presumed Cambrian rocks. The small bodies in the Double Cove area and the body near Albina Creek at CP575055 are closely associated with basalt lavas (€ab) of that area and so are probably comagmatic with them. The gabbro is coarse grained dark green-grey. In Double Cove at CP625114 intrusive contacts of one of the bodies can be clearly seen. Another small body of gabbro occurs intruding the siltstone (€ac) at CP640077.

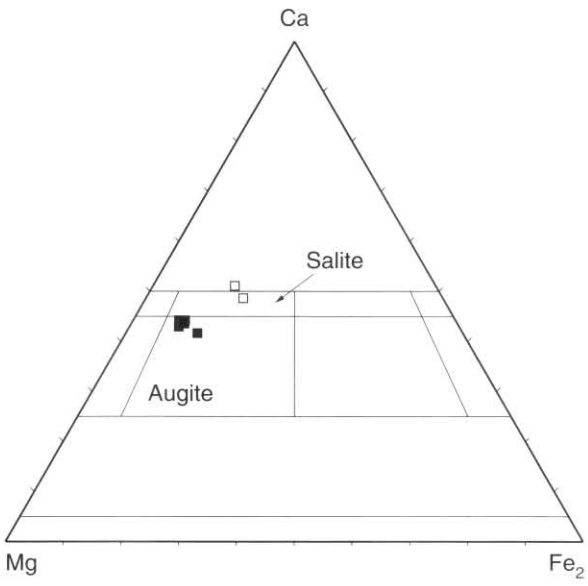

Figure 8. Plot of pyroxene compositions from a gabbro bodies at CP613016 in the Nielson River (MH314, ■) and at CP640077 (MH333, □).

In thin section the various gabbro bodies are very similar consisting of cloudy very altered plagioclase, ophitic clinopyroxene and opaque grains. The pyroxene of one (MH333) is salite (see table 9 and fig. 8) and is partly altered to actinolite and chlorite. Minor quantities of epidote and sphene are present in some samples.

Tonalite/quartz gabbro (€x)

Rocks of this unit occur in two small areas in the Point Hibbs Mélange Belt. The outcrops at CN657987 are assumed to be in faulted contact with the surrounding sheared serpentinite (€ss) whereas those at CN659977 occur at the southern end of an elongated block of gabbro (€g) and are assumed to be faulted against a highly sheared rock unit composed mainly of chlorite and quartz (€tc).

In outcrop the rock type is coarse grained with a medium dark green/grey colour and is very similar to the gabbro (€g).

In thin section a sample from the southern of the two bodies is coarse grained and has a primary mineralogy of plagioclase, clinopyroxene, quartz and opaques. The plagioclase has extensive cloudy alteration and the clinopyroxene is partly altered to chlorite and actinolite. Quartz, which forms about 10% of the rock, is intergranular to the other minerals and encloses smaller crystals of plagioclase. The opaque grains are large and sparse with one enclosing small laths of plagioclase. Micro probe analysis show that they are ilmenite. Another sample from the same body has a similar coarse-grained texture and consists of quartz, plagioclase, actinolite, chlorite and opaques. The plagioclase has abundant small inclusions of chlorite. Quartz is more abundant than in the previous sample and forms about 40% of the rock. It encloses small laths of plagioclase and crystals of actinolite and chlorite.

Samples from the other body are very similar in texture and mineralogy. One sample contains plagioclase with extensive cloudy alteration but still retaining signs of zoning. Clinopyroxene in the same sample is partly altered to actinolite and chlorite. In a more altered sample clinopyroxene has been entirely replaced by actinolite and chlorite and epidote is present as granular patches, replacing some of the plagioclase, and also as veins. Quartz is intergranular and ranges from 15% to 20% of the rock.

Table 10. SPINEL COMPOSITIONS FROM SERPENTINISED PYROXENITE (€sp, €ss)

	MH15 _2/2	MH15 _1/2	MH15 _1/1	MH15 _2/1	MH230 _3/1	MH228 _3/1	MH230 _3/2	MH218 _1/3	MH218 _1/1	MH218 _3/1	MH218 _2/1	MH218 _1/4	MH218 _3/2
SiO_2	<0.15	<0.15	<0.15	<0.15	<0.15	<0.15	<0.15	<0.15	0.36	<0.15	<0.15	<0.15	<0.15
TiO_2	<0.15	0.22	<0.15	<0.15	<0.15	0.21	<0.15	<0.15	<0.15	<0.15	0.21	<0.15	<0.15
Al_2O_3	3.98	3.52	3.64	3.60	10.72	7.31	11.75	17.02	16.65	17.15	17.73	17.30	17.33
Cr_2O_3	67.49	67.41	67.40	67.16	58.59	57.69	55.97	50.49	50.40	50.16	50.13	50.03	49.97
Fe_2O_3	0.25	0.80	0.91	1.06	2.75	4.02	4.82	3.16	3.58	3.42	2.69	3.32	3.22
FeO	19.90	19.44	19.39	19.75	17.00	26.21	15.40	19.16	18.33	18.95	18.67	19.15	19.51
MnO	<0.15	<0.15	<0.15	<0.15	<0.15	<0.15	<0.15	<0.15	<0.15	<0.15	<0.15	<0.15	<0.15
MgO	8.37	8.62	8.66	8.42	10.93	4.55	12.07	10.17	10.69	10.31	10.56	10.21	9.97
CaO	<0.15	<0.15	<0.15	<0.15	<0.15	<0.15	<0.15	<0.15	<0.15	<0.15	<0.15	<0.15	<0.15
Na_2O	<0.15	<0.15	<0.15	<0.15	<0.15	<0.15	<0.15	<0.15	<0.15	<0.15	<0.15	<0.15	<0.15
K_2O	<0.15	<0.15	<0.15	<0.15	<0.15	<0.15	<0.15	<0.15	<0.15	<0.15	<0.15	<0.15	<0.15
H_2O	<0.15	<0.15	<0.15	<0.15	<0.15	<0.15	<0.15	<0.15	<0.15	<0.15	<0.15	<0.15	<0.15
Si	0	0	0	0	0	0	0	0	0.092	0	0	0	0
Ti	0	0.045	0	0	0	0.044	0	0	0	0	0.040	0	0
Al	1.290	1.139	1.180	1.169	3.314	2.403	3.590	5.150	5.023	5.180	5.333	5.225	5.242
Fe^3	0.052	0.165	0.187	0.220	0.543	0.843	0.941	0.610	0.689	0.660	0.516	0.641	0.621
Cr	14.650	14.650	14.630	14.610	12.140	12.710	11.460	10.240	10.190	10.160	10.110	10.130	10.130
Σ	16.000	16.000	16.000	16.000	16.000	16.000	16.000	16.000	16.000	16.000	16.000	16.000	16.000
Fe^2	4.572	4.469	4.454	4.546	3.728	6.109	3.338	4.112	3.924	4.061	3.984	4.103	4.187
Mn	0	0	0	0	0	0	0	0	0	0	0	0	0
Mg	3.428	3.531	3.546	3.454	4.272	1.891	4.662	3.888	4.076	3.939	4.016	3.897	3.813
Ca	0	0	0	0	0	0	0	0	0	0	0	0	0
Na	0	0	0	0	0	0	0	0	0	0	0	0	0
K	0	0	0	0	0	0	0	0	0	0	0	0	0
Σ	8.000	8.000	8.000	8.000	8.000	8.000	8.000	8.000	8.000	8.000	8.000	8.000	8.000
Mg*	0.42	0.44	0.44	0.43	0.53	0.23	0.58	0.48	0.50	0.49	0.50	0.48.	0.47
Cr*	0.91	0.92	0.92	0.92	0.78	0.84	0.76	0.66	0.66	0.66.	0.65	0.65	0.65

	MH7 _1/2	MH218 _2/2	MH7 _1/1	MH208 _1/1	MH208 _2/2	MH208 _1/2	MH208 _2/1	MH208 _4/1	MH208 _3/2	MH207 _5/1	MH214 _4/1	MH208 _3/1
SiO_2	<0.15	<0.15	<0.15	<0.15	<0.15	<0.15	<0.15	<0.15	<0.15	<0.15	<0.15	2.70
TiO_2	<0.15	<0.15	<0.15	<0.15	<0.15	<0.15	<0.15	0.26	0.25	0.10	<0.15	<0.15
Al_2O_3	19.91	17.63	19.91	16.31	16.46	16.38	16.32	16.74	16.49	23.45	23.68	11.47
Cr_2O_3	49.88	49.83	49.46	49.36	49.31	49.15	48.68	48.60	48.47	44.14	42.21	37.26
Fe_2O_3	1.57	3.22	2.14	4.46	4.26	4.58	5.10	4.64	4.99	3.43	4.98	18.60
FeO	16.28	18.93	15.83	20.95	21.18	21.02	21.06	20.52	20.76	15.99	16.42	22.21
MnO	<0.15	<0.15	<0.15	<0.15	<0.15	<0.15	<0.15	<0.15	<0.15	<0.15	0.26	0.47
MgO	12.37	10.38	12.65	8.91	8.78	8.87	8.84	9.24	9.05	12.90	12.46	7.29
CaO	<0.15	<0.15	<0.15	<0.15	<0.15	<0.15	<0.15	<0.15	<0.15	<0.15	<0.15	<0.15
Na_2O	<0.15	<0.15	<0.15	<0.15	<0.15	<0.15	<0.15	<0.15	<0.15	<0.15	<0.15	<0.15
K_2O	<0.15	<0.15	<0.15	<0.15	<0.15	<0.15	<0.15	<0.15	<0.15	<0.15	<0.15	<0.15
H_2O	<0.15	<0.15	<0.15	<0.15	<0.15	<0.15	<0.15	<0.15	<0.15	<0.15	<0.15	<0.15
Si	0	0	0	0	0	0	0	0	0	0	0	0.723
Ti	0	0	0	0	0	0	0	0.051	0.048	0.018	0	0
Al	5.859	5.313	5.851	4.994	5.041	5.015	5.001	5.107	5.042	6.785	6.869	3.626
Fe^3	0.295	0.620	0.402	0.871	0.834	0.895	0.998	0.903	0.974	0.633	0.922	3.752
Cr	9.846	10.060	9.747	10.130	10.120	10.090	10.000	9.939	9.936	8.564	8.209	7.898
Σ	16.000	16.000	16.000	16.000	16.000	16.000	16.000	16.000	16.000	16.000	16.000	16.000
Fe^2	3.398	4.047	3.301	4.551	4.600	4.566	4.578	4.439	4.502	3.281	3.378	4.981
Mn	0	0	0	0	0	0	0	0	0	0	0.053	0.107
Mg	4.602	3.953	4.699	3.449	3.400	3.434	3.422	3.561	3.498	4.719	4.569	2.912
Ca	0	0	0	0	0	0	0	0	0	0	0	0
Na	0	0	0	0	0	0	0	0	0	0	0	0
K	0	0	0	0	0	0	0	0	0	0	0	0
Σ	8.000	8.000	8.000	8.000	8.000	8.000	8.000	8.000	8.000	8.000	8.000	8.000
Mg*	0.57	0.49	0.58	0.43	0.42	0.42	0.42	0.44	0.43	0.58	0. 57	0.36
Cr*	0.62	0.65	0.62	0.66	0.66	0.66	0.66	0.66	0.66	0.55	0.54	0.68

Rocks from these two bodies though considerably altered retain much of their original igneous texture.

Quartz-epidote-chlorite rock (€q)

A small body of this rock unit occurs at CP684025 in the Point Hibbs Mélange Belt and is surrounded by gabbro (€g).

In outcrop it is a coarse grained, massive, medium-dark grey rock which weathers to a rusty gritty material.

In thin section it is a coarse grained and consists of a granular mass of quartz, epidote, chlorite and opaques. Quartz forms 60% to 70% of the rock and the other major original mineralogy has been replaced by the epidote and chlorite. The opaques are leucoxene after ilmenite.

It seems probable that this rock type has been produced by the extreme alteration of the tonalite (€x) rock type.

Felsic intrusions (?) of rhyolite chemical composition (€ri, €rip)

Two bodies of light coloured fine- to medium-grained igneous rock occur in the northern part of the Timbertops area at CN677965 and CN688970. These bodies lie within the area of the intermediate probable extrusives and intrusives of andesite chemical composition (€ta) and have been described as stock-like bodies (White, 1975). Their relationship to the surrounding rocks is unclear and they are petrographically and chemically very similar to the nearby quartz and feldspar felsic porphyries of rhyolite chemical composition.

In thin section the larger body (€ri) centred on CN688970 is fine- to medium-grained, consisting of a mass of thin plagioclase laths, quartz, chlorite and opaque grains. The plagioclase is cloudy with abundant small sericite inclusions. In some samples it shows flow alignment. The other body (€rip) at CN677965 consists of a fine-grained granular mass of plagioclase, quartz and chlorite with corroded and embayed phenocrysts of quartz, and glomerophyric patches of plagioclase. Small lath shaped phenocrysts of biotite, largely altered to chlorite and fine opaque grains, are also present. The plagioclase is extensively altered to sericite

Schistose possible tuff or lava (€tc)

Rocks of this unit occur as a number of elongate blocks in the Point Hibbs Mélange Belt and are assumed to be faulted against the other rock types of the belt. Due to the highly

Table 11. PYROXENE COMPOSITIONS FROM THE PYROXENITES (Csp) OF THE POINT HIBBS MÉLANGE BELT

	MH207 _1/1	MH207 _2/1	MH207 _5/2	MH228 _2/1	MH228 _1/1	MH228 _2/2	MH214 _1/1	MH214 _1/3	MH214 _2/1	MH214 _3/1
SiO_2	56.1	56.51	56.93	56.07	55.91	54.28	53.06	53.16	53.18	52.88
TiO_2	<0.15	<0.15	<0.15	<0.15	<0.15	<0.15	<0.15	<0.15	<0.15	<0.15
Al_2O_3	1.80	1.75	1.51	0.28	0.18	0.22	2.08	1.90	1.77	1.67
Cr_2O_3	0.65	0.58	0.50	0.16	0.11	0.62	1.42	1.32	1.14	1.19
Fe_2O_3	0.71	0.23	<0.15	0.27	0.17	<0.15	0.26	0.35	0.72	1.37
FeO	5.50	5.72	6.05	11.57	11.86	6.43	2.000	1.87	1.49	1.35
MnO	<0.15	<0.15	<0.15	0.16	0.14	0.20	<0.15	<0.15	<0.15	<0.15
MgO	32.78	33.42	34.28	31.30	31.42	20.82	17.33	17.25	17.29	18.45
CaO	2.47	1.79	0.72	0.19	0.20	17.42	23.85	24.15	24.41	23.10
Na_2O	<0.15	<0.15	<0.15	<0.15	<0.15	<0.15	<0.15	<0.15	<0.15	<0.15
K_2O	<0.15	<0.15	<0.15	<0.15	<0.15	<0.15	<0.15	<0.15	<0.15	<0.15
H_2O	<0.15	<0.15	<0.15	<0.15	<0.15	<0.15	<0.15	<0.15	<0.15	<0.15
Si	1.945	1.953	1.962	1.981	1.979	1.974	1.931	1.935	1.936	1.922
Al^4	0.055	0.047	0.038	0.012	0.008	0.010	0.069	0.065	0.064	0.072
Σ	2.000	2.000	2.000	1.993	1.986	1.984	2.000	2.000	2.000	1.994
Al^8	0.019	0.025	0.024	0	0	0	0.021	0.017	0.012	0
Ti	0	0	0	0	0	0	0	0	0	0
Fe^3	0.018	0.006	0	0.007	0.004	0	0.007	0.010	0.020	0.037
Cr	0.018	0.016	0.014	0.004	0.003	0.018	0.041	0.038	0.033	0.034
Mg	1.694	1.721	1.761	1.649	1.657	1.129	0.940	0.936	0.938	1.000
Fe^2	0.159	0.165	0.175	0.342	0.351	0.196	0.061	0.057	0.045	0.041
Mn	0	0	0	0.005	0.004	0.006	0	0	0	0
Ca	0.092	0.066	0.027	0.007	0.008	0.679	0.930	0.942	0.952	0.900
Na	0	0	0	0	0	0	0	0	0	0
K	0	0	0	0	0	0	0	0	0	0
Σ	2.000	2.000	2.000	2.014	2.028	2.028	2.000	2.000	2.000	2.012
Mg*	91.41	91.25	90.96	82.82	82.51	85.20	93.90	94.25	95.42	96.06

Table 12. AMPHIBOLE COMPOSITIONS FROM MH6B AND GARNET COMPOSITIONS FROM MH34

	amphiboles							garnet		
	MH6B_1/2	MH6B_1/4	MH6B_1/3	MH6B_2/3	MH6B_4/1	MH6B_4/3		MH34_1/1	MH34_2/1	MH34_3/1
SiO_2	53.52	51.61	48.31	47.64	48.53	47.29	SiO_2	38.66	38.72	38.58
TiO_2	<0.15	0.36	0.43	1.30	1.44	1.58	TiO_2	<0.15	<0.15	<0.15
Al_2O_3	3.93	3.82	6.97	7.85	6.82	7.49	Al_2O_3	23.57	23.49	24.66
Cr_2O_3	<0.15	<0.15	<0.15	<0.15	<0.15	<0.15	Cr_2O_3	0.33	0.33	0.36
Fe_2O_3	1.34	4.70	9.92	8.54	8.67	8.39	Fe_2O_3	<0.15	<0.15	<0.15
FeO	8.80	6.72	3.39	6.07	5.29	6.32	FeO	0.34	0.35	0.48
MnO	2.82	3.78	1.34	<0.15	0.21	<0.15	MnO	2.51	2.51	2.11
MgO	15.46	15.15	16.67	14.10	14.9	14.26	MgO	<0.15	<0.15	<0.15
CaO	11.46	11.10	10.03	10.77	10.71	11.10	CaO	34.59	34.60	33.81
Na_2O	0.42	0.48	0.61	1.48	1.17	1.34	Na_2O	<0.15	<0.15	<0.15
K_2O	0.15	0.19	0.23	0.15	0.16	0.17	K_2O	<0.15	<0.15	<0.15
H_2O	2.10	2.08	2.10	2.08	2.09	2.08	H_2O	<0.15	<0.15	<0.15
Si	7.642	7.432	6.898	6.851	6.95	6.82	Si	5.841	5.849	5.802
Al^4	0.358	0.568	1.102	1.149	1.050	1.180	Ti	0	0	0
Σ	8.000	8.000	8.000	8.000	8.000	8.000	Al	4.197	4.184	4.371
Al^8	0.303	0.081	0.071	0.181	0.102	0.092	Fe^3	0	0	0
Ti	0	0.039	0.046	0.144	0.155	0.171	Cr	0.040	0.040	0.042
Fe^3	0.144	0.509	1.066	0.924	0.935	0.910	Fe^2	0.043	0.045	0.061
Cr	0	0	0	0	0	0	Mn	0.321	0.321	0.269
Fe^2	1.051	0.809	0.404	0.730	0.634	0.762	Mg	0	0	0
Mn	0.341	0.462	0.162	0	0.026	0	Ca	5.599	5.600	5.447
Mg	3.291	3.252	3.548	3.022	3.180	3.064	Na	0	0	0
Σ	5.130	5.152	5.297	5.000	5.031	5.000	K	0	0	0
EXM	0.130	0.152	0.297	0	0.031	0	OH	0	0	0
Ca	1.753	1.713	1.534	1.659	1.643	1.715	Σ	16.040	16.030	15.990
NAM	0.117	0.135	0.169	0.341	0.326	0.285				
Σ	1.870	1.848	1.703	2.000	1.969	2.000				
NAA	0.117	0.135	0.169	0.412	0.326	0.374				
K	0.028	0.036	0.042	0.028	0.030	0.031				
Σ	0.028	0.036	0.042	0.099	0.030	0.120				
OH	2.000	2.000	2.000	2.000	2.000	2.000				
Mg*	0.76	0.80	0.90	0.81	0.83	0.80				

tectonised and altered state of the rocks, identification of the original rock type is difficult.

In thin section rocks of this unit are strongly foliated and generally consist of varying proportions of chlorite and quartz with minor opaques. At CN660975 a less altered, fine-grained sample (MH501) was obtained which consists of abundant cloudy plagioclase laths with intergranular chlorite and opaques. The opaques occur as fine grains and irregular shaped patches. This rock is probably a highly altered basalt.

Fine-grained units of andesite and rhyolite chemical composition (Cti)

Rocks of this type occur in three areas in the Point Hibbs Mélange Belt and are assumed to be faulted against the neighbouring units. At CP702066 the rock is generally highly sheared and contains blocks of unsheared fine-grained light grey-green material. At the other two areas, CP694045 and CP680013, the rock has a similar character to the unsheared material.

In thin section the rock generally consists of a fine- to medium-grained mass of plagioclase laths with intergranular chlorite, quartz and opaques. Some samples have sparse plagioclase phenocrysts and sparse biotite phenocrysts partly altered to chlorite may be present. Patches of secondary carbonate are common. The chlorite is associated with fine grains of actinolite in some samples.

Serpentinised pyroxenite (Csp)

Rocks of this type occur in fault-bounded, elongate blocks in the Point Hibbs Mélange Belt which trends south-west from Asbestos Point to Point Hibbs.

Plate 13. Igneous layering in serpentinite (Ɛss) at CP676007.

In some areas unit Ɛsp is massive and coarse-grained (e.g. near the upper part of Hills Creek, CN650960) but elsewhere it is generally fine-grained and highly tectonised with an anastomosing foliation approximately parallel to the trend of the blocks and is marked as Ɛss. The colour varies from pale to dark green. Igneous layering (plate 13) is present in a small area of massive serpentinite at CP676007. Massive small (<1 m) blocks of gabbro are present in strongly foliated serpentinite at Asbestos Point [CP702070] and also at CP681034.

In thin section the foliated serpentinite and also most of the more massive rock consists of serpentine minerals with minor amounts of small, dark brown or opaque grains of spinel (table 10). The spinel is generally the only original mineralogy remaining. In many cases the serpentine minerals pseudomorph the original mafic mineral whose grain size ranges up to 5 mm. In some areas e.g. at CP679027 the original mineralogy has been entirely converted to talc, chlorite and colourless amphibole (probably cummingtonite or tremolite). In the more massive rock some samples show only partial replacement of the original pyroxenes by serpentine minerals. On the basis of a very few samples the rocks were dominantly orthopyroxene with less than 5% clinopyroxene (table 11). In one sample (MH214) however, the surviving mineralogy consists entirely of diopside (fig. 9).

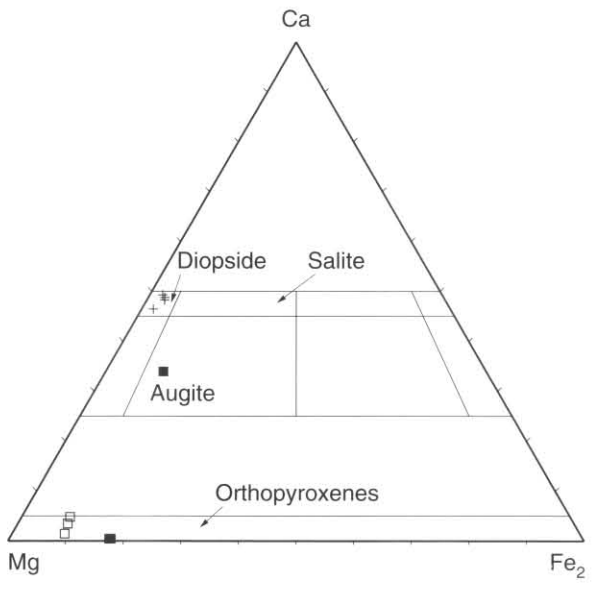

Figure 9. Pyroxene compositions from the pyroxenites (Ɛsp) of the Point Hibbs Mélange Belt. MH228 (■), MH207(□), MH214 (×).

Gabbroic blocks within the sheared serpentinite consist of fine sericite after plagioclase together with amphibole and chlorite. A sample from Asbestos Point contains pale brown hornblende (table 12) while the amphibole in a sample from CP681034 contains pale green actinolite. The later sample also contains plagioclase altered to fine sericite and grossular garnet (table 12).

Mafic dykes of high Mg chemical composition (Ɛbd)

At CP548034 on the west coast a 70 m wide, steep dyke trending north-east and consisting of a fine-grained light grey-green igneous rock intrudes dark grey mudstone of the mudstone/lithicwacke sequence (Ɛaml). Another smaller dyke of similar character is present close by. The foliation in the country rock continues through the dyke, and the margin at one point is folded parallel to the bedding. The country rock close to the dyke has been strongly hornfelsed.

In thin section the dyke rock is composed mainly of colourless amphibole and chlorite with subordinate talc (confirmed by XRD). A very small proportion of fine opaque grains are also present. The chlorite defines the foliation.

Intermediate dykes (Ɛid)

A group of fine-grained, pale grey, steep, igneous dykes intrude dark grey mudstone of the mudstone/lithicwacke sequence (Ɛaml) on the west coast near CN558999. The dykes average about 6 m thick, trend north-east, and share the same foliation as the country rock. At some places the dyke boundaries are parallel to bedding whereas elsewhere the truncate it. The margins of the dykes have a finer grain size due to chilling.

In thin section the dykes are composed of an unorientated mass of cloudy plagioclase laths with intergranular colourless chlorite, opaque grains, quartz and secondary carbonate.

Peridotite bodies (Ɛp, Ɛpd)

A small mass of coarse-grained unfoliated mafic rock (Ɛp) crops out in a creek at CN710947. Its relationship to neighbouring units is unknown.

In thin section it consists of abundant grain supported olivine crystals pseudomorphed by pale green serpentine. Intergranular clinopyroxene is mostly altered to chlorite. An opaque mineral occurs as fine secondary grains along cleavage cracks and as larger probably primary grains. The grain supported olivine crystals indicates that the rock is an accumulate.

A rock unit (Ɛpd) of very similar character also unfoliated, occurs as dyke shaped bodies on the north-west margin of the Precambrian rocks in the Nielson River area between CP608023 and CP623037. The dykes follow the faulted boundary between the Precambrian rocks and the rocks of probable Cambrian age to the north-west and so their position may have been controlled by the line of weakness provided by the fault.

In thin section the rock consists of grain supported crystals of olivine pseudomorphed by colourless serpentine. Intergranular and poikolitic clinopyroxene (chrome rich salite, see table 13) is partly altered to brown amphibole (kaersutite, see table 13) and biotite. Pale green chlorite (see table 13) is also present as intergranular patches and may have been secondary after orthopyroxene. Opaque mineral is

Table 13. MINERAL COMPOSITIONS FROM PERIDOTITE BODIES (€pd)

	amphibole			chlorite		ilmenite		pyroxene				
	MH307 _5/1	MH307 _5/2	MH368 _4/1	MH368 _3/1		MH368 _7/1		MH307 _1/1	MH307 _2/1	MH368 _3/1	MH368 _5/1	MH368 _6/1
SiO_2	42.75	42.07	44.17	32.57		<0.15	SiO_2	50.63	50.29	49.23	49.69	49.01
TiO_2	5.40	5.37	4.42	<0.15		49.11	TiO_2	1.71	1.67	1.69	1.44	2.04
Al_2O_3	11.2	11.73	10.02	16.34		<0.15	Al_2O_3	3.45	3.83	5.10	5.35	3.4
Cr_2O_3	0.14	0.19	<0.15	<0.15		0.86	Cr_2O_3	0.57	1.03	1.31	1.38	0.75
Fe_2O_3	<0.15	<0.15	0.43	<0.15		<0.15	Fe_2O_3	1.05	0.76	1.23	<0.15	0.46
FeO	7.40	7.65	7.08	7.42		43.65	FeO	4.03	4.09	3.68	4.93	7.15
MnO	<0.15	<0.15	<0.15	<0.15		5.87	MnO	<0.15	<0.15	<0.15	<0.15	<0.15
MgO	15.86	15.37	16.54	31.00		0.52	MgO	15.45	15.5	15.08	15.03	16.45
CaO	11.66	11.73	11.62	<0.15		<0.15	CaO	22.83	22.64	22.45	22.20	20.75
Na_2O	3.15	3.36	3.20	<0.15		<0.15	Na_2O	0.27	0.20	0.23	<0.15	<0.15
K_2O	0.36	0.45	0.44	0.12		<0.15	K_2O	<0.15	<0.15	<0.15	<0.15	<0.15
H_2O	2.08	2.07	2.08	12.55		<0.15	H_2O	<0.15	<0.15	<0.15	<0.15	<0.15
Si	6.176	6.100	6.365	Si	6.224	Ti	1.892	Si	1.865	1.852	1.814	1.830	1.824
Al^4	1.824	1.900	1.635	Al^4	1.776	Cr	0.035	Al^4	0.135	0.148	0.186	0.170	0.149
Σ	8.000	8.000	8.000	Σ	8.000	Fe^2	1.870	Σ	2.000	2.000	2.000	2.000	1.973
Al^8	0.083	0.106	0.068	Al^8	1.905	Mn	0.255	Al^8	0.014	0.019	0.036	0.062	0
Ti	0.587	0.586	0.479	Ti	0	Mg	0.04	Ti	0.047	0.046	0.047	0.040	0.057
Fe^3	0	0	0.047	Fe^3	0	Σ	4.091	Fe^3	0.029	0.021	0.034	0	0.013
Cr	0.016	0.022	0	Cr	0			Cr	0	0.030	0.038	0.040	0.022
Fe^2	0.894	0.928	0.854	Fe^2	1.186			Mg	0.848	0.851	0.828	0.825	0.913
Mn	0	0	0	Mn	0			Fe^2	0.124	0.126	0.114	0.152	0.222
Mg	3.415	3.321	3.552	Mg	8.83			Mn	0	0	0	0	0
Σ	4.995	4.963	5	Ca	0			Ca	0.901	0.893	0.887	0.876	0.827
EXM	0	0	0	Na	0			Na	0.019	0.014	0.016	0	0
Ca	1.805	1.823	1.794	K	0.029			K	0	0	0	0	0
NAM	0.195	0.177	0.206	Σ	11.95			Σ	2.000	2.000	2.000	1.994	2.054
Σ	2.000	2.000	2.000	OH	16.000			Mg*	0.87	0.87	0.88	0.84	0.80
NAA	0.689	0.769	0.688	Mg*	0.88								
K	0.067	0.083	0.080										
Σ	0.755	0.852	0.768										
OH	2.000	2.000	2.000										
Mg*	0.79	0.78	0.81										

present as coarse probably primary grains and also as abundant fine secondary grains along cleavage cracks. Probe analysis (see table 13) of some of the larger opaque grains show that they are manganese rich ilmenite. The grain supported olivine crystals indicate that the rock is an accumulate.

Cretaceous (?) *

M. P. McClenaghan

Lamprophyre dykes and intrusive bodies (Cl)

A number of dyke-shaped intrusions of similar petrographic character occur in the area are assumed to have been produced by the same magmatic event.

At CP692076 a 0.5 m wide dyke with variable attitude (165°/68°W, 21°/71°W, 145°/68°SW) cuts mudstone of the mudstone/lithicwacke sequence (€tl). The dyke is medium grained, unfoliated and has fine-grained chilled margins. It was only possible to trace it for about 5 m.

In thin section the rock has abundant thin lath shaped phenocrysts of biotite set in a fine-grained matrix which includes chlorite and cloudy feldspar. Some chlorite patches have shapes suggesting that they were derived from olivine. Small opaque grains are also present.

At CP681025 and CP682034 dykes approximately 0.5 m wide occur intruding the sheared serpentinite (€ss). The dykes are unfoliated and fine to medium grained. At CP677007 another fine-grained dyke occurs intruding gabbro (€g).

In thin section a sample collected from the dyke at CP682034 consists of abundant phenocrysts of biotite and clinopyroxene which show a size range with the matrix. Serpentine patches occur with shapes suggesting that they were derived from olivine. Feldspar in the matrix is cloudy and contains abundant sericite. Faint polysynthetic twinning indicates that some of the feldspar was plagioclase. Samples from the other two localities are similar but more highly weathered.

Close (1972) and White (1975) identified hornblende phenocrysts in addition to biotite and clinopyroxene from samples of dykes intruding the serpentinite in this area.

At CN574980 a coarse-grained body approximately 6 m wide occurs which is of undetermined shape. It is an unfoliated rock intruded into grey mudstone belonging to the Precambrian sequence of the Nielson River area.

In thin section it has abundant phenocrysts of biotite and clinopyroxene. The biotite and clinopyroxene are partly altered to chlorite. The matrix consists dominantly of K-feldspar with lesser amounts of quartz, plagioclase and opaques. The quartz and K-feldspar show micrographic texture and accessory small euhedral apatite crystals are present.

Another small, medium-grained intrusion occurs at CN573991 intruded into siltstone of the variably calcareous mudstone/siltstone/sandstone sequence (€ac) of probable Cambrian age. It was not possible to determine the form of the body but it had a minimum width of 2 m at one point.

In thin section the rock is similar to the one at the previous locality but is more altered with clinopyroxene pseudomorphed by actinolite.

At the northern part of Varna Bay an approximately circular body 0.5 km in diameter of coarse-grained rock is intruded into calcareous mudstone of the €ac unit. The body consists of pale coloured and dark coloured rock. The dark rock is present in the other as variably shaped bodies with sharp boundaries. The bodies range in size from approximately 0.5

* At the time of preparation of the Macquarie Harbour map the age of the lamprophyre dyke suite was thought likely to be Cretaceous, based on the view of Sutherland and Corbett (1974). Recent radiometric age determinations (McClenaghan *et. al.*, in press) indicate a Devonian age.

m to 5 m long. The proportion of dark rock becomes greater to the south of the intrusion and dykes of the pale rock intrude the darker.

In thin section the dark rock has very abundant large and sometimes aligned laths of biotite and abundant actinolite pseudomorphs after clinopyroxene set in a mosaic of K-feldspar and plagioclase with accessory opaques and apatite. The K-feldspar shows cloudy alteration. Some samples contain quartz and have graphic intergrowths of quartz and K-feldspar. The pale coloured rock consists of a coarse-grained mosaic of K-feldspar, quartz, plagioclase and carbonate. The K-feldspar is cloudy and perthitic and has graphic intergrowths with quartz. Microcline twinning is present in some of the K-feldspar. Minor small patches of muscovite, chlorite and fine-grained opaque grains may be the product of alteration from biotite. Carbonate is present as intergranular patches and is probably secondary.

On the northern side of the body a fine-grained dyke 6 m wide with an attitude of 160°/75°E is intruded into the sedimentary country rock. It was not possible to trace it into the larger body.

In thin section the dyke rock consists of abundant thin lath-shaped crystals of biotite set in a fine-grained granular matrix of feldspar and carbonate. The biotite is mostly altered to chlorite. Pseudomorphs of serpentine after olivine are common.

A small intrusion of coarse-grained rock of undetermined shape occurs at CP572015 which is in an area of the mudstone/lithicwacke sequence (€aml). It has been included in the same group as the bodies described above though it has a slightly different petrographic character.

In thin section it consists of a coarse-grained mosaic of plagioclase, actinolite, zoisite, chlorite and opaque grains. It is a strongly altered rock with little of the original texture remaining.

The petrographic character of most of the rocks described in this section indicates that they are minettes, kersantites and vogesites.

HEMATITE BODIES (hp)

Small lenticular bodies consisting dominantly of hematite but with variable small amounts of pyrite and chlorite occur near the Nielson River between CN580990 and CP620040. The bodies lie along north-east trending faults and it appears that the faults have provided a pathway for mineralising fluids that have deposited the bodies. Veins up to 30 mm wide of hematite with or without pyrite, quartz and chlorite and veins of pyrite alone, are common in this area. The country rock is frequently rich in freshly crystallised hematite, chlorite and pyrite and it appears that these features were produced in the same mineralising event.

GEOCHEMISTRY

M. P. McClenaghan

Introduction

Whole rock and trace element analyses were made of igneous rocks from the map sheet in order to characterise and compare them with similar units elsewhere in Tasmania (tables 14–16). Because two methods of analysis were used for the rare earth elements (REE) those results have been presented in different tables. The two methods (neutron activation (NA) and inductively coupled plasma-mass spectrometry (ICP-MS)), are closely comparable as can be seen from the duplicate analyses of samples MH104 and MH194B. There is also duplication in the analysis of some other elements such as Ce, La, Nd and Th for some of the samples. Most elements were analysed by XRF as well as by NA, ICP-MS or both. Where NA or ICP-MS analyses were also available for an element, they were used on the diagrams in preference to the XRF analyses and NA analyses were used for samples MH104 and MH194B instead of the ICP-MS analyses.

Where possible, terminology used in describing the various igneous rock units follows that of White (1975).

The pillow and massive basalts indicated on the map by the symbol €ba and cropping out in a zone from the Double Cove area south-west to the western coast of the peninsula are the Lucas Creek Volcanics. Another two isolated outcrops of pillow basalt occur on the coast farther south and are also indicated by the same symbol. As will be shown later these two occurrences have a slightly different geochemical characteristics. These basalts centred on CP555007 and CP554003 will be referred to as west coast basalt north and south respectively.

Massive basalts cropping out on the western side of the southern part of Birchs Inlet and indicated on the map by the symbol €tbc are the Birchs Inlet Volcanics.

The Noddy Creek Volcanics include a number of intrusive and extrusive units cropping out east of the Point Hibbs Mélange Belt in the central part of the peninsula. They are shown on the map with the symbols, €tr, €al, €ri, €ta, €rip and €g.

Details of the these units and other smaller units which have not been distinguished by formal names are presented in Table 17.

Classification, geochemical characteristics, correlations and tectonic settings of Cambrian igneous rocks

MAIN IGNEOUS GROUPS: LUCAS CREEK, BIRCHS INLET AND NODDY CREEK VOLCANICS

Classification

Based on the classification system of Le Maitre (1984) the Lucas Creek Volcanics and the Birchs Inlet Volcanics range from basalt to basaltic andesite. The Noddy Creek Volcanics form two composition groups, andesite/ trachyandesite and rhyolite (see fig. 10).

Using an alternative classification system based on K_2O–SiO_2 plots (see fig. 11) (Peccerillo and Taylor, 1976) the three main igneous groups range across the volcanic series from arc tholeiite to shoshonite. The Lucas Creek and Birchs Inlet Volcanics include low-K tholeiite and high-K tholeiite basalt. The Noddy Creek Volcanics are mostly high-K andesite, rhyolite and high-K rhyolite. The wide spread in K_2O content of the rocks may be due to alteration and so may not be an indication of their original composition. This suggestion is supported by the widespread alteration of plagioclase to sericite which would not be possible without the addition of K_2O.

The three main igneous groups have been plotted on FeO*/MgO–SiO_2, FeO*/MgO–FeO* and Na_2O+K_2O–FeO*–MgO diagrams (fig. 12–14) in order to distinguish tholeiitic and calc-alkaline trends (see Miyashiro, 1974). The Lucas Creek Volcanics and Birchs Inlet Volcanics show trends typical of tholeiitic rocks whereas the Noddy Creek Volcanics show a calc-alkaline trend. Isolated rocks near the magnesium rich end of these trends may be difficult to assign since there is overlap between the two types of trend. A plot on a Zr–Ti–Y diagram (see fig. 15) shows the tholeiitic and calc-alkaline groups falling in different areas without overlap. As Zr, Ti and Y are generally accepted to be among the least mobile elements and so representative of the original composition, this type of diagram and the fields for the Lucas Creek–Birchs Inlet rocks and the Noddy Creek rocks will be used to distinguish between the two trends for the other minor groups from the area and also as a diagram to discriminate between tholeiitic and calc-alkaline rocks.

Table 14. WHOLE ROCK MAJOR AND TRACE ELEMENT ANALYSES FROM THE MACQUARIE HARBOUR MAP SHEET

Grid Ref.	CP616123	CP620122	CP623118	CP623116	CN557949	CP555008	CP554007	CP554005	CP554004	CP548021
Symbol	€ab	€ab	€ab	€ab	€l	€ab	€ab	€ab	€ab	€ab
Field No.	MH101	MH104	MH105	MH106	MH111	MH158	MH161	MH163	MH165	MH177
Anal No.	820296	820297	820298	820299	820300	820301	820302	820303	820304	820305
SiO_2	44.48	48.70	48.69	47.77	48.12	45.21	44.16	47.08	47.05	48.08
TiO_2	0.73	1.66	1.85	3.44	1.17	0.90	0.84	1.14	0.48	1.35
Al_2O_3	14.36	13.68	14.45	12.73	10.52	17.31	16.67	13.85	14.19	14.48
Fe_2O_3	2.11	3.14	2.55	7.01	2.51	3.88	3.29	2.58	1.89	2.77
FeO	8.62	9.68	8.92	8.01	5.05	9.30	10.75	7.56	7.43	9.56
MnO	0.19	0.22	0.20	0.21	0.11	0.24	0.26	0.16	0.16	0.21
MgO	13.61	5.84	6.61	5.22	11.64	6.70	8.67	10.41	12.49	7.36
CaO	8.10	9.80	10.25	8.39	5.09	7.87	4.86	10.42	7.67	9.81
Na_2O	1.18	3.35	1.93	3.24	1.49	2.53	1.45	1.18	1.12	2.46
K_2O	1.51	0.29	1.59	1.03	3.11	0.31	2.28	0.41	1.87	0.22
P_2O_5	0.16	0.32	0.29	0.47	0.75	0.57	0.53	0.21	0.22	0.23
CO_2	0.14	0.24	0.18	0.10	5.88	0.17	0.17	0.10	0.21	0.14
SO_3	0.17	0.22	<0.05	<0.05	0.20	0.22	<0.05	<0.05	<0.05	0.05
H_2O^+	3.95	3.44	2.92	2.69	3.69	4.65	5.76	4.83	5.09	3.57
H_2O^-	0.13	0.18	0.04	0.17	0.48	0.18	0.05	0.05	0.06	0.04
Total	99.44	100.76	100.47	100.48	99.81	100.04	99.74	99.98	99.93	100.28
Ag	n.d.	n.d.	n.d.	n.d.	n.d.	n.d.	n.d.	n.d.	n.d.	n.d.
As	<10	<10	<10	<10	<10	18	<10	<10	11	<10
Ba	420	150	550	210	2000	320	320	310	1150	81
Cd	n.d.	n.d.	n.d.	n.d.	n.d.	n.d.	n.d.	n.d.	n.d.	n.d.
Ce	26	43	40	76	110	105	94	55	42	28
Co	61	43	38	40	38	54	37	34	53	43
Cr	1400	67	190	83	560	33	32	420	1300	165
Cu	78	210	115	57	81	70	68	130	370	105
Ga	12	13	16	21	12	11	8	13	11	16
In	n.d.	n.d.	n.d.	n.d.	n.d.	n.d.	n.d.	n.d.	n.d.	n.d.
La	<6	<6	<6	<6	33	48	43	14	18	<6
Mo	<2	<2	<2	<2	<2	<2	<2	<2	<2	<2
Nb	<3	9	<3	13	7	52	52	12	11	3
Nd	<9	14	10	22	41	17	25	18	<9	<9
Ni	480	63	105	76	81	70	68	130	390	105
Pb	<4	<4	<4	<4	<4	<4	<4	4	<4	<4
Rb	47	12	36	19	185	9	31	12	45	8
Sb	n.d.	n.d.	n.d.	n.d.	n.d.	n.d.	n.d.	n.d.	n.d.	n.d.
Sc	34	37	35	38	33	30	23	36	49	40
Sn	<3	<3	5	3	<3	3	3	5	<3	4
Sr	95	220	210	360	100	560	470	180	150	270
Th	3	4	3	6	20	7	9	6	7	<3
U	<4	<4	<4	<4	6	<4	<4	4	<4	<4
V	230	400	330	460	210	145	150	240	210	340
W	n.d.	n.d.	n.d.	n.d.	n.d.	n.d.	n.d.	n.d.	n.d.	n.d.
Y	20	35	26	39	26	31	29	29	20	23
Zn	79	97	99	93	50	99	120	78	95	88
Zr	42	97	105	220	170	100	100	135	42	62

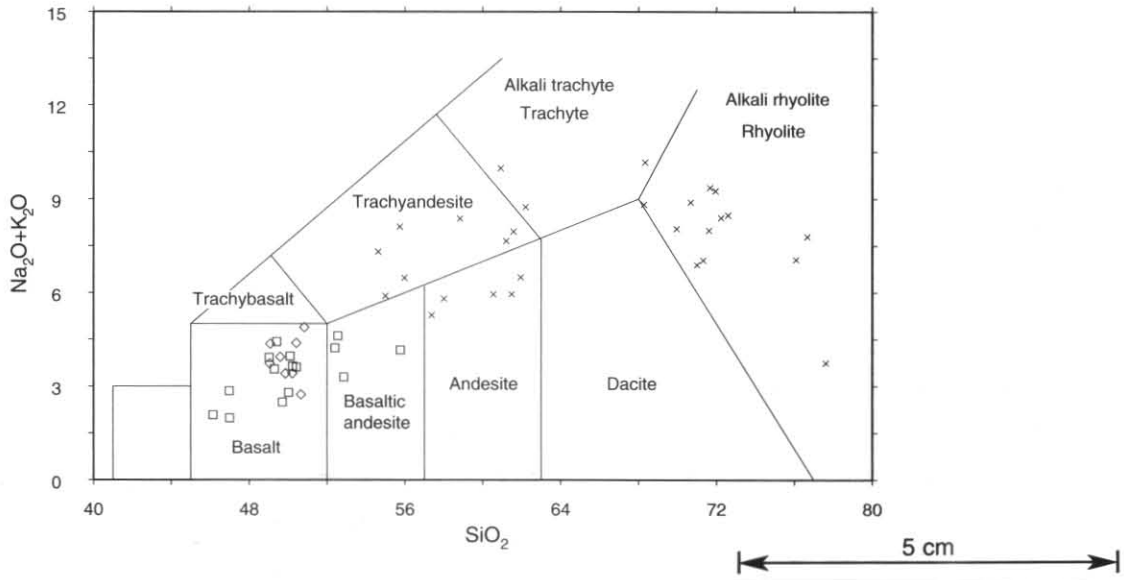

Figure 10. SiO_2–Na_2O+K_2O diagram, Lucas Creek Volcanics (□), Birchs Inlet Volcanics (◇) and Noddy Creek Volcanics (×). Fields from Le Maitre (1984).

Comparison between the main volcanic groups in the Macquarie Harbour area

The Lucas Creek and Birchs Inlet Volcanics are very similar in their major and trace element composition (see tables 14–16; fig. 10–19). The Birchs Inlet Volcanics show two types of REE pattern (fig. 20) suggesting that two magma types are present. Two analyses show a LREE (light rare earth element) depleted pattern whereas another analysis shows slight LREE enrichment with a steady negative slope toward HREE (heavy rare earth element). The REE pattern for the Lucas Creek Volcanic analyses (fig. 21) also show LREE enrichment which is rather similar to the single analysis from

Table 14. WHOLE ROCK MAJOR AND TRACE ELEMENT ANALYSES FROM THE MACQUARIE HARBOUR MAP SHEET (continued)

Grid Ref.	CP548027	CN730955	CN729955	CN726927	CN726927	CN735960	CN735959	CN736936	CP692022	CP546038
Symbol	€ab	€tbc	€tbc	€tbc	€tbc	€tbc	€tbc	€tbc	€tr	€ab
Field No.	MH178	MH192	MH193	MH194A	MH194B	MH195	MH196	MH200	MH209	MH245
Anal No.	820306	830636	830637	830638	830639	830640	830641	830642	830643	830644
SiO_2	47.51	48.22	47.17	47.67	47.74	48.46	48.64	49.12	71.55	52.10
TiO_2	3.45	2.11	2.34	0.76	0.76	2.56	2.29	1.27	0.32	0.96
Al_2O_3	12.73	14.24	14.18	14.41	14.36	12.85	14.19	13.99	14.32	15.86
Fe_2O_3	3.09	4.91	9.57	4.63	5.45	10.30	5.00	2.00	0.65	0.76
FeO	11.31	7.42	5.26	5.97	5.50	4.94	7.95	10.26	2.09	9.55
MnO	0.22	0.15	0.08	0.15	0.15	0.15	0.24	0.20	0.08	0.21
MgO	6.22	7.35	8.27	8.70	9.18	5.93	6.75	7.29	0.75	7.10
CaO	8.68	7.36	5.28	10.49	9.64	6.33	8.82	10.30	0.43	3.13
Na_2O	1.88	3.05	2.61	2.62	2.65	3.57	2.41	2.49	5.49	2.67
K_2O	0.49	1.13	0.60	1.15	0.99	1.08	0.88	0.15	2.86	1.21
P_2O_5	0.46	0.24	0.25	0.09	0.08	0.24	0.24	0.14	0.06	0.08
CO_2	0.10	0.04	0.10	0.09	0.07	0.10	0.07	0.04	0.11	1.10
SO_3	<0.05	<0.05	<0.05	0.05	0.06	0.14	0.05	0.16	0.06	0.07
H_2O^+	4.18	3.03	3.68	3.03	3.11	2.61	2.53	3.03	1.23	5.01
H_2O^-	0.03	0.39	0.56	0.23	0.28	0.62	0.41	0.08	0.05	0.08
Total	100.35	99.64	99.95	100.04	100.02	99.88	100.47	100.52	100.05	99.89
Ag	n.d.	n.d.	n.d.	n.d.	n.d.	n.d.	n.d.	n.d.	n.d.	n.d.
As	<10	<10	20	10	<10	<10	<10	<10	<10	20
Ba	125	89	125	43	61	120	78	44	590	210
Cd	n.d.	n.d.	n.d.	n.d.	n.d.	n.d.	n.d.	n.d.	n.d.	n.d.
Ce	67	53	66	27	30	60	47	28	57	35
Co	43	37	42	44	44	48	39	45	<6	54
Cr	96	190	200	280	290	140	100	130	<5	100
Cu	77	35	56	58	58	110	70	280	97	10 120
Ga	20	24	22	13	14	17	19	14	14	12
In	n.d.	n.d.	n.d.	n.d.	n.d.	n.d.	n.d.	n.d.	n.d.	n.d.
La	<6	8	<6	<6	<6	<6	<6	<6	18	<6
Mo	<2	<2	<2	<2	<2	<2	<2	<2	<2	<2
Nb	9	6	8	<3	<3	6	6	<3	10	<3
Nd	27	15	22	<9	<9	20	14	11	11	11
Ni	77	104	86	130	130	80	76	96	3	72
Pb	<4	870	4	<4	<4	<4	<4	<4	5	<4
Rb	15	22	12	17	15	10	12	10	93	40
Sb	n.d.	n.d.	n.d.	n.d.	n.d.	n.d.	n.d.	n.d.	n.d.	n.d.
Sc	35	34	37	44	43	33	31	39	<9	56
Sn	3	4	<3	<3	5	6	3	<3	3	<3
Sr	340	180	145	250	210	170	200	135	130	230
Th	7	4	<3	<3	7	6	<3	5	21	3
U	5	4	<4	5	<4	0	4	<4	8	4
V	450	360	420	280	300	410	400	320	45	320
W	n.d.	n.d.	n.d.	n.d.	n.d.	n.d.	n.d.	n.d.	n.d.	n.d.
Y	39	27	28	24	24	31	28	21	25	22
Zn	130	190	110	77	75	145	105	92	60	89
Zr	210	135	145	31	33	149	138	59	105	51

Table 15. RARE EARTH AND OTHER ELEMENT ANALYSES FROM THE MACQUARIE HARBOUR MAP SHEET ANALYSED BY THE NEUTRON ACTIVATION METHOD

Grid Ref.	CP616123	CP616123	CP554004	CN729955	CN726926	CN726927	CP620122	CP555008	CN672964
Symbol	€ab	€ab	€ab	€tbc	€tbc	€tbc	€ab	€ab	€ta
Field No.	41575	MH101	MH165	MH193	41508	MH194B	MH104	MH158	41516
La	3.35	3.41	12.30	10.70	1.47	1.14	8.63	36.50	32.60
Ce	8.37	8.49	24.40	26.80	4.12	3.06	21.20	73.10	73.10
Nd	5.21	5.52	10.00	19.30	5.00	4.53	13.70	24.30	31.00
Sm	1.75	1.85	2.41	6.16	1.93	1.72	4.17	4.75	6.24
Eu	0.69	0.87	0.70	2.04	0.75	0.71	1.26	1.38	1.31
Tb	0.45	0.40	0.40	1.10	0.49	0.52	1.07	0.92	0.47
Ho	0.59	0.54	0.62	1.18	0.74	0.80	1.61	1.19	0.63
Yb	1.57	1.62	1.82	2.25	2.11	2.21	3.73	3.17	1.90
Lu	0.23	0.26	0.27	0.30	0.37	0.34	0.47	0.48	0.31
Hf	1.24	1.26	1.15	3.97	1.00	1.00	2.78	2.23	2.72
Ta	0.55	<0.40	0.53	1.16	0.88	0.50	1.05	3.35	0.40
Th	0.78	0.36	2.60	0.85	0.25	<0.20	1.87	5.50	10.90

Table 16. RARE EARTH ELEMENT ANALYSES FROM THE MACQUARIE HARBOUR MAP SHEET ANALYSED BY THE ICP–MS METHOD

Grid Ref.	CP620122	CP554007	CP554005	CP548021	CN726927	CN660975	CN656989	CP669002	CP548035	CN677972	CN692999	CN675963
Symbol	€ab	€ab	€ab	€ab	€tbc	€tc	€g	€g	€bd	€g	€al	€tm
Field No.	MH104	MH161	MH163	MH177	MH194B	MH501	MH517	MH520	MH552	MH565	41530	41543
La	9.7	40	16	4.4	1.2	0.1	0.4	<0.1	0.2	19	28	3.3
Ce	25	83	41	11	3.4	0.7	1.0	<0.1	0.3	42	65	7.1
Pr	2.8	8.1	4.7	1.5	0.5	<0.1	0.1	<0.1	<0.1	4.4	6.9	0.8
Nd	13	29	18	7.8	2.8	0.6	0.5	0.1	0.6	17	27	3.1
Sm	3.8	1.3	4.0	2.4	1.6	0.2	<0.1	<0.1	<0.1	3.0	4.0	0.9
Eu	1.0	<0.1	1.2	1.0	0.6	<0.1	<0.1	<0.1	<0.1	0.7	0.4	0.2
Gd	5.0	4.2	4.8	3.7	2.3	0.2	0.2	0.3	0.8	3.0	3.4	0.9
Tb	0.8	0.6	0.7	0.6	0.4	<0.1	<0.1	<0.1	0.1	0.6	0.7	0.2
Dy	6.0	4.7	4.8	3.5	3.1	0.5	0.2	0.3	1.0	3.8	3.9	0.4
Ho	1.2	1.1	0.9	0.7	0.7	0.1	<0.1	<0.1	0.2	0.8	1.1	0.1
Er	3.6	3.2	2.7	2.5	2.2	0.3	0.3	0.3	0.8	2.4	2.5	0.4
Tm	0.5	0.4	0.3	0.2	0.3	<0.1	<0.1	<0.1	0.1	0.3	0.5	0.1
Yb	3.3	3.8	2.2	1.7	2.4	0.4	0.5	0.4	1.0	1.8	2.0	0.3
Lu	0.5	0.5	0.3	0.3	0.4	<0.1	0.1	<0.1	0.2	0.4	0.4	0.1

Table 14. WHOLE ROCK MAJOR AND TRACE ELEMENT ANALYSES FROM THE MACQUARIE HARBOUR MAP SHEET (continued)

Grid Ref.	CP572016	CP558035	CN734963	CN726926	CN688961	CN683961	CN675964	CN672964	CN671960	CN672962
Symbol	€t	€ab	€tbc	€tbc	€ri	€ta	€rip	€ta	€ta	€ta
Field No.	MH258	MH269	41507	41508	41509	41513	41514	41516	41517	41524
Anal No.	830645	830646	830656	830657	830658	830659	830660	830661	830662	830663
SiO_2	45.93	51.03	46.44	46.77	66.42	52.08	69.66	54.47	59.41	54.95
TiO_2	0.51	0.58	2.02	0.62	0.39	0.66	0.26	0.46	0.69	0.87
Al_2O_3	20.77	14.30	13.13	14.29	14.58	17.18	14.6	14.55	16.07	17.20
Fe_2O_3	2.07	3.31	5.97	4.46	3.27	3.22	2.25	1.40	4.67	4.95
FeO	5.55	6.70	7.77	6.40	2.76	5.99	1.93	8.07	3.13	8.07
MnO	0.16	0.14	0.20	0.16	0.16	0.16	0.07	0.16	0.08	0.16
MgO	7.87	8.32	6.54	8.87	0.78	4.67	0.84	6.90	2.64	3.07
CaO	9.68	8.66	8.82	10.62	0.51	4.43	0.30	3.87	1.40	0.27
Na_2O	2.73	3.76	3.00	2.43	4.14	4.16	4.46	3.69	7.26	5.40
K_2O	0.20	0.71	1.11	1.11	4.43	2.80	4.29	1.31	2.46	0.09
P_2O_5	0.19	0.05	0.27	0.12	0.14	0.28	0.10	0.17	0.14	0.17
CO_2	0.15	0.11	0.17	0.13	0.04	0.17	0.13	0.46	0.07	0.08
SO_3	<0.05	<0.05	0.08	0.06	<0.05	0.38	0.06	0.15	0.05	0.12
H_2O^+	4.49	2.65	3.19	3.38	1.65	3.02	1.40	2.73	1.35	3.60
H_2O^-	0.22	0.20	0.36	0.28	0.19	0.18	0.14	0.34	0.28	0.34
Total	100.52	100.52	99.07	99.70	99.46	99.38	100.49	98.73	99.7	99.34
Ag	n.d.	n.d.	n.d.	n.d.	n.d.	n.d.	n.d.	n.d.	n.d.	n.d.
As	<10	12	<10	30	<10	<10	<10	125	<10	<10
Ba	140	45	120	57	920	750	750	970	155	15
Cd	n.d.	n.d.	n.d.	n.d.	n.d.	n.d.	n.d.	n.d.	n.d.	n.d.
Ce	64	18	41	29	78	88	110	92	98	130
Co	27	75	44	42	<6	30	9	24	17	14
Cr	580	195	200	300	<5	<5	<5	155	<5	<5
Cu	23	80	280	53	14	22	10	17	12	5
Ga	9	15	24	11	14	14	12	<4	11	18
In	n.d.	n.d.	n.d.	n.d.	n.d.	n.d.	n.d.	n.d.	n.d.	n.d.
La	19	<6	<6	<6	32	40	48	39	43	72
Mo	<2	<2	<2	<2	<2	<2	<2	<2	<2	<2
Nb	17	<3	6	<3	10	4	11	3	4	8
Nd	15	<9	20	<9	24	31	29	27	27	32
Ni	120	77	92	135	3	4	3	63	7	<3
Pb	4	<4	12	10	4	18	33	30	10	<4
Rb	8	16	12	18	200	39	175	46	24	7
Sb	n.d.	n.d.	n.d.	n.d.	n.d.	n.d.	n.d.	n.d.	n.d.	n.d.
Sc	40	53	32	43	<9	22	<9	29	15	13
Sn	<4	11	<3	<3	5	<3	4	<3	<3	<3
Sr	490	200	120	230	49	540	44	200	44	38
Th	4	<3	4	4	22	13	25	15	14	15
U	<4	<4	4	<4	6	6	8	5	5	6
V	120	280	390	300	60	210	42	185	190	195
W	n.d.	n.d.	n.d.	n.d.	n.d.	n.d.	n.d.	n.d.	n.d.	n.d.
Y	14	19	25	26	37	27	20	25	23	25
Zn	91	81	100	72	83	85	59	36	53	77
Zr	42	23	135	31	220	115	180	95	135	150

Table 17. GROUPINGS OF IGNEOUS SAMPLES FROM THE MACQUARIE HARBOUR AREA WHICH ARE DISTINGUISHED ON GEOCHEMICAL PLOTS AND DISCUSSED IN THE TEXT

Lucas Creek Volcanics (€ab)	Samples 41567, 41569, 41570, 41571, 41572, 41575, MH101, MH104, MH105, MH106, MH464, MH473, MH254, MH269, MH177, MH178
West coast basalt north (€ab)	Samples MH158, MH161
West coast basalt south (€ab)	Samples MH163, MH165
Birchs Inlet Volcanics (€tbc)	Samples 41507, 41508, MH192, MH193, MH194A, MH194B, MH195, MH196, MH200
Noddy Creek Volcanics (€tr, €al, €ri, €ta, €rip, €g)	Samples 41509, 41511, 41513, 41514, 41515, 41516, 41517, 41518, 41524, 41525, 41526, 41527, 41528, 41529, 41530, 41531, 41533, 41534, 41535, 41536, MH209, MH491, MH493, MH564, MH565, MH574, MH575A, MH582
Basalt (€tba) in the mudstone/lithicwacke succession (€tl) near CN710948	Samples MH442, MH443
Andesite and rhyolite (€ti) in the Point Hibbs Mélange Belt	Samples MH10, MH39, MH286
Schistose possible tuff or lava (€tc) in the Point Hibbs Mélange Belt	Samples 41521, MH501
Mafic probable lavas (€tm) from the Timbertops area	Samples 41543, 41546
Mafic dykes of high Mg composition (€bd) on the west coast at CP548035 intrusive into mudstone/lithicwacke (€aml)	Sample MH552
Gabbro (€g) and associated tonalite/quartz gabbro (€x) Point Hibbs Mélange Belt	Samples MH20, MH205, MH219, MH284, MH289, MH497, MH511, MH513, MH517, MH520
Serpentinised pyroxenite (€sp) from the Point Hibbs Mélange Belt	Samples MH7, MH15, MH208, MH218, MH230
Peridotite with brown amphibole (€pd) at CP617022	Sample MH307
Gabbro (€g) intruding Precambrian rock at CP669081, CN564942 and CP613016	Samples MH60, MH120, MH314
Gabbro intruding the variably calcareous mudstone/siltstone/ sandstone sequence (€ac) at CP644077	Samples MH331, MH333
Lamprophyre dykes and intrusive bodies (Cl)	Samples MH111, MH258

Table 14. WHOLE ROCK MAJOR AND TRACE ELEMENT ANALYSES FROM THE MACQUARIE HARBOUR MAP SHEET (continued)

Grid Ref.	CN678973	CN683984	CN692999	CP685002	CP694038	CP625114	CP624118	CP624118	CP623120	CP620122
Symbol	€tr	€tr	€al	€al	€tr	€ab	€ab	€ab	€ab	€ab
Field No.	41525	41527	41530	41531	41536	41567	41569	41570	41571	41572
Anal No.	830664	830665	830666	830667	830668	830669	830670	830671	830672	820673
SiO_2	75.25	66.83	53.44	59.52	70.59	49.98	47.80	48.16	50.07	43.38
TiO_2	0.22	0.59	0.49	0.53	0.28	1.41	3.14	1.52	0.91	0.38
Al_2O_3	13.65	15.42	16.93	14.30	14.28	14.26	12.67	14.51	13.34	12.38
Fe_2O_3	0.72	4.38	3.00	3.57	0.90	1.52	4.04	0.96	1.52	1.94
FeO	0.34	0.45	5.98	3.83	2.08	9.90	10.09	10.43	10.17	5.33
MnO	0.08	0.04	0.23	0.13	0.06	0.15	0.22	0.16	0.22	0.12
MgO	0.25	0.10	4.87	4.26	0.76	5.93	5.82	6.97	7.93	9.80
CaO	0.02	0.26	3.25	5.11	0.33	8.28	8.01	9.38	7.60	11.92
Na_2O	3.89	3.88	3.51	3.07	4.56	3.55	3.23	2.41	2.74	2.76
K_2O	3.75	6.05	4.26	2.68	4.65	0.47	0.54	1.03	0.37	0.70
P_2O_5	0.03	0.20	0.19	0.13	0.07	0.21	0.38	0.21	0.14	0.10
CO_2	0.09	0.12	0.15	0.19	0.07	0.15	0.11	0.12	0.19	5.94
SO_3	<0.05	0.07	0.08	0.08	0.06	0.06	0.05	0.09	0.09	0.05
H_2O^+	1.46	0.91	2.63	2.40	1.13	2.85	3.04	3.05	3.85	4.15
H_2O^-	0.24	0.15	0.11	0.09	0.08	0.17	0.20	0.12	0.31	0.13
Total	99.99	99.45	99.12	99.89	99.90	98.89	99.34	99.12	99.45	99.08
Ag	n.d.	n.d.	n.d.	n.d.	n.d.	n.d.	n.d.	n.d.	n.d.	n.d.
As	<10	<10	<10	67	<10	<10	<10	<10	12	<10
Ba	720	2600	1500	650	890	210	195	410	110	330
Cd	n.d.	n.d.	n.d.	n.d.	n.d.	n.d.	n.d.	n.d.	n.d.	n.d.
Ce	140	120	96	83	90	44	72	43	40	23
Co	<6	6	39	26	4	48	40	48	48	45
Cr	<5	<5	5	105	<5	115	82	195	300	1000
Cu	7	14	19	13	9	110	115	110	105	32
Ga	13	13	17	12	13	13	22	20	13	7
In	n.d.	n.d.	n.d.	n.d.	n.d.	n.d.	n.d.	n.d.	n.d.	n.d.
La	65	51	47	30	45	<6	<6	<6	7	<6
Mo	<2	<2	<2	<2	<2	<2	<2	<2	<2	<2
Nb	8	13	<3	5	10	4	11	3	4	<3
Nd	30	38	25	21	21	9	27	11	14	<9
Ni	<3	<3	24	39	<3	83	76	105	135	330
Pb	<4	13	<4	<4	11	<4	<4	<4	<4	8
Rb	128	140	125	125	160	15	17	23	12	14
Sb	n.d.	n.d.	n.d.	n.d.	n.d.	n.d.	n.d.	n.d.	n.d.	n.d.
Sc	<9	<9	21	23	<9	40	34	37	41	37
Sn	<3	3	<3	5	<3	<3	<3	<3	3	<3
Sr	44	105	230	240	115	300	300	250	180	120
Th	32	28	14	13	23	<3	3	5	4	<3
U	6	4	4	<4	7	4	<4	5	4	<4
V	16	110	240	155	43	380	460	330	300	150
W	n.d.	n.d.	n.d.	n.d.	n.d.	n.d.	n.d.	n.d.	n.d.	n.d.
Y	12	25	19	27	24	26	39	26	25	14
Zn	15	18	69	61	100	8	130	110	86	48
Zr	135	220	84	185	110	95	220	99	71	15

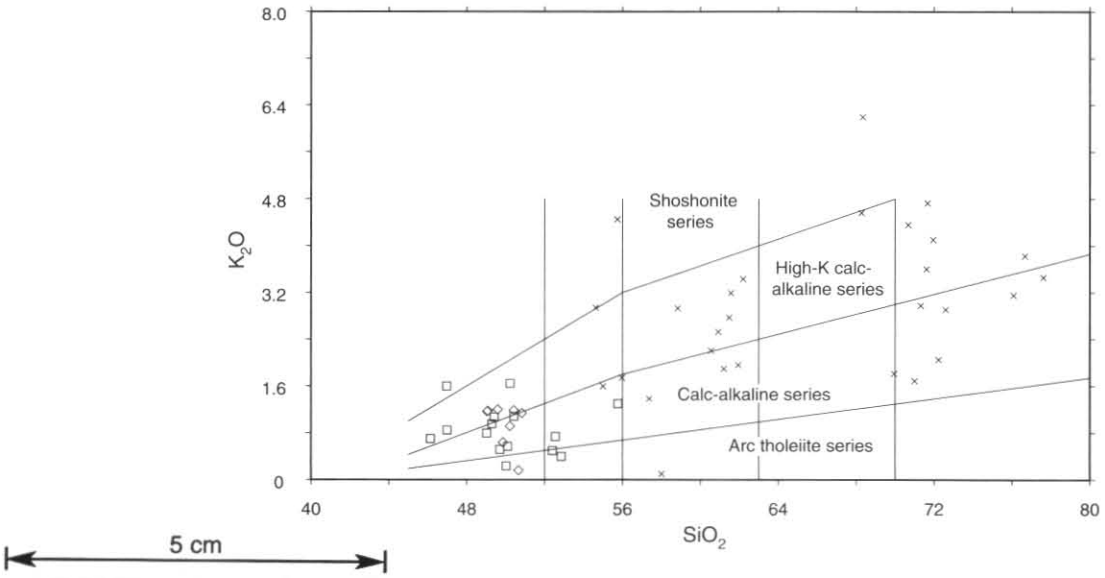

Figure 11. SiO_2–K_2O diagram, Lucas Creek Volcanics (□), Birchs Inlet Volcanics (◇) and Noddy Creek Volcanics (×). Fields from Peccerillo and Taylor, 1976).

the Birchs Inlet Volcanics. The varying amount of REE in the Lucas Creek Volcanics is consistent with fractionation of a single magma type. This compositional data suggest that the two units overlap for a large part of their range but that there are compositions present in the Birchs Inlet Volcanics not present or not sampled in the Lucas Creek Volcanics.

The Noddy Creek Volcanics clearly have a different composition range from the Lucas Creek and Birchs Inlet volcanics (fig. 10–15). The REE pattern (fig. 22) for the Noddy Creek Volcanics show strong LREE enrichment with flat HREE. The LREE enrichment is much greater than for the Lucas Creek Volcanics. One analysis shows Eu depletion

Table 14. WHOLE ROCK MAJOR AND TRACE ELEMENT ANALYSES FROM THE MACQUARIE HARBOUR MAP SHEET (continued)

Grid Ref.	CP616123	CN688957	CN672963	CN676972	CN644966	CN682982	CN679989	CN692999	CP683001	CP686017
Symbol	€ab	€ri	€ta	€g	€tc	€tr	€al	€al	€al	€tr
Field No.	41575	41511	41515	41518	41521	41526	41528	41529	41533	41534
Anal No.	839674	860304	860305	860306	860307	860308	860309	860310	860311	860312
SiO_2	44.11	70.03	60.22	53.87	61.4	73.25	57.81	60.3	60.22	69.15
TiO_2	0.58	0.34	0.47	0.55	0.22	0.14	0.62	0.60	0.54	0.39
Al_2O_3	13.21	14.25	13.9	14.72	12.77	11.72	15.71	14.79	14.54	15.25
Fe_2O_3	0.51	0.86	0.96	3.86	0.83	0.74	3.07	4.78	2.58	0.60
FeO	9.97	3.44	5.29	5.51	4.02	1.10	6.58	2.79	4.99	3.57
MnO	0.16	0.07	0.12	0.17	0.13	0.08	0.22	0.15	0.26	0.14
MgO	14.06	2.12	5.65	7.03	8.47	1.59	3.84	4.03	4.81	1.26
CaO	9.49	0.15	4.16	4.6	3.25	2.27	2.03	3.00	3.03	0.28
Na_2O	1.06	3.98	5.66	4.55	5.95	0.26	3.57	4.66	4.40	5.06
K_2O	0.79	2.92	1.86	1.67	0.17	3.26	2.10	3.12	1.90	1.64
P_2O_5	0.12	0.09	0.16	0.06	0.11	0.02	0.20	0.15	0.17	0.09
CO_2	0.17	0.02	0.30	0.02	0.10	3.20	0.98	0.17	0.17	0.09
SO_3	0.27	<0.05	<0.05	<0.05	<0.05	<0.05	<0.05	<0.05	<0.05	<0.05
H_2O^+	5.13	1.85	1.34	3.11	2.16	1.75	3.26	1.72	2.36	2.07
H_2O^-	0.07	n.d.	n.d.	n.d.	n.d.	n.d.	n.d.	n.d.	n.d.	n.d.
Total	99.70	100.12	100.09	99.72	99.58	99.38	99.99	100.26	99.97	99.59
Ag	n.d.	<5	<5	<5	<5	<5	<5	<5	<5	<5
As	<10	<10	<10	<10	<10	<10	<10	11	<10	<10
Ba	300	970	450	360	105	1600	1100	1350	1300	410
Cd	n.d.	<4	<4	<4	<4	<4	<4	<4	<4	<4
Ce	34	220	65	82	31	160	165	100	105	72
Co	64	13	29	40	25	4	18	22	23	5
Cr	1350	110	145	480	360	30	78	135	170	35
Cu	72	8	5	58	24	10	36	9	56	8
Ga	12	16	9	14	6	12	15	14	13	17
In	n.d.	<3	<3	<3	<3	<3	<3	<3	<3	<3
La	<6	100	<7	18	<7	83	66	32	30	12
Mo	<2	4	6	5	5	4	4	4	3	5
Nb	<3	11	<3	3	3	9	8	8	7	11
Nd	<9	80	59	49	<9	51	72	37	44	26
Ni	430	41	79	190	130	3	15	27	33	<3
Pb	5	7	5	5	<4	16	31	6	12	92
Rb	23	110	50	41	15	140	95	115	86	110
Sb	n.d.	<4	<4	<4	<4	<4	8	<4	<4	<4
Sc	37	12	26	28	15	<10	25	24	22	<10
Sn	<3	<4	<4	<4	<4	<4	<4	<4	<4	<4
Sr	66	77	120	175	27	76	300	240	290	97
Th	<3	32	11	11	<4	36	25	22	21	18
U	<4	9	5	5	<5	11	<5	6	5	8
V	210	55	200	270	74	13	220	165	220	85
W	n.d.	<9	<9	<9	<9	<9	<9	<9	<9	<9
Y	17	45	15	20	8	27	32	22	18	16
Zn	81	170	19	120	44	26	100	105	165	74
Zr	37	240	100	82	120	105	150	195	155	120

indicating that it may have undergone considerable feldspar fractionation or has been considerably altered. The range of enrichment of the samples is consistent with fractionation of a single magma type.

Comparison between the main volcanic groups in the Macquarie Harbour area and other Cambrian volcanic rocks in western Tasmania

The tholeiitic Birchs Inlet Volcanics are petrologically and chemically very similar to the Mainwaring Volcanics (Brown, in prep.) (see fig. 16, 17, 19), which are a sequence of mafic lavas occurring on the Montgomery map sheet to the south (shown by symbol Evv; Brown, 1988). The continuity of the magnetic anomaly pattern produced by the lavas across the intervening unmapped area supports the view that they belong to the same unit. The geochemical similarity between the two groups is also evident in the REE pattern (see fig. 20, 23) as two samples from the Mainwaring Volcanics show the LREE depletion present in some of the Birchs inlet Volcanics though to a greater degree. They were probably comagmatic with some of the Birchs Inlet basalts and have been produced by less fractionation or a greater amount of melting. Also present are more common samples with a slight LREE enrichment with a negative slope towards HREE similar to the pattern for the Lucas Creek Volcanics (fig. 21) and one of the samples from the Birchs Inlet Volcanics (fig. 20). This pattern differs slightly from that of the Lucas Creek and Birchs Inlet Volcanics as it is almost flat for the LREE. Also present are two samples with a concave pattern due to relative enrichment of LREE and HREE. These three types of pattern suggest that three magma types are present.

The Lucas Creek and Birchs Inlet Volcanics also have geochemical similarity to basaltic rocks intercalated in the Eocambrian sequence of the Smithton region (Smithton basalts) (Brown *et al.*, 1989) and among the Eocambrian lithicwacke of the Crimson Creek Formation in the Dundas Trough (Brown, 1986), (see fig. 24–27). The Crimson Creek basalts have two types of REE pattern (fig. 28). Two of the samples have slight LREE enrichment with a steady negative slope towards HREE which is similar to the pattern for some of the Lucas Creek, Birchs Inlet and Mainwaring Volcanics (fig. 20–21, 23). A third sample has a more marked LREE enrichment but is otherwise similar to the other two samples.

The Miners Ridge basalts in the Queenstown area and basaltic rocks from the Henty Fault Wedge have tholeiitic character (McClenaghan and Corbett, 1985) and also show similarities to the tholeiitic rocks of the Sorell Peninsula – Elliott Bay region and the basaltic rocks from the Crimson Creek Formation and the Eocambrian sequence of the Smithton region mentioned above (compare fig. 24, 26–27, 29 with fig. 16–19). The Miners Ridge basalt (data from Crawford, Corbett, Everard, 1992) shows LREE depletion (fig. 29) for three samples which is very similar to that for some samples from the Birchs Inlet and Mainwaring Volcanics (fig. 20, 23). Another sample shows only very slight LREE depletion and has a greater total REE content and may not be comagmatic. Four samples (fig. 29) from the Henty Fault Wedge (data from Crawford, Corbett, Everard, 1992) show slight REE enrichment patterns with a steady negative slope towards HREE. This pattern is very similar to that shown by some of the samples from Crimson Creek

Table 14. WHOLE ROCK MAJOR AND TRACE ELEMENT ANALYSES FROM THE MACQUARIE HARBOUR MAP SHEET (continued)

Grid ref.	CP92037	CN675963	CN671966	CN640953	CN709948	CN712948	CP598077	CP597101	CN669967	CN677961
Symbol	€tr	€tm	€tm	€tc	€tba	€tba	€ab	€ab	€tr	€ta
Field No.	41535	41543	41546	41550	MH442	MH443	MH464	MH473	MH491	MH493
Anal No.	860313	860314	860315	860316	860317	860318	860319	860320	860321	860322
SiO_2	70.25	50.79	52.42	52.06	47.04	51.80	43.70	47.26	60.43	57.70
TiO_2	0.24	0.11	0.11	0.08	0.51	0.71	3.58	1.82	0.81	0.83
Al_2O_3	14.52	6.38	6.79	9.26	15.66	17.65	14.26	14.53	19.06	17.01
Fe_2O_3	0.60	1.71	1.22	2.08	4.36	1.64	3.62	1.97	1.21	3.61
FeO	2.98	7.04	9.92	8.63	5.64	6.32	12.65	12.29	4.54	4.80
MnO	0.11	0.11	0.09	0.20	0.11	0.13	0.21	0.22	0.07	0.22
MgO	1.19	26.05	21.44	16.49	13.65	8.72	6.02	6.75	2.18	3.10
CaO	0.37	0.46	0.43	4.63	4.10	3.21	8.86	7.72	0.21	2.66
Na_2O	4.30	0	0	0.51	2.31	3.25	1.30	2.48	5.15	5.33
K_2O	3.53	0	0.17	0.03	1.15	1.66	0.66	0.91	3.33	2.87
P_2O_5	0.04	0.02	0.07	0.08	0.11	0.09	0.36	0.26	0.26	0.27
CO_2	0.04	0.06	0.27	0.18	0.09	0.35	0.26	0.07	0.33	0.09
SO_3	<0.05	<0.05	<0.05	<0.05	<0.05	<0.05	<0.05	<0.05	<0.05	<0.05
H_2O^+	1.52	7.21	6.82	5.83	5.21	4.12	4.48	3.89	2.13	2.01
H_2O^-	n.d.	n.d.	n.d.	n.d.	n.d.	n.d.	n.d.	n.d.	n.d.	n.d.
Total	99.69	99.94	99.75	100.06	99.94	99.65	99.96	100.17	100.31	100.50
Ag	<5	<5	<5	<5	<5	<5	<5	<5	<5	<5
As	<10	<10	<10	<10	<10	<10	<10	<10	<10	<10
Ba	1050	24	18	27	520	1650	570	570	1800	690
Cd	<4	<4	4	<4	<4	<4	<4	<4	<4	<4
Ce	100	32	40	32	28	56	97	63	145	135
Co	5	73	76	50	50	36	44	48	5	20
Cr	89	2600	3100	1600	940	145	92	97	43	51
Cu	5	6	18	10	13	150	175	95	24	6
Ga	14	4	6	6	13	14	30	20	18	16
In	<3	<3	<3	5	<3	<3	3	3	<3	<3
La	38	<7	<7	<7	<7	<7	<7	<7	44	47
Mo	3	4	6	6	5	4	10	6	2	5
Nb	12	3	<3	<3	<3	<3	15	8	13	10
Nd	20	23	31	18	17	<9	61	34	40	49
Ni	<3	800	570	380	430	70	82	77	16	14
Pb	4	<4	<4	<4	<4	<4	5	<4	42	26
Rb	125	6	34	19	36	34	53	47	97	96
Sb	<4	<4	5	14	<4	<4	<4	5	5	7
Sc	<10	15	30	42	37	34	52	50	21	15
Sn	<4	<4	4	<4	<4	<4	<4	<4	<4	<4
Sr	145	11	10	14	85	200	420	260	155	180
Th	26	<4	<4	<4	4	15	4	<4	30	14
U	<5	<5	<5	<5	<5	<5	<5	<5	<5	<5
V	37	59	165	200	300	270	640	530	160	250
W	<9	10	<9	<9	<9	<9	<9	<9	<9	<9
Y	16	5	<2	<2	10	25	37	24	13	28
Zn	62	67	85	71	69	125	140	125	60	93
Zr	110	44	28	6	26	90	250	130	200	160

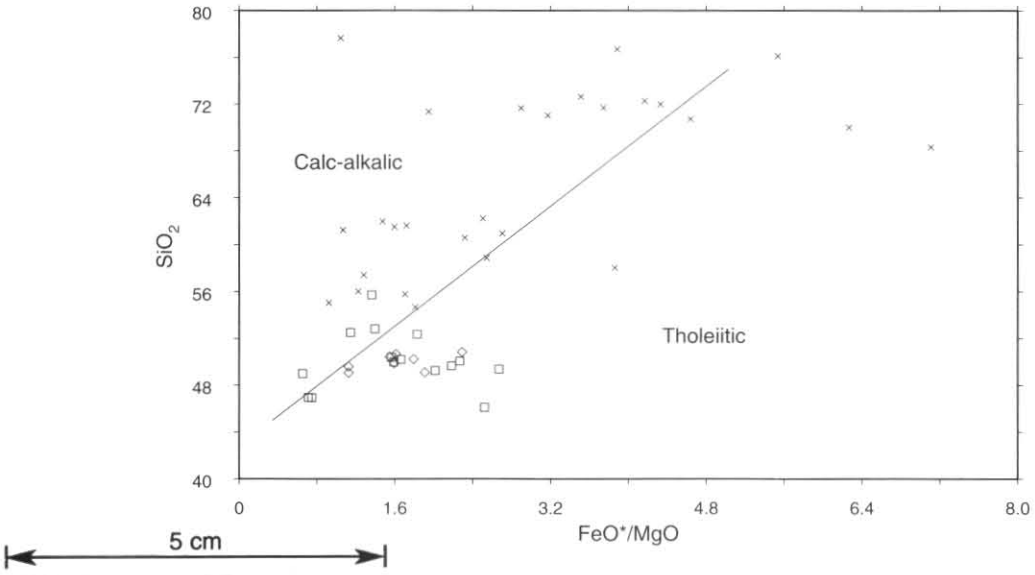

Figure 12. FeO*/MgO–SiO_2 diagram, Lucas Creek Volcanics (□), Birchs Inlet Volcanics (◇) and Noddy Creek Volcanics (×). Boundary from Miyashiro (1974).

Formation basalts, and the Lucas Creek, Birchs Inlet and Mainwaring Volcanics.

REE patterns for western Tasmanian non calc-alkaline rocks are discussed more generally in a later section.

It is evident that there is range of geochemical character in most of the tholeiitic units discussed above, based on their least mobile element composition, and that parts of some units share a very similar geochemical character.

The calc-alkaline Noddy Creek Volcanics are petrologically and geochemically similar to a sequence of basaltic andesite, andesite and dacite in the Montgomery area (shown by €vv, €vs and €mv, Brown, 1988). These rocks are also calc-alkaline (Brown, in prep.) and mostly plot in the same field as the Noddy Creek Volcanics on the Zr–Ti–Y diagram (fig. 30) and are probably part of the same unit. The REE pattern for these rocks (fig. 31; data from Brown, in prep.)

Table 14. WHOLE ROCK MAJOR AND TRACE ELEMENT ANALYSES FROM THE MACQUARIE HARBOUR MAP SHEET (continued)

Grid Ref.	CN660975	CN657986	CN656989	CP548035	CN680977	CN677972	CN685975	CN686977	CN679962	CP640077	CP701069
Symbol	€tc	€x	€g	€bd	€tr	€g	€tr	€tr	€rip	€g	€sp
Field No.	MH501	MH513	MH517	MH552	MH564	MH565	MH574	MH575A	MH582	MH333	MH7
Anal No.	860323	860324	860325	860326	860327	860328	860329	860330	860331	876011	881742
SiO_2	54.26	54.68	46.27	50.23	75.12	52.88	71.3	71.64	71.12	44.69	39.84
TiO_2	0.64	0.55	0.05	0.14	0.19	0.51	0.19	0.21	0.24	1.01	0.03
Al_2O_3	15.40	15.62	18.93	10.34	13.95	14.28	14.40	14.26	14.6	15.92	2.01
Fe_2O_3	1.69	1.49	1.34	0.64	0.99	1.89	3.94	0.86	1.19	2.44	4.18
FeO	13.59	8.37	6.39	6.58	1.07	7.04	2.85	2.76	1.69	11.18	1.80
MnO	0.12	0.13	0.17	0.12	0	0.25	0.07	0.06	0.01	0.31	0.14
MgO	6.69	5.69	8.20	18.09	0.35	9.06	1.04	0.84	0.63	5.41	38.00
CaO	0.17	5.22	12.33	6.72	0.09	4.60	0.23	0.21	0.23	8.19	0.05
Na_2O	1.94	4.00	0.86	1.40	3.85	4.13	6.35	6.29	5.09	2.58	0.11
K_2O	0.06	0.61	1.50	0.44	3.11	1.53	1.84	2.03	4.05	1.05	0.05
P_2O_5	0.16	0.13	0.15	0.13	0.09	0.13	0.08	0.08	0.09	0.60	0.01
CO_2	0.08	0.05	0.03	0.29	0.18	0.10	0.08	0.08	0.05	0.43	0.20
SO_3	<0.05	<0.05	<0.05	<0.05	<0.05	<0.05	<0.05	<0.05	<0.05	0.33	0.04
H_2O^+	5.84	3.32	4.19	5.00	1.52	3.55	1.27	1.21	1.16	4.17	12.67
H_2O^-	n.d.	n.d.	n.d.	n.d.	n.d.	n.d.	n.d.	n.d.	n.d.	n.d.	n.d.
Total	100.64	99.66	100.40	100.12	100.51	99.95	103.53	100.15	98.31	99.13	99.13
Ag	<5	<5	<5	<5	<5	<5	<5	<5	<5	<5	<6
As	<0	<10	<10	<10	<10	<10	<10	<10	<10	<10	<22
Ba	110	330	1100	570	720	580	740	760	730	2600	<23
Cd	<4	<4	<4	<4	<4	<4	<4	<4	<4	17	<6
Ce	30	20	16	24	155	66	110	115	110	77	<29
Co	45	31	40	63	<4	42	4	5	5	54	75
Cr	125	160	175	2800	95	610	115	130	78	64	3530
Cu	16	81	9	88	10	73	12	13	10	120	<4
Ga	14	14	11	6	13	12	14	12	15	12	<3
In	<3	<3	<3	<3	<3	<3	<3	<3	5	6	<8
La	<7	<7	<7	<7	76	11	51	46	53	32	<25
Mo	6	5	4	4	5	5	6	6	4	<2	<5
Nb	<3	<3	<3	<3	8	<3	9	11	9	72	<8
Nd	<9	19	9	<9	53	37	42	30	20	40	<9
Ni	100	68	155	820	9	230	3	5	6	45	718
Pb	<4	6	<4	<4	9	<4	4	<4	9	<4	<11
Rb	21	31	56	28	150	40	40	42	185	26	<6
Sb	11	<4	<4	<4	<4	4	<4	<4	<4	<5	8
Sc	45	39	42	39	<10	28	<10	<10	<10	33	15
Sn	<4	<4	<4	<4	<4	<4	<4	<4	<4	n.d.	<8
Sr	11	145	320	57	65	150	59	61	53	310	<7
Th	<4	<4	11	4	35	13	27	29	26	<4	<10
U	<5	<5	<5	<5	<5	<5	8	<5	6	<5	<12
V	620	350	145	165	14	220	20	22	40	195	27
W	<9	<9	<9	<9	<9	<9	<9	<9	<9	n.d.	92
Y	<2	9	<2	2	6	20	15	15	17	49	<6
Zn	135	83	33	46	39	210	70	66	49	200	33
Zr	20	20	13	6	160	83	130	130	175	115	<6

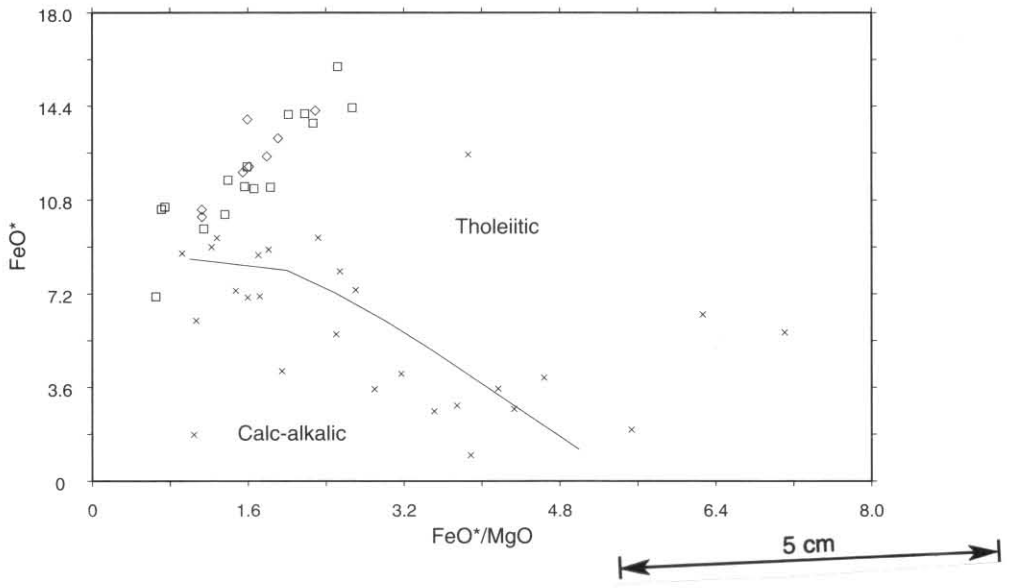

Figure 13. FeO*/MgO–FeO* diagram, Lucas Creek Volcanics (□), Birchs Inlet Volcanics (◇) and Noddy Creek Volcanics (×). Boundary from Miyashiro (1974).

show the same strong LREE enrichment and flat HREE with high overall REE abundance, seen for the Noddy Creek Volcanics (compare fig. 22 and 31).

The Noddy Creek Volcanics also have strong petrological and geochemical similarity to the calc-alkaline part of the Mt Read Volcanics from the Queenstown to Hellyer area (Corbett in Burrett and Martin, 1989). Samples from the Mt Read Volcanics mostly plot in the Noddy Creek Volcanics field on the Zr-Ti-V diagram (fig. 32).

Crawford, Corbett and Everard (1992) have distinguished three calc-alkaline suites from the Mt Read Volcanics based principally on TiO_2, P_2O_5 and REE content. Suite I includes

Table 14. WHOLE ROCK MAJOR AND TRACE ELEMENT ANALYSES FROM THE MACQUARIE HARBOUR MAP SHEET (continued)

Grid Ref.	CP702065	CP669028	CP708061	CP669081	CP677011	CP678009	CP676007	CP674005	CP679017	CP687037
Symbol	€ti	€sp	€g	€g	€g	€sp	€sp	€g	€sp	€g
Field No.	MH10	MH15	MH20	MH60	MH205	MH208	MH218	MH219	MH230	MH284
Anal No.	881743	881744	881745	881746	881747	881748	881749	881750	881751	881752
SiO_2	72.03	44.03	48.82	41.97	47.31	38.25	40.08	48.65	39.48	49.19
TiO_2	0.16	0.01	0.30	1.16	0.07	0.01	0.01	0.05	0	0.76
Al_2O_3	15.11	0.60	10.56	16.77	17.38	0.71	0.78	19.37	0.27	16.02
Fe_2O_3	0.50	3.27	3.76	2.09	0.90	7.56	2.78	1.32	3.64	1.24
FeO	1.78	2.81	10.89	6.74	4.65	4.88	2.82	4.88	0.21	9.21
MnO	0.04	0.24	0.28	0.16	0.13	0.16	0.10	0.19	0.03	0.22
MgO	1.10	34.55	10.33	8.60	10.77	35.62	39.69	9.55	41.89	9.44
CaO	0.54	3.66	7.30	14.85	10.81	0.06	0.04	8.17	0.01	6.07
Na_2O	7.14	0.11	2.66	1.76	1.28	0.20	0.06	2.30	0.41	1.71
K_2O	0.18	0.03	0.18	0.06	1.76	0.05	0.02	1.24	0.03	0.92
P_2O_5	0.03	0.07	0.10	0.28	0.22	0	0.02	0.08	0	0.10
CO_2	0.40	0.27	0.83	0.10	0.07	0.10	0.14	0.14	0.19	0.15
SO_3	0.06	0.03	0.03	0.98	0.05	0.02	0.02	0.07	0.30	0.07
H_2O^+	0.94	9.89	4.11	5.41	4.33	11.15	12.49	4.13	13.26	4.95
H_2O^-	0	0	0	0	0	0	0	0	0	0
Total	100.01	99.57	100.15	100.93	99.73	98.77	99.05	100.14	99.72	100.05
Ag	<6	<6	<6	<6	<6	<6	<6	<6	<6	<6
As	<22	<22	<22	<22	<22	<22	<22	<22	<22	<22
Ba	57	<23	42	24	1500	<23	<23	390	<23	450
Cd	<6	<6	<6	<6	<6	<6	<6	<6	<6	<6
Ce	68	<29	<29	<29	<29	<29	<29	<29	<29	<29
Co	<7	63	n.d.	49	38	124	99	40	63	55
Cr	131	3470	491	484	504	6430	4060	299	2210	460
Cu	<4	<4	6	76	<4	<4	<4	<4	<4	107
Ga	10	<3	9	12	6	<3	<3	8	<3	9
In	<8	<8	<8	<8	<8	<8	<8	<8	<8	<8
La	39	<25	<25	<25	<25	<25	<25	<25	<25	<25
Mo	8	5	<5	8	6	11	15	15	<5	<5
Nb	12	<8	<8	9	<8	<8	<8	<8	<8	<8
Nd	<26	<26	<26	<26	<26	<26	<26	<26	<26	<26
Ni	17	409	131	137	142	1560	1200	116	1590	142
Pb	<11	<11	<11	46	<11	<11	<11	15	<11	<11
Rb	<6	7	13	13	57	6	<6	26	<6	43
Sb	<6	8	10	8	9	8	<6	9	<6	9
Sc	<8	<8	74	48	47	11	10	42	<8	59
Sn	<8	<8	<8	<8	<8	<8	<8	<8	<8	<8
Sr	51	13	29	29	211	<7	<7	257	<7	133
Th	29	<10	<10	<10	<10	<10	12	<10	17	<10
U	<12	<12	<12	<12	<12	<12	<12	<12	<12	<12
V	11	13	286	270	121	32	24	99	9	290
W	203	107	n.d.	134	152	193	303	347	<11	16
Y	20	<6	14	23	<6	<6	<6	<6	<6	15
Zn	13	41	60	132	41	42	26	130	10	74
Zr	128	<6	18	84	<6	<6	<6	<6	<6	37

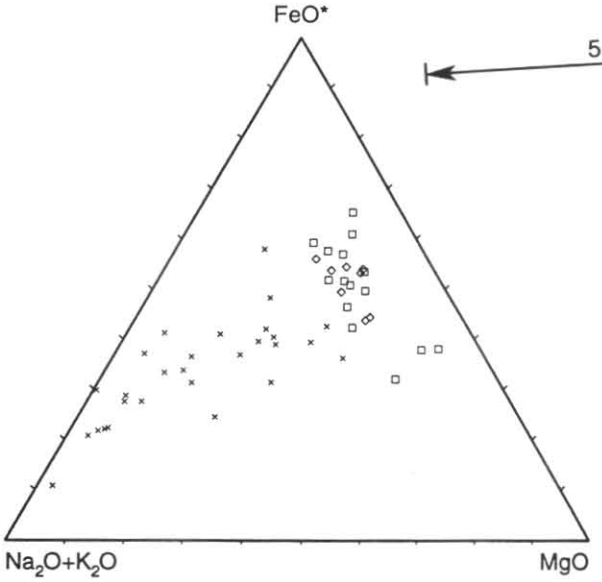

Figure 14. Na_2O+K_2O–FeO*–MgO diagram, Lucas Creek Volcanics (□), Birchs Inlet Volcanics (◇) and Noddy Creek Volcanics (×).

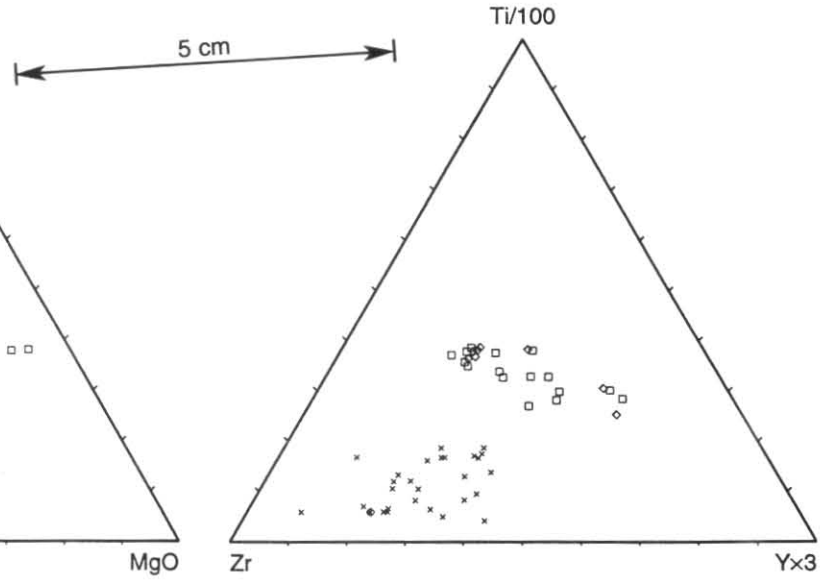

Figure 15. Zr–Ti–Y diagram, Lucas Creek Volcanics (□), Birchs Inlet Volcanics (◇) and Noddy Creek Volcanics (×).

the Eastern Sequence, Central Volcanic Complex, Tyndall Group, the intrusive quartz-feldspar porphyries and granitoids, and the andesite lavas of the Que–Hellyer Footwall sequence. Suite II comprises intrusive and extrusive rocks mainly from the upper part of the southern Central Volcanic Complex. Rocks from this suite are more P_2O_5-rich and have a higher La/Yb ratio than suite I rocks. Suite III rocks include lavas from the Que–Hellyer Hangingwall sequence, the Lynch Creek basalt and intrusive basalts in the Howards Plain area. Suite III rocks show a wide range of P_2O_5/TiO_2 and LREE enrichment. Some of the suite III lavas are regarded as shoshonites. In order to compare

Table 14. WHOLE ROCK MAJOR AND TRACE ELEMENT ANALYSES FROM THE MACQUARIE HARBOUR MAP SHEET (continued)

Grid Ref.	CP694045	CP696045	CP617022	CP613016	CN659977	CN657985	CP669002	CP715047
Symbol	€ti	€g	€pd	€g	€x	€x	€g	€ti
Field No.	MH286	MH289	MH307	MH314	MH497	MH511	MH520	MH39
Anal No.	881753	881754	881755	881756	881757	881758	881759	881760
SiO_2	61.36	54.33	36.77	46.01	69.65	56.48	49.57	53.95
TiO_2	0.15	0.64	0.68	0.79	0.41	0.34	0.07	0.45
Al_2O_3	9.69	16.54	7.20	17.98	11.86	15.09	8.05	14.71
Fe_2O_3	0.51	0.58	4.61	1.29	4.18	1.70	0.93	1.10
FeO	5.02	5.58	7.12	6.30	4.63	6.31	8.73	5.99
MnO	0.14	0.14	0.15	0.14	0.05	0.13	0.19	0.11
MgO	7.05	6.53	28.76	8.66	1.07	5.35	18.93	6.20
CaO	4.37	6.56	3.00	11.20	0.35	7.39	8.83	4.15
Na_2O	1.89	4.38	0.39	2.72	4.64	4.31	0.32	5.76
K_2O	0.25	1.56	0.36	0.42	0.24	0.31	0.05	0.52
P_2O_5	0.10	0.10	0.11	0.19	0.11	0.17	0.10	0.16
CO_2	5.87	0.10	0.12	0.12	0.15	0.04	0.10	2.50
SO_3	0.04	0.03	0.06	0.43	0.02	0.02	0.16	1.05
H_2O^+	3.60	2.57	9.67	3.98	2.32	2.55	3.87	3.21
H_2O^-	0	0	0	0	0	0	0	0
Total	100.04	99.64	99.00	100.23	99.68	100.19	99.90	99.86
Ag	<6	<6	<6	<6	<6	<6	<6	<6
As	<22	<22	<22	<22	<22	<22	<22	<22
Ba	40	560	39	105	56	100	43	115
Cd	<6	<6	<6	<6	<6	<6	<6	<6
Ce	<29	<29	<29	<29	<29	<29	<29	69
Co	30	20	126	43	26	37	71	34
Cr	519	83	2130	428	135	111	1320	61
Cu	<4	<4	<4	73	<4	12	<4	23
Ga	7	12	5	11	10	8	3	9
In	<8	<8	<8	<8	<8	<8	<8	<8
La	<25	<25	<25	<25	<25	<25	<25	<25
Mo	5	<5	<5	<5	6	5	<5	<5
Nb	<8	9	<8	8	<8	<8	<8	<8
Nd	<26	<26	<26	<26	<26	<26	<26	31
Ni	78	8	818	150	10	54	231	51
Pb	<11	<11	<11	<11	<11	<11	<11	<11
Rb	13	82	21	18	11	11	7	31
Sb	7	9	7	10	8	9	8	9
Sc	11	24	18	33	21	38	55	20
Sn	<8	<8	<8	<8	<8	<8	<8	<8
Sr	28	369	16	225	23	226	51	170
Th	<10	<10	<10	<10	<10	<10	<10	16
U	<12	<12	<12	<12	<12	<12	<12	<12
V	55	185	112	190	11	273	130	212
W	60	74	11	20	34	28	<11	32
Y	<6	21	7	16	21	12	<6	19
Zn	49	49	93	58	28	31	49	23
Zr	51	103	62	52	46	21	<6	60

Noddy Creek Volcanics and their correlates in the Montgomery area with these suites, plots of SiO_2–TiO_2 and SiO_2–P_2O_5/TiO_2 are presented which also show the fields for the three Mt Read Volcanic suites (fig. 33–34). It is clear that the Noddy Creek Volcanics and their correlates in the Montgomery area overlap to a large extent with the three suites, however, the more extreme compositions from suite III with high P_2O_5 and high P_2O_5/TiO_2 ratios are not present. Comparison of REE plots for the three suites (fig. 35–37) with that for the Noddy Creek Volcanics and their correlates in the Montgomery area (fig. 38) show that the plots are very similar except that some of the suite III samples have a greater LREE enrichment than the Noddy Creek Volcanics and their correlates in the Montgomery area. These plots confirm that the Mt Read Volcanics from the Queenstown to Hellyer area are geochemically extremely similar to the Noddy Creek Volcanics and their correlates in the Montgomery area except for the absence P_2O_5 and LREE enriched rocks in the latter areas.

Tectonic setting of volcanic rocks from the Macquarie Harbour area and other parts of western Tasmania

A number of diagrams have been used to assess the tectonic setting of the various volcanic rock groups discussed in the last section. On the Zr–Ti–Y diagram (Pearce and Cann, 1973; fig. 16, 26) the calc-alkaline correlates of the Noddy Creek Volcanics from the Montgomery area, a single sample from the Noddy Creek Volcanics and the calc-alkaline part of the Mt Read Volcanics plot in the volcanic arc calc-alkaline fields. On the Zr–Ti–Sr diagram (Pearce and Cann, 1973; fig. 17, 27) the same samples again plot in the

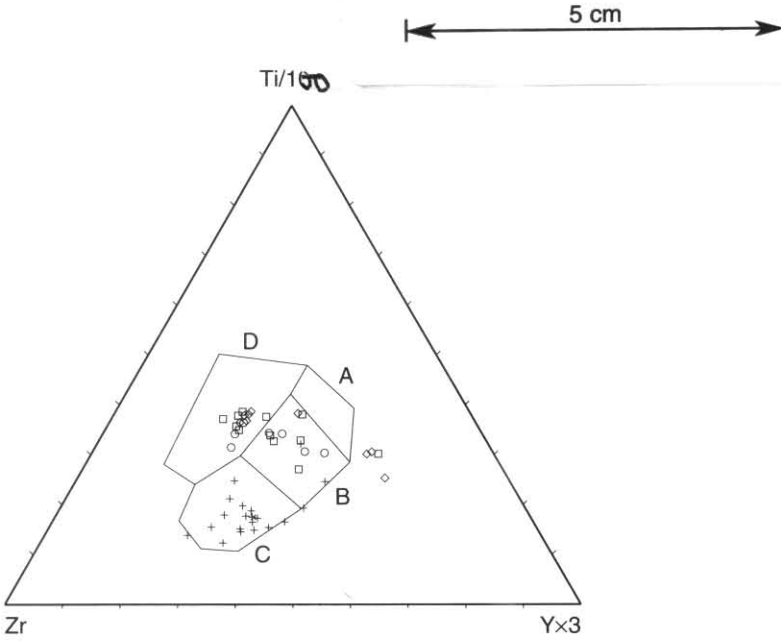

Figure 16. Zr–Ti–Y discriminant diagram with fields from Pearce and Cann (1973). A is low-K tholeiite, B is ocean-floor basalt or low-K tholeiite or calc-alkali basalt, C is calc-alkali basalt and D is within plate basalt (ocean island or continental). Lucas Creek Volcanics as (□), Birchs Inlet Volcanics (◇), Noddy Creek Volcanics (×), Noddy Creek Volcanics correlates in the Montgomery area (+) and Mainwaring Volcanics from the Montgomery area (○). Only samples with 12% < CaO+MgO < 20% have been plotted.

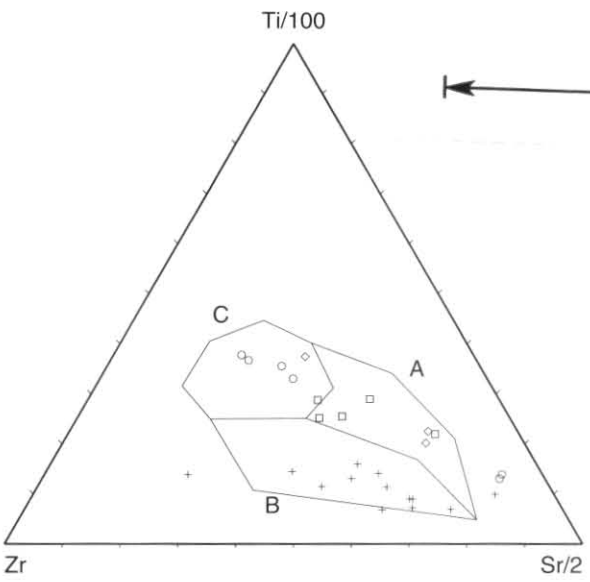

Figure 17. Zr–Ti–Sr discriminant diagram with fields from Pearce and Cann (1973). A is low-K tholeiite, B is calc-alkali basalt, C is ocean floor basalt. Symbols as for Figure A. Only samples with 12% < CaO+MgO < 20% and lying outside the within plate field on Figure A have been plotted.

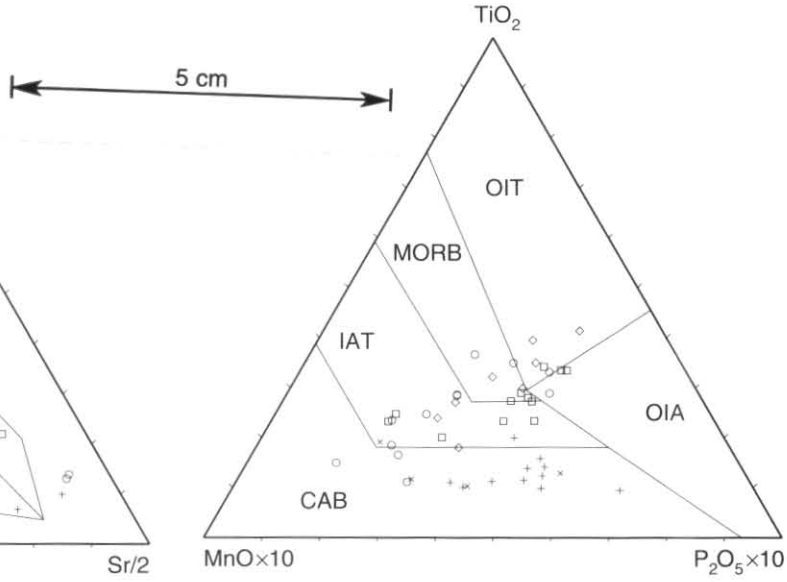

Figure 18. MnO–TiO_2–P_2O_5 discriminant diagram with fields from Mullen (1983). MORB is mid-ocean ridge basalt, IAT is island arc tholeiite, CAB is island arc calc-alkaline basalt, OIT is ocean island tholeiite and OIA is ocean island alkalic basalt. Symbols as for Figure A. Only samples with 45% < SiO_2 < 54% have been plotted.

volcanic arc calc-alkaline field. A volcanic arc setting is also indicated by the MnO–TiO_2–P_2O_5 diagram (Mullen, 1983; fig. 18, 25 where they plot in the island arc calc-alkaline basalt field. On the Th–Hf–Ta diagram (Wood, 1980; fig. 39) a single sample from the Noddy Creek Volcanics and a number of samples from the calc-alkaline correlates of the Noddy Creek Volcanics from the Montgomery area plot in the destructive plate-margin field.

An indication of the tectonic setting can also be obtained from clinopyroxene compositions (Leterrier *et al.*, 1982). This method avoids the problem of post-emplacement alteration which may have changed the whole rock composition but will not affect non-altered clinopyroxene. Leterrier *et al.* (1982) define various tectonic setting as follows. Orogenic basalts are those from destructive plate margins such as arc tholeiites, calc-alkali basalts from continental margins and island arc shoshonitic lavas. Non-orogenic basalts are tholeiites from distensive areas such as transitional basalts from rift zones, abyssal tholeiites, back-arc basin tholeiites, oceanic island tholeiites and continental tholeiites. The pyroxene compositions from Noddy Creek Volcanics have been plotted on the diagrams devised by Leterrier *et al.* (1982) to distinguish these settings. On the Ca–Ti+Cr diagram (fig. 40) the Noddy Creek Volcanics pyroxenes fall in the orogenic basalt field as expected on the basis of their major and trace element composition, however, on the $Al_{(total)}$–Ti diagram (fig. 41) they plot in tholeiitic field rather than the calc-alkali field. It is assumed that this is because the analysed pyroxenes occurred in andesite which is in the part of the calc-alkaline composition range closest to the composition of the tholeiitic rocks and that the method is not sufficiently sensitive to distinguish between the two rock types.

It seems clear that the calc-alkaline Mt Read Volcanic rocks from the Sorell Peninsula–Elliott Bay region and the Queenstown to Hellyer area were produced in an island arc setting.

On the Zr–Ti–Y diagram (Pearce and Cann, 1973) (fig. 16, 26) the various tholeiitic volcanic groups from western Tasmania, discussed above, generally plot in the within-plate field or the ocean-floor, low-K and calc-alkali basalt field. On the Zr–Ti–Sr diagram (Pearce and Cann, 1973) (fig. 17, 27) those samples which fall outside the within-plate field on the Zr–Ti–Y diagram have been plotted and the various tholeiitic groups mostly plot both in the ocean floor basalt and low-K tholeiite fields.

On the MnO–TiO_2–P_2O_5 diagram (Mullen, 1983) (fig. 18, 25) the tholeiitic groups generally range across the fields from ocean island tholeiite to island arc calc-alkaline basalt fields. On the Th–Hf–Ta diagram (Wood, 1980) (fig. 39) the Lucas Creek, Birchs Inlet and Mainwaring Volcanics samples generally plot in the field for E-type MORB and tholeiitic within-plate basalts and differentiates. A range of tectonic settings is also indicated by the Ti–V diagram (Shervais, 1982) (fig. 19, 24) where the tholeiitic groups have Ti/V ratios ranging from those expected for MORB to those for island arc volcanics. The pyroxene composition from basalts of the Lucas Creek and Birchs Inlet Volcanics also give an ambiguous indication of tectonic setting. On the Ca–Ti+Cr diagram (Leterrier *et al.*, 1982) (fig. 40) the Lucas Creek and Birchs Inlet Volcanics pyroxenes are mostly in the non orogenic field but partly extend into the orogenic field. This feature is also evident for pyroxene compositions (Brown, 1986) from the Crimson Creek basalts (see fig. 42).

The consistent feature of the discriminant diagrams is that the tholeiitic groups show a range of geochemical character consistent with MORB to island arc tectonic settings. Shervais (1982) points out that back-arc basin basalts may have either arc-like or MORB-like Ti/V ratios, and sample suites from single back-arc basins may have Ti/V ratios ranging from 10 to 50 and that this range in Ti/V ratios in samples from a restricted geographic area may be diagnostic of the back arc setting. Saunders and Tarney (1984) also point out that many back-arc basins have basalts transitional in chemistry between N-type MORB and island-arc or even calc-alkaline basalts (enrichment of large ion lithophile (LIL) elements (K, Rb, Ba, Th) relative to high field strength (HFS) elements (Nb, Ta, Zr, Hf, Ti)). Figure 43 shows a multi-element plot of samples from the Lucas Creek, Birchs Inlet and Mainwaring Volcanics, normalised by N-type MORB composition and it is clear that they show the varying enrichment in LIL elements suggested as typical of back-arc basins. The enrichment of Ta evident in the diagram, however, is not typical of back-arc basalts and is generally a characteristic of E-type MORB.

A back-arc basin assignment for the tholeiitic volcanics appears inconsistent with the fore-arc character of closely associated boninitic and low-Ti tholeiitic sequences (Brown

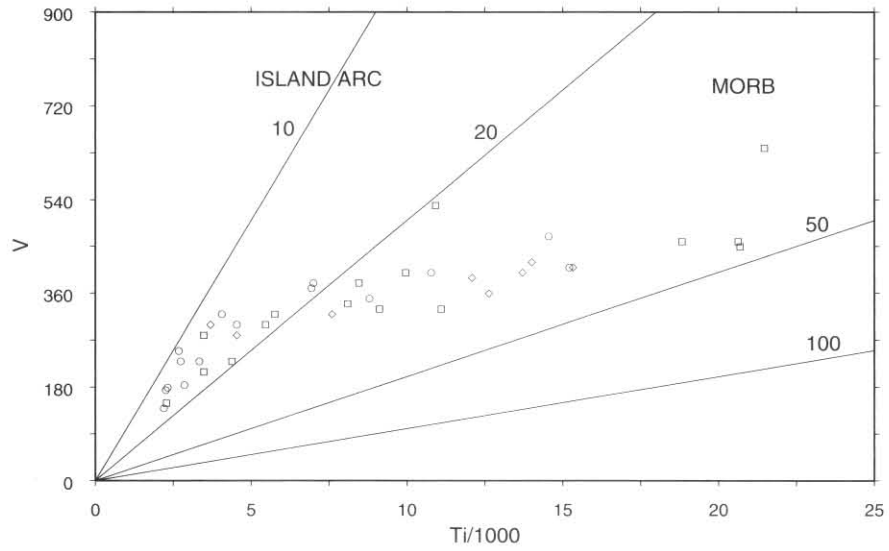

Figure 19. Ti–V discriminant diagram with fields from Shervais (1982). Lucas Creek Volcanics (□), Birchs Inlet Volcanics (◇) and Mainwaring Volcanics from the Montgomery area (○). Ti/V ratios indicated. Island arc rocks Ti/V < 20 and MORB Ti/V > 20.

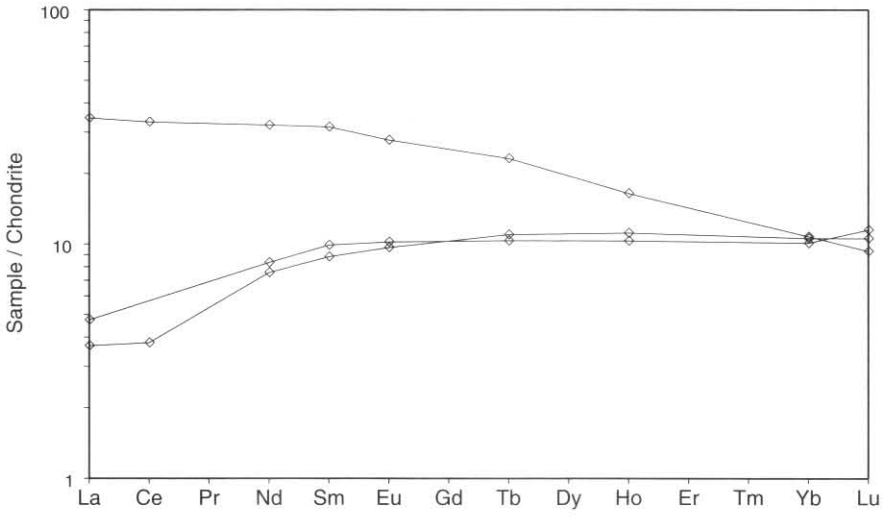

Figure 20. Chondrite-normalised REE patterns for the Birchs Inlet Volcanics.

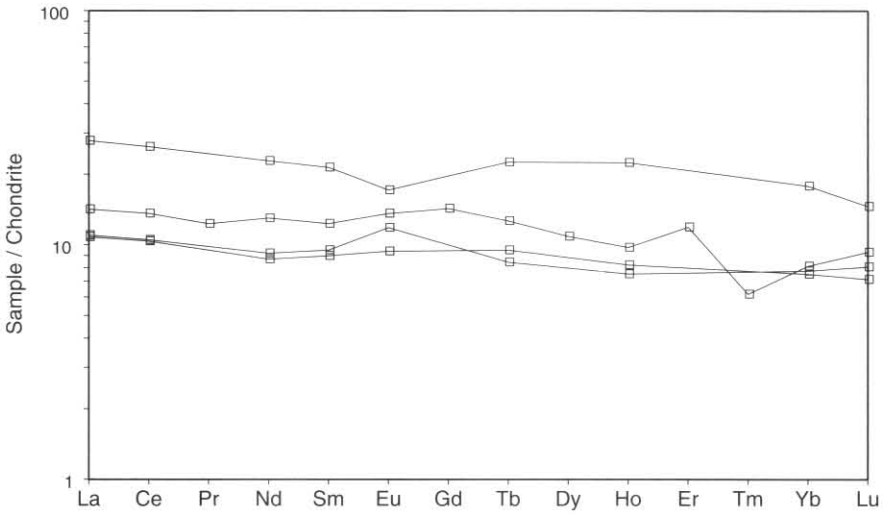

Figure 21. Chondrite-normalised REE patterns for the Lucas Creek Volcanics.

5 cm

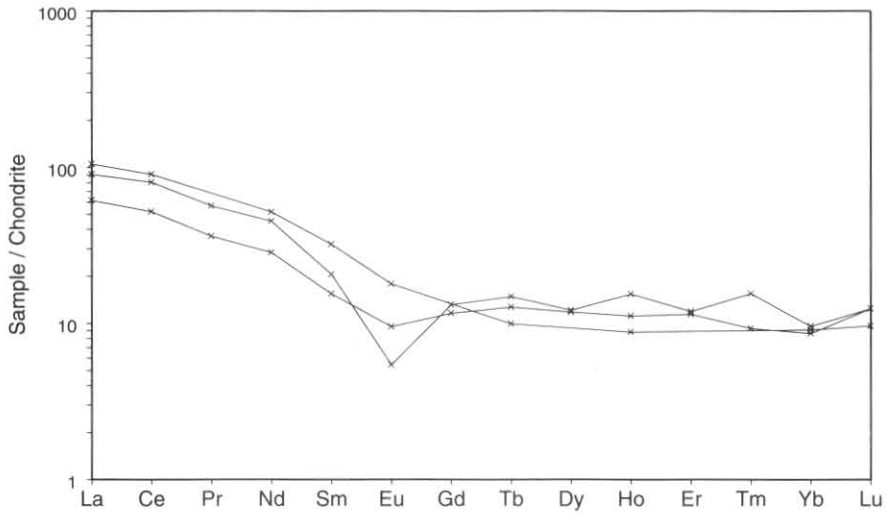

Figure 22. Chondrite-normalised REE patterns for the Noddy Creek Volcanics.

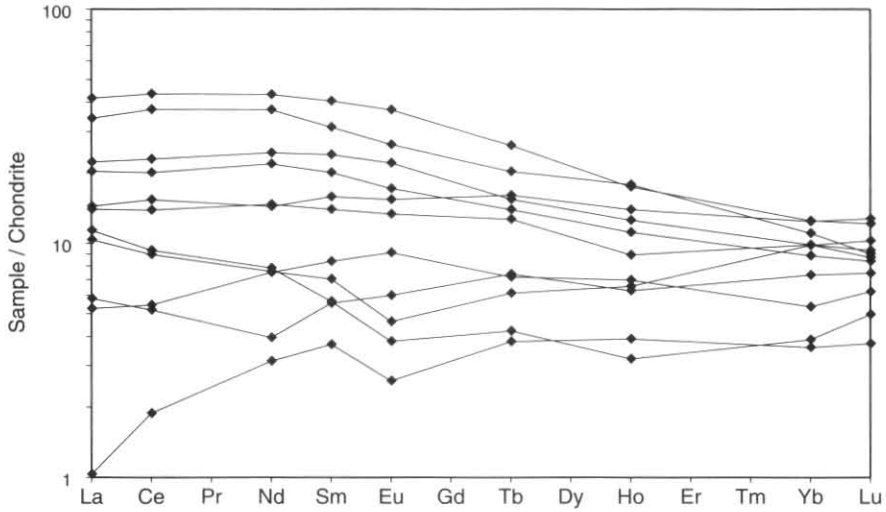

Figure 23. Chondrite-normalised REE patterns for the Mainwaring Volcanics from the Montgomery area.

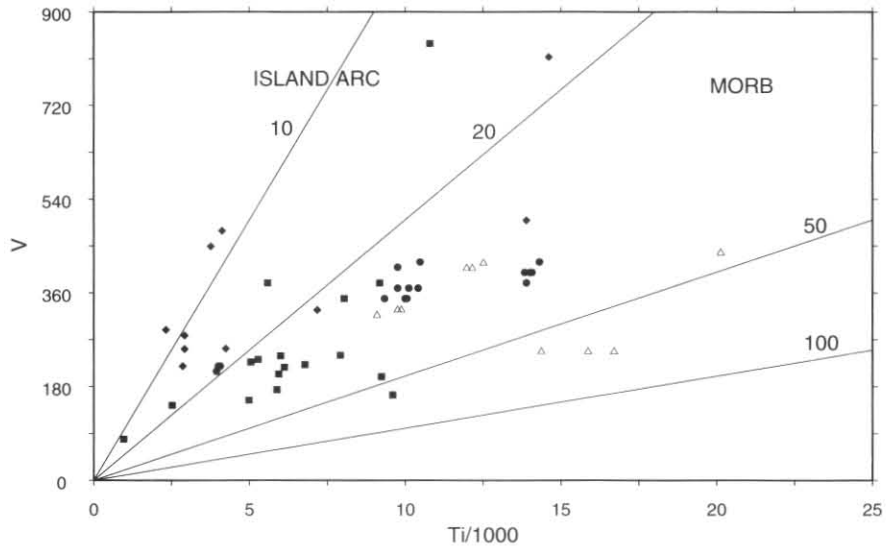

Figure 24. Ti-V discriminant diagram with fields from Shervais (1982). Smithton basalts (●), Crimson Creek basalts (△), Miners Ridge basalts (◆) and Henty Fault Wedge basalts (■). Ti/V ratios indicated. Island arc rocks Ti/V < 20 and MORB Ti/V > 20.

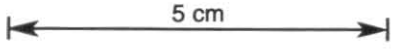

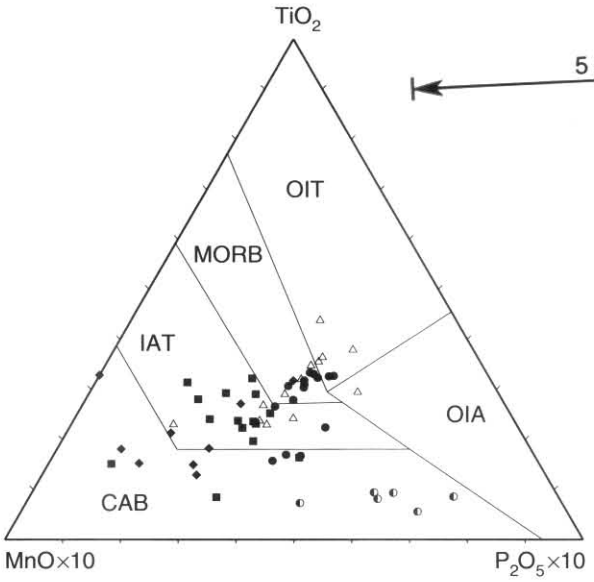

Figure 25. MnO–TiO_2–P_2O_5 discriminant diagram with fields from Mullen (1983). MORB is mid-ocean ridge basalt, IAT is island arc tholeiite, CAB is island arc calc-alkaline basalt, OIT is ocean island tholeiite and OIA is ocean island alkalic basalt. Symbols as for Figure 24 with the addition of calc-alkali rocks from the Mt Read Volcanics (◐).

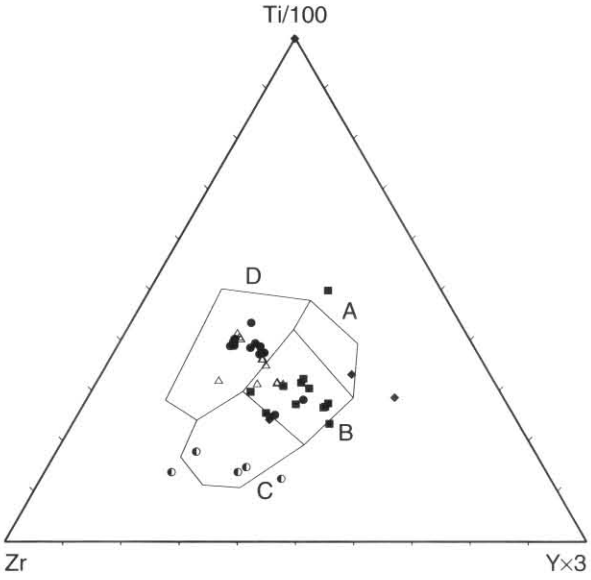

Figure 26. Zr–Ti–Y discriminant diagram with fields from Pearce and Cann (1973). A is low-K tholeiite, B is ocean-floor basalt or low-K tholeiite or calc-alkali basalt, C is calc-alkali basalt and D is within plate basalt (ocean island or continental). Symbols as for Figure 24 with the addition of calc-alkali rocks from the Mt Read Volcanics (◐). Only samples with 12% CaO+MgO 20% have been plotted.

and Jenner, 1990), however, the complex tectonic history of western Tasmania leaves the possibility open.

Discussion of possible grouping of western Tasmanian non calc-alkaline igneous rocks based on REE composition

Examination of REE patterns for non calc-alkaline rocks from western Tasmania indicate that there may be five main groups (see fig. 44–48 and table 18). Similarity of REE pattern suggests that the rocks were formed by a similar process at the same time and so may be a guide to correlation.

The rocks of group 1 are all characterised by very low TiO_2 as well as LREE depletion and this grouping suggests a

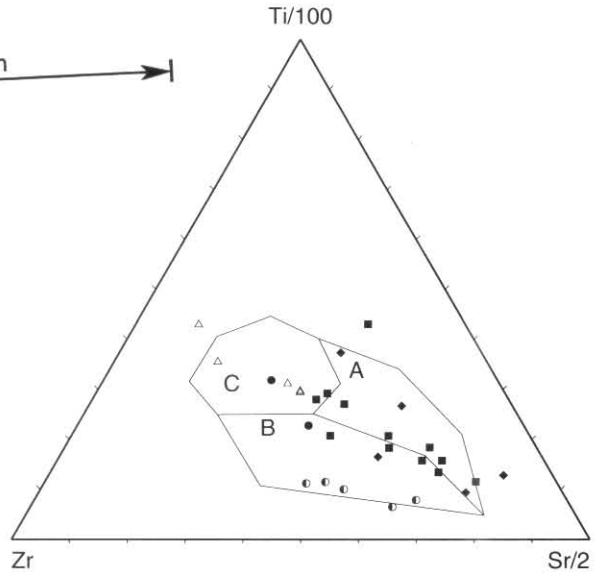

Figure 27. Zr–Ti–Sr discriminant diagram with fields from Pearce and Cann (1973). A is low-K tholeiite, B is calc-alkali basalt, C is ocean floor basalt. Symbols as for Figure 24 with the addition of calc-alkali rocks from the Mt Read Volcanics (◐). Only samples with 12% < CaO+MgO < 20% and lying outside the within plate field on Figure 26 have been plotted.

correlation between the Birchs Inlet Volcanics, Mainwaring Volcanics, Miners Ridge basalt of the Queenstown area and the low-Ti basalt of the Dundas Trough. A correlation is also indicated with gabbro and possible lava present in the mafic-ultramafic complex of the Point Hibbs Mélange Belt. The inclusion in this group of a mafic dyke from the Albina Creek area which intruded into sedimentary rocks interbedded with the Lucas Creek Volcanics, suggest that the correlation may extend to the Lucas Creek Volcanics. A single analysis of a basalt (41572, table 14) with TiO_2 of 0.38% from the Lucas Creek Volcanics was not analysed for REE, however, unpublished data of Crawford (Crawford, Corbett and Everard, 1992) indicates the presence of highly REE depleted tholeiites with TiO_2 contents less than 0.5% in the Lucas Creek Volcanics at Double Cove. The correlation of the Miners Ridge basalts with low-Ti basalt sequences in western Tasmania was considered by Crawford, Corbett and Everard (1992) but rejected because of the presence of TiO_2 rich rocks as well as TiO_2 poor ones in the Miners Ridge basalts. One sample (table 18, C3 in group 2) from the Miners Ridge basalt, which is richer in TiO_2 and REE than the others, appears not to belong to this group and so indicates that the Miners Ridge basalts include more than one magma type. Crawford Corbett and Everard (1992) correlate the Miners Ridge basalts with the Crimson Creek Formation basalts, however, none of the Crimson Creek Formation basalts have the very low TiO_2 values and LREE depleted pattern characteristic of most of the Miners Ridge basalts and other group 1 lavas.

The group 2 lavas show higher REE and TiO_2 values with an approximately flat REE pattern. The grouping suggests that there is a correlation between the Lucas Creek Volcanics, Mainwaring Volcanics, Henty Fault Wedge basalts, Henty Dyke Swarm basalts and Crimson Creek Formation basalts. The single Miners Ridge basalt sample, already discussed above, may also belong to this group though it is slightly richer in HREE than the other samples.

The pattern for the group 4 lavas differs only slightly from that of group 2 and supports a correlation between the Birchs Inlet Volcanics and the Mainwaring Volcanics.

Group 3 lavas show a LREE enrichment pattern and suggest a correlation between Sock Creek basalts and Henty Fault Wedge basalts. In spite of a sample of Crimson Creek Formation basalt and west coast south basalt having a similar

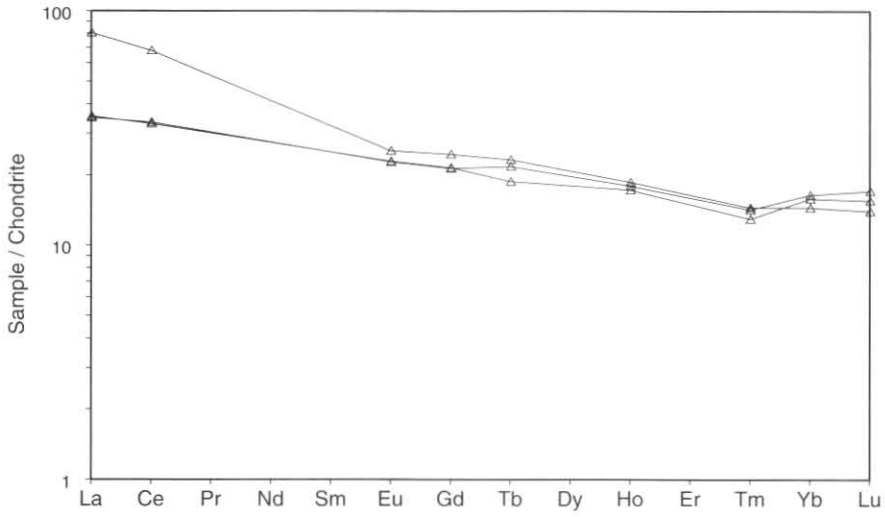

Figure 28. Chondrite-normalised REE patterns for the Crimson Creek basalts.

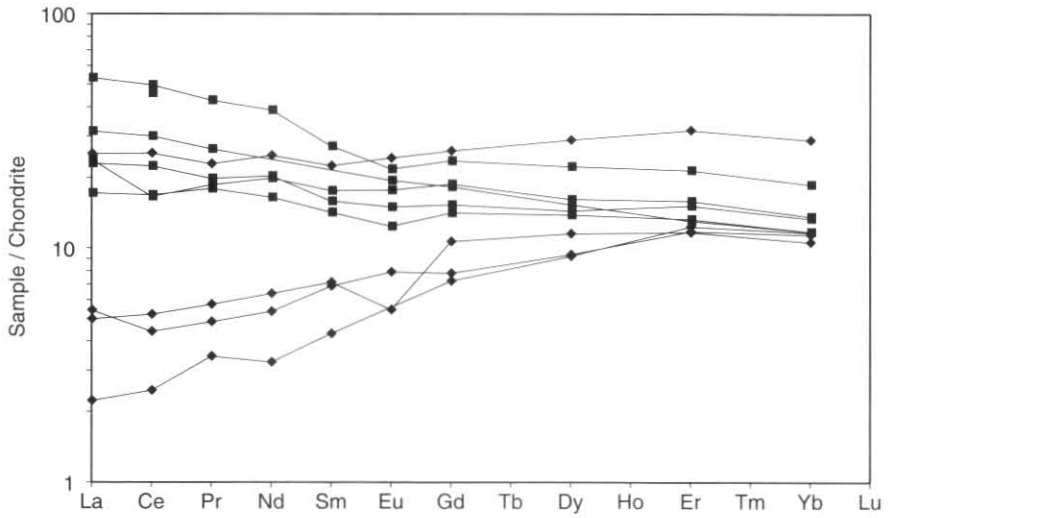

Figure 29. Chondrite-normalised REE patterns for the Miners Ridge basalts (◆) and Henty Fault Wedge basalts (■).

REE pattern they have much higher TiO_2 and Zr values with similar MgO values and so are unlikely to be correlates.

The sample from the mafic volcanic unit (€vv) of the Montgomery area has similar TiO_2 and Zr values to the Sock Creek and Henty Fault Wedge basalts and so may be a correlate.

The group 5 lavas have low REE values similar to those for the group 1 lavas but don't show the LREE depletion of the group 1 lavas. This grouping links the high-Mg andesites of the Dundas Trough and the Timbertops area with lavas in the Mainwaring Volcanics.

It is clear from these groupings that most of the major rock units include several REE patterns indicating that they were produced by more than a single magma type. The Mainwaring Volcanics are noteworthy for including samples from four of the five groups. Crawford, Corbett and Everard (1992) suggested that the Henty Dyke Swarm and the Henty Fault Wedge tholeiitic rocks are comagmatic, however, the linking of two of the Henty Fault Wedge rocks to the Sock Creek rocks rather than the other Henty Fault Wedge and Henty Dyke Swarm rocks on the basis of REE pattern suggests that more than one magma type is present.

MINOR IGNEOUS ROCK GROUPS

M. P. McClenaghan

Classification and correlation

The west coast basalts north and south have a different composition from the Lucas Creek Volcanics as is indicated by their position on the Zr–Ti–Y diagram (fig. 49) where they plot closer to the field of the Noddy Creek Volcanics than to the field of the Lucas Creek Volcanics. The two samples from the northern basalts have Y/Nb ratios of 0.57 and 0.56 which indicate that they are alkalic (see Pearce and Cann, 1973) whereas all other basalts from the area have ratios greater than 1 indicating a tholeiitic character. The REE pattern (fig. 50) shows LREE enrichment and greater total REE content than the Lucas Creek Volcanics. This pattern is similar to that of the calc-alkaline Noddy Creek Volcanics.

Two samples (MH10, MH39) of fine-grained rock of andesite and rhyolite chemical composition (€ti) from the Point Hibbs Mélange Belt plot in the same area as the calc-alkaline Noddy Creek Volcanics on the Zr–Ti–Y diagram (fig. 51). This suggests that they are part of the Noddy Creek Volcanics that have been faulted into the mélange belt. A single sample (41521) from the schistose

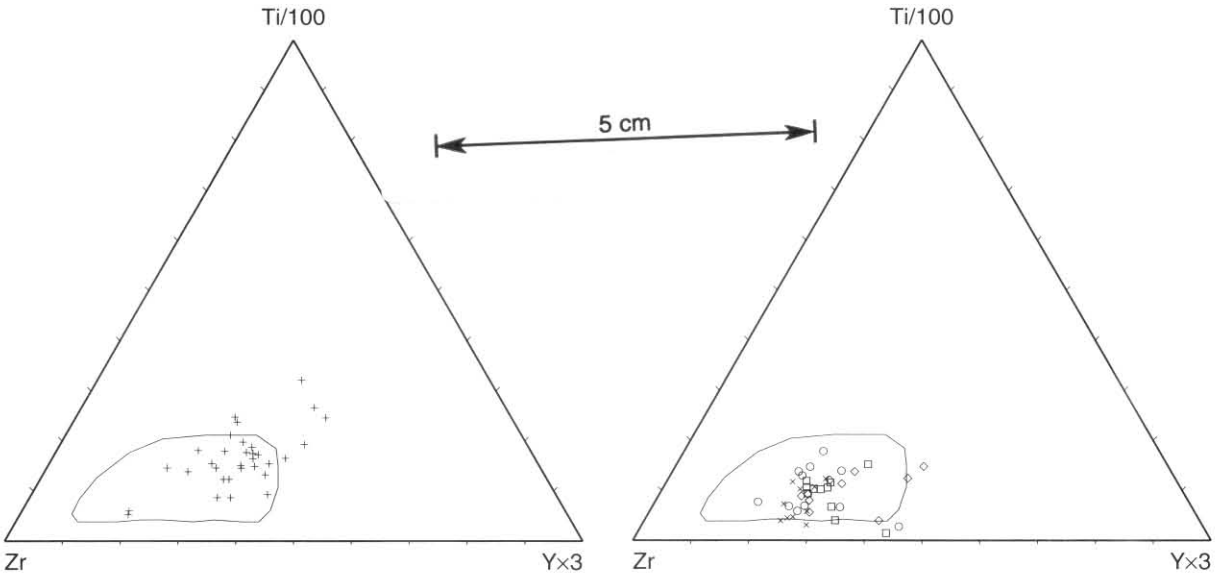

Figure 30. Zr–Ti–Y diagram with field for the Noddy Creek Volcanics taken from Figure 15. Noddy Creek Volcanics correlates in the Montgomery area (+).

Figure 32. Zr–Ti–Y diagram with field for the Noddy Creek Volcanics taken from Figure 15. Calc-alkaline Mt Read Volcanics with western sequence (◇), southern central volcanic complex rocks (×), northern central volcanic complex rocks (□) and Que–Hellyer rocks (○).

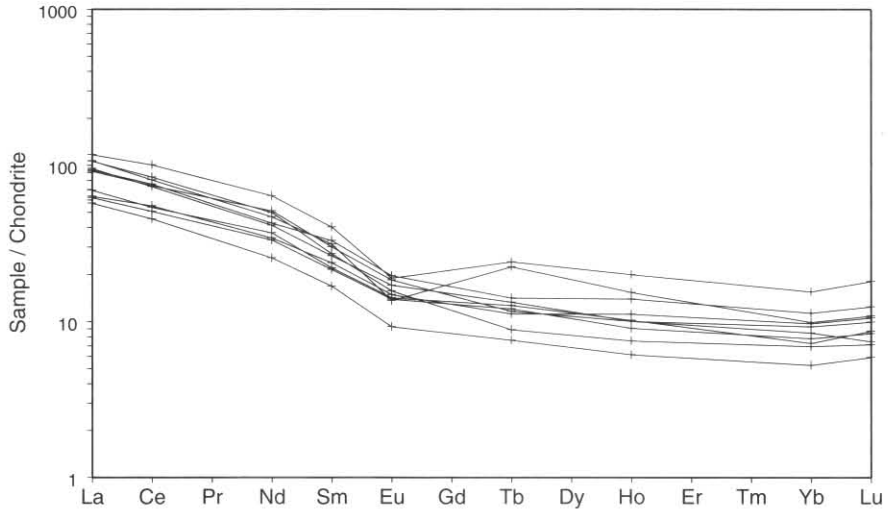

Figure 31. Chondrite-normalised REE patterns for Noddy Creek Volcanics correlates in the Montgomery area.

possible tuff or lava unit (Ctc) also plots in the Noddy Creek Volcanics field and probably also belongs to this group. Another sample from the Ctc rock unit (MH501) has a different character and has low REE content (see fig. 54) with slight depletion of LREE which is quite different from the greater REE content and LREE enrichment of the Noddy Creek Volcanic calc-alkaline rocks. This pattern is similar to that of low-Ti basalts described from the Dundas Trough (Brown, 1986).

A Zr–Ti–Y plot (fig. 53) of gabbro samples from the Point Hibbs Mélange Belt show that most samples plot in the area of tholeiitic rocks whereas one sample (MH289) plots in the calc-alkaline area. This sample came from a gabbro unit on the eastern side of the belt [CP696045] adjacent to the Noddy Creek Volcanics and so it is possible that it is rock from that unit that has been faulted into the belt.

REE patterns for two of the gabbro samples (see fig. 54) are low in total REE content and LREE depletion for one sample (MH520) (some LREE below detection limits) with the other sample (MH517) having an almost flat pattern for LREE and slight HREE enrichment also with low total REE. These patterns are quite different from those of the calc-alkaline rocks and the pattern of MH520 resembles that for low-Ti basalts whereas that for MH517 is similar to high-Mg andesite or boninite from the Dundas Trough (Brown, 1986). However, the mineralogy and major element composition of MH517 is inconsistent with it being a boninite.

Two samples of mafic probable lavas (Ctm; table 14, 41543, 41546) from the Timbertops area have chemical compositions resembling boninites, as indicated by their high SiO_2, MgO, Cr, and Ni contents and their concave to LREE enriched REE patterns (fig. 55). They also have low abundances of high field strength elements and contain Cr-rich spinel (see fig. 56). They resemble boninitic lavas described from the Dundas Trough farther north (fig. 52; Brown, 1986).

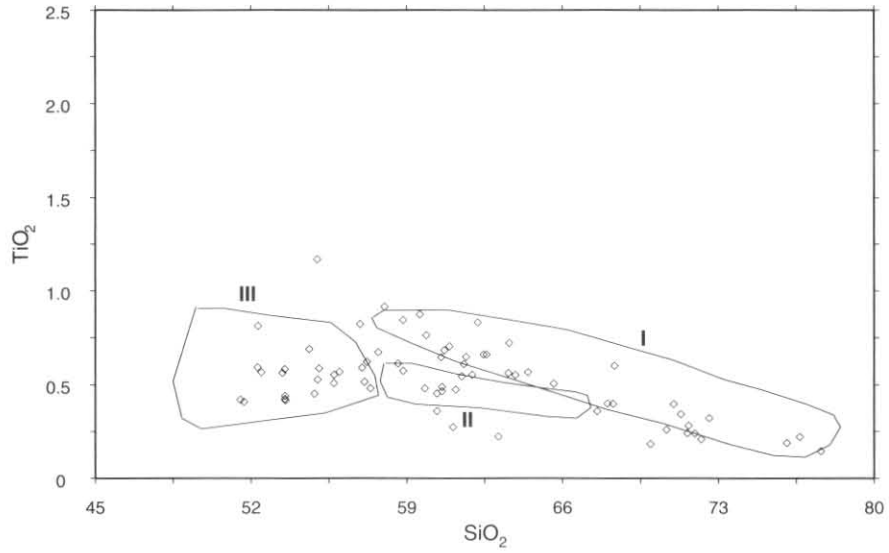

Figure 33. SiO_2-TiO_2 diagram for the Noddy Creek Volcanics and their correlation in the Montgomery area. Fields for suites I – III from Crawford *et al.* (1992) indicated.

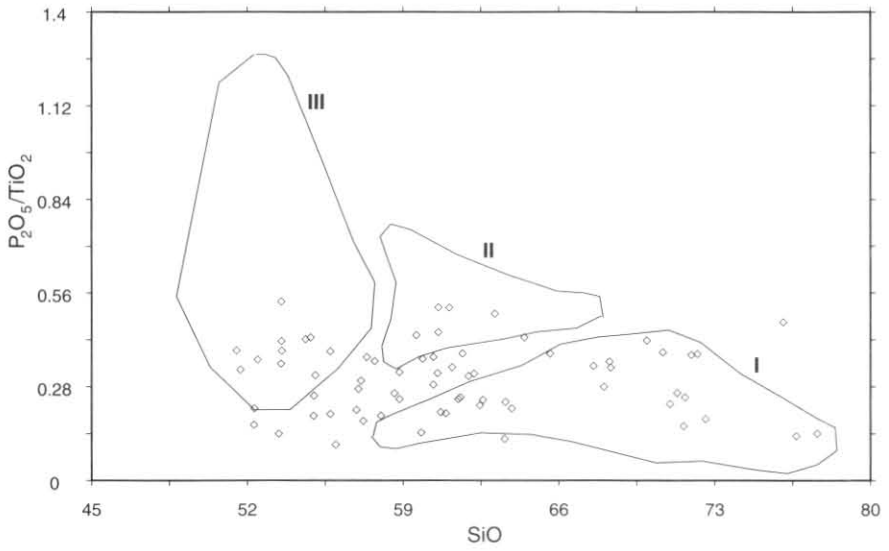

Figure 34. SiO_2-P_2O_5/TiO_2 diagram for the Noddy Creek Volcanics and their correlation in the Montgomery area. Fields for suites I – III from Crawford *et al.* (1992) indicated.

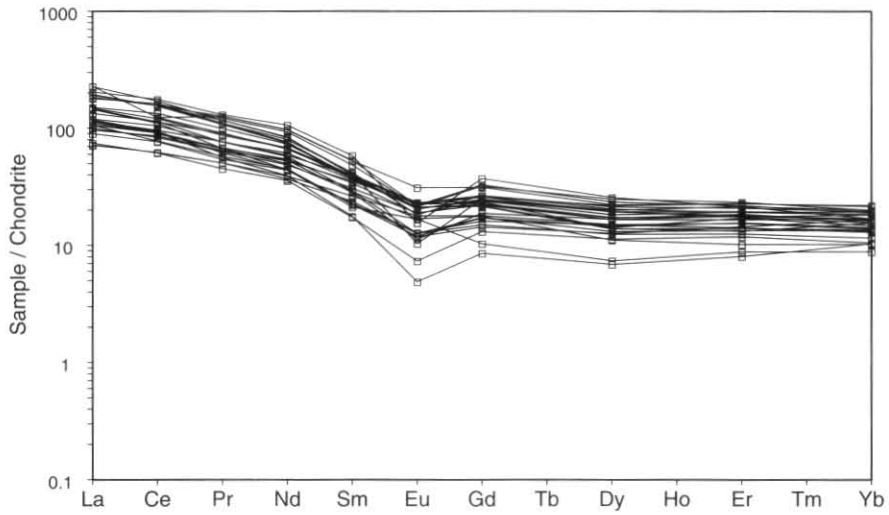

Figure 35. Chondrite-normalised REE patterns for suite I rocks form Crawford *et al.* (1992).

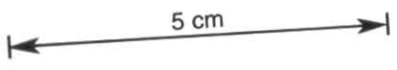

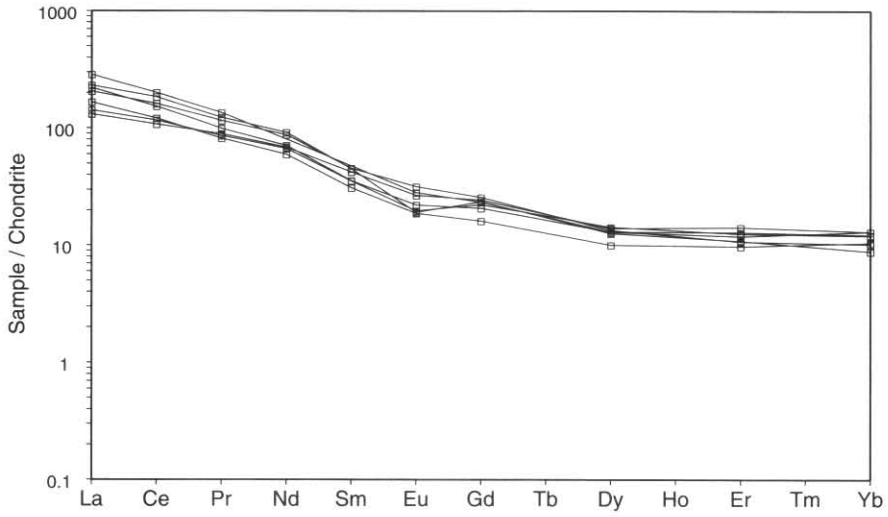

Figure 36. Chondrite-normalised REE patterns for suite II rocks form Crawford *et al.* (1992).

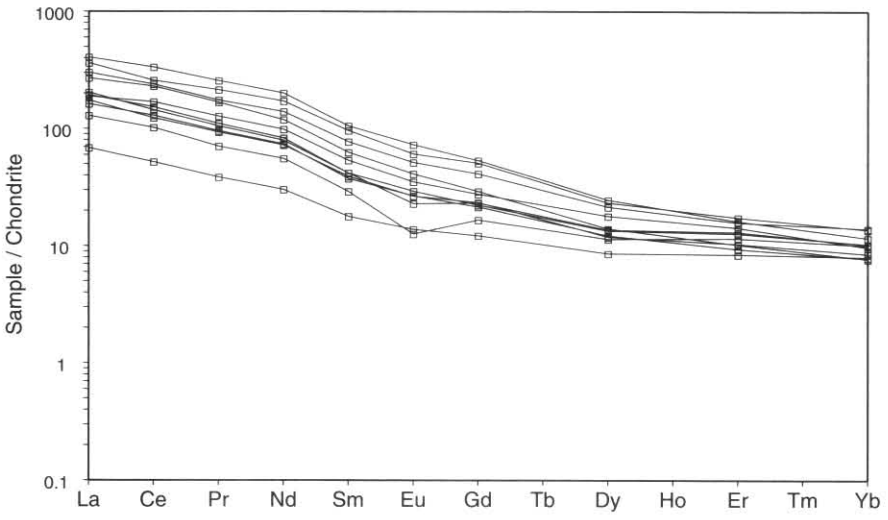

Figure 37. Chondrite-normalised REE patterns for suite III rocks form Crawford *et al.* (1992).

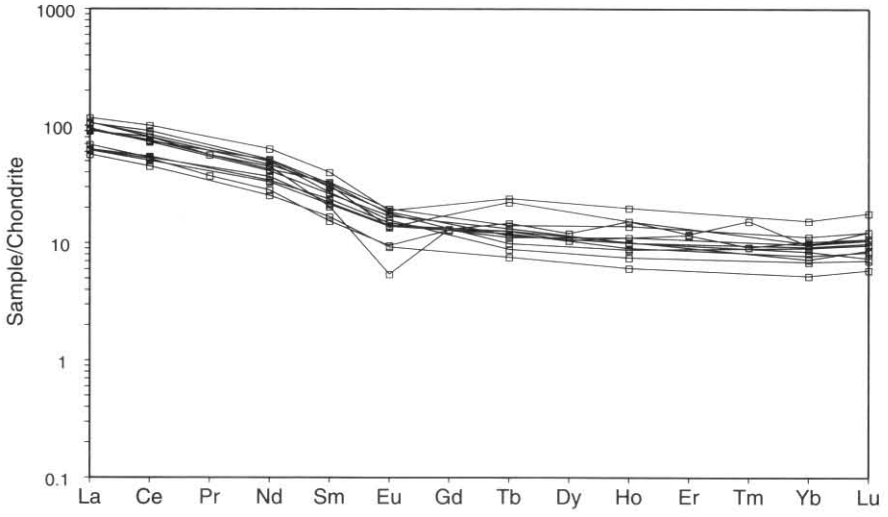

Figure 38. Chondrite-normalised REE patterns for Noddy Creek Volcanics and their correlates in the Montgomery area. Key to symbols given in Table 18.

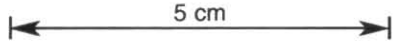

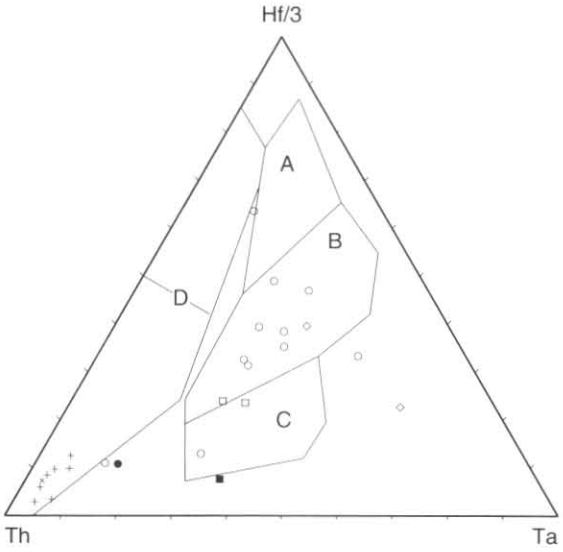

Figure 39. Ta–Hf–Th discriminant diagram with fields from Wood (1980). A is N-type MORB, B is E-type MORB and tholeiitic within plate basalts and differentiates, C is alkaline within plate basalts and differentiates and D is destructive plate-margin basalts and differentiates. Symbols as for Figure A. with in addition west coast basalt south (■) and west coast basalt north (●).

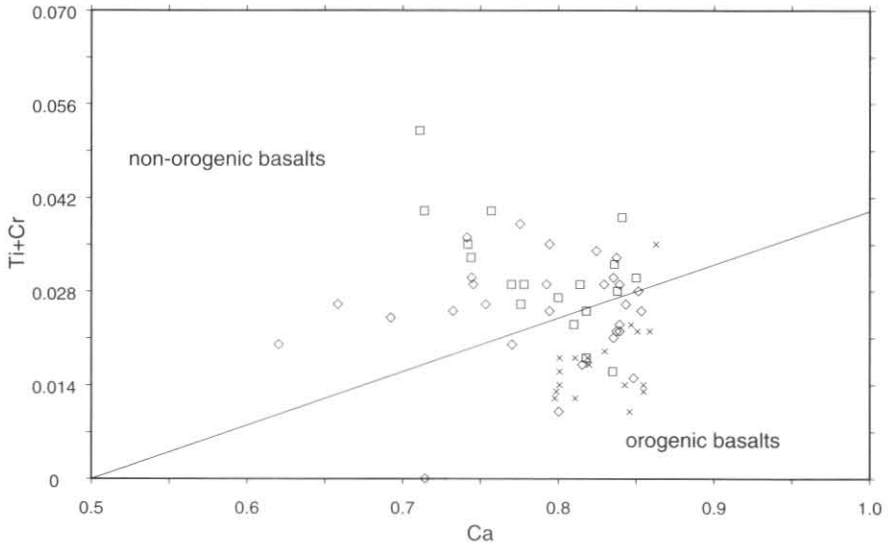

Figure 40. Ca–Ti+Cr discriminant diagram for pyroxene compositions. Fields from Leterrier *et al.* (1982). Lucas Creek Volcanics (□), Birchs Inlet Volcanics (◇) and Noddy Creek Volcanics (×).

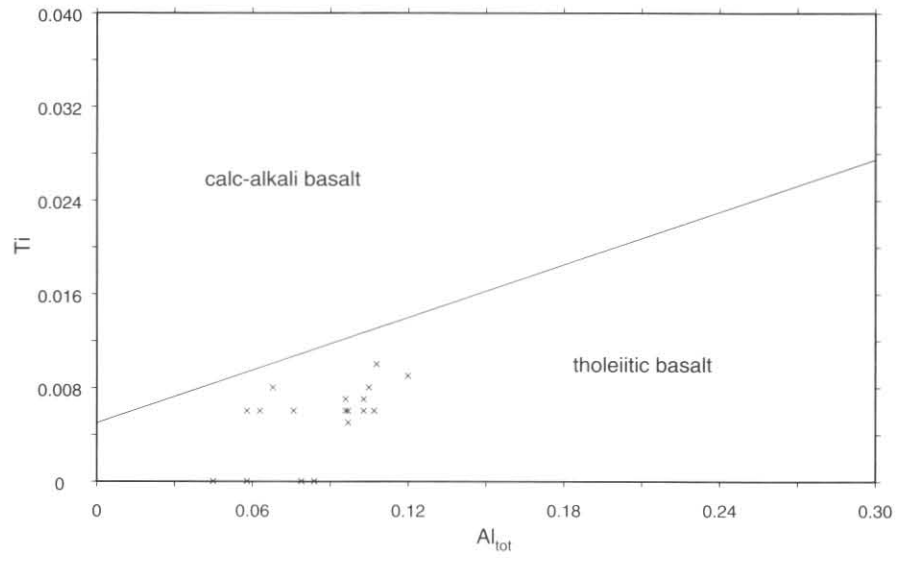

Figure 41. $Al_{(total)}$–Ti discriminant diagram for pyroxene compositions. Fields from Leterrier *et al.* (1982). Noddy Creek Volcanics (×).

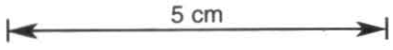

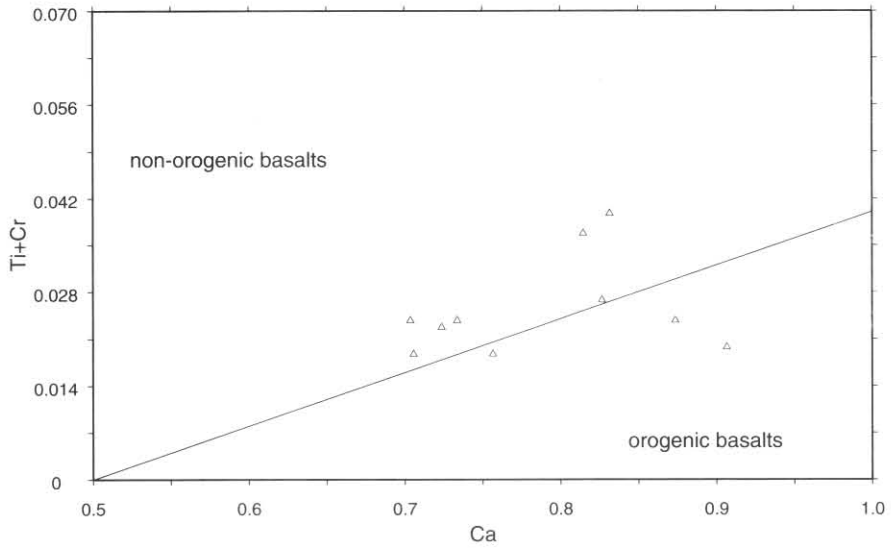

Figure 42. Ca–Ti+Cr discriminant diagram for pyroxene compositions. Fields from Leterrier *et al.* (1982). Crimson Creek basalts as triangles.

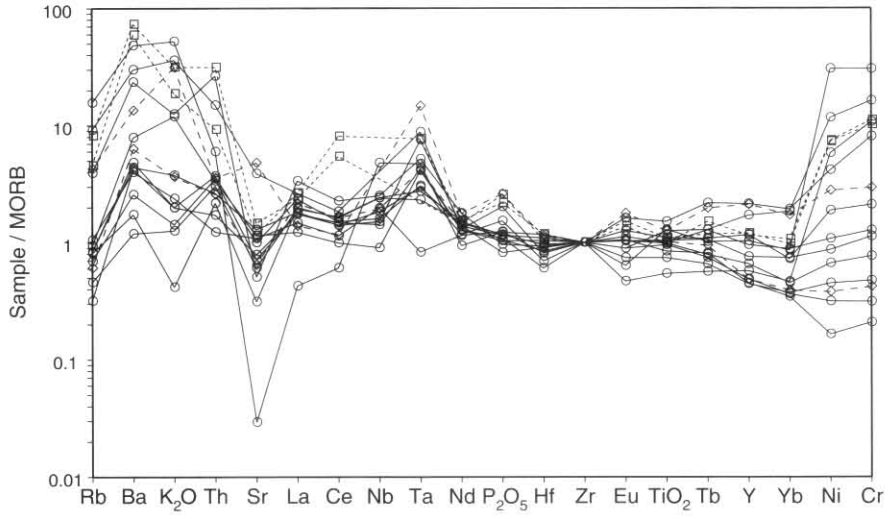

Figure 43. Multi-element diagram. Lucas Creek Volcanics (□), Birchs Inlet Volcanics (◇) and Mainwaring Volcanics from the Montgomery area (○). Compositions have been normalised to give constant Zr levels inorder to partly eliminate the effects of low pressure fractionation.

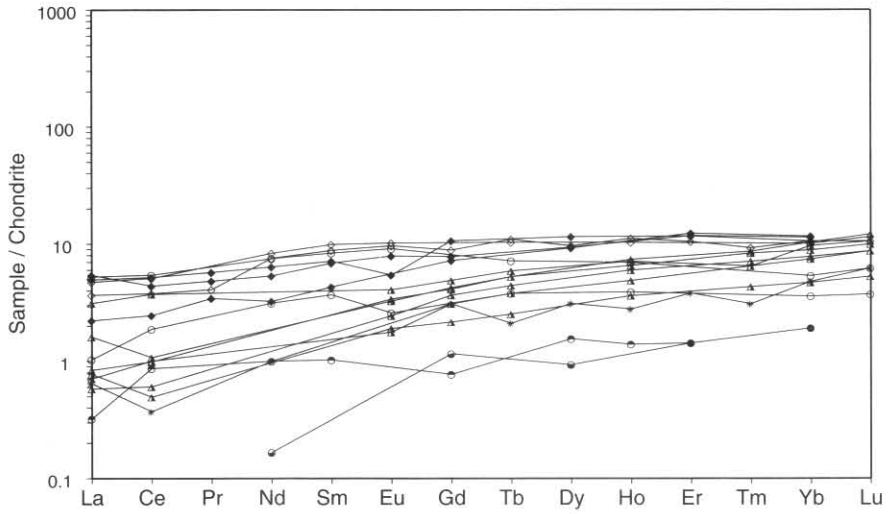

Figure 44. Chondrite-normalised REE patterns for group 1 non calc-alkaline igneous rocks from western Tasmania. Key to symbols given in Table 18.

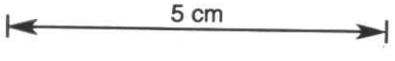

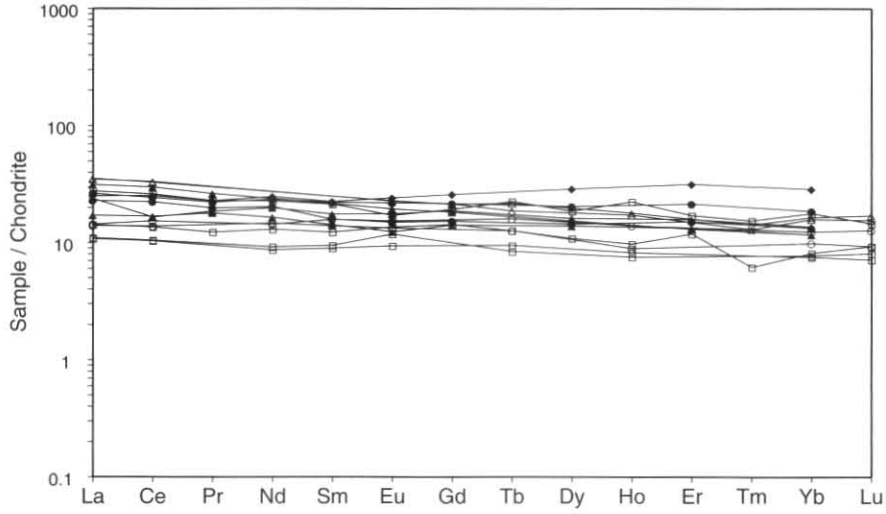

Figure 45. Chondrite-normalised REE patterns for group 2 non calc-alkaline igneous rocks from western Tasmania. Key to symbols given in Table 18.

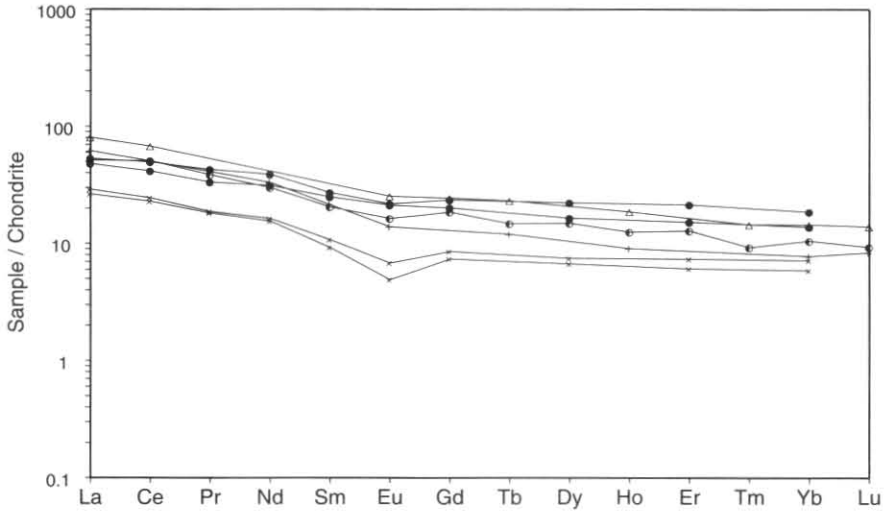

Figure 46. Chondrite-normalised REE patterns for group 3 non calc-alkaline igneous rocks from western Tasmania. Key to symbols given in Table 18.

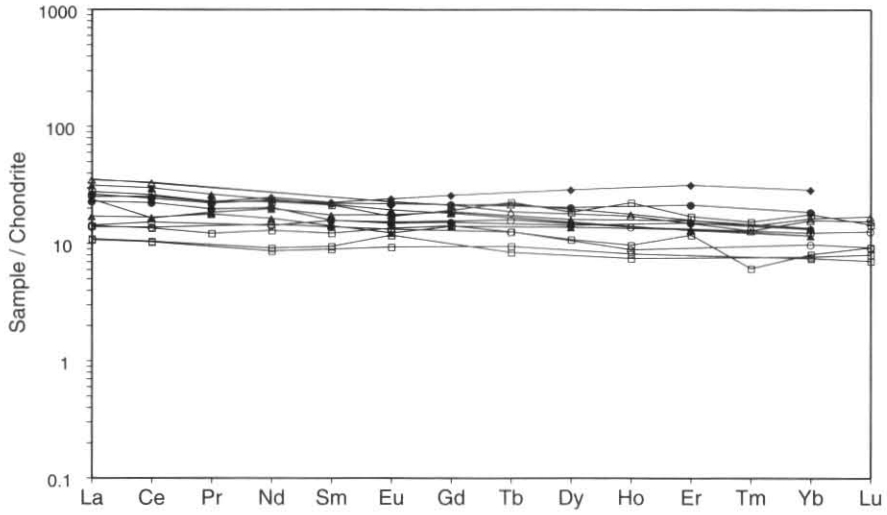

Figure 47. Chondrite-normalised REE patterns for group 4 non calc-alkaline igneous rocks from western Tasmania. Key to symbols given in Table 18.

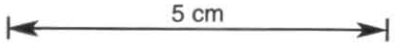

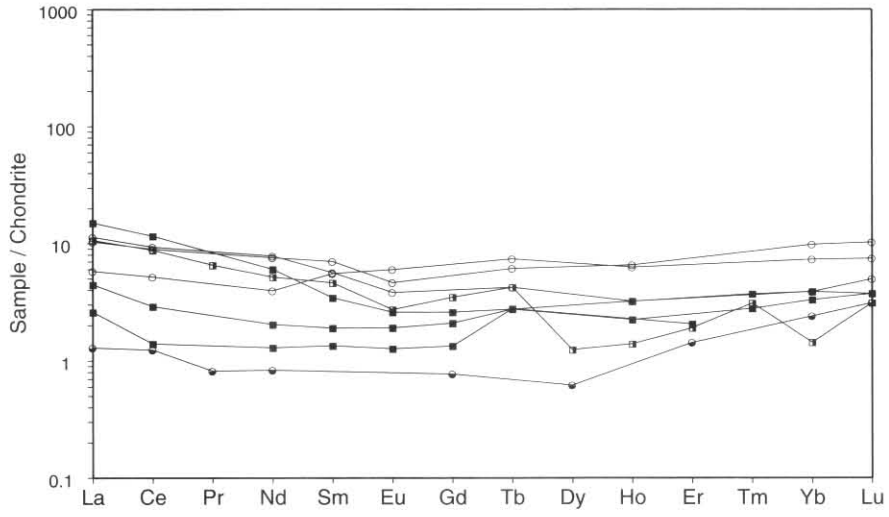

Figure 48. Chondrite-normalised REE patterns for group 5 non calc-alkaline igneous rocks from western Tasmania. Key to symbols given in Table 18.

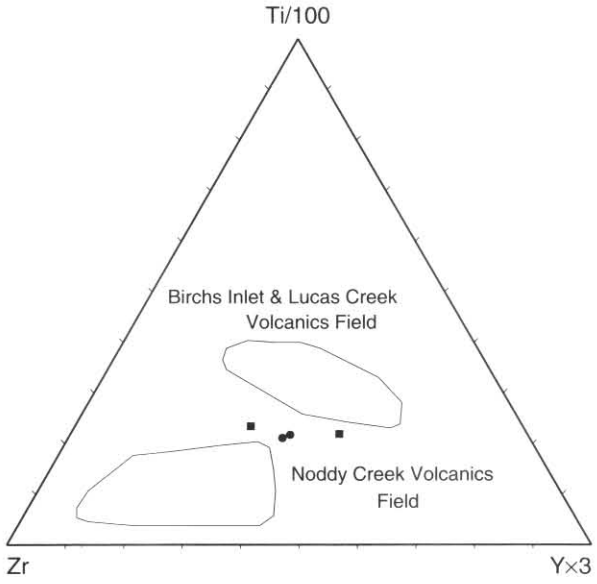

Figure 49. Zr–Ti–Y diagram with fields for Birchs Inlet/Lucas Creek Volcanics and Noddy Creek Volcanics taken from Figure 15. West Coast basalt north (●) and West Coast basalt south (■).

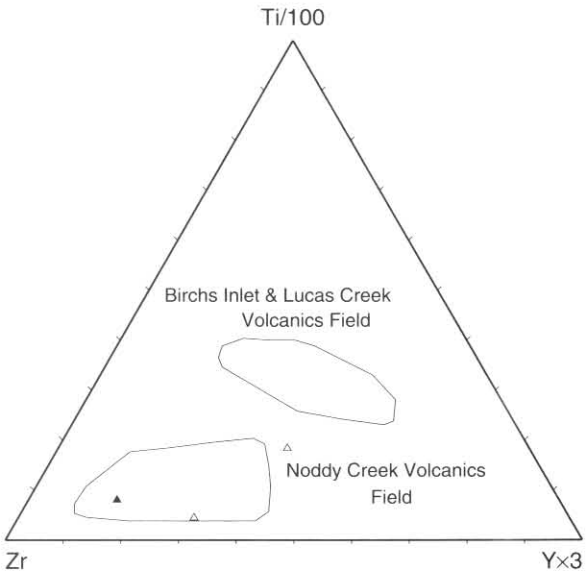

Figure 51. Zr–Ti–Y diagram with fields for Birchs Inlet/Lucas Creek Volcanics and Noddy Creek Volcanics taken from Figure 15. Fine-grained andesite and rhyolite (Ꞓti) (△) and schistose possible tuff or lava (Ꞓtc) (▲).

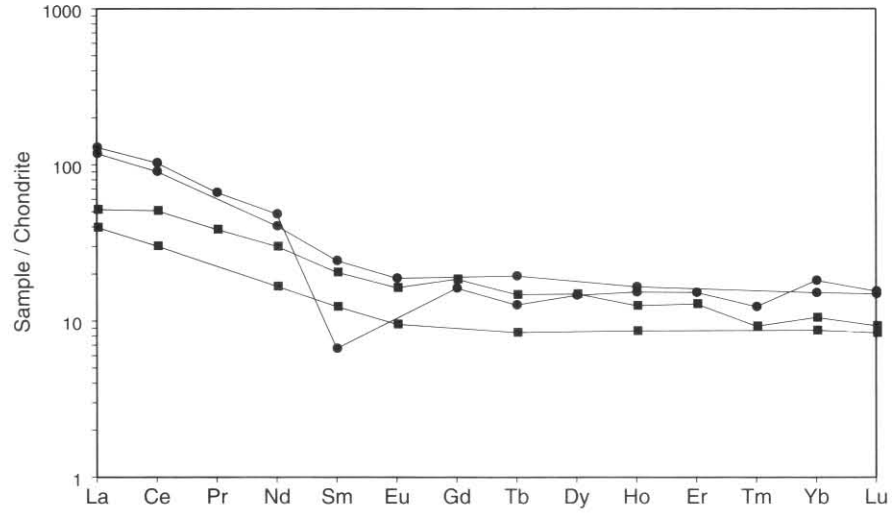

Figure 50. Chondrite-normalised REE patterns for the west coast basalt north (●) and west coast basalt south (■).

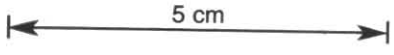

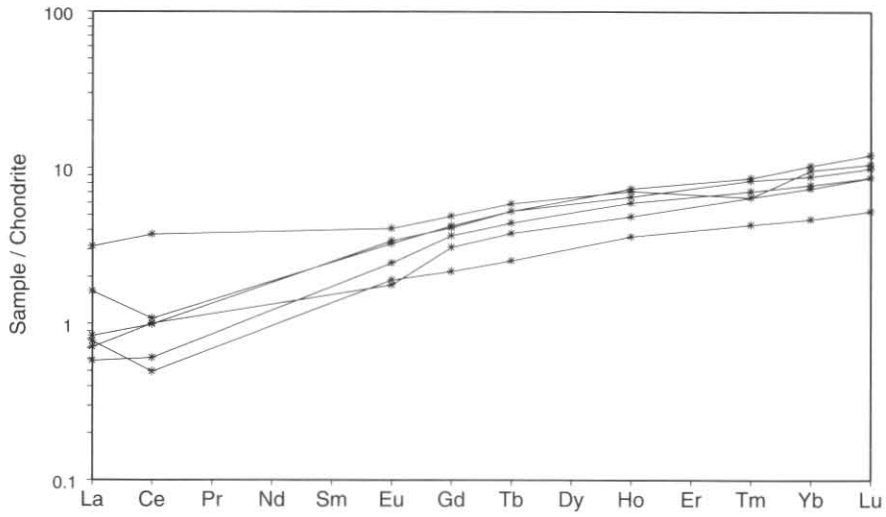

Figure 52. Chondrite-normalised REE patterns for low-Ti basalts from the Dundas Trough (Brown, 1986).

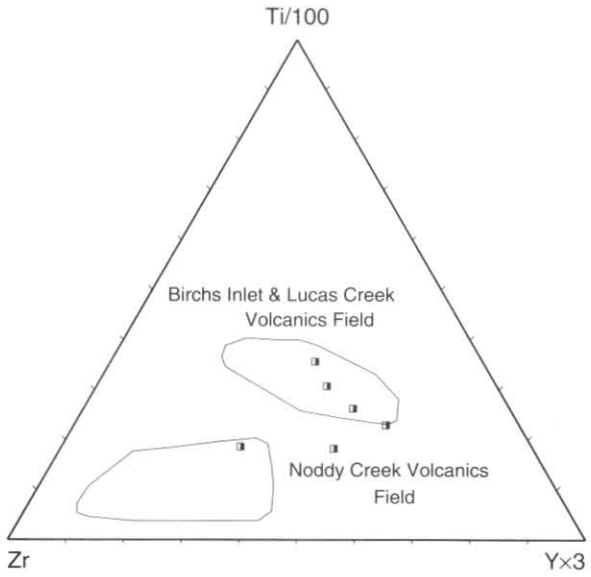

Figure 53. Zr–Ti–Y diagram with fields for Birchs Inlet/Lucas Creek Volcanics and Noddy Creek Volcanics taken from Figure 15. Gabbro (Ꞓg) samples from the Hibbs Mélange Belt.

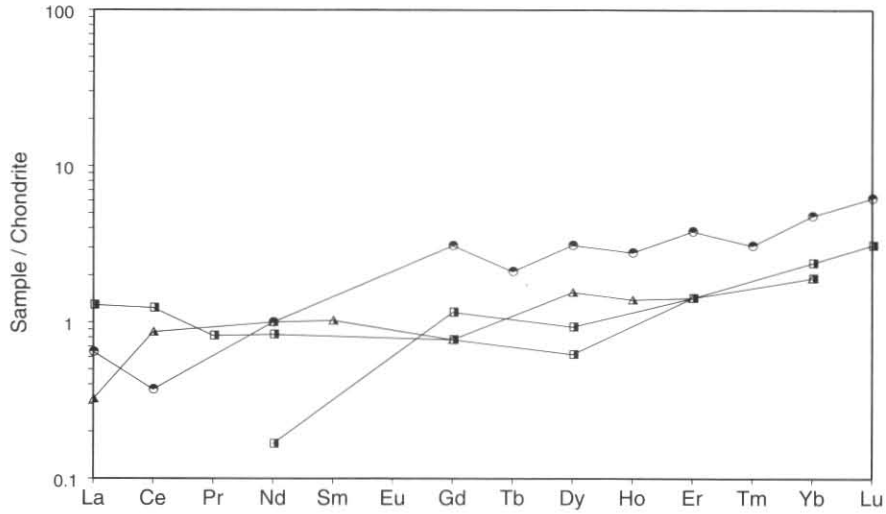

Figure 54. Chondrite-normalised REE patterns for schistose possible tuff or lava (Ꞓtc) (▲) and gabbro (Ꞓg) (◨) from the Hibbs Mélange Belt. High Mg mafic dyke (Ꞓbd) from the Albina Creek area (◓).

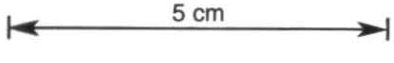

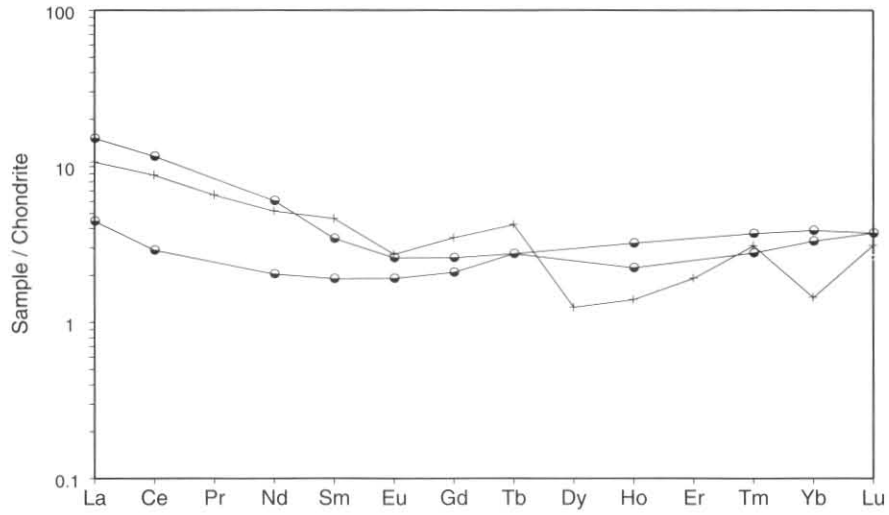

Figure 55. Chondrite-normalised REE patterns for mafic probable lava (Ctm) (+) and boninitic lavas from the Dundas Trough (Brown, 1986) (◒).

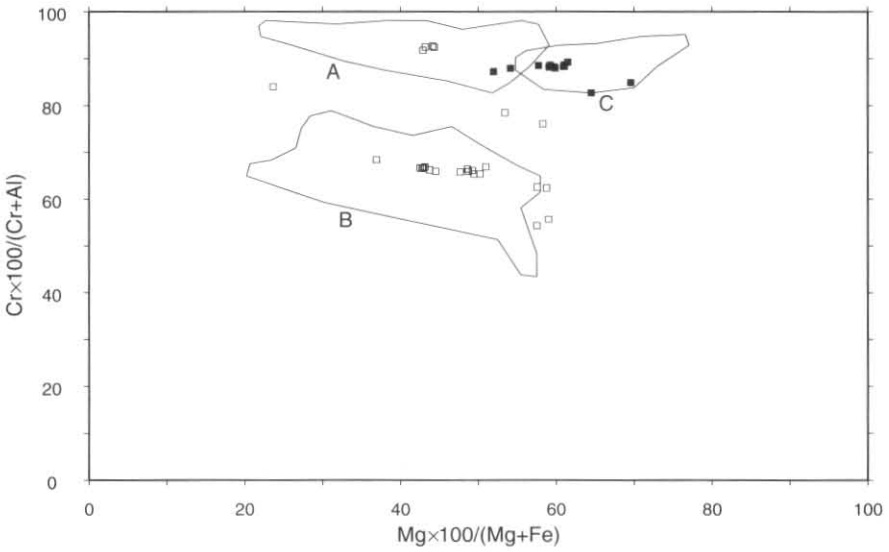

Figure 56. (Cr×100)/(Cr+Al)–(Mg×100)/(Mg×100)/(Mg+Fe^{2+}) diagram with spinels from the mafic probable lavas (Ctm)(■) and spinels from the serpentinised pyroxenite (□). Field A is for the layered dunite-harzburgite succession (LDH), field B for the layered pyroxenite-dunite succession (LPD) and field C is for high-Mg andesite or boninite from the Dundas Trough (Brown, 1986).

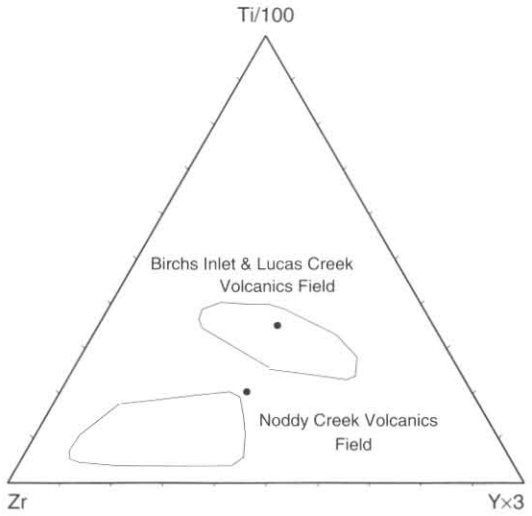

Figure 57. Zr–Ti–Y diagram with fields for Birchs Inlet/Lucas Creek Volcanics and Noddy Creek Volcanics taken from Figure 15. Basalt (Ctba) in the mudstone/lithicwacke succession (Ctl) near CN710948.

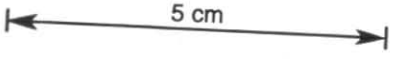

Table 18. GROUPING OF WESTERN TASMANIAN NON CALC-ALKALINE IGNEOUS ROCKS BASED ON REE COMPOSITION

ROCK UNIT AND PLOT SYMBOL	GROUP 1	GROUP 2	GROUP 3	GROUP 4	GROUP 5
Birchs Inlet Volcanics (◇)	MH194B 41508			MH193	
Lucas Creek Volcanics (□)		MH101 MH104 MH177 41575			
Mafic dyke, Albina Creek area (✳)	MH552				
Gabbro, Point Hibbs Mélange Belt (◒)	MH520				
Possible lava, Point Hibbs Mélange Belt (◓)	MH501				MH517
West coast basalt, south (◐)			MH163		
Mafic probable lava Timbertops area (◨)					41543
Mainwaring Volcanics (Evv) from the Montgomery area (Brown, in prep.) (○)	883674 873019	873017 873036		883703 873035 873018 883702	873008 873006 873009
Mafic volcanic rock (Ɛvv) from the Montgomery area (Brown, in prep.) (+)			883686		
Low-Ti basalt, Dundas Trough (Brown and Jenner,1989) (▲)	60903 60919 60900 850032 850033 850034				
Miners Ridge Basalts (Crawford, Corbett and Everard, 1992) (◆)	W64 LE196 C2	C3			
Henty Fault Wedge (Crawford, Corbett and Everard, 1992) (●)		HR126 206	1984/11 225		
Henty Dyke Swarm (Crawford, Corbett and Everard, 1992) (▲)		R8 STP234 R195			
Sock Creek (Crawford, Corbett and Everard, 1992) (×)			Z7250 Z7247		
Crimson Creek Formation (Brown, 1986) (△)		C302 C447(i)	C313		
High-Mg andesite (Brown and Jenner, 1989) (■)					850028 850023 850025

A single sample (MH552) of a high Mg mafic dyke from the west coast shows low abundances of high field strength elements and strong depletion of the LREE (see fig. 54). These characteristics are similar to low-Ti basalts described from the Dundas Trough (Brown, 1986; fig. 52) though this sample is richer in MgO and Ni and so must have a more primitive composition.

Two samples from a small area of basalt present in the mudstone/lithicwacke succession near CN710948 plot in different positions on the Zr–Ti–Y diagram (fig. 57) with one sample falling in the calc-alkaline area and the other in the tholeiitic field.

STRUCTURAL GEOLOGY

Proterozoic rocks

LIBERTY POINT TO GORGE POINT AREA

R. H. Findlay

This region (fig. 58) has been affected by a minimum of four fold events of which generally two or three are evident in most outcrops. These structures are overprinted by a subsequent cleavage which follows the orientation of the axial plane cleavage seen in the post-Ordovician Timbertops Syncline in the southern part of the Sorell Peninsula. Also present are numerous joints which have not been studied in detail. Faults have been inferred from the interpretation of aerial photographs; and these Proterozoic rocks are also thrust along a flat-lying fault over the Cambrian sequence.

Within the quartzitic beds, cross-bedding permits construction of a regional form-line map of bedding, and which highlights the complex nature of the folding in the region. Additional regional structural data have been gained from interpretation of aerial photographs of the peninsula, and the two sets of data have been combined to form the form-line map of Figure 58.

This map highlights:

(1) large-scale refolded isoclinal folds to the north and west of the Betsys Bay region (fig. 58; Domain 1);

(2) large-scale variably plunging NW- to NE-trending upright to asymmetric folds between Betsys Bay and Liberty Creek (fig. 58, Domains 4 and 5);

(3) large-scale warps of the folds outlined in (2) across steeply dipping W-trending axial surfaces.

Locally, the structural geology is invariably complex, with a minimum of two cleavage-forming events being recognisable in pelitic units, and, less commonly, a maximum of four folding events at some localities. The nature of the low-grade metamorphism during these events makes difficult the tracking of cleavages between the isolated inland outcrops; this problem is compounded by considerations concerning the possible effects of strain partitioning on the recognition of cleavages according to their local morphology.

The interpretation of the geological structure outlined below depends principally on a relatively few key exposures within the six structural domains which make up the region. Of importance to the structural correlation between these domains is the recognition of the different types of

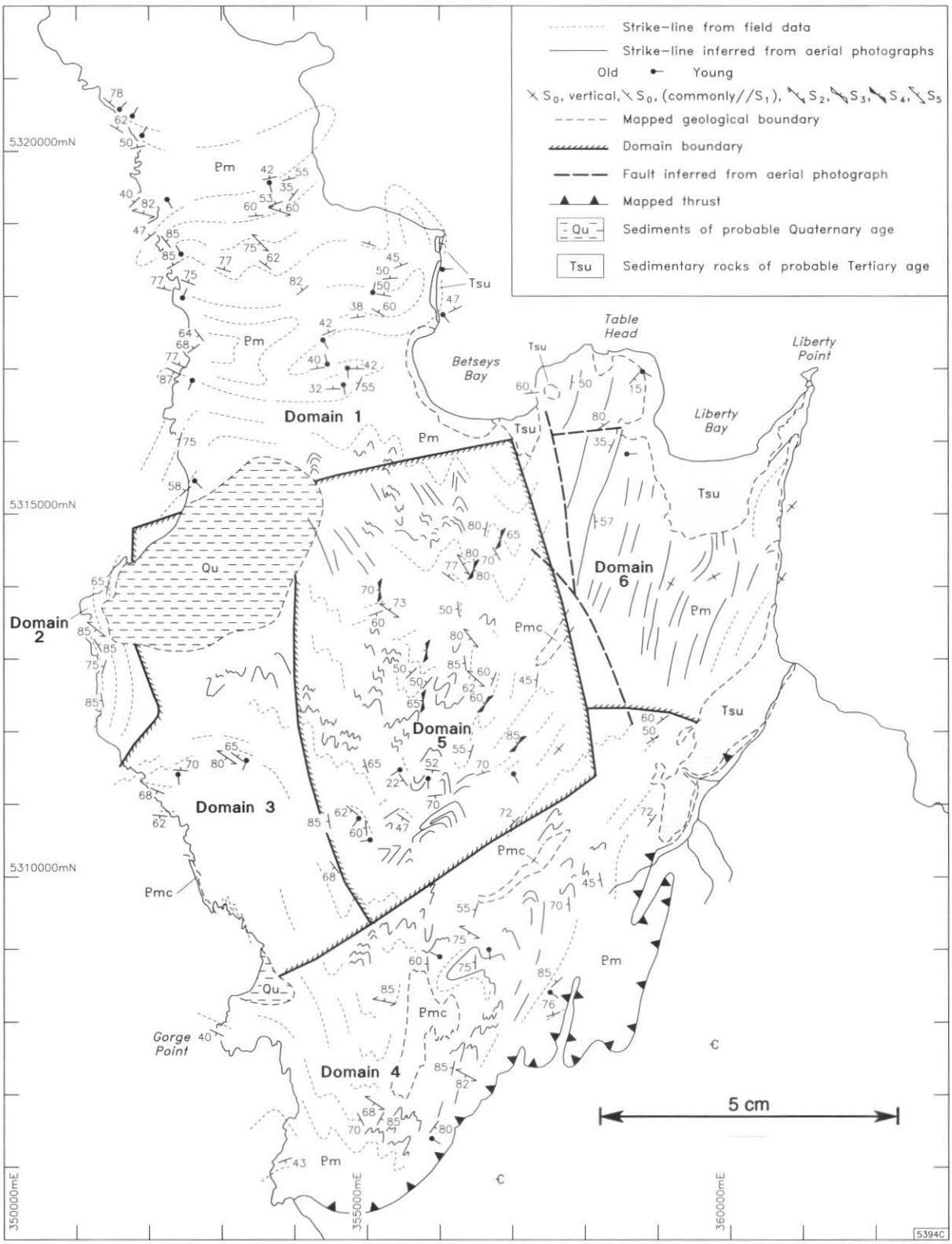

Figure 58. Domain map of Proterozoic rocks of the Sorell Peninsula.

interference pattern generated by the cross-folding observed at the key localities. In summary, five deformational events are recognised, as outlined below:

D_1 produced a low-grade metamorphic differentiation layering (S_1) in pelitic beds and a schistosity in quartzites, during isoclinal folding (F_1) which led to partial transposition of bedding.

D_2 produced large-scale isoclinal folds (F_2) in Domain 1 (fig. 58), but these folds are less dominant further south. An S_2 crenulation cleavage was also developed and may be observed in pelitic beds.

D_3 also produced isoclinal structures (F_3) which are recognised principally in the regions occupied by Domains 2, 3, 5 and 6 (fig. 58); these folds were accompanied by formation of a crenulation cleavage, again best developed in pelitic rocks.

D_4 produced generally upright N-trending folds (F_4) on a regional scale, although F_4 folds are much more open in Domain 1 (fig. 58) than elsewhere. A variably-developed steeply W-dipping crenulation cleavage was also produced. Interference between mesoscopic F_2 and F_4 folds has produced Type 3 interference patterns,

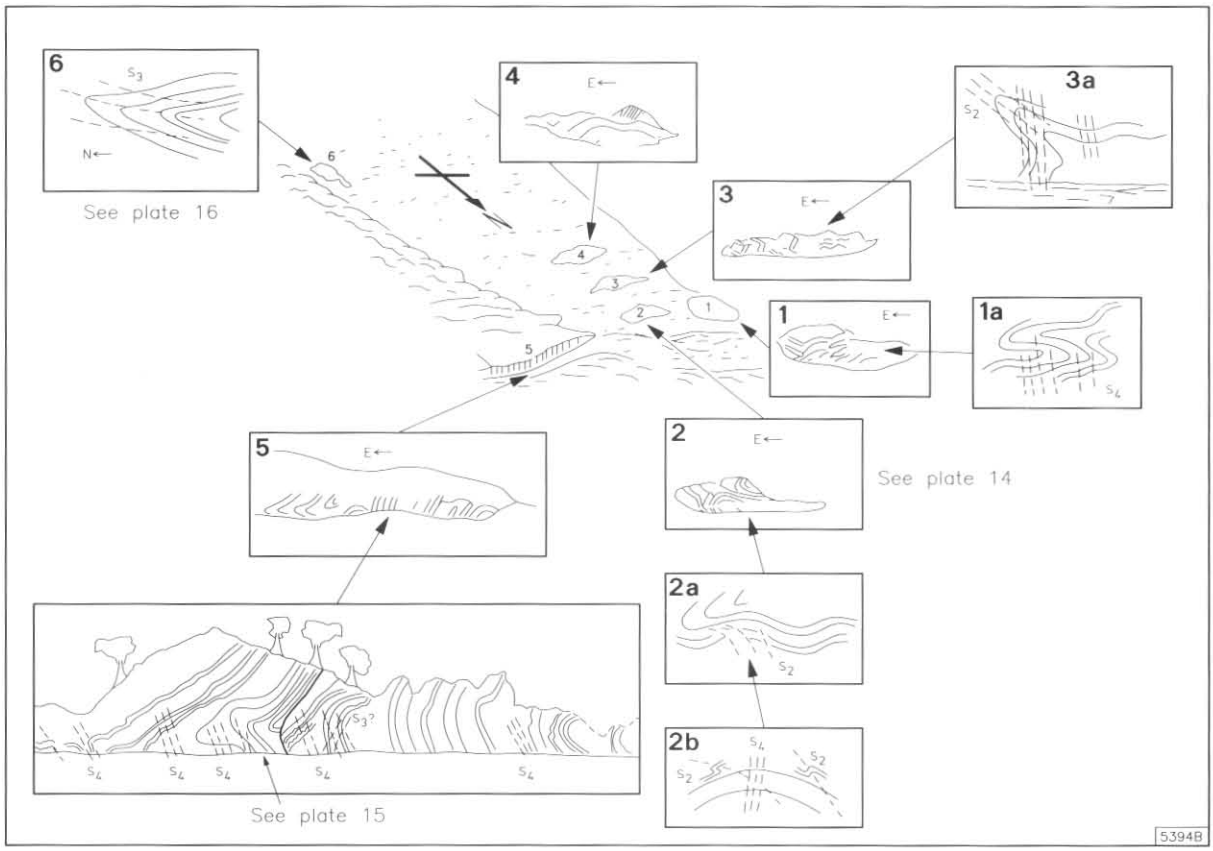

Figure 59. Outcrop data for beach outcrop at CP535090. See text for full explanation.

Plate 14. F_2 folds at outcrop 2, view to south. The reclined and recumbent F_2 folds here close to the east and west and are cross-folded by upright N-trending F_4 warps.

Plate 16. Recumbent N-closing F_3 fold forming outcrop 6 at CP535090. Note collapse of fold hinge, thickening of pelitic beds at fold hinge, and strong axial plane cleavage. View down plunge.

Plate 15. F_2 folds at outcrop 5. View down plunge.

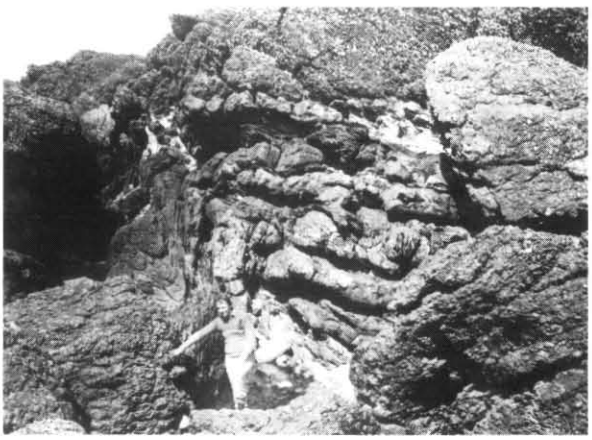

Plate 17. Outcrop at CP515103 showing massive conglomerate and sandstone horizons folded by asymmetric SSW-plunging F_4 fold. View down plunge.

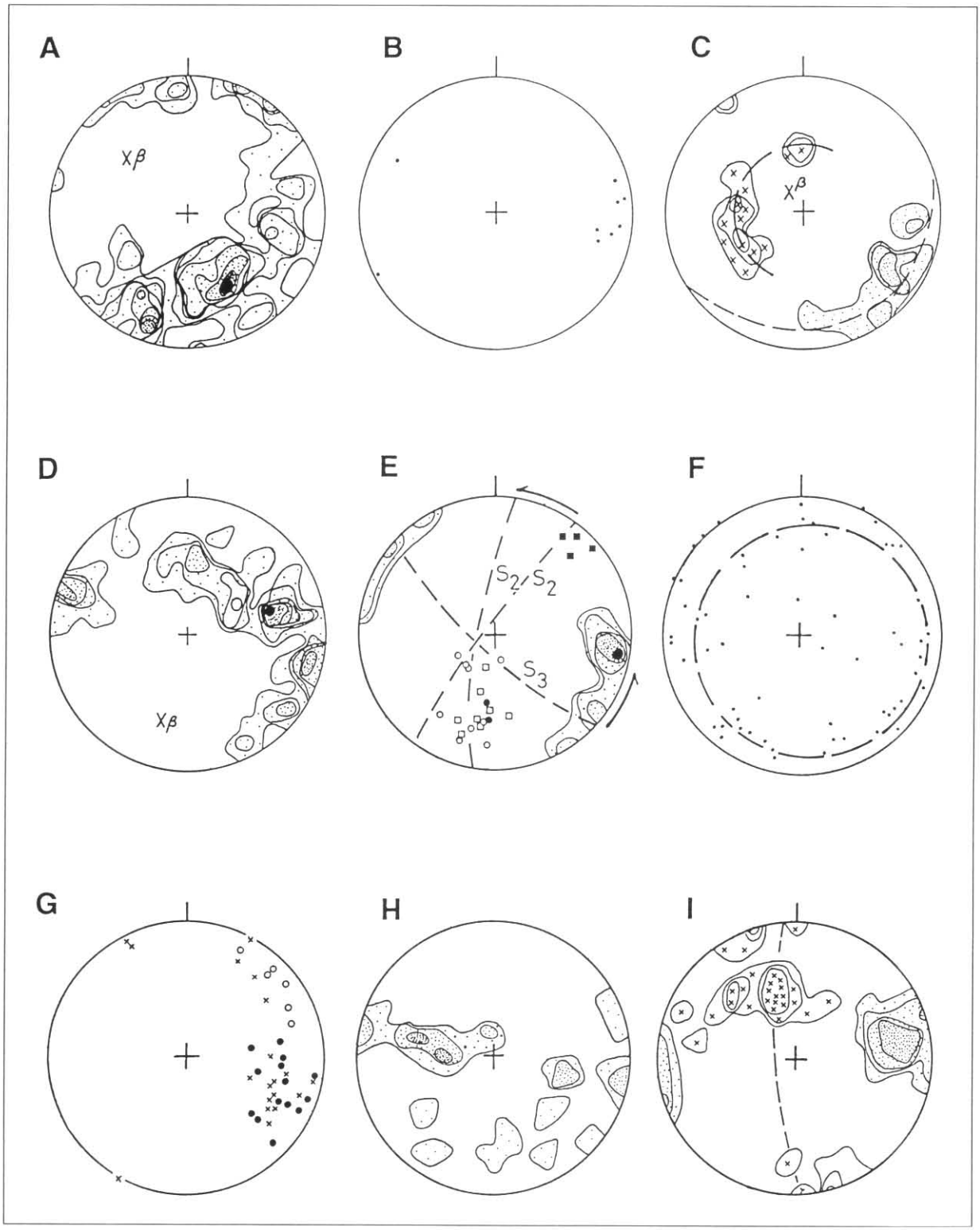

Figure 60. Equal area, southern hemisphere projection stereographic nets showing key structural data for domains 1, 2, 4, 5 and 6. Domain 3 contains mesoscopic folds of too great a complexity for resolution as domains within Figure 58 and 60, and the structure of this region is explained in terms of key outcrops as at CP535090 (fig. 59).

Stereo-net A: Domain 1, poles to bedding (S_0); contours at 1, 2, ... 9 points per 1% area, 98 points. β 50° to 294°. ***Stereo-net B:*** Domain 2, poles to S_0. ***Stereo-net C:*** Stipple, poles to S_0;crosses local F_3 fold axes; locality CP512138. Note that the warping of the local F_3 axes occurs about an F_4 axis within the axial plane of the post-Ordovician Timbertops Syncline. Contours to local S_3 at 1, 2, 3 points per 1% area, 16 points. Contours to fold axes 1, 2, 3 points per 1% area, 10 points. ***Stereo-net D:*** Domain 4, poles to S_0; contours at 1, 2, ...6 points per 1% area; 52 points. β 35° to 198°, corresponding to local B_2^0 fold axis orientation.***Stereo-net E:*** Domain 4, stippled area shows poles to local S_2; open circles local L_2^0; open squares local B_2^0; solid circles elongation of prolate pebbles; solid squares local S_3 cleavage, also plotted as great circle, which is parallel to cleavage in the post-Ordovician Timbertops Syncline. *Note:* 1 – rotation of S_2 (see text) through 30–40° from south-western to north-eastern part of Domain 4; and 2 – the distribution of L_2^0 and B_2^0 along S_2 through plunges of 20–75°. This, allied to the pebble extension along the L_2^0 and B_2^0 direction may be evidence for otherwise unsubstantiated sheath folding. ***Stereo-net F:*** Domain 5, poles to S_0. Note small circle distribution indicating complexity of folding. Thus the few shallowly-dipping beds measured could provide an argument for sheath-folding although such folds were not recognised in the field. ***Stereo-net G:*** Domain 5, crosses local S_1; solid circles local S_2; open circles local S_3. The S_3 direction corresponds to the orientation of the cleavage in the Timbertops Syncline. ***Stereo-net H:*** Domain 6; poles to S_0; contours at 1, 2, 3 points per 1% area; 26 points. ***Stereo-net I:*** Domain 6, stippled area poles to local S_3.; crosses poles to local B_3^0 and L_3^0. S_0 contours at 1, 2, 3, 5 points per 1% area, 27 points; B_3^0, L_3^0 contours at 1, 2, 3, 5 points per 1% area, 30 points.

whereas interference between F_3 and F_4 folds has produced Type 2 interference structures. Interference structures produced by refolding of F_2 by F_3 are less evident.

D_5 was responsible for overprinting the D_1–D_4 structures by a steeply south-west dipping crenulation cleavage whose orientation appears affected by the later E-W warping about steep axes. This SW-dipping cleavage coincides with the orientation of the axial surface of the Timbertops Syncline, which folds the Ordovician siliciclastics and limestones of the Wurawina Supergroup in the southern part of the map sheet.

Domain 1

Here (fig. 58), geopetal indicators confirm large-scale isoclinal folding, and local mesoscopic structural studies confirm the regional π-pole plot to bedding (A, fig. 60) that these folds plunge to the north-west at 40–50° (β to S_0 is 50° to 308° true). The regional structural pattern resembles the Type 3 interference pattern of Ramsay (1967), the isoclinal folds being cross-folded about a W- to SW-dipping axial surface parallel to the trend of a W- to SW-dipping cleavage in this structural domain which is later identified as the regional S_4 surface.

At CP519197 the coastal exposure contains a W-plunging sinistral fold of 3–4 m scale which folds a bedding-parallel schistosity. At CP519199 this fabric is axial planar to partly-transposed isoclinal folds in bedding. The west-plunging sinistral fold is overprinted by a crenulation cleavage dipping at 60–75° to 230–250° and which produces small folds incongruent to the shallowly-dipping north-western limb of the larger sinistral fold. As the orientation of the axis and axial plane of the sinistral fold corresponds to those inferred from the regional π-pole plot for Domain 1 (fig. 60a) and the regional form line map (fig. 58), the sinistral fold is regarded as part of these structures.

In pelitic beds further north [CP518202] bedding has been transposed on S_1 to form a new fabric which has been refolded isoclinally about a steep crenulation cleavage and then cross-folded by a weak crenulation cleavage dipping 80° to 015°. The orientation of this crenulation cleavage coincides with that of a weak crenulation cleavage seen further south, as well as a common spaced cleavage in the quartzitic beds, and also with the axial plane trend of the Timbertops Syncline; that is, it may correlate with the regional post-Ordovician S_5 fabric.

Additional complexity is indicated by cross-folding relations exposed at CP518202 where Type 2 (Ramsay, 1967) interference structures occur in thinly inter-laminated sandstone and pelite beds. Here, the sinistral folds described above are reduced in scale to 25– 50 mm.

Using these data the following hierarchy of structural events can be determined:

Local F_1; isoclinal folding with transposition of bedding in thinly-bedded pelite-sandstone sequences to produce S_1 fabric.

Local F_2; refolding of S_1 to produce isoclinal structures on small and regional scale, and production of crenulation cleavage S_2.

Subsequent deformations have produced regional Type 3 fold interference patterns and small-scale Type 2 interference structures; it will be argued later that the Type 2 structures are the result of folding F_3 by F_4 and the Type 3 structures formed by folding F_2 folds by F_4.

It is inferred that the NE-dipping crenulation cleavage is a fifth generation structure (S_5), formed during folding of the Ordovician rocks of the Timbertops Syncline.

Domain 2

In Domain 2 (fig. 58) thick quartzite beds dominate the coastal outcrop and dip predominantly west (B, fig. 60). However, the thinner sandstone beds and pelitic units display clear evidence for multiple deformation.

The earliest structures occur in pelitic beds, at CP512138 where a schistosity is folded by rootless isoclinal folds. These are folded by chevron folds which contain an axial plane crenulation cleavage and which is warped about a steeply-plunging (~80°) axis within a steep NW-dipping axial surface. This surface is developed strongly as a crenulation cleavage at CP515142, and the folding related to production of this cleavage is responsible for the small-circle distribution of chevron fold axes in stereonet c, Figure 60.

A few hundred metres south, at CP513130 sinistrally-verging NW-plunging upright folds contain a crenulation cleavage which here follows the orientation of a steeply west-dipping spaced cleavage in the sandstone beds. This spaced cleavage overprints minor warps about an axial plane dipping steeply to 325–345°and these warps fold a schistosity here slightly oblique to S_0.

These data are interpreted as follows

Local F_1; rootless isoclinal folds in bedding with a axial plane schistosity.

Local F_2; minor warps about an axial plane S_2 crenulation cleavage dipping steeply to 325–345°.

Local F_3; chevron folds and an associated crenulation cleavage S_3; the F_3 folds and S_3 have been rotated about to form steeply plunging open warps about an axial plane trending north (Local F_4).

Domain 3

The geology of this area (fig. 58) is well exposed in the coastal section where can be seen mesoscopic Type 2 and Type 3 (Ramsay, 1967) interference folds, and it is clear that at least four folding episodes are involved. The structural geology is best described in terms of the outcrops in the beach at CP535090 (fig. 59), which can be used to interpret the complex mesoscopic structures seen as far north as CP515118.

The scattered outcrops (fig. 59) in the beach at CP535090 present evidence for four folding events. The first event is represented by a bedding parallel schistosity (S_1); bedding is not transposed strongly. S_1 is folded by isoclinal folds (F_2) which here are recumbent and close east and west (fig. 59; outcrops 1, 2, 5; plates 14, 15).

The F_2 folds contain an axial plane crenulation cleavage, clearly visible in the pelitic beds, and are crossed by a crenulation cleavage (S_3) which is axial planar to north-closing F_3 recumbent folds (fig. 59, outcrop 6; plate 16). The S_3 cleavage is folded about a steeply E-W dipping crenulation cleavage (S_4). Steeply south to SE-dipping to vertical fractures postdate these structures.

Interference of these different fold generations would produce Type 2 (Ramsay 1967) structures in the case of the F_3 and F_4 deformations, Type 3 (Ramsay 1967) structures in the case of interference between F_2 and F_4, and isoclinally refolded isoclinal structures forming very tight Type 3 folds in the case of F_2 refolding F_3.

Type 2 interference folds occur further north in the complexly folded region at CP526104. Here, coarse pebble and cobble conglomerates within a sequence of more thinly bedded quartzites and pelites are folded into large SSW-plunging asymmetric folds which verge east (plate 17); note that folds of like style occur a few hundred metres north but verge west, thus indicating an intervening synclinorial axis. These folds fold smaller near-recumbent N-verging folds which develop an axial plane crenulation cleavage; this cleavage in the pelitic beds cross-cuts small isoclinal folds marked by colour banding and which contain an axial plane

schistosity formed of oriented phyllosilicate minerals. That is, here there are represented three folding events: the asymmetric SSW-plunging folds are correlated with F_4 on the basis of the orientation of their axial-plane cleavage; and the N-closing recumbent structures are thought equivalent to F_3 according to their orientation. The small-scale isoclinal folds seen only in the pelites are attributed to F_1 insofar as they are responsible for the bedding-parallel schistosity within the pelitic units, although note that it is also possible that they could correlate with F_2.

Smaller Type 2 interference structures are exposed also in the sandstone beds some 100 m to the north where they are cut by a spaced cleavage dipping 55°to 315°.

Type 3 interference folds are exposed at CP524106 where NE/SW-closing, west to NW-plunging open reclined folds refold isoclinal structures and overlie a shallowly west-dipping shear zone. The orientation and style of the open reclined folds resembles that of the F_3 generation at CP535090. In addition, about 50 to 100 m north of CP524106 there are Type 3 interference structures whose geometry is consistent with refolding of F_2 by F_4.

Domain 4

Here, poles to bedding and a bedding-parallel schistosity (local S_1) define a great circle whose pole plunges 35° to 198 (D, fig. 60) and corresponds to the maximum of the F_2 fold axes folding S_1 and crenulation lineations (E, fig. 60). Poles to a locally second crenulation cleavage (E, fig. 60) form a maximum plunging steeply east (E, fig. 60), and which is cut by a surface named locally as S_3 which dips steeply south-west. Passing from the south-west of the domain to the north-east, there is evidence for rotation of the local S_2 by some 30°(fig. 58; E, fig. 60); there are not enough data to show whether the local S_3 has been so rotated.

From interpretation of aerial photographs and field data (fig. 58) the dominant structures are chevron folds with an axial plane striking north. These fold structures are identical in orientation and style to the mesoscopic folds described above as F_2 folds, which fold a schistosity seen elsewhere to be axial planar to isoclinal structures. The orientation and cleavage style of the chevron folds follows that of the F_4 structures in Domain 3; the later crenulation cleavage known locally in Domain 4 as S_3 is identical in style and orientation to that known as S_5 elsewhere.

Domain 5

The exposures here consist of outcrops of both massive and laminated weathered quartzite units with very small isolated outcrops of pelitic rocks exposed patchily within the button-grass. The small-circle of poles to bedding (F, fig. 60) indicates complexity of folding. Locally, the earliest deformational event, here called F_1, is indicated by a quartz-mica-chlorite differentiation layering (local S_1) in the pelitic beds; this is axial plane to very rare probable isoclinal hinges (local F_1) in the quartzitic interbeds and is commonly crenulated by a steeply W- to WNW-dipping crenulation cleavage.

At CP562139 the S_1 fabric is thrown into a Type 2 (Ramsay 1967) fold interference pattern formed of N-S-closing recumbent structures (local F_2) which have been cross-folded (local F_3) by folding across a NNE-striking axial plane. The orientation of this surface follows that of the WNW-dipping crenulation cleavage outlined above. Larger-scale Type 2 interference folds occur also at CP565140 where they have been mapped according to the distribution of rubbly quartzite beds.

The geometrical similarities of this folding with the Type 2 interference folds in domain 3 lead to the following correlation: F_3 here is correlated with the regional F_4 as seen in domain 3; F_2 here is correlated with F_3 in domain 3; and the S_1 quartz-chlorite-mica foliation here and elsewhere is thought to correspond with S_1 in domain 3.

Domain 6

Poles to bedding plot in general on a steeply north-dipping great circle (H, fig. 60), whose pole coincides with the maximum (I, fig. 60) for fold axes, cleavage bedding intersection lineations and minor crenulations on the predominantly bedding-parallel schistosity. Poles to the dominant crenulation cleavage form steeply E- and W-plunging maxima indicating a dominant N-striking cleavage direction. Although these data suggest a simple fold history of formation of an early bedding-parallel schistosity, followed by folding about a north-trending crenulation cleavage to produce upright N-plunging folds, detailed studies at Liberty Point, Table Head, and in Betsys Bay confirm greater complexity.

In the Table Head to Betsys Bay region there occur N-trending folds which fold a bedding-parallel schistosity (local S_1). The N-trending axial planes of these structures are followed by a crenulation cleavage (local S_2) in which the fold axes plunge variably from shallowly to 25° south to dominantly 30–60° north-west (the geometry of these structures in shown in stereonets H and I (fig. 60)). At Table Head, the outcrop pattern of the pelitic beds is suggestive of Type 2 interference folding. As the local S_1 is parallel to S_0, this interference pattern would indicate a generation of folds intervening between the S_1 event and the supposed S_2 event. This may point to a generation of folds intervening between the production of the S_1 fabric (D_1) and the local apparent F_2 folds. These structures are overprinted by sinistrally and dextrally verging kink-bands whose mutual age relations are unknown; the sinistral kink-bands have steeply dipping north to NE-striking axial surfaces and the axial surface of the dextral kink-bands dip steeply and strike north-west.

At CP568163 in Betsys Bay, small isoclinal folds in bedding contain the local S_1 as an axial plane fabric and are crossed by the local N-trending S_2 crenulation cleavage; this is the same surface morphologically as the supposed S_2 surface at Table Head. Also present is a moderately steeply SW-dipping spaced cleavage associated with kinking of the S_1 fabric.

At Liberty Point the sequence is folded into what is interpreted as a Type 2 interference pattern about axes plunging north-west to NNW at between 35 and 45°; these structures resemble on a larger scale those inferred in the pelitic units at Table Head. Note that in the thicker sandstone beds, the local S_2 cleavage fans markedly.

Further south, at CP606163, W-verging shallowly N- to shallowly S-plunging chevron and multi-hinged folds (local F_2) verge west and refold generally S-verging structures (local F_1) with an axial plane schistosity. In the thicker quartzitic beds, this schistosity forms a diverging fan. At this locality, the local F_1 folds appear to be near recumbent and their axes plunge shallowly west.

Yet further south [CP606143] there is confirmation that the local F_2 described above form the third generation (F_3) folds in Domain 6. Here, the dominant folds are chevron-style structures which plunge south and whose axial planes dip west at 60–70°; these structures are geometrical correlates of the local F_2 folds at CP606163. They refold a schistosity locally oblique to bedding, and also a distinctly different schistosity which follows bedding and is axial plane to isoclinal folds in bedding.

Finally, the chevron folds here are warped about steeply plunging axes; this deformation is thought to have produced the regional scatter of B_3^0 and L_3^0 lineations shown in the north-west quadrant of stereonets H and I (fig. 60).

Discussion

As summarised previously, there is evidence for five deformational events in these Precambrian rocks, which were accompanied by low greenschist facies metamorphism. The age of these events is uncertain and all the

D_1–D_4 events would appear to precede the thrusting of the Precambrian sequence over the Cambrian rocks. The D_5 event produced a cleavage whose trend follows that of the axial plane of the post-Ordovician/pre-Tertiary Timbertops Syncline in the southern part of the map sheet area; this cleavage trend also occurs in the Cambrian rocks south of the thrust contact. However, this evidence is not sufficient to argue that the thrust between the Precambrian and Cambrian rocks preceded the D_5 cleavage and the possibly contemporaneous formation of the Timbertops Syncline.

No evidence of sheath folding has been observed, although it could be argued on a geometrical basis that the Type 2 and Type 3 interference structures could be the result of cross-folding one generation of sheath folds (here represented by the F_2 and F_3 structures) by F_4 folds. The key area for resolving this question is the foreshore platform on the west coast between CP535090 and CP524106 where there exist both mesoscopic Type 2 and Type 3 interference structures. Based on observations at CP535090, F_2 and F_3 would appear to be separate events.

Finally, it is noteworthy that no obvious high-strain zones have been recognised, despite the evidence for at least two generations of recumbent structures. If such high-strain zones exist, then they must be narrow, and possibly confined to the relatively poorly exposed pelitic units.

NIELSON RIVER AREA

M. P. McClenaghan

Due to the difficulties of access to some areas and the weathering state of outcrops, structural information from this area is uneven in quality. Well-exposed rocks on the west coast at Varna Bay and on the east coast north of Bryans Bay provided abundant data on mesoscopic folds of various styles and orientations. Good outcrops also occur in the Nielson River and the upper parts of Birthday Creek. Outcrops on the buttongrass plains and in the smaller creeks were usually of poor quality. Air photo interpretation of the buttongrass areas indicate that the dominant structural trend is north-east, confirmed by ground measurements in localities selected for their better exposure.

Five deformation events (D_1–D_5) have been recognised with chronological relationships having been deduced from the interactions and relative positions of planar and linear structures and the distribution of these structures. The full sequence of deformation events is based on the structures in the coastal rocks north of Bryans Bay and only some of the later events can be recognised in the other parts of the area. The lack of lithological marker horizons has prevented the mapping of major folds and large faults. D_4 is the dominant deformation in the northern part of the area (Domain 1, fig. 61) whereas, to the south it becomes progressively less intense.

Domain 1

This domain is dominated by an intense north-east trending, steep, cleavage (S_4) which is best developed in the more pelitic rocks. In the dark grey mudstone it is a slaty cleavage, in the lighter grey siltstone a closely spaced crenulation cleavage and in the quartzwacke rocks a more widely spaced cleavage crenulating other widely spaced cleavages. It is considered to be S_4 based on the relationships seen at a number of key outcrops between CP662087 and CP666085 on the coast north of Bryans Bay. The first of these is at CP662087 near the mouth of Butler Creek and consists of a single large outcrop of quartzwacke. Three coarse cleavages occur in this rock (S_1–S_3, plates 18, 19) and a clear chronology was established based on cross cutting relationships. Poles to the latest cleavage here (S_3, fig. 62) define a girdle which is consistent with the cleavage having been folded about a NNE trend (best fit fold axis 41° to 023°). A short distance farther to the south (at CP665085) the S_3 cleavage is crenulated by a later, steep cleavage (S_4) trending

Plate 18. Coarsely developed S_2 cleavage crenulating the S_1 cleavage in quartzwacke of unit Pnq at CP662087. Same outcrop as for Plate 19.

Plate 19. Coarsely developed S_3 cleavage crenulating the S_2 cleavage in quartzwacke of unit Pnq at CP662087. Same outcrop as for Plate 18.

north-east which farther south is dominant in the coastal outcrops. On the basis of similarity of attitude it is considered to be the same as the dominant cleavage in the domain (fig. 63). Its attitude is consistent with its production by the deformation event that folded the S_3 cleavage (fig. 62).

Tight, upright, mesoscopic folds in bedding with wavelengths generally less than one metre, are common in coastal outcrops and in the inland parts of the domain near the Nielson River. The S_4 cleavage is approximately axial planar to the folds which show a wide range of plunges (fig. 64). The folds from the coastal outcrops plunge at intermediate angles to the south-west, whereas folds from the Nielson River area plunge at steep to low angles to the north-west. The poles to bedding (fig. 65) reflect the pattern shown by the mesoscopic folds. The folds may include folds produced by the D_1 to D_3 events as well as the dominant D_4 event.

Minor kink-like folds are present in coastal rocks; these fold the S_4 cleavage and represent the D_5 event. They have moderately to steeply dipping axial planes trending north-west (fig. 66). A poorly-developed crenulation cleavage follows the axial planes of some of these folds. The attitude of these surfaces is similar to that of the cleavage in the post-Ordovician deformation of the Timbertops area and so they may be the same one.

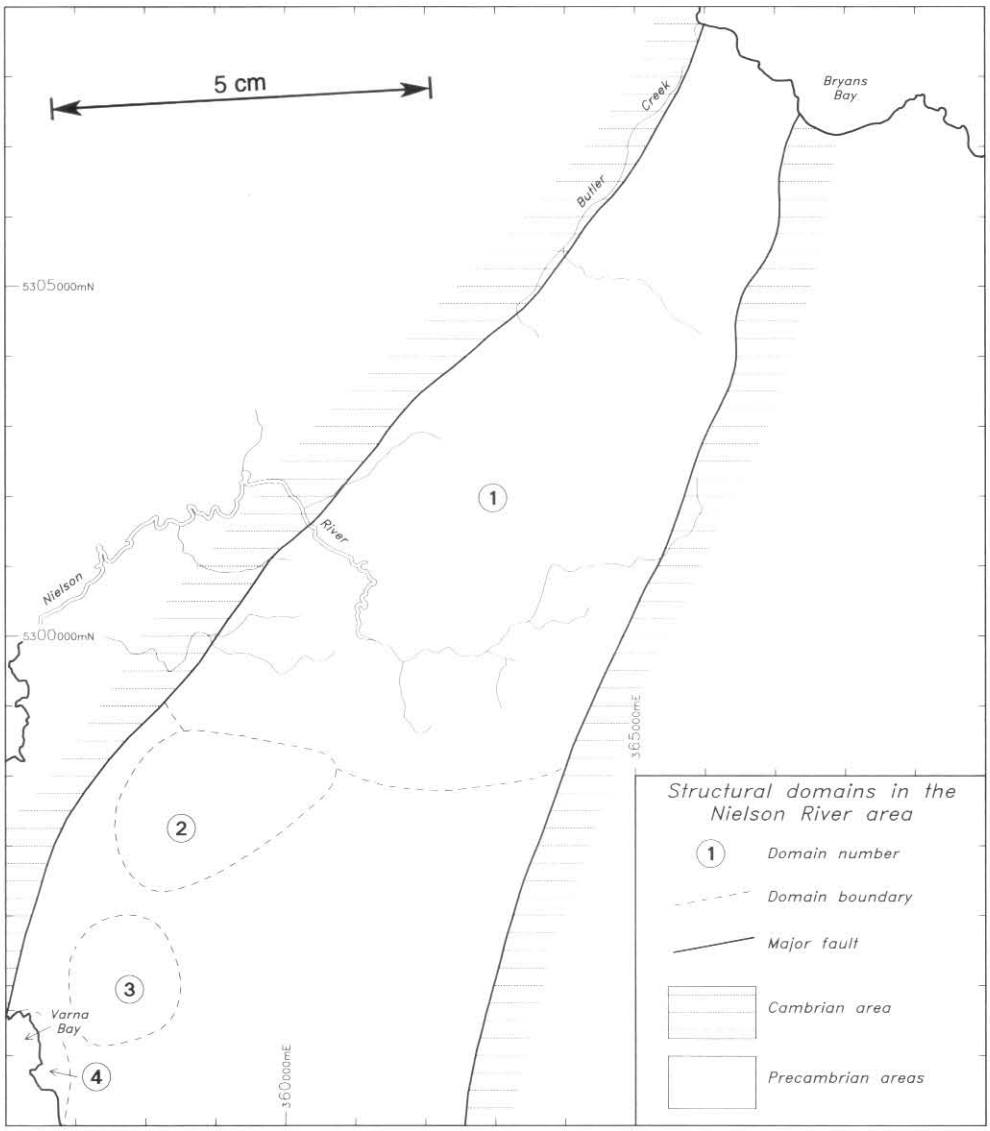

Figure 61. Structural domains in the Nielson River area.

Domain 2

In this domain most measurements were obtained from dolomite-rich mudstone and siltstone and the cleavage is a closely spaced slaty type. Recrystallisation of the dolomite made it difficult to recognise whether more than one cleavage was present. The cleavage is generally steep and strikes north-east, however, although some shallow dips were recorded. The poles to this cleavage approximately define a girdle consistent with folding of the cleavage about an axis plunging at a low angle to the north-east (fig. 67). It seems probable that most of the cleavage readings were for S_4 and that some earlier cleavages were also measured and these were folded by the D_4 event. The poles to bedding (fig. 68) also define a girdle consistent with folding plunging at a low angle to the north-east. Mesoscopic folds in bedding (fig. 69) generally plunge at low angles to the north-east.

Domain 3

Rocks in this domain are similar to Domain 2, consisting of carbonate-rich mudstone and siltstone, here however, a generally slaty cleavage is strongly developed and a crenulation cleavage is much less common. Poles to cleavage lie on a broad girdle consistent with folding about axes plunging at low angles to the south-west (fig. 70). No mesoscopic folds were recorded. These features are broadly similar to those in Domain 2 except that the plunge of cleavage folding is to the south-west rather than north-east.

Domain 4

Carbonate-rich sequences of mudstone, siltstone and sandstone of this domain (fig. 61) in the Varna Bay area provided abundant good coastal outcrops. At CN564941 very tight mesoscopic folds of bedding, with wavelengths less than 0.5 m, have an axial plane cleavage (local S_1) which is crossed by a more strongly developed cleavage (local S_2) which is also axial planar to tight folds of bedding (local F_2). Elsewhere the earlier cleavage is difficult to recognise and appears to be subparallel to bedding. The local F_2 fold hinges plunge west south-west and north-east at low angles (fig. 71) and the axial planes have variable strikes and low angle dips (fig. 72).The broad spread of the poles to the axial planes of the local F_2 folds (fig. 72) and the local S_2 cleavage (fig. 73) indicate that there was a later, gentle folding event with a south-west trend. The poles to bedding display a similar broad girdle consistent with gentle folding with a south-west trend (fig. 74). It seems likely that this south-west trending fold event is the D4 event recognised in the previous domains so that the local D1 and D_2 could be equated with D_1 and D_2 events in the domains to the north. This correlation indicates that the D_4 event is most intense in the northern part of the Precambrian area where it is at its most narrow and is very much less intense in the south-west where it is at its widest. This difference in the development of the D_4 event also coincides with the change from non-carbonate rocks to carbonate-rich rocks.

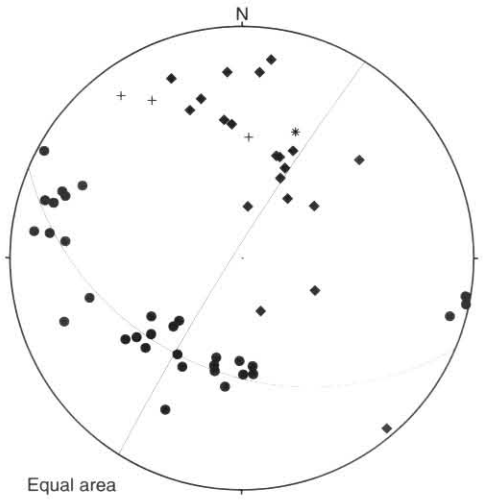

Figure 62. Domain 1. Poles to S_1(+), poles to S_2 (◆), poles to S_3 (●), best fit axis of fold in S_3 (✳), NW-trending great circle is best fit great circle to S_3 and NE-trending great circle is average S_4.

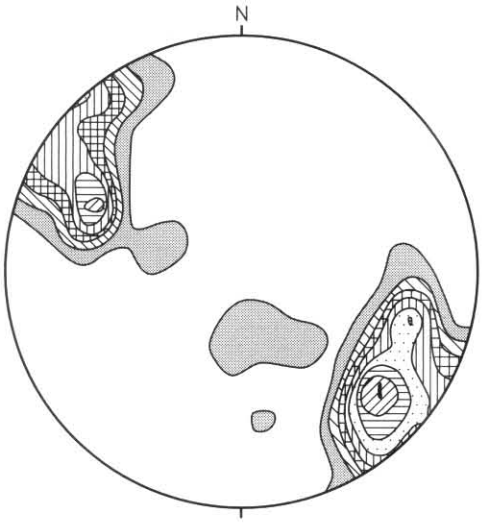

Figure 65. Domain 1. Contoured diagram of poles to bedding contoured at 1 to 8 × uniform distribution; 130 readings.

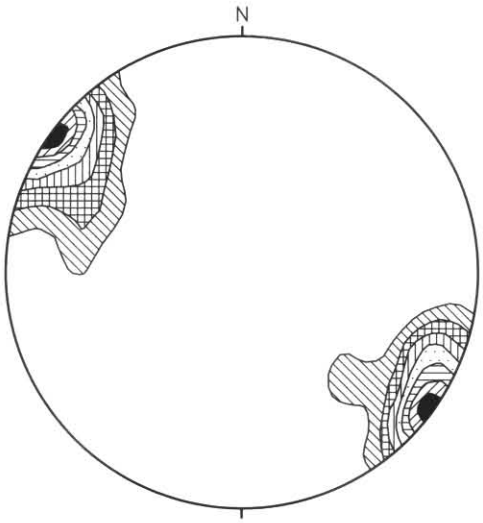

Figure 63. Domain 1. Poles to S_4 cleavage contoured at 2, 4, 6, ... uniform distribution; 90 readings.

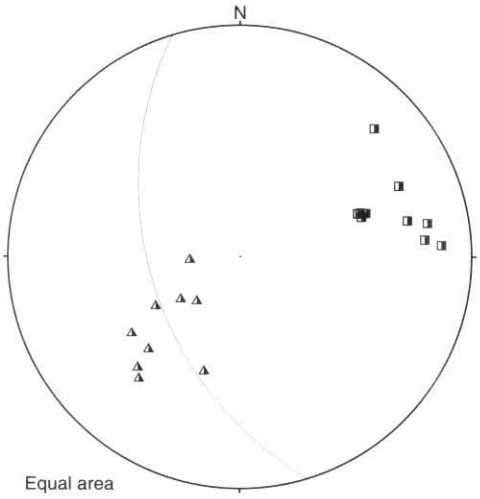

Figure 66. Domain 1. Kink style folds folding S_4. Poles to axial planes (◨) and hinges (◭). The great circle is the average axial surface plane.

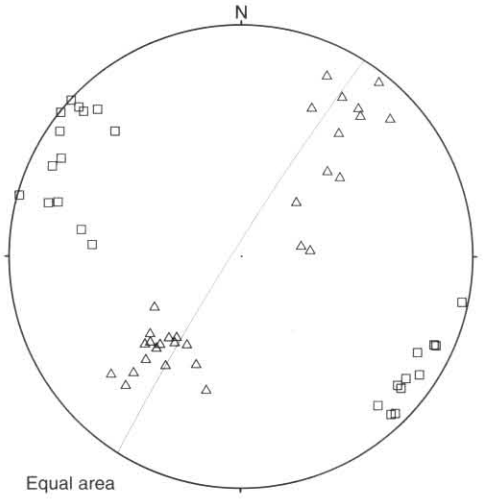

Figure 64. Domain 1. Hinges to folds of bedding (△), squares are poles to axial planes of folds of bedding (□) and the great circle is the average S_4 cleavage.

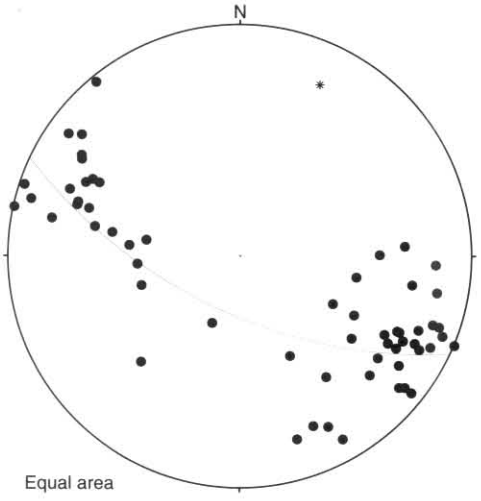

Figure 67. Domain 2. Poles to dominant cleavage (●), best fit fold of cleavage (✳) and great circle is best fit great circle to cleavage.

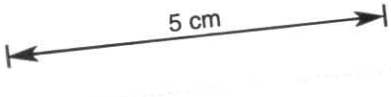

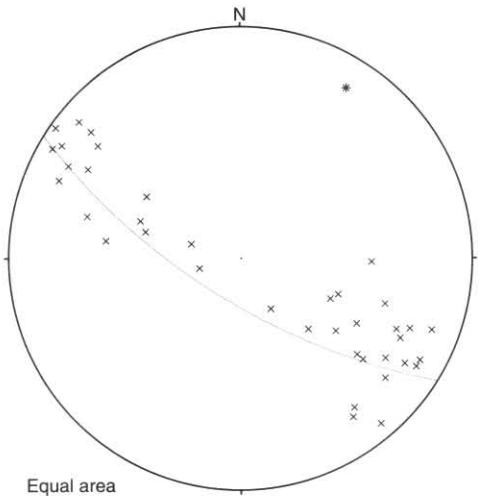

Figure 68. Domain 2. Poles to bedding (×), axis of best fit fold in the bedding (∗) and great circle is best fit great circle to bedding.

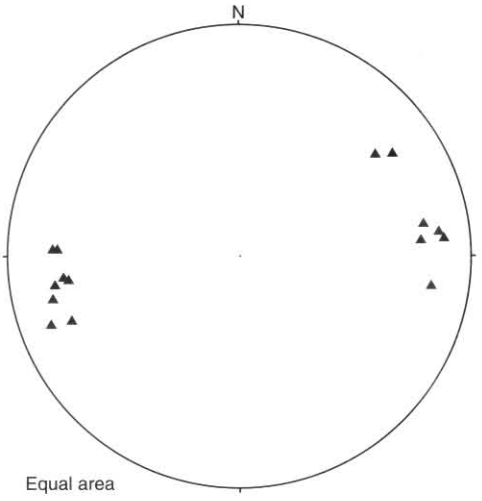

Figure 71. Domain 4. Hinges of folds in the bedding of locally F_2 folds (▲).

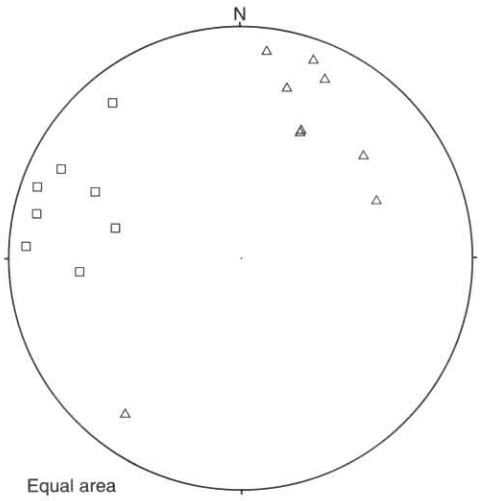

Figure 69. Domain 2. Hinges of folds in bedding (△) and poles to axial planes of folds in bedding (□).

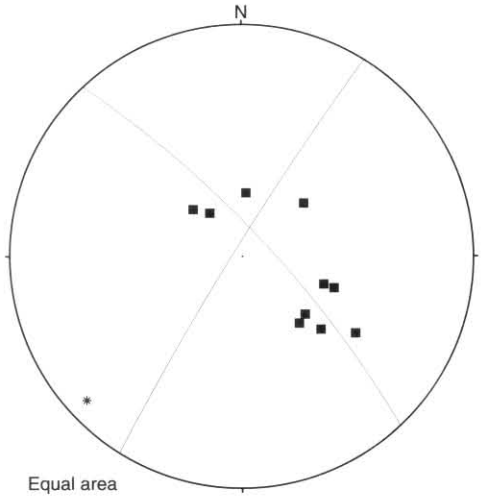

Figure 72. Domain 4. Poles to axial planes of folds of bedding of locally F_2 folds (■). The SW-trending great circle is the average S_4 cleavage in Domain 1 and the NW-trending great circle is the best fit great circle to the axial planes of the F_2 folds. Axis of the best fit fold of the axial planes of the F_2 folds (∗).

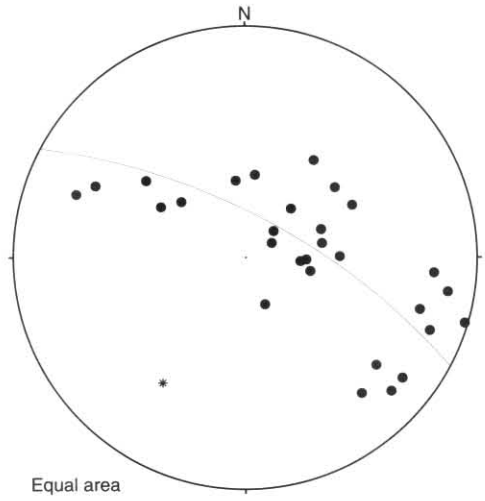

Figure 70. Domain 3. Poles to cleavage (●), best fit axis of folding of cleavage (∗) and great circle is best fit great circle to cleavage.

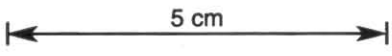

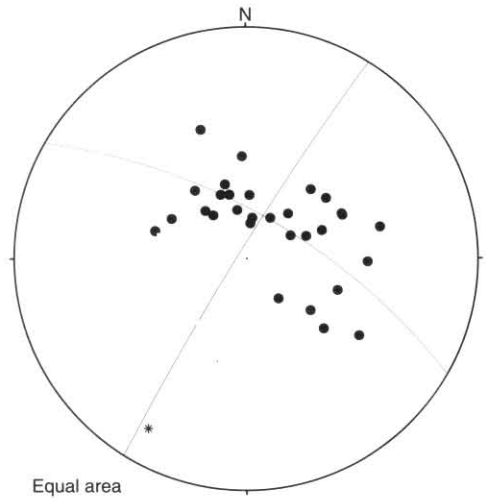

Figure 73. Domain 4. Poles local S_2 cleavage (●). The SW-trending great circle is average S_4 cleavage from Domain 1 and the NW-trending great circle is the best fit great circle to the local S_2 cleavages. Axis of the best fit fold of the S_2 cleavages (∗).

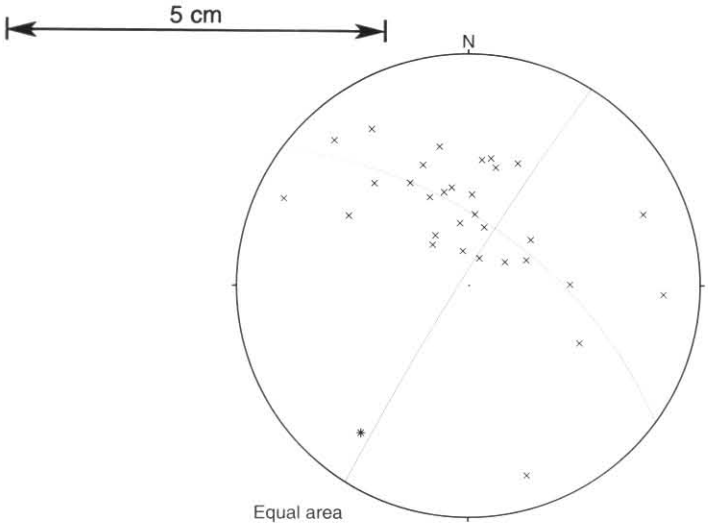

Figure 74. Domain 4. Poles to bedding (×). The SW-trending great circle is average S_4 cleavage from Domain 1 and the NW-trending great circle is the best fit great circle to the bedding. Axis of the best fit fold of the bedding (*).

At several localities e.g. CN563946 there is a steep weakly developed crenulation cleavage trending north-west (average value 89° to 245°) which is axial planar to sparse mesoscopic folds. This appears to be the latest deformation event in the domain and so is assumed to be D_5. The similarity of trend of these structures to those of the post-Ordovician event in the Timbertops area suggest that they were produced by the same event.

Lower Palaeozoic (Cambrian–Devonian)

M. P. McClenaghan

SARAH ISLAND TO TIMBERTOPS AREA

The structure of this region (fig. 75) is dominated by two large folds of different orientation and age, and is further complicated by thrusts and steeply-dipping faults. The two major folds are the NW-trending post-Ordovician, possibly Devonian, Timbertops Syncline and the SE-trending Commandant Creek structure which affects only rocks of Cambrian age; the Commandant Creek structure is crossed by the Timbertops Syncline, and restoration of the Ordovician beds to the horizontal indicates a marked angular unconformity between the Cambrian and Ordovician sequences.

The region has been divided into five structural domains (1–5). Domain 1 is occupied solely by the Ordovician rocks of the Timbertops Syncline; Domains 2 to 5 are occupied by the Cambrian sequence, with 2 being subdivided according to changes in orientation of the probably post-Early Ordovician cleavage seen here.

In Domain 1, poles to bedding measurements confirm that the Timbertops Syncline plunges about 20° to 140° (fig. 76); an anastomosing closely-spaced to slaty cleavage is developed in the more pelitic units in the core of the syncline and dips very steeply north-east and south-west (fig. 78). Statistically, this post-Early Ordovician cleavage follows the axial plane of the Timbertops syncline (fig. 76). This NW-trending cleavage also follows the trend of the cleavage in the Carboniferous tillite of the Zeehan area (Goscombe, 1991) as well as cleavage trends seen in Devonian rocks further north. This cleavage therefore provides an important datum for interpretation of the cleavages affecting the underlying Cambrian sequence.

Sub-domains 2a and 2b contain a complex fold, the Commandant Creek structure (fig. 75). In Sub-domain 2a bedding measurements and photo-lineations suggest the presence of an upright antiformal structure with a low northward plunge; in Sub-domain 2b bedding measurements and limited geopetal data suggest a S-plunging syncline. The Commandant Creek structure would appear therefore to be a N-plunging antiformal / S-plunging synclinal fold couple. Poles to bedding are distributed about a broad small circle girdle within which some readings from scattered localities fall on to a great circle girdle, with a SW-plunging pole (fig. 77). These data confirm the general outcrop pattern of a general south-westerly trend to the Commandant Creek structure, as distinct from the south-easterly trend of the Timbertops Syncline, and the complexity of the π-diagram also points to subsequent cross-folding by this post-Early Ordovician fold.

A cleavage following the trend of the axial cleavage of the Timbertops Syncline has been recognised in the Cambrian beds of Sub-domains 2a and 2b. This cleavage is predominantly a spaced cleavage, although in some pelitic units a slaty cleavage has also been seen following this orientation. Because of this the NW-trending cleavage in the Domains 2a and 2b is accorded a post-Early Ordovician age.

No axial-plane cleavage has been recognised in outcrop as associated with the Commandant Creek structure. Figure 79 is a plot of poles to cleavage measured in Sub-domains 2a and 2b and from which have been removed those cleavages correlated with the post-Early Ordovician cleavage. The plot consists of two morphological groups of cleavage; a fine schistosity in the coarser units together with a very fine slaty cleavage in pelitic beds, and a non-penetrative cleavage formed of closely spaced fractures. The poles to the first morphological group lie principally in the north-west and south-east quadrants of the stereonet in Figure 79 although there is the suggestion that these readings lie on a small circle. That is, these data may point to a deformed but principally N-trending cleavage; note that the dominant cleavage trend (fig. 79) would trend through the sparse cleavage/bedding intersection lineations and stretched pebble lineations in this region. Thus this NE-trending cleavage may be axial planar to the NE-trending Commandant Creek structure. The significance of the few spaced cleavages, which form the second morphological group, is unknown.

At CN676962, CN673965 and CN668957 unit €ta is sheared at or close to its contact with unit €tm. These poorly exposed sheared rocks contain a C-S fabric. The geometry of the C-S fabric at CN676962 and CN668957 is in accordance with the interpretation that the fabric has been folded by the Timbertops Syncline. An attempt to restore the original dips of the C-S fabrics at these two localities by restoration of the Ordovician strata to the horizontal increased the divergence between the orientation of the two fabrics. Similarly, restoration of the pre-Ordovician orientation of the Cambrian beds flanking the Timbertops Syncline also indicated a greater pre-Ordovician divergence in dip of bedding; on restoration of the pre-Ordovician orientation of the Cambrian bedding, the reconstruction produced the possibility of a SE-trending asymmetric synform. When combined, these two reconstructions could be interpreted as indicating that the reconstructed fold folded the earlier C-S fabric; however, the data are not adequate to restore the original dip of the fabric.

In Sub-domains 2c–2f the post-Early Ordovician cleavage ranges in trend from ≈010° to 330° (fig. 75, 81, 84, 85, 87). These differences in cleavage trend may indicate large-scale kinking. This cleavage is axial planar to mesoscopic folds which plunge steeply north and occur in Sub-domain 2d (fig. 80). They have wavelengths of 0.5–200 m and closely follow the statistical fold axis derived from the bedding orientations. The statistical fold axis shows a decreasing plunge going north from Sub-domain 2d to 2f (fig. 80, 82, 85), and in Sub-domain 2g two measured fold hinges plunge at low to moderate angles to the south. Bedding in most of Sub-domain 2g dips and youngs to the east.

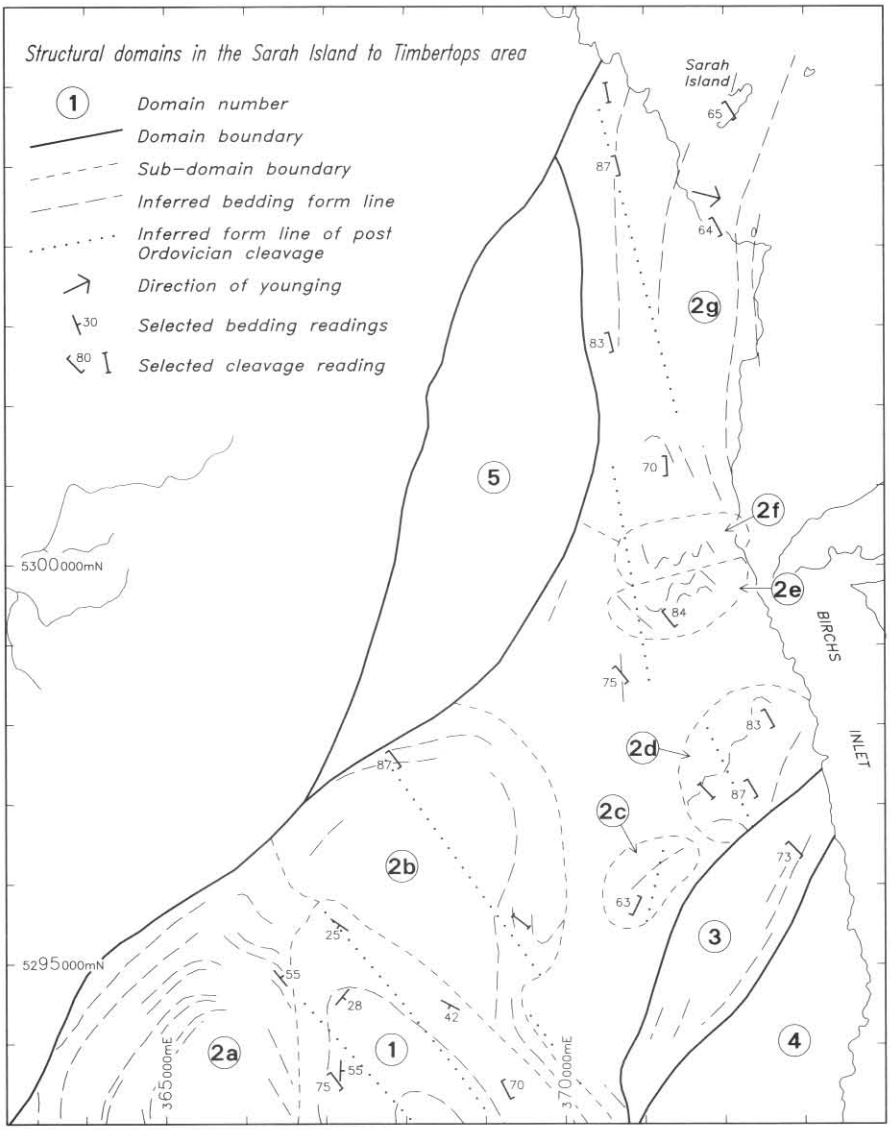

Figure 75. Structural domains in the Sarah Island – Timbertops area.

In Domain 3, the clastic rocks of unit €ts are inferred on the basis of a distinct photo-lineament, which truncates bedding, to be faulted against the rocks to the north. Bedding dips both north-west and south-east indicating gently plunging, upright folds on a north-east to south-west trend (fig. 88) and of less than 200 m in wavelength. A single steep cleavage recorded at CN730967 trends north-west, cutting across the trend of the inferred folds. If this cleavage is the post-Early Ordovician cleavage, as is suggested by its orientation, then this folding was produced by an event earlier than the one that produced the folding in Sub-domains 2c, 2d, 2e and 2f.

Domain 4 is distinguished by its lack of structure. The rocks here consist of massive basalt lava (€tbc); they have a north-east trending faulted contact against the clastic rocks of Domain 3.

Domain 5 consists of rock unit €al flanked to the north and south by rocks of unit €tr. It is separated from Domain 2 by a W-dipping thrust fault and on the western margin it abuts the Point Hibbs Mélange Belt. The rocks within this domain are generally massive and poorly exposed and did not yield any structural information. The distribution of rock units €al and €tr suggest a large north-east trending fold.

ALBINA CREEK AREA

M. P. McClenaghan

Structural information in this area was obtained mainly from coastal outcrops and a few of the larger creeks. Most of the interior of the peninsula is heavily vegetated and difficult of access. The structural interpretation is further complicated by several north-east trending faults (fig. 89) some of which have low angle dips to the north-west and are therefore thrusts. According to cross-cutting cleavage relationships seen at a number of restricted localities five deformations are recognized (D_1–D_5). D_1 produced folds but no cleavage, D_2–D_5 produced cleavages and folds (S_2–S_5; F_2–F_5), and D_3 is the regionally dominant deformation responsible for producing a regional generally north-east to north striking cleavage of variable local intensity. Three structural domains are recognized according to the orientation of the S_3 structure (fig. 89).

Domain 1

Near CP632113 two styles of F_1 folds occur; kink folds dominate the pelitic sequences whereas in the more thickly bedded sandstone/pelite sequence, folds resembling the Class 2 style of Ramsay (1967) (similar folds) occur. These folds are cut by the regional S_3 fabric (fig. 90).

Around CP658090, near Hogan Cove D_2 folds occur. These F_2 folds were identified as such because they contain a weak slaty cleavage (S_2) crossed by the regional S_3 fabric which here is a crenulation cleavage. The F_2 folds are tight with wavelengths of about 0.5 m. Both S_2 and S_3 are found in the Hogan Cove area, but S_3 becomes better developed farther north to form a slaty cleavage, whereas S_2 dies out.

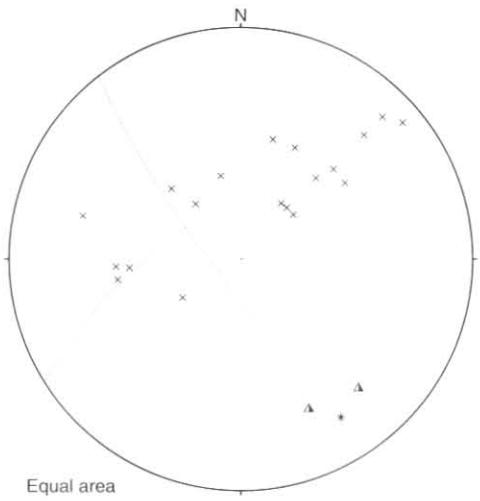

Figure 76. Domain 1. Poles to bedding (×), ✳ is axis of best fit great circle to bedding poles and follows bedding/cleavage intersections (▲) which lie close to great circle to the average cleavage orientation.

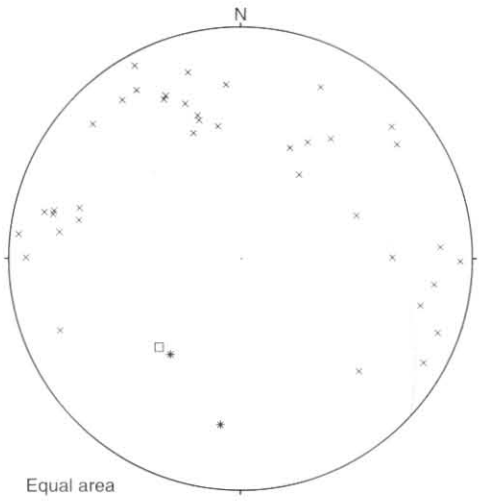

Figure 77. Poles to bedding (×) in Sub-domains 2a and 2b. The majority of bedding poles fall on the great circle shown whose pole (□) plunges at 46° to 223° close to one of two stretched pebble lineations (✳). The nine poles plunging towards between 270° and 240° lie off this great circle; these readings, obtained from the region between CN667953 and CN667959, lie adjacent to the west limb of the younger Timbertops Syncline and their displacement may reflect refolding during the younger 'Timbertops event'.

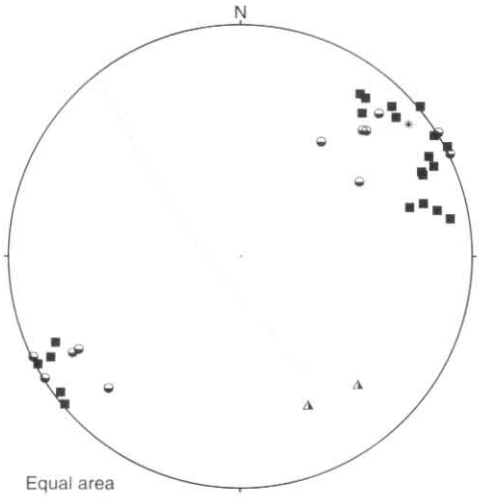

Figure 78. Poles to cleavage in the Timbertops Syncline (◒); average post Early Ordovician cleavage orientation from Figure 77 (great circle and ✳) is 81° to 232°. Cleavage seen in the Cambrian sequence of the Commandant Creek Structure but which crosses this complex fold (■). As these readings follow the cleavage poles in the Timbertops Syncline they are thought to represent the same cleavage. Cleavage/bedding intersection lineation in the Timbertops Syncline (▲).

5 cm

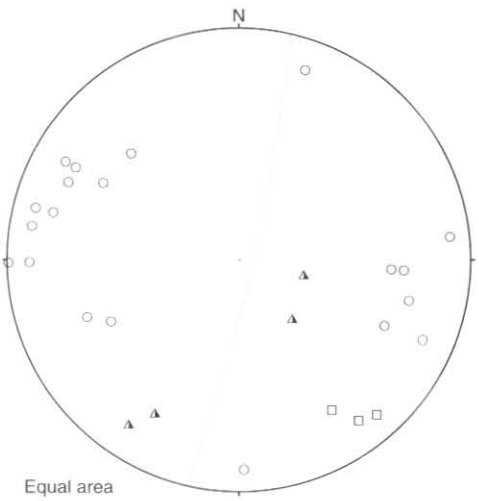

Figure 79. Poles to cleavage (○), close-spaced fractures (□) in Sub-domains 2a and 2b (Commandant Creek structure), and bedding/cleavage intersection lineations (▲). Great circle is average morphological group one cleavage plane.

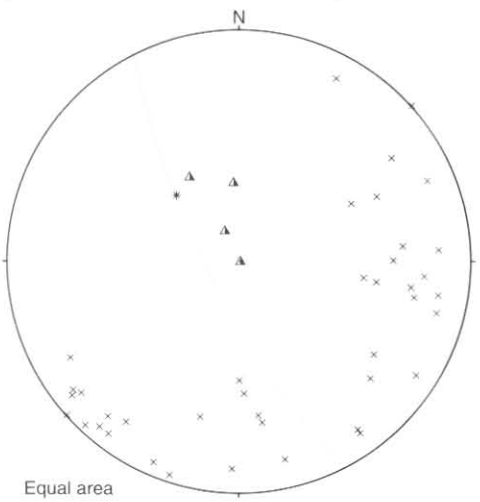

Figure 80. Domain 2d, poles to bedding (×), great circle is average post-Early Ordovician cleavage, ✳ is axis of best fit fold axis to the bedding, ▲ – hinges to minor folds in bedding.

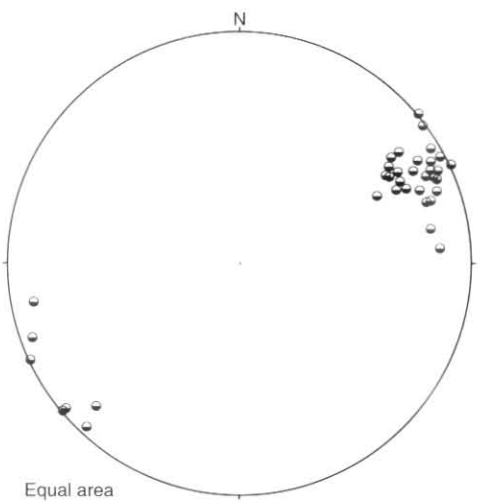

Figure 81. Domain 2d, poles to post-Lower Ordovician cleavage.

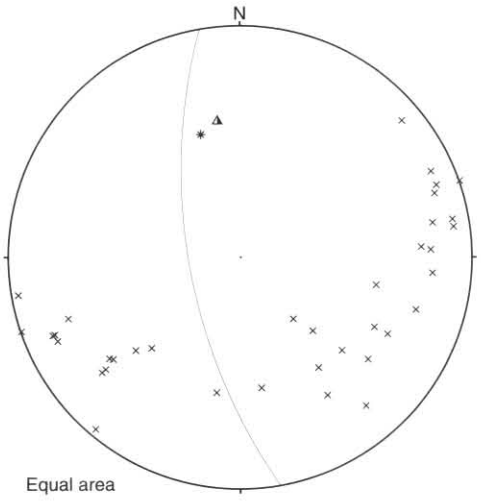

Figure 82. Domain 2e, poles to bedding (×), great circle is trace of average post-Early Ordovician cleavage, ✳ is axis of best fit fold axis to the bedding, ▲ – hinge to minor fold of bedding.

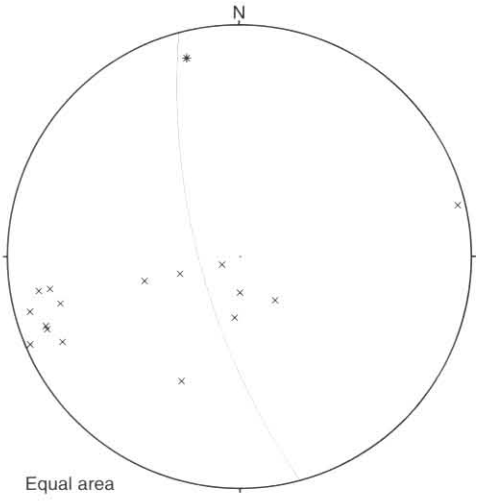

Figure 85. Domain 2f, poles to bedding (×) great circle is trace of average post-Early Ordovician cleavage, ✳ is axis of best fit fold to the bedding.

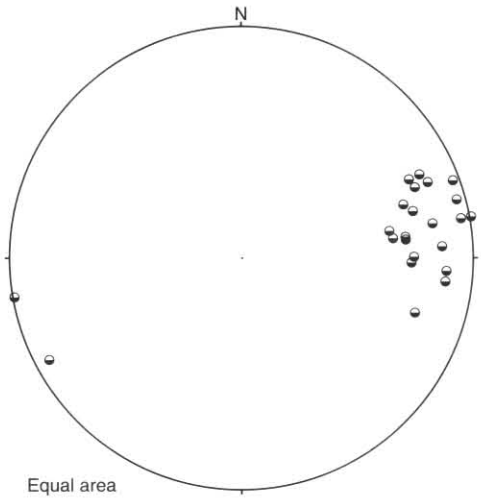

Figure 83. Domain 2e, poles to post-Early Ordovician cleavage.

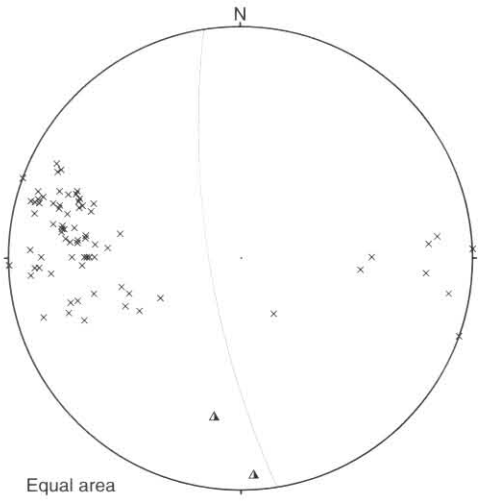

Figure 86. Domain 2g, poles to bedding (×), great circle is trace of average post-Early Ordovician cleavage, hinges to minor folds of bedding (▲).

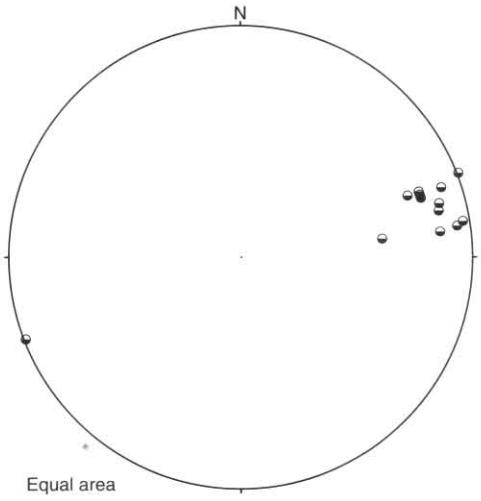

Figure 84. Domain 2f, poles to post-Early Ordovician cleavage.

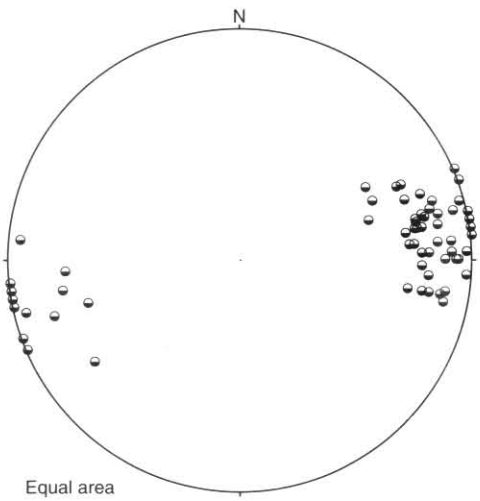

Figure 87. Domain 2g, poles to post-Early Ordovician cleavage.

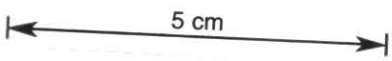

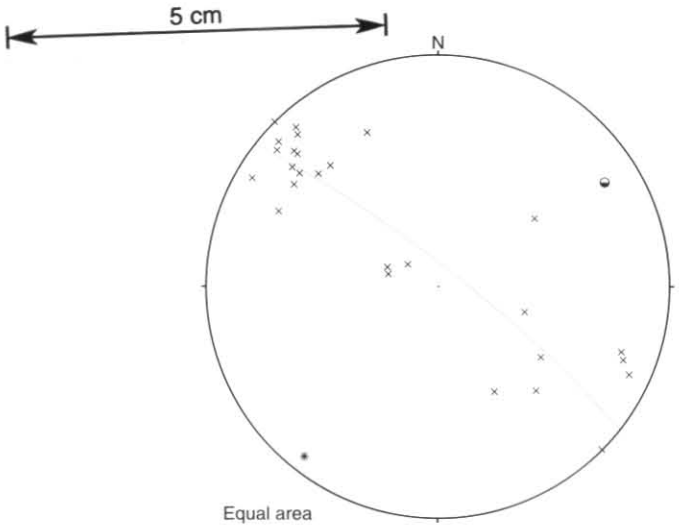

Figure 88. Poles to bedding (×) in Domain 3. Best fit great circle to bedding poles shown with its axis (✳) plunging at 7° to 218°. Pole to coarse fracture cleavage (◒).

Domain 2

The dominant cleavage here strikes at 56° (fig. 92) in contrast to the dominant S_3 cleavage in Domain 1 which strikes at 28° (fig. 91). However as it is a slaty cleavage identical to S_3 in Domain 1, and is axial planar to folds of like appearance to the F_3 folds in Domain 1, this cleavage is correlated with S_3 in Domain 1. The difference in orientation may be due to rotation by faulting.

The S_3 cleavage is very strongly developed in the pelitic rocks but is generally not evident in the massive, pure carbonate units which are less obviously deformed. Exceptions to this generalisation occur at CP552013 and CP552015 on the west coast, where there are two zones of extremely intense cleavage development with the cleavage being shown by sharp upstanding ridges with the very tightly folded bedding being almost obliterated by transposition.

Domain 3

The rocks in this domain consist of massive, sparsely current bedded calcareous sandstone with beds up to one metre thick interbedded with minor thinner units of calcareous siltstone. These rocks are less deformed and have a moderately well developed, steep, platy cleavage developed trending approximately north-south (fig. 89, 93) which is axial planer to large (≈5 m wavelength), gently plunging, open folds (plate 20 and front cover). This cleavage may also be the S_3 but its slightly different morphology makes this uncertain.

F_3 fold plunges

D_3 folds in Domains 1 and 2 as seen in the coastal outcrops from the eastern and western coasts, show a wide range of plunge orientations (fig. 94, 95). The fold hinges lie on or close to the average cleavage S_3 plane (fig. 94, 95). A few fold hinges in Domain 2 (fig. 95) that depart from the average cleavage plane occur in areas where the axial planar cleavage has locally a slightly different orientation. This may be due to later kinking. Fold hinges with a wide range of plunges lying in the cleavage plane is a feature that is unlikely to occur if the variation of plunge was due to folding of already folded rocks. Other explanations are sheath folding or shear folding.

S_4 and S_5 cleavages

At CP551016 in Domain 2, over a small area, the S_3 cleavage is folded into tight, upright, mesoscopic folds (0.5 m wavelength) with a weakly developed crenulation cleavage (S_4). This follows the F_4 axial planes and has a slightly different orientation to the S_3. Due to the localised nature of this deformation close to a fault it seems possible that it was related to the faulting. A weakly developed crenulation cleavage is also developed in the area around CN553953 in Domain 1; this is later than the dominant S_3 cleavage and may also be S_4. This cleavage also has an orientation only slightly different to the S_3 cleavage (fig. 96).

At CP649097 in Domain 1 there is a poorly developed, steep, crenulation cleavage trending north-west which cuts across the mesoscopic folds associated with the dominant S_3 cleavage. This is clearly a later cleavage but its very different orientation to the S_4 cleavage described above suggests that it is related to another deformation event (D_5?). At several other places in Domains 1 and 2 there are steep cleavages with a similar north-west trend (e.g. CP568031, CP630085 and CN553968). The cleavage at CP568031 is a crenulation cleavage. These cleavages may also have been produced by the same event and the similarity of their attitude to that of the cleavage produced by the post-Ordovician deformation of the Timbertops area may mean that they represent that event.

Plate 20. Open folds in massively bedded calcareous sandstone of unit Cac at CN551967.

Faulting

The Macquarie Harbour map sheet area contains numerous faults and shear-zones. It is most notable for two structures whose interpretation is of prime importance in a regional context; these are the Liberty Creek Thrust and the very complex Point Hibbs Mélange Belt, both of which affect rocks of Precambrian to lower Palaeozoic age. Also present are steep NE-trending faults in the Cambrian sequence of the Sorell Peninsula and faults of extremely low angle within the Tertiary sequence on the eastern side of Macquarie Harbour.

LIBERTY CREEK THRUST

M. P. McClenaghan
R. H. Findlay

The Liberty Creek Thrust is a very shallowly dipping structure which has been tested by four drill holes, two of which are about one kilometre north-west in a cross-strike direction from the thrust front near Liberty Creek. The thrust juxtaposes Precambrian rocks (unit Pm) over sedimentary rocks of inferred Cambrian age. An outlier of the thrusted Precambrian sequence overlies with a flat contact thrusted and steeply faulted, probably Cambrian rocks some 4–5 km south-east of the thrust front.

No exposures of the fault rock between the Cambrian and Precambrian sequence have been found, and thus it is extremely difficult to be certain of the movement sense of the thrust. Brown *et al.* (1991) have suggested the likelihood of north to NW-directed thrusting on the basis of work recently carried out by D. Seymour in the Point Hibbs Quadrangle (Seymour *et al.*, in prep.). Alternatively, given the recent

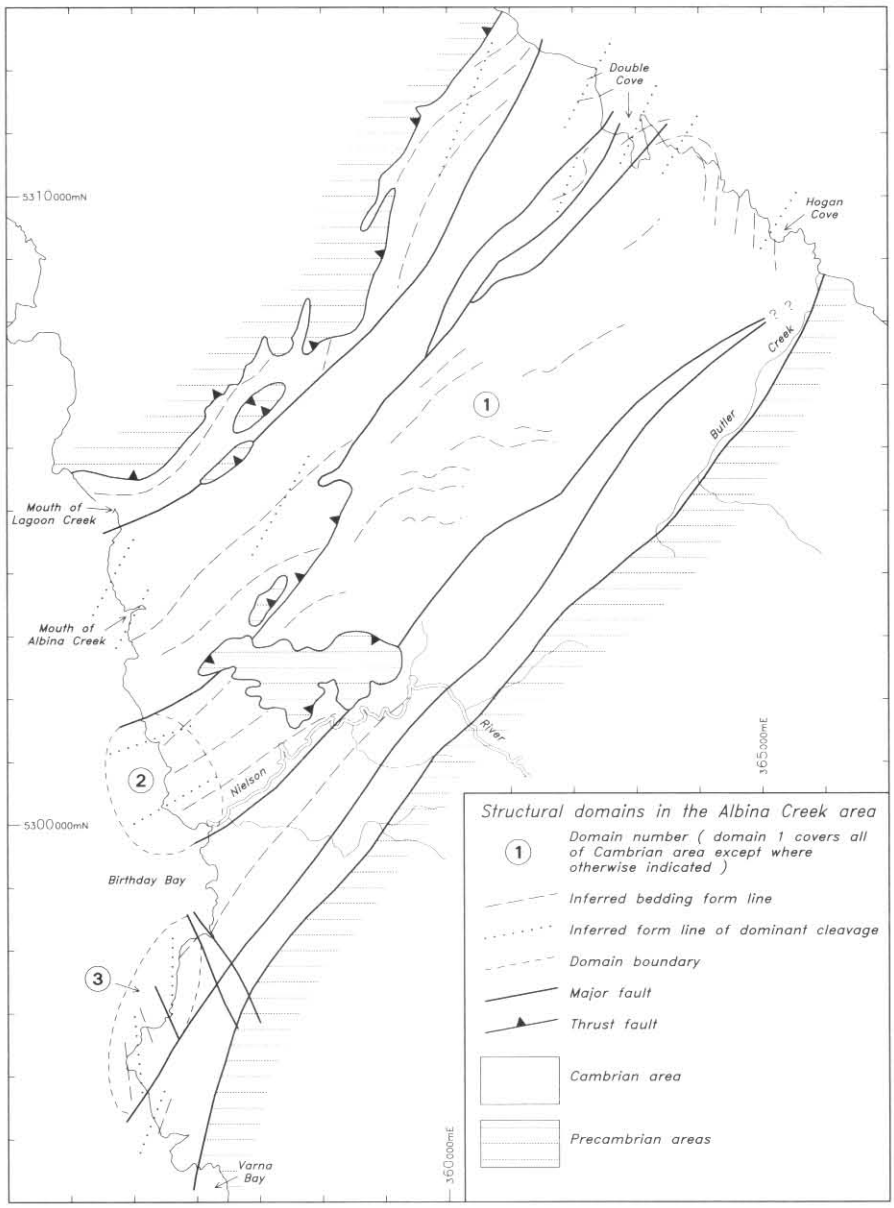

Figure 89. Structural domains in the Albina Creek area.

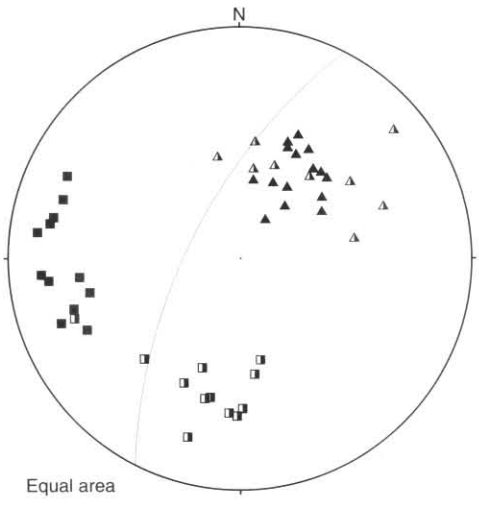

Figure 90. Albina Creek area Domain 1, area near CP632113. Folds in bedding: ▲, △ – hinges; ■, ◨ – squares are poles to axial planes. Kink style folds as filled symbols and folds resembling similar style folds as half filled symbols. The great circle is the average S_2 cleavage for the area near CP632113.

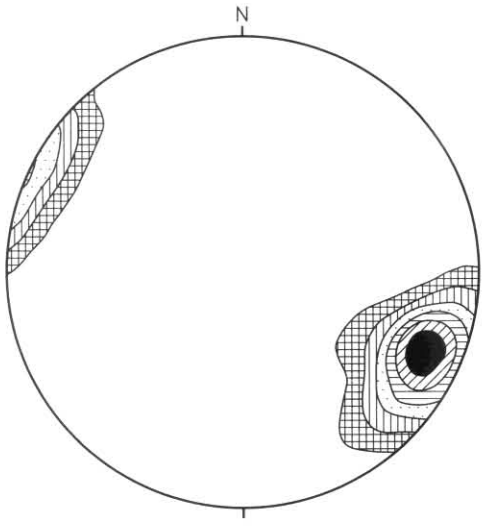

Figure 91. Albina Creek area, Domain 1. Poles to dominant S_3 cleavage. Contoured at 2, 4, 6, 8, 10, 12 and 14 × uniform distribution; 241 readings.

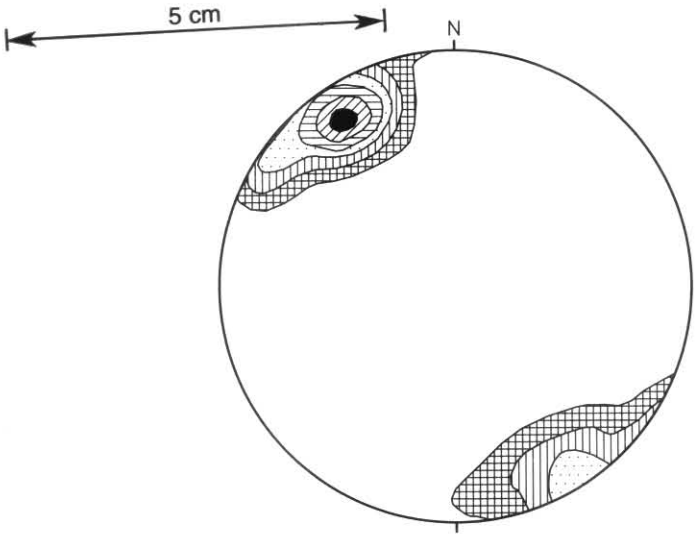

Figure 92. Albina Creek area, Domain 2. Poles to dominant S_3 cleavage. Contoured at 2, 4, 6, 8, 10 and 12 × uniform distribution; 53 readings.

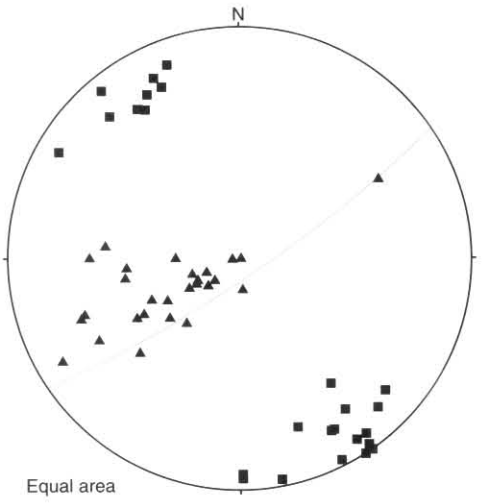

Figure 95. Albina Creek area, Domain 2. F_3 hinges (▲) and poles to F_3 axial planes (■). Average S_3 cleavage shown as a great circle.

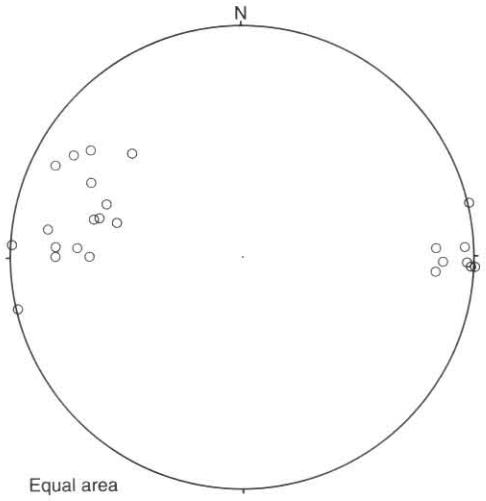

Figure 93. Albina Creek area, Domain 3. Poles to cleavage.

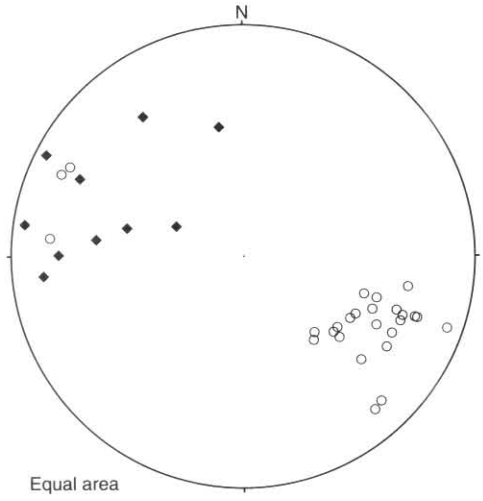

Figure 96. Albina Creek area, Domain 1 in the area around CN553953. Poles to dominant earlier S_3 cleavage (○) and poles to later crenulation cleavage – S_4 (◆).

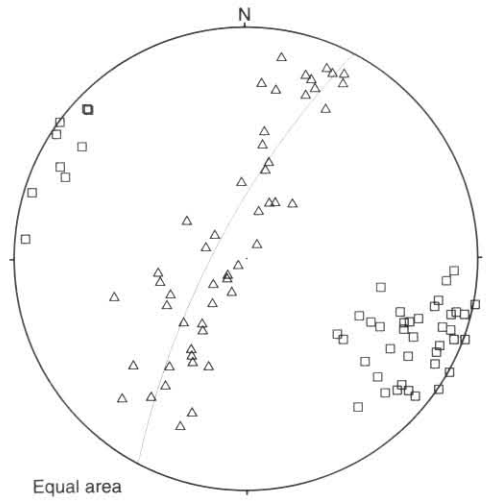

Figure 94. Albina Creek area, Domain 1. F_3 hinges (▲) and poles to F_3 axial planes (■). Average S_3 cleavage is shown as a great circle.

work in the Zeehan quadrangle (Findlay and Brown, 1992), southward-directed thrusting may also be possible.

The age of the Liberty Point Thrust is unknown. The Precambrian and underlying Cambrian units contain a weak cleavage following the trend of the post-Ordovician Timbertops Syncline, and the drill-hole data indicates the possibility of very young (Tertiary?) cave deposits in the possibly Cambrian carbonate rocks underlying the thrust.

POINT HIBBS MÉLANGE BELT

R. H. Findlay

This narrow zone (fig. 97) is complexly faulted and sheared, and the rocks show evidence of several phases of continuous and discontinuous deformation. The region is dominated by schistose serpentinised ultramafic rocks and subordinate enclaves of sheared sedimentary, volcanic and intrusive units. The mélange belt's northern boundary consists of an extensive steep fault separating a thin Cambro-Ordovician sequence from Precambrian rocks to the north; the southern boundary is more complex and involves both steep and shallow faults.

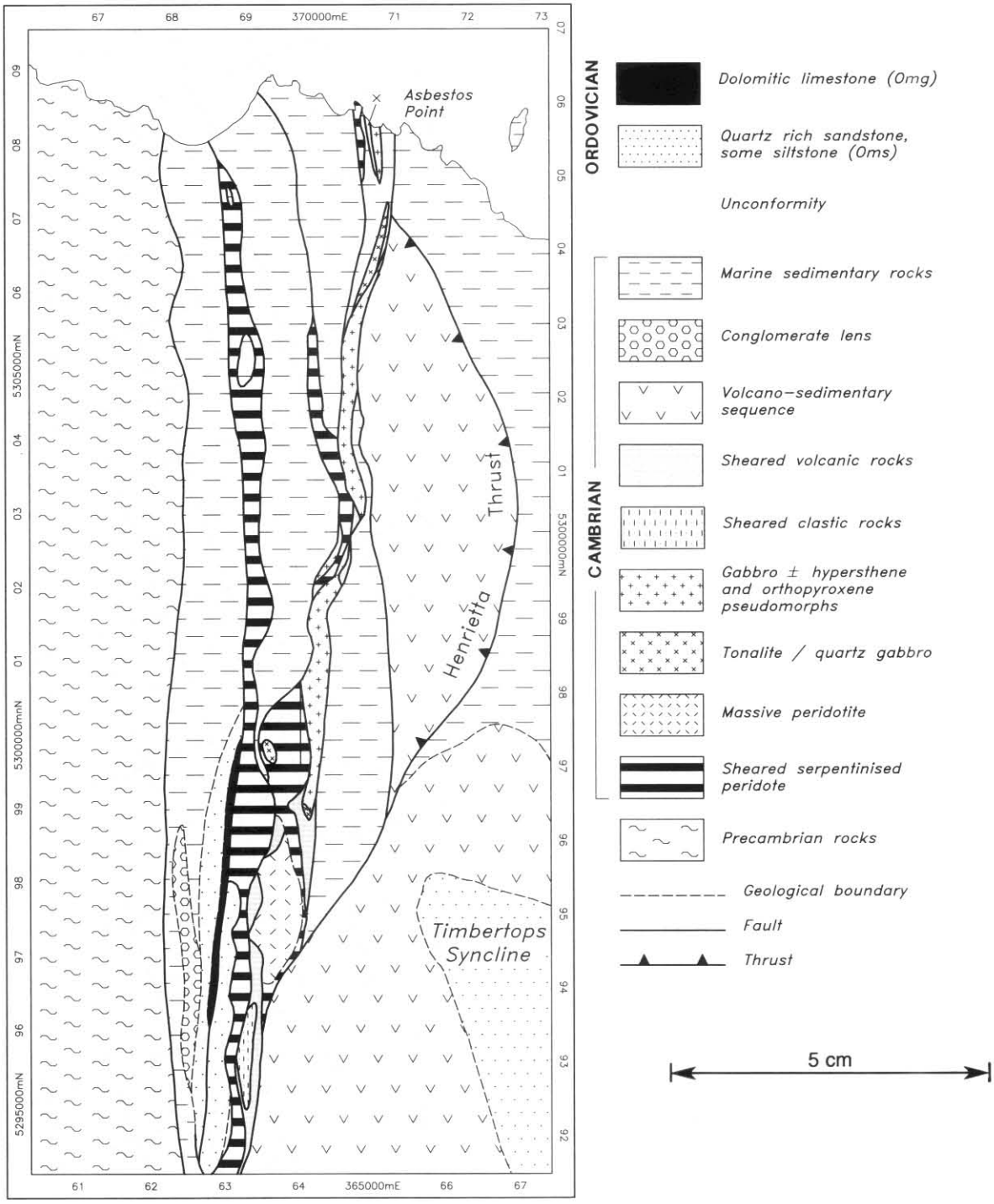

Figure 97. Simplified geological map of the Point Hibbs Mélange Belt, from McClenaghan and Findlay (1989).

McClenaghan and Williams (1989) first attempted to assess movements within the mélange belt through their study of fabric relations in fault-bound schistose serpentinite exposed at Asbestos Point. They found marked variations in extension directions during development of the north to NNE-trending cleavage and reported NNE-trending shear zones showing a horizontal dextral component of movement.

The present study was focused principally on the southern part of the mélange belt in the map-sheet area. The possible kinematics of the belt were investigated by :

(1) attempting various restorations in the continuity of certain marker units (e.g. the dolomite bed Omg and sandstone Oms);

(2) study of small-scale structures which resemble in places a C-S fabric; and

(3) study of the later discontinuous deformation as exemplified by asbestos fibre and quartz-chlorite striations on fault surfaces within the belt.

These studies produced useful albeit ambiguous results.

Restoration of marker units

Figures 98 and 99 show the results of treating the mélange belt as a strike-slip system, which is supported by the numerous minor faults containing strike-slip and oblique-slip slickenlines (see later discussion). Figure 98 shows the result of treating the belt as a sinistral strike-slip system; this reconstruction co-incidentally closes the southern end of the Macquarie Harbour Graben. Note that the serpentinised ultramafic units retain their double-pronged topology, although the belt is shortened.

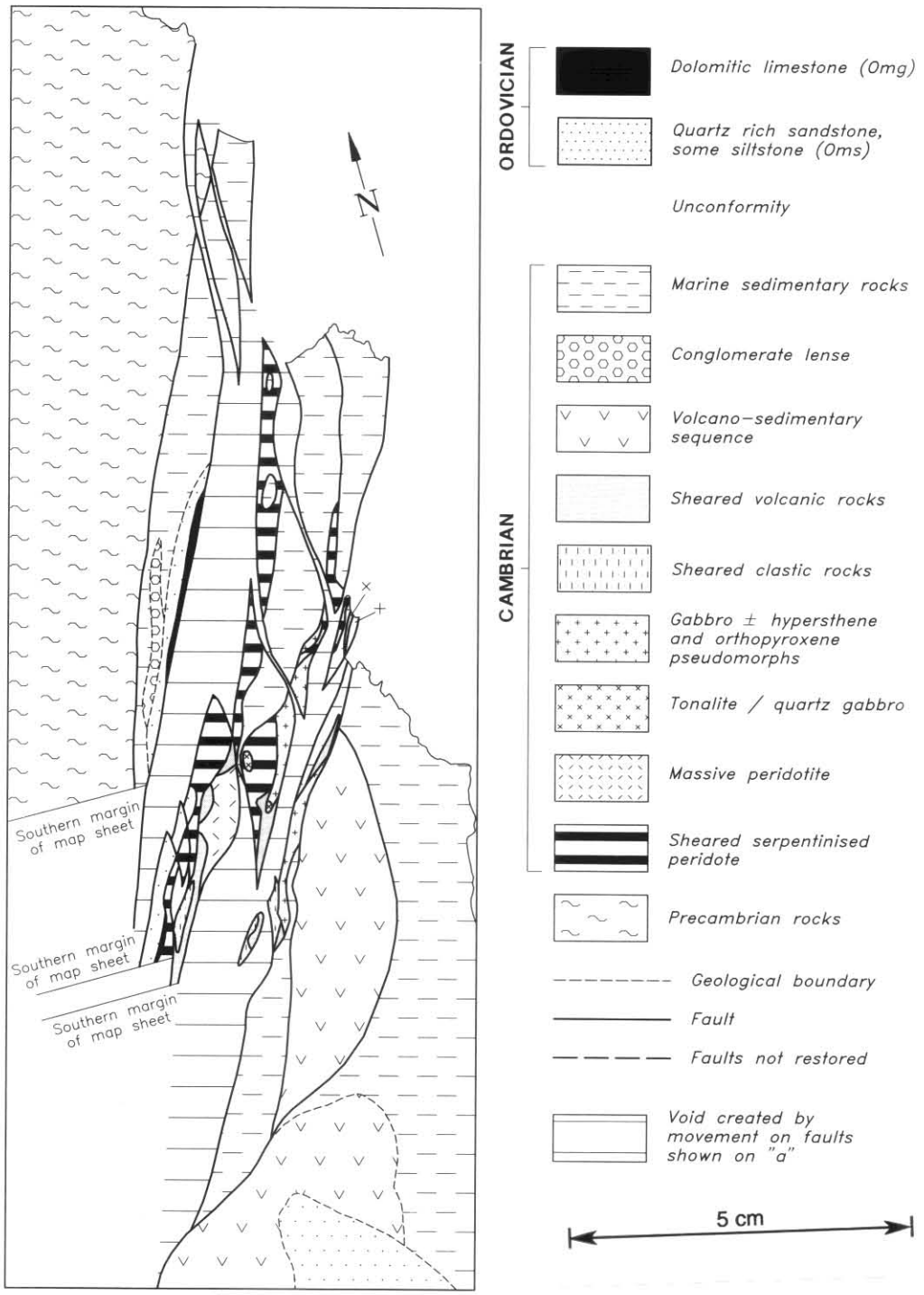

Figure 98. Point Hibbs Mélange Belt after restoration of possible sinistral strike-slip movement.

Figure 99 shows the results of treating the belt as a dextral strike-slip system. The serpentinised units retain their double-pronged topology but are somewhat attenuated; the Henrietta Thrust becomes an essential part of the system and may be interpreted as part of a tulip structure.

Both reconstructions create voids, and the supposed strike-slip movement would have been transpressive which could have caused at least some rotation of the beds to their present steep dip, and possibly some of the thrusting interpreted in the region of CN645953 (see cross-section C-D, McClenaghan and Findlay, 1989).

It is re-emphasised here that these reconstructions are reasonable speculations.

Fabric studies

Structures resembling C-S fabrics and crenulation cleavages occur within the sheared serpentinite in the southern part of the mélange belt (fig. 100, insets A–I), and C-S structures have been recognised also by McClenaghan and Williams (1989) to the north. The structures identified by these workers indicate dextral shear; their original orientation is not known.

The present study focused on the schistose rocks, generally serpentinitic, within the southern end of the mélange belt (fig. 100). Three morphological groups of structure were recognised:

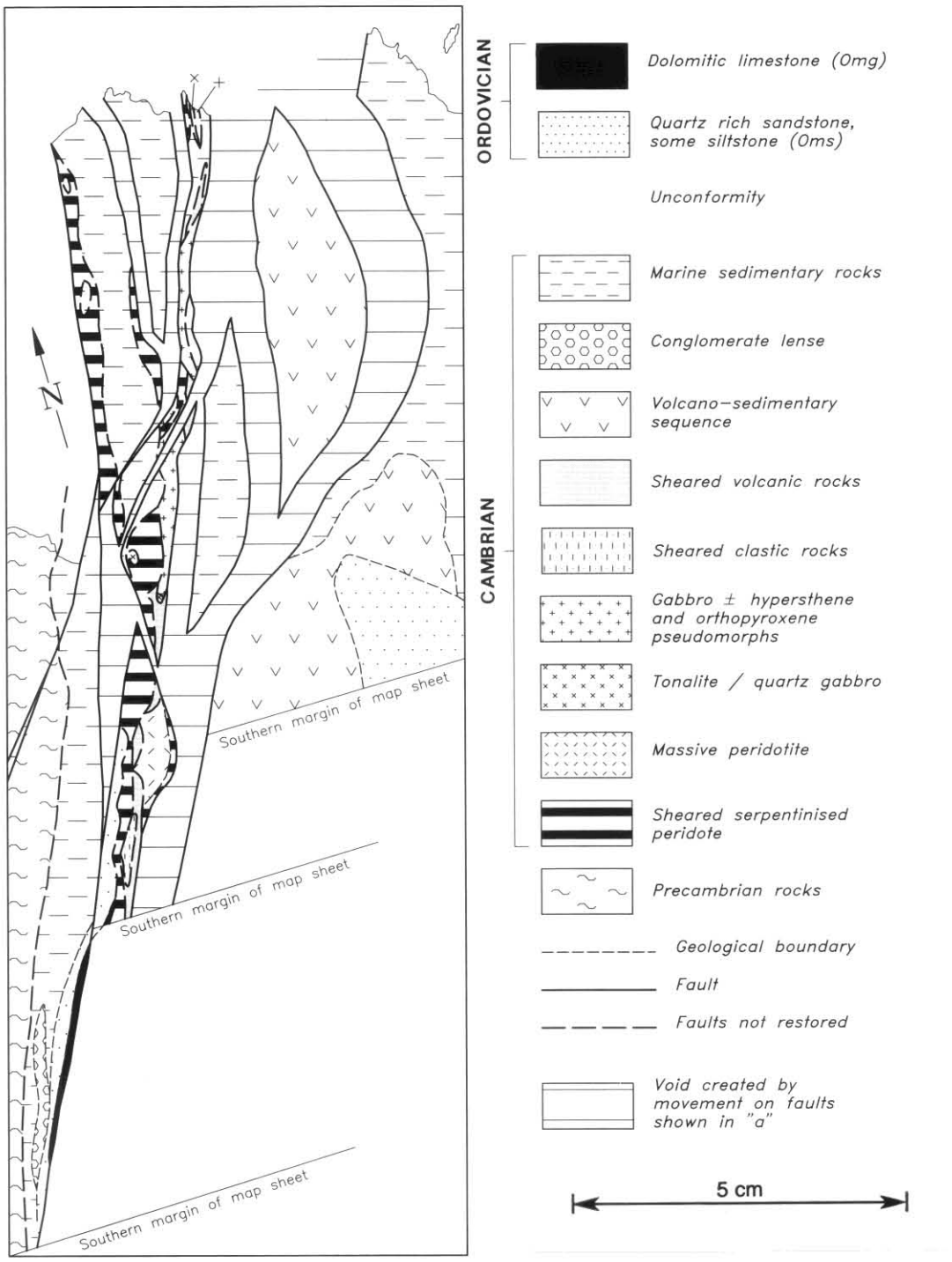

Figure 99. Point Hibbs Mélange Belt after restoration of possible dextral strike-slip movement.

(1) those such as illustrated in insets A and B, where occur phacoids within which the schistosity is diverted sigmoidally between zones of generally plane parallel schistosity;

(2) structures which contain distinct planar to curviplanar discontinuities between which the schistosity is rotated either sigmoidally or is folded (insets C, D, E, F, G); and

(3) structures formed of minor fault arrays between which the schistosity is rotated or folded and which in part may resemble those forming group 2 (e.g. inset H, I).

The group 1 structures display a sinistral vergence. As elsewhere a schistosity morphologically identical to that surrounding the group 1 phacoids is cut by the planar discontinuities of groups 2 and 3, these phacoidal structures may be the earliest deformation evident in the serpentinite and may represent transposed fold limbs or an early C-S fabric.

The group 2 structures may represent formation of a younger crenulation cleavage and folding of the schistosity (note that near the locality of inset H, variably-plunging small upright NW-trending folds fold the schistosity) and the variable vergence illustrated identifies different locations on the major fold limbs. Alternatively, morphological group 2 may contain two distinct fabrics, a crenulation cleavage (insets E, F, G) and a C-S fabric (insets C and D). Note that insets C and D indicate respectively dextral and sinistral shear, and that the supposed C-planes are at an angle of some 40° to each other.

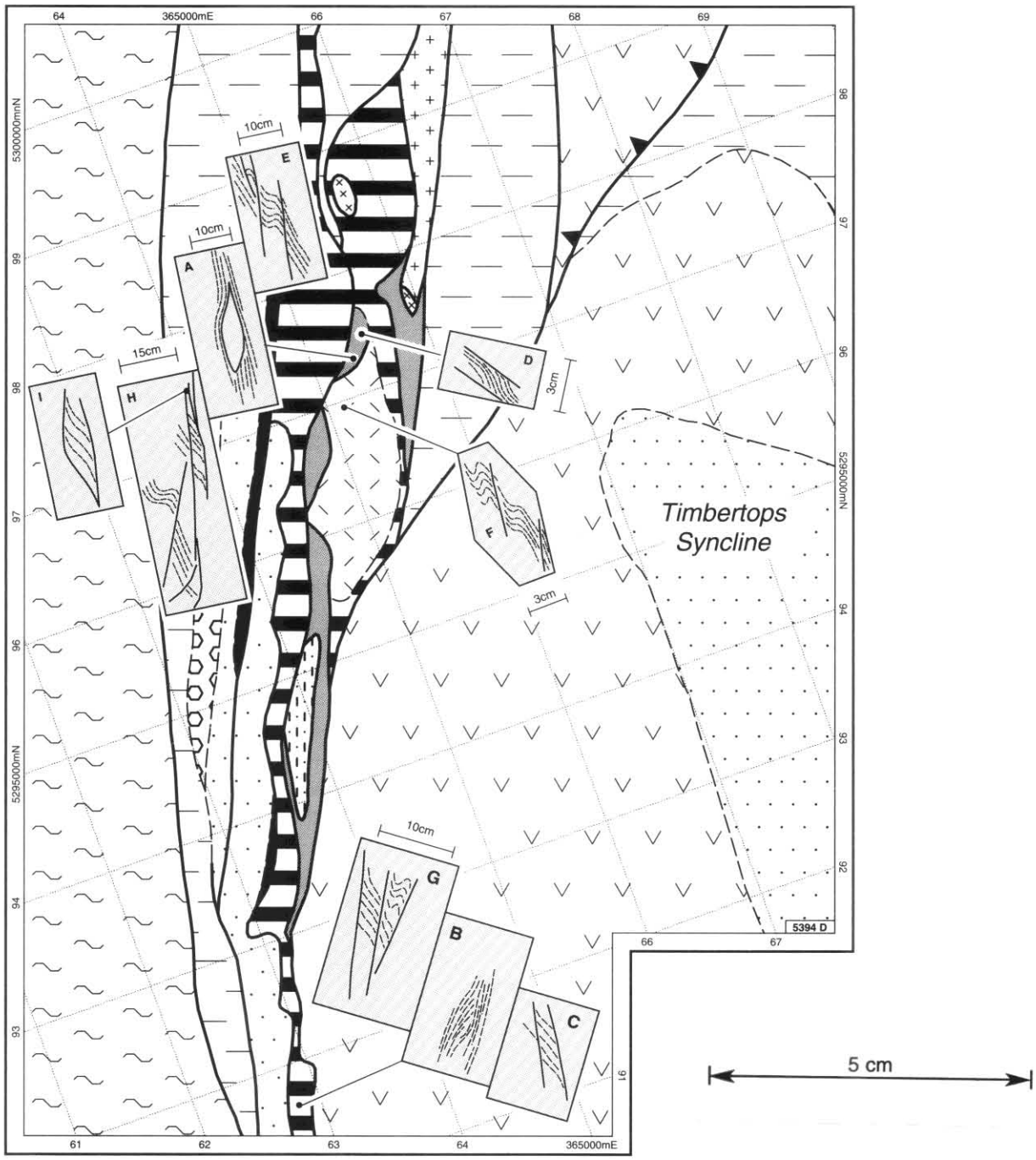

Figure 100. Minor structures within serpentinite, sheared volcanic units, and massive peridotite in southern part of Point Hibbs Mélange Belt. Localities of insets indicated. Legend as for Figures 97–99).

The group 3 structures appear to be small faults; it is not clear whether the rotation of the schistosity occurred during or before faulting. Note that the relations between faulting and schistosity at inset I could indicate dextral slip (in agreement with G, C and E) whereas the S-shaped fold in schistosity (inset H) corresponds to similar structures in insets G, E and F).

Fault striation analysis

It has long been recognised that striations on fault surfaces are useful for developing a kinematic picture of faulting and that appropriate statistical analysis of such structures can reveal the regional stress tensor, and indeed track changes in the regional stress tensor (*cf.* Bott, 1959; Findlay, 1980; Etchecopar *et al.* 1981; Angelier 1984). This type of analysis requires measurement of a large number of fault surfaces (>100) on which the slip sense is known. The present study is therefore markedly limited as only 53 striations were measured on 48 faults. Of these only eight had an identifiable slip sense.

The localities of the faults measured are given in Figure 101, together with the orientation of the faults measured. The localities lie generally within or adjacent the serpentinised peridote exposed in the vicinity of CN650960, although samples from minor faults in rocks flanking the mélange belt were included in this study. Within the serpentinised peridotite, the faults' surfaces contain asbestos fibres thought to track the movement of the faults; in the other rocks, the mineral fibres are of quartz.

Figure 101 confirms that no one fault orientation is unique to one location; at no locality was found evidence for different ages of faulting.

Figure 102 is a summary of the geometries of the faults and their M-planes; there is no obvious preferred orientation of

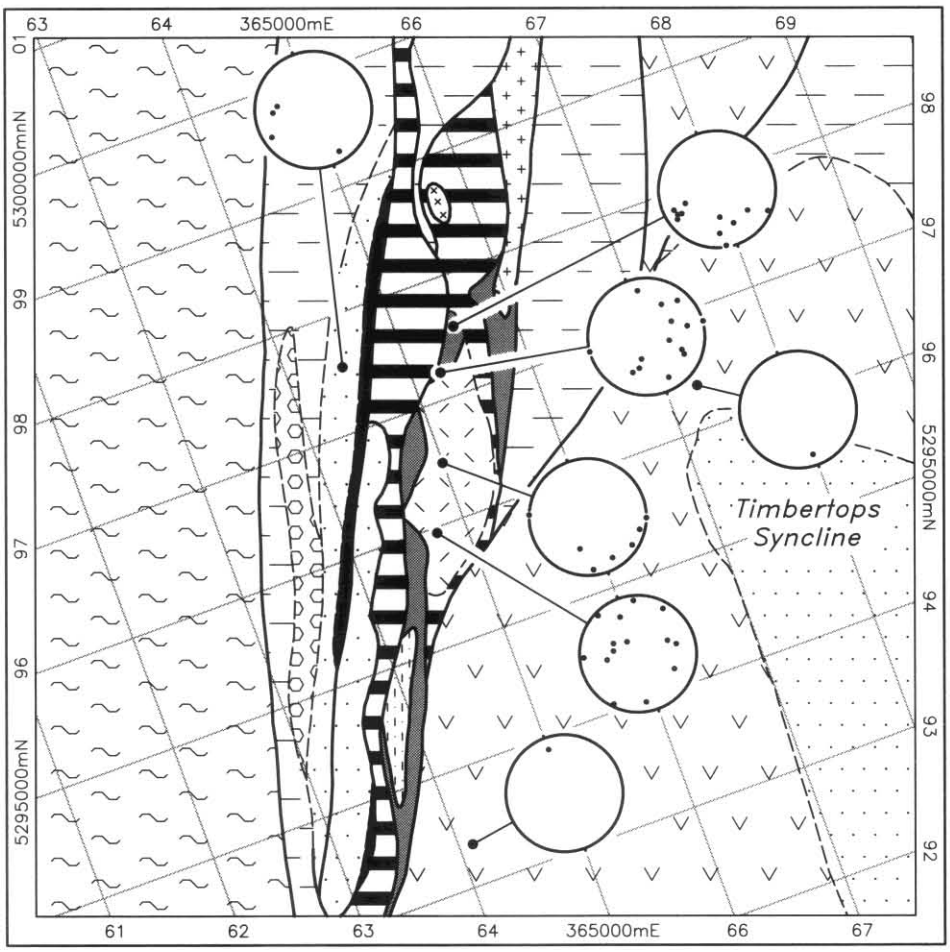

Figure 101. Localities for fault striation analysis within the Point Hibbs Mélange Belt. Stereo-nets are equal area, southern hemisphere projections and show poles to faults studied.

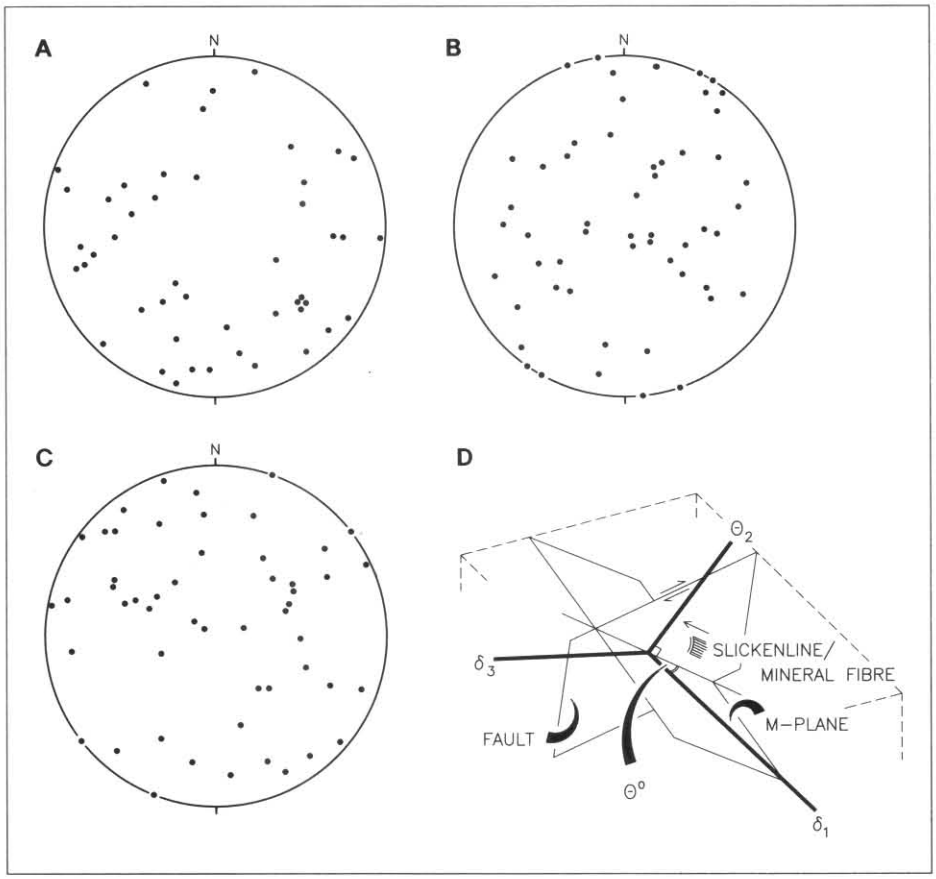

Figure 102. Equal area southern hemisphere stereo-nets showing: A – poles to all faults; B – all striations; C – poles to all M-planes. D defines the geometry of fault, slickenline, movement direction, σ_1, σ_2, σ_3 and M-plane.

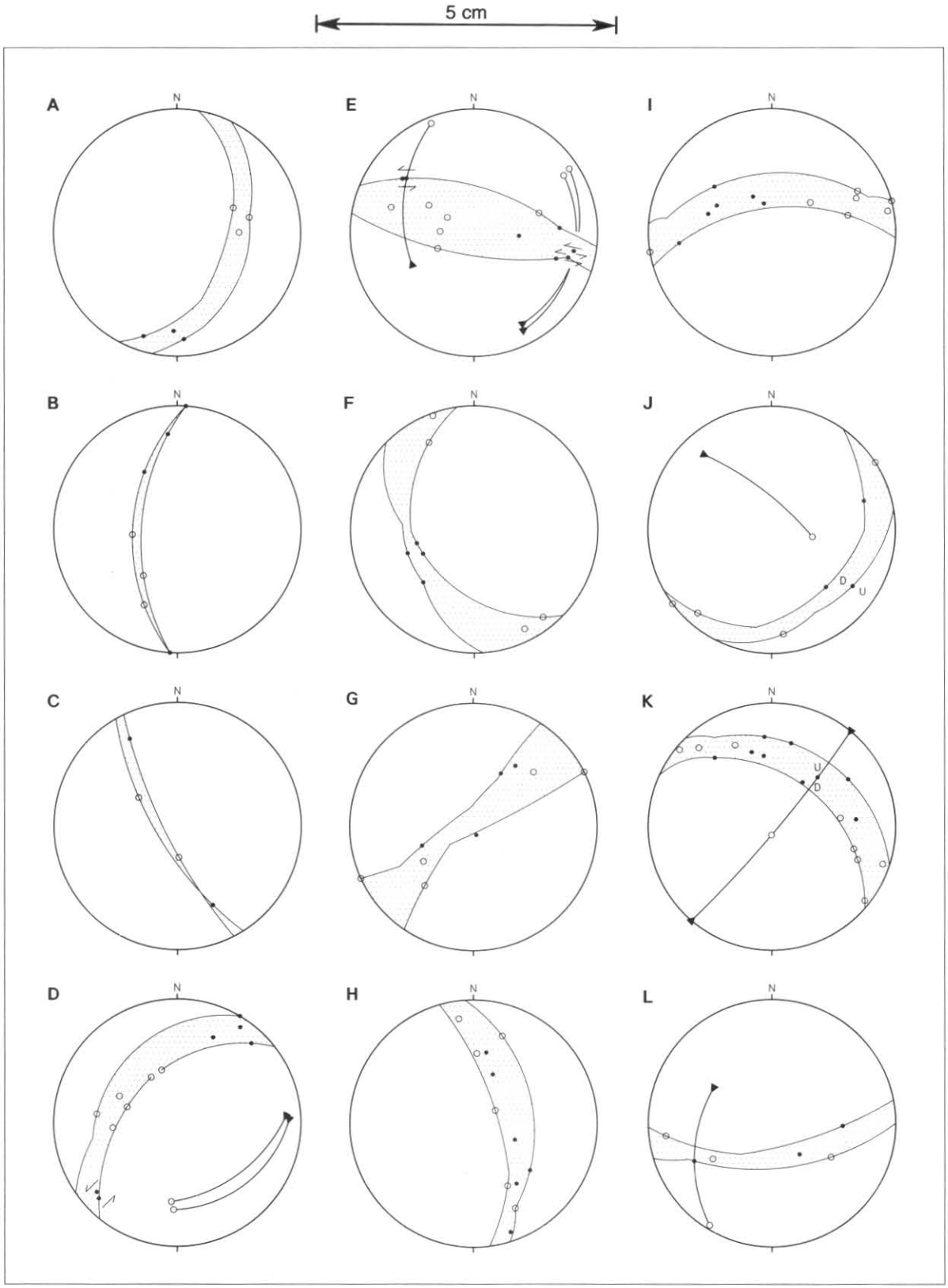

Figure 103. Equal area southern hemisphere stereographic projections showing assignment of faults into groups according to firstly fault orientation and as a second criterium striation orientation. Stippled area shows fault measurements; ● – striation orientation; ○ – σ_2 orientation; ▲ – σ_3. σ_1 and σ_3 have been derived using $\theta = 45°$. See text for discussion.

faults, striations and consequently M-planes (see D, fig. 102 for definition of M-plane). Figure 103 shows the faults divided into sub-groups according to their orientation. Broadly, two sets of sub-groups are present; sub-groups A–E are dominantly strike-slip faults, whereas sub-groups F-L are faults on which both strike-slip and dip-slip have occurred. This illustrates the complexity of the faulting and suggests a multi-phase fault history. However, the exposures are such that it was not possible to recognise the history of faulting in the field.

σ_1 and σ_3 were determined graphically for the eight faults on which the slip sense was identifiable, and for two values of θ, 30° and 45° (see A and B, fig. 104). Although work by Spörli (1979), Findlay (1980) and Rattenbury and Spörli (1985) has suggested that 30° is the appropriate value for θ

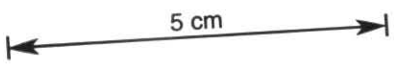

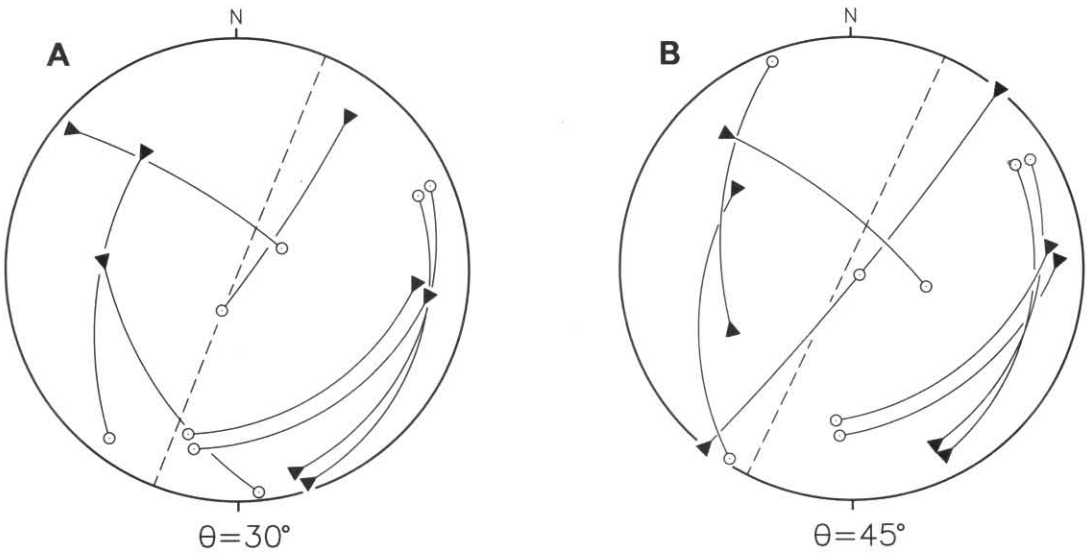

Figure 104. Equal area southern hemisphere stereographic projections showing: A – calculated σ_1 and σ_3 directions for $\theta = 30°$; B – calculated σ_1 and σ_3 directions for $\theta = 45°$. Symbols as for Figure 103.

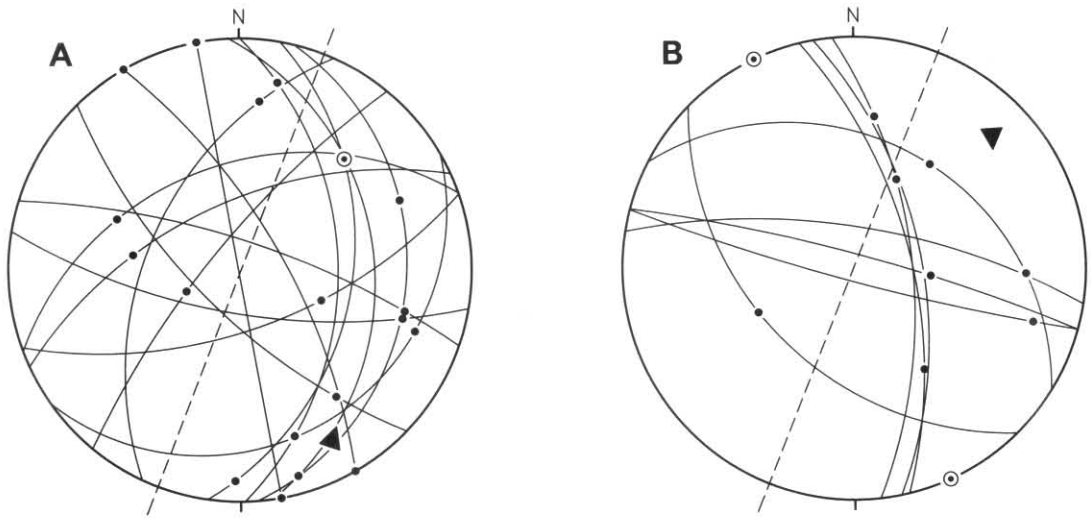

Figure 105. A – Faults found to be compatible statistically with SE-plunging σ_1 (▲) and NE-plunging σ_3 (⊙), ● – fault striations. B – Faults found to be compatible statistically with NE-plunging σ_1 (▲) and SE-directed σ_3 (⊙), ● – fault striations. Dashed line shows strike of the mélange belt.

in the anisotropic metagreywacke of the Torlesse terrane of New Zealand, this may not be the case in the present study; the data in Figure 104 (A and B) can be interpreted as indicating a NW-SE and a NE-SW directed σ_1, and there is slightly closer clustering of σ_1 where $\theta = 45°$.

The NW- and NE-directed orientations of σ_1 were tested for all faults using the STRIA TEST program held by R. F. Berry (University of Tasmania) (see Etchecopar *et al.* 1981), to assess which faults might be mechanically compatible with the σ_1–σ_3 orientations derived for the eight faults whose slip-sense is known. This included the assignment of movement senses to the faults, given the striation orientation, and culling and re-testing with the opposed movement sense those faults which had proved incompatible with the given stress tensor.

The results of this study are limited. Fifteen faults (A, fig. 105) proved statistically to be mechanically compatible with σ_1 plunging 20° to 150° and σ_3 plunging 35°to 046°; if this is a true indication of the regional stress tensor then sinistral slip would have occurred on the major NNE-trending faults in the mélange belt. Eleven faults (fig. 105) are mechanically compatible with σ_1 plunging 20° to 035° and σ_3 plunging 0°to 140°. This would produce dextral slip on the NNE-trending faults of the mélange belt.

There are four major reservations pertinent to these conclusions:

(1) the movement history is unknown and multi-phase faulting is very likely;

(2) the number of faults measured (48) is too low for adequate statistical analysis;

(3) of the 48 faults measured, too few contained striations whose slip sense is known;

(4) neither this study, nor those on which it was based, fully take into account the possibility of rotation of the stress tensor during faulting, nor do they take into account the development of secondary stress fields at the tips of propagating faults.

These reservations notwithstanding, this study is a guide to future work.

OTHER FAULTS IN THE CAMBRIAN SEQUENCES

The region between the northern and southern Precambrian sequences is broken by NNE-trending steeply-dipping faults; these trend parallel to sub-parallel the fault forming the northern boundary of the Point Hibbs Mélange Belt.

The kinematics of only one of these faults have been studied. This fault, which crops out at CP615123, displays a 6 m-thick tectonised zone marked by brecciation and fault-controlled angular boudinage of bedding in the marginal part of the fault zone together with disrupted isoclinal folds, and more internally, a black, finely comminuted, schistose fault-rock containing linear phacoids of sandstone. C-S structures and asymmetric pressure shadows around phacoids within this fault rock (fig. 106) confirm a sinistral strike-slip component; other phacoids display symmetrical pressure shadows indicative of flattening.

Assuming that the linear phacoids track the movement of the fault, and noting that fold hinges within the fault rock also follow the orientation of these phacoids, then σ_1 may have plunged 30° to 132°and σ_3 30°to 242° during faulting. Again no account has been taken of rotation of the stress tensor during faulting; note that this orientation for σ_1 would produce the observed dextral slip on minor fault (1) (fig. 106). However, it would produce reverse, and not the observed dextral, slip on minor fault (2); again these faults may have formed before production of the fault rock and the stretched phacoids, and when σ_1 could have had a more easterly trend.

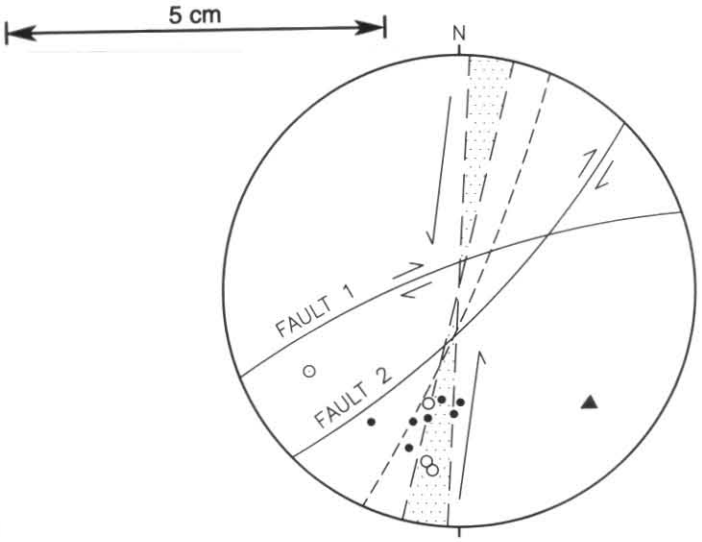

Figure 106. Equal area southern hemisphere stereographic projection showing structural elements of fault zone at CP615123. Plunge of elongate phacoids (●), plunge of fold axes (○). The stippled area indicates the orientation of the fault zone; ▲ – possible orientation of σ_1; ⊙ – possible orientation of σ_3. Whilst the σ_1 orientation is compatible with the observed sinistral slip in the fault zone and dextral faulting on the possible Riedel shear Fault 1, it would produce reverse and not the apparent dextral slip on Fault 2.

TERTIARY FAULTING

In the Farm Cove–Sophia Point region the Tertiary Macquarie Beds are faulted against siliciclastic rocks correlated with the Late Cambrian–Ordovician Denison Group. As discussed earlier, the influx of gravels in Pliocene times indicates uplift of these siliciclastic rocks which form the West Coast Ranges. The presence of local low-angle angular and erosional unconformities between conglomeratic layers assigned, on lithological grounds only, to unit Tsg, are indicative of post-Tss to syn-Tsg uplift. The rapid influx of the conglomerates overlying unit Tss, and its overall coarsening upwards character, confirm rapid, and possible increasingly so, uplift of the east side of the Macquarie Harbour region during Late Tertiary times.

Low angle faults occur within unit Tss at CP703156, CP731129, and CP735111 (fig. 6 on p. 25). No cataclastically deformed rocks, nor mylonites occur along the fault planes and minor structures associated with these faults indicate normal slip; at CP735113 finely laminated sandstone layers within the fault zone are disrupted and folded, and a pinnate cleavage, which transposes some thin sandstone beds with the fault zone, has been formed (fig. 6).

The geometry of those structures is consistent with their interpretations as lystric normal faults formed by gravitational collapse of the thickened sedimentary pile. The apparent unconformity below beds of possible Eocene age overlying the faults in the cliff at CP735113 would suggest that these faults are of probable intra-Eocene age.

REFERENCES

ANGELIER, J. 1984. Tectonic analysis of fault slip data sets. *J. geophys. Res.* B89:5835–5848.

BAILLIE, P. W.; CORBETT, K. D. 1985. Geological atlas 1:50 000 series, sheet 57 (7913N), Strahan. *Department of Mines, Tasmania.*

BOTT, M. H. P. 1959. The mechanics of oblique slip faults. *Geol. Mag.* 96:109–117.

BRADLEY, J. 1954. The geology of the West Coast Range of Tasmania. Part I: Stratigraphy. *Pap. Proc. R. Soc. Tasm.* 88:193–243.

BROWN, A. V. 1986. Geology of the Dundas–Mt Lindsay–Mt Youngbuck region. *Bull. geol. Surv. Tasm.* 62.

BROWN, A. V. 1988. Geological atlas 1:50 000 series, sheet 78 (7912S), Montgomery. *Department of Mines, Tasmania.*

BROWN, A. V. (comp.) 1989. Geological atlas 1:50 000 series, sheet 21 (7916S), Smithton. *Explan. Rep. geol. Surv. Tasm.*

BROWN, A. V. in prep. Geological atlas 1:50 000 series, sheet 78 (7912S), Montgomery. *Explan. Rep. geol. Surv. Tasm.*

BROWN, A. V.; JENNER, G.A. 1989. Geological setting, pertology and chemistry of Cambrian boninite and low-Ti tholeiitic lavas in western Tasmania, *in:* CRAWORD, A. J. (ed.) *Boninites and related rocks:* 233–263 Hyman Unwin : London.

BROWN, A. V.; FINDLAY, R. H.; MCCLENAGHAN, M. P. 1991. Summary of the regional geology of the Macquarie Harbour, Pt Hibbs, and Montgomery 1:50 000 map sheets. *Rep. Dep. Mines Tasm.* 1991/02.

CLOSE, R. J. 1972. The geology and economic potential of the Hibbs Ultramafic Belt in the Noddy Creek area of south west Tasmania. *Rep. explor. Dep. BHP* 1230 [TCR 72-889].

CRAWFORD, A. J.; CORBETT, K. D.; EVERARD, J. L. 1992. Geochemistry of the Cambrian volcanic-hosted massive sulfide-rich Mount Read Volcanics, Tasmania, and some tectonic implications. *Econ. Geol.* 87:597–619.

ETCHECOPAR, A.; VASSEUR, G.; DAIGNIERES, M. 1981. An inverse problem in microtectonics for the determination of stress tensors from fault striation analysis. *J. struct. Geol.* 3:51–65.

FINDLAY, R. H. 1980. *Structure of the Hooker and Copland Valleys, central Southern Alps, N.Z.* Ph.D. thesis, University of Auckland..

FINDLAY, R. H.; BROWN, A. V. 1992.The 10th Legion Thrust, Zeehan district. Distribution, interpretation, and regional and economic significance. *Rep. Divn Mines miner. Resour. Tasm.* 1992/02.

JAGO, J. B. 1971. An abrupt Upper Middle Cambrian faunal change, Christmas Hills, Tasmania, Australia. *Pap. Proc. R. Soc. Tasm.* 105:83–85.

HALL, W. D. M.; MCINTYRE, M.I.; CORBETT, E. B.; MCGREGOR, P. W.; FENTON, G. R.; ARNDT, C. D.; BUMSTEAD, E. D. 1969*a*. Report on field work. E.L. 13/65. S.W. Tasmania 1967–68. *Rep. explor. Dep. BHP* 793 [TCR 69-555].

HALL, W. D. M.; MCINTYRE, M.I.; HALL, K. 1969*b*. E.L. 13/65. South-west Tasmania. Geological report. 1966–67. *Rep. explor. Dep. BHP* 778 [TCR 69-552]. [TCR 86-2618].

JONES, P. A. 1986. Final report. Macquarie EL 31/83, Tasmania. *Rep. Cyprus Exploration* 505.

LANGLANDS, J. G. 1971. Exploration for chrysotile asbestos in the Hibbs Belt, Noddy Creek. 1970/71. *Rep. explor. Dep. BHP* 1056 [TCR 71-805].

LE MAITRE, R. W. 1984. A proposal by the IUGS Subcommission on the Systematics of Igneous Rocks for a chemical classification of volcanic rocks based on the total alkali silica (TAS) diagram. *Aust. J. earth. Sci.* 31:243–255.

LETERRIER, J.; MAURY, R. C.; THONON, P.; GIRARD, D.; MARCHAL, M. 1982. Clinopyroxene composition as a method of identification of the magmatic affinities of paleo-volcanic series. *Earth planet. Sci. Letters* 59:139–154.

MCCLENAGHAN, M. P.; CORBETT, K. D. 1985. Geochemical diagrams of Cambrian volcanic rocks and associated intrusives from western Tasmania. *Unpubl. Rep. Dep. Mines Tasm.* 1985/63.

MCCLENAGHAN, M. P.; FINDLAY, R. H. 1989. Geological atlas 1:50 000 series. Sheet 64 (7913S). Macquarie Harbour. *Department of Mines, Tasmania.*

MCCLENAGHAN, M. P.; SEYMOUR, D. B.; VILLA, M. in press. Radiometric dating of a lamprophyre dyke suite from western Tasmania and the age of thrust faulting in the Point Hibbs area.

MCCLENAGHAN, M. P.; WILLIAMS, E. 1989. Tectonic transport of rock-units near Asbestos Point, Macquarie Harbour. *Rep. Dep. Mines Tasm.* 1989/18.

MCGREGOR, P. W. 1972. Exploration for chrysotile asbestos. Pad 2 to Hibbs Lagoon, E.L. 13/65. S.W. Tasmania. January to March 1972. *Rep. explor. Dep. BHP* 1126. [TCR 71-862].

MIYASHIRO, A. 1974. Volcanic rock series in island arcs and active continental margins. *Am. J. Sci.* 274:321–355.

MULLEN, E. D. 1983. $MnO/TiO_2/P_2O_5$: a minor element discriminant for basaltic rocks of oceanic environments and its implication for petrogenesis. *Earth planet. Sci. Letters* 62:53–62.

PALETHORPE, C. E. 1972. *A geochemical and geotectonic comparison of selected Australian ultramafic associations.* Ph.D. thesis, University of Queensland.

PEARCE, J. A.; CANN, J. R. 1973. Tectonic setting of basic volcanic rocks determined using trace element analysis. *Earth planet. Sci. Letters* 19:290–300.

PECCERILLO, A.; TAYLOR, S. R. 1976. Geochemistry of Eocene calc-alkaline volcanic rocks from the Kastamonu area, northern Turkey. *Contrib. Mineral. Petrology* 58:63–81.

RATTENBURY, M. S.; SPÖRLI, K. B. 1985. Paleostress orientations from striations in Torlesse rocks, Otaki Forks, Tararua Range, New Zealand. *N.Z. J. Geol. Geophys.* 28:435–442.

SAUNDERS, A. P.; TARNEY, J. 1984. Geochemical characteristics of basaltic volcanism within back-arc basins. *Spec. Publ. geol. Soc. Lond.* 16:59–76.

SHERVAIS, J. W. 1982. Ti-V plots and the petrogenesis of modern and ophiolitic lavas. *Earth planet. Sci. Letters* 59:101–118.

SPORLI, K. B. 1979. Structure of the South Island Torlesse in relation to the origin of the Southern Alps. *Bull. R. Soc. N.Z.* 18:99–104.

SUTHERLAND, F. L.; CORBETT, E. B. 1974. The extent of Upper Mesozoic igneous activity in relation to lamprophyric intrusion in Tasmania. *Pap. Proc. R. Soc. Tasm.* 105:175–190.

WHITE, N. C. 1975. *Cambrian volcanism and mineralisation, south-west Tasmania.* Ph.D. thesis, University of Tasmania : Hobart.

WOOD, D. A. 1980. The application of a Th-Hf-Ta diagram to problems of tectonomagmatic classification and to establishing the nature of crystal contamination of basaltic lavas of the British Tertiary Volcanic Province. *Earth planet. Sci. Letters* 50:11–30.

Appendix A

ECONOMIC GEOLOGY

J. Pemberton

Introduction

The Macquarie Harbour sheet (McClenaghan and Findlay, 1989) contains Cambrian mafic, ultramafic and felsic volcanic rocks with associated sedimentary rocks. They are regarded as prospective for volcanic-hosted massive sulphides, platinoids, nickel and gold.

In 1815 Capt. J. Kelly was the first to note the economic potential of the area when he reported the presence of brown coal in Tertiary sediments on the northern shores of Macquarie Harbour (Bacon in Baillie *et al.*, 1985). The modern exploration era started in 1956 with Lyell E.Z. Explorations (L.E.E.) working from Macquarie Harbour south to the Wanderer River (see Scott, 1957; Scott, 1960*a, b*; Scott *et al.*, 1959 and Elms *et al.*, 1959). During this period an airborne magnetics and electromagnetic survey was flown with ground follow-up employing mapping, geophysics, geochemistry and some drilling. Broken Hill Pty Co. Ltd (BHP) had an exploration licence over most of south-west Tasmania in the late 1960s (see McGregor, 1969; Hall *et al.*, 1969*a, b*; Langlands, 1971 and Langlands and Rees, 1971). Using reconnaissance mapping and geochemistry to eliminate areas of low prospectivity they reduced the licence to cover the area from Macquarie Harbour to Elliott Bay. Work was concentrated on the asbestos in the Noddy Creek area and copper at Cypress Creek to the south of the Macquarie Harbour sheet. During the 1980s Amoco Minerals Australia Co. held the area. Airborne Dighem electromagnetic and magnetic surveys were flown with ground based follow-up using geophysics, geochemistry and mapping (see Kary, 1985). Part of the area is presently held by Plutonic Operations Ltd as the Muddy Cove Creek E.L. 4/92 of 243 km^2.

Metallic minerals

COPPER PROSPECTS

Pelias Cove [CP635118]

The maps of Scott (1957) and McGregor (1969) show this prospect 200 m south-west of its position as shown on the Macquarie Harbour sheet of McClenaghan and Findlay (1989). In the initial phase of exploration Lyell E.Z. Explorations (L.E.E.) discovered a 12 m wide zone of mineralisation of which 6 m was a hematitic-pyritic gossan. Bands of sulphide had selectively replaced a volcaniclastic sediment. An average of three samples from Scott (1957) gave the following results: 0.2% Cu, 1.5% Pb, 0.9% Zn, 4.6 g/t Ag, 0.18 g/t Au, 42.1%Fe.

In May, 1957, six short diamond holes were attempted by L.E.E. Recovery was poor with the best hole (L4) sited on the gossanous outcrop giving 2.59% Cu, trace Pb and 43.4% Fe from 0 m to 35.7 m. Scott (1960*a*) concluded that the drilling and E.M. survey showed that the mineralisation did not continue along strike or at depth and no further work was warranted.

Two lines of soil sampling by BHP (McGregor, 1969) were anomalous in copper to the east of the area sampled and drilled by L.E.E. These results led McGregor to surmise that the mineralised zone was a NW-striking fault dipping east, and that L.E.E. had not located it. No further work was done on this prospect.

Birthday Bay [CN562992]

These copper prospects were first reported by Waller(1902) between Birthday Bay and Nielson Creek in Cambrian dolomite and mudstone. Chalcopyrite, bornite and copper carbonates were noted in quartz-carbonate veins, disseminated through the sediments and along shears. An average of 1% Cu was obtained from five bulked rock chips across the various prospects while some two tons of chalcocite-rich gossan reputedly yielded 40% Cu but exhausted the available ore.

Waller (1902) concluded with an optimistic assessment of the future of the prospects, but no further work has taken place.

HEMATITE-MAGNETITE-PYRITE PROSPECTS

Iron Creek [CN584997] (also called Big Creek, Deep Creek, Anomaly 129 or 10/8)

L.E.E. discovered the hematite-magnetite-pyrite body at what is now called Iron Creek while following up a large airborne magnetic anomaly (see Scott *et al.*, 1959). The ironstone is some 396 m long and from 4.5 m to 76 m wide. Scott *et al.* (1959) interpreted it as outcropping between the Precambrian and Cambrian units whereas the Macquarie Harbour sheet (McClenaghan and Findlay, 1989) shows it associated with a fault within the Cambrian sequence. An assay gave 68.9% Fe, 0.03% S, 1.48% SiO_2, 500 ppm Zn, trace Pb and some copper staining was noted. A later report by Scott (1960) used a length of 450 m, a width of 52 m and a depth of 91 m to calculate that there was a total 4.7 million tons of iron oxide.

One hole was drilled to 100.9 m where it was abandoned due to drilling difficulties (see Hall *et al.*, 1969*b*). A brief summary of the hole was given as:

0–96.6 m	Schistose quartzite, quartzite and argillite.
96.6–97.5 m	70% pyrite, 30% hematite.
97.5–100.9 m	Schistose quartzite.

Assays of the core were not anomalous. Although the intersection was narrow, the change to a sulphide-rich rock does suggest either a secondary weathering effect or primary zonation.

Other hematite-magnetite-pyrite bodies.

During the mapping of the Macquarie Harbour sheet three other ironstone bodies were noted to the north of Iron Creek at CP591011, CP591015 and CP601029 (McClenaghan and Findlay, 1989). A sample from the ironstone at CP601029 collected by the Department of Mines and assayed by Amoco (see Kary, 1985) had 0.15 ppm Au.

PROSPECTS ASSOCIATED WITH THE ULTRAMAFIC ROCKS

Nickel

During the thorough search for asbestos by B.H.P., some nickel mineralisation was detected. Hall *et al.* (1969) record pentlandite from sheared serpentinites at about CP680021. It occurs as disseminated rounded blebs to 2 mm and assayed up to 1200 ppm Ni.

McGregor (1969) reports the above occurrence as well as specks of pentlandite in a costean 300 m south and smears of pentlandite on shear planes in DDH 1 a further 100 m south.

Chrome, osmiridium and gold [CP680060]

In the report by Scott (1957), prospector G. Abel details the discovery of chromite, gold and osmiridium in stream sediments from a branch of what is now called Baylee Creek (Abel referred to the alluvials as the Gravelly Beach prospect).

Chromite was obtained from the length of the creek whereas gold and osmiridium occurred in patches. A1.5kg black sand sample assayed 39.6% Cr_2O_3, 29.4% SiO_2, 15.7% FeO, 7.00% MgO and 5.1% Al_2O_3 (see Scott, 1957). The small

tonnage and length of the creek made it an impractical and uneconomic proposition. Ultramafic rocks in the headwaters were regarded as the source of this mineralisation. This is confirmed by the work of Close (1972) who found an average of 3000 ppm Cr in the ultramafics at Noddy Creek, where it occurred as disseminated grains of chromite.

MACQUARIE HARBOUR BOTTOM SEDIMENTS

Initial interest in the potential of the Recent sediments on the bottom of Macquarie Harbour was shown by Planet Mining Co. Pty Ltd, with a report by Campe (1966) summarising source areas for possible accumulations of detrital mineralisation. The King River delta (on the Strahan 1:50 000 geological map – see Baillie *et al.*, 1985) has attracted most explorers interested in the mineral potential of the harbour. Jinks (1976), working for Citco International Minerals Co., calculated a reserve in the delta of 100 million tons containing 3.5% S in pyrite and 0.11% Cu mainly as chalcopyrite.

Fimiston Minerals N.L. (Roots, 1971) recognised the highly mineralised hinterland as a source for possible mineralisation in the sediments and suggested two methods of concentration in the harbour:

(1) Transport by humic acids with deposition by chemical or biochemical reaction under reducing conditions.

(2) By mechanical transport and detrital deposition in the harbour. Anomalous results were obtained for Ni in the Double Cove to Sarah Island area and one sample from Double Cove had 950 ppm Cu.

A detailed geochemical survey by Citco International Mining Co. (Harvey, 1986) of the whole harbour returned two anomalous samples from the Macquarie Harbour sheet:

(1) From CP610208: 730 ppm Cu, 20 ppm Pb, 160 ppm Zn, 32 ppm Co and 20 ppm Mo.

(2) From CP700130: 700 ppm Cu, 12 ppm Pb, 180 ppm Zn, 30 ppm Co and 15 ppm Mo.

The results to date from this work all point to the King River delta as the most prospective part of the harbour.

Industrial minerals

ASBESTOS

Chrysotile asbestos is restricted to the ultramafic belt between Asbestos Point and Point Hibbs. The first report of asbestos at Asbestos Point is in Hills (1914) with H. Grice being granted a reward claim in 1900. Nye (1929) and Rae (1941) both visited the area and reported small scale prospecting.

The work of Taylor (1955) gives a detailed account of asbestos in numerous trenches and of the styles of asbestos formation at Asbestos Point. He reported three generations of cross-fibre chrysotile:

(1) Fibre in serpentinites parallel to the serpentinite-pyroxenite contact.

(2) Occasional fibre in massive serpentinite associated with shearing.

(3) Fibre associated with tensional cracks. Taylor (1955) concluded that the Asbestos Point serpentinite was a thin sill with no strike extent or connection to the Spero River serpentinite and that the area offered little encouragement.

An airborne survey was flown for BHP in 1966 who started ground work in 1969 when Hall *et al.* (1969*a*) noted that asbestos veins were common in the ultramafics in the Noddy Creek area. Follow-up work (Hall *et al.*, 1969*b*) in this area detailed an eastern and western zone with approximately 3 km strike length of asbestos-bearing ultramafics. Extensive costeaning allowed a tonnage estimate of 4.89 million tons at 2.6% asbestos for the western belt and 3.63 million tons at 1.9% asbestos for the eastern belt.

In the summer of 1971 BHP drilled 9 holes (centred on DHNC 6 at CP680021) in the Noddy Creek area (see Langlands and Rees, 1971). A later report by Langlands (1971) suggested possibly 11.7 million tons of ore grade material which fell well short of the required 25 million tons at 4.5% fibre.

A study of the Hibbs ultramafic belt by Close (1972) discusses the various factors controlling the formation of the chrysotile asbestos and related metasomatic minerals (stichtite, talc and magnesite) as well as the regional geology.

TALC

Alteration of the ultramafic rock to form talc occurs in areas of intense shearing. Close (1972) suggests that some of the high quality talc in the Noddy Creek area has the potential to produce an economic deposit.

DOLOMITE

Precambrian dolomitic limestone outcrops in the Birthday Creek–Timms Creek area. An assay reported by Elms *et al.* (1959) gave 41.08% CaO, 37.10% CO_2, 15.6% SiO_2, 5.31% Al_2O_3 and 3.0% MgO.

Two lenses of Cambrian dolomite occur in the Nielson River–Iron Creek area.

STICHTITE

The rare carbonate mineral stichtite ($Mg_6Cr_2(CO_3)(OH)_{16}.4H_2O$.), valued by mineral collectors, is reported by Close (1972) to occur in the Noddy Creek area. It usually takes the form of oval blebs (4 mm in diameter) but does occasionally form stichtite rich lenses up to 1.25 m wide and 3 m long.

Fuel minerals

COAL

Thin beds of uneconomic brown coal in Tertiary sediments outcrop in the Farm Cove area and to the south along Birchs Inlet. A full account of the history and recent exploration is detailed by Bacon in Baillie *et al.*(1985).

OIL

The search for oil on the Macquarie Harbour sheet has been brief and unsuccessful. Amoco (1981) shot one 10 km line of seismic reflection along Macquarie Harbour. They concluded that the depth to basement was too shallow and turned their attention to the offshore Sorell Basin.

Asphaltic bitumen samples were collected widely from the west and south-west coast of Tasmania around the turn of the century. Hills collected a sample in 1913 from the coast about 5 km south of Albina Creek in the vicinity of Birthday Bay (Volkman *et al.*, 1992). Subsequent detailed analyses of this sample with fifteen others led Volkman *et al.* (1992) to conclude that these samples most likely originate from seepages off Tasmania or South Australia from rocks of mid-Triassic age or younger (e.g. Sorell Basin or Otway Basin).

REFERENCES

AMOCO. 1981. *Final report of operations and field work. March 1-16, 1981.* Amoco Australia Petroleum Company. West Tasmania Basin. [TPR OR-092]

BACON, C. A. 1985. Fuel minerals Coal, *in*: BAILLIE, P. W.; CORBETT, K. D.; GREEN, G. R. Geological atlas 1:50 000 series. Sheet 57(7913N). Strahan. *Explan. Rep. geol. Surv. Tasm.*

BAILLIE, P. W.; CORBETT, K. D.; GREEN, G. R. 1985. Geological atlas 1:50 000 series. Sheet 57(7913N). Strahan. *Explan. Rep. geol. Surv. Tasm.*

CAMPE, G. C. 1966. *Geology of the hinterland of E.L. 5/66, Maquarie Harbour, Tasmania.* [TCR 66-427]

CLOSE, R. J. 1972. *The geology and economic potential of the Hibbs Ultramafic Belt in the Noddy Creek area of south west Tasmania.* Broken Hill Pty Co. Ltd. [TCR 72-889]

ELMS, R. G.; SCOTT, B; BONIWELL, J. B. 1959. *Regional report on Modder River area.* Lyell E.Z. Explorations. [TCR 59-279]

HALL, W. D. M.; MCINTYRE, M.I.; CORBETT, E. B.; MCGREGOR, P. W.; FENTON, G. R.; ARNDT, C. D.; BUMSTEAD, E. D. 1969*a*. Report on field work. E.L. 13/65. S.W. Tasmania 1967–68. *Rep. explor. Dep. BHP* 793 [TCR 69-555].

HALL, W. D. M.; MCINTYRE, M.I.; HALL, K. 1969*b*. E.L. 13/65. South-west Tasmania. Geological report. 1966–67. *Rep. explor. Dep. BHP* 778 [TCR 69-552]. [TCR 86-2618].

HARVEY, S. R. M. 1986. *Macquarie Harbour mineral exploration project Phase II. E.L. 2/74.* Citco International Minerals Company. [TCR 86-2543]

HILLS, C. L. 1914. Geological reconnaissance of the country between Cape Sorell and Point Hibbs. *Bull. geol. Surv. Tasm.* 18.

JINKS, D. D. 1976. *Tasmania copper project. Phase III – final report Macquarie Harbor, Tasmania, Australia.* Citco International Minerals Company : Tulsa. [TCR 84-2303]

KARY, G. L. 1985. Progress report to September 1985, Sorell Peninsula, Exploration Licences 35/83, 36/83 and 37/83 Tasmania. *Rep. Amoco Minerals Aust. Co.* 454. [TCR 85-2466]

LANGLANDS, J. G. 1971. *E.L. 13/65 Cape Sorell peninsula, south-west Tasmania. Exploration for chrysotile asbestos in the Hibbs Belt, Noddy Creek, 1970/71.* Broken Hill Pty Co. Ltd. [TCR 71-758]

LANGLANDS, J. G.; REES, R. C. 1971. *Report to the Tasmanian Mines Department on exploration for chrysotile asbestos in E.L. 13/65. December, 1970 to June, 1971.* Broken Hill Pty Co. Ltd. [TCR 71-758]

MCGREGOR, P. N. 1969. *Report on 1968-69 field work. E.L. 13/65. South West Tasmania.* Exploration Dep. Broken Hill Pty Co. Ltd. : Melbourne. [TCR 69-586]

MCCLENAGHAN, M. P.; FINDLAY, R. H. 1989 Geological atlas 1:50 000 series. Sheet 64 (7913S). Macquarie Harbour. *Department of Mines, Tasmania.*

NYE, P. B. 1969. Report on the asbestos deposits at Asbestos Point, Macquarie Harbour. *Rep. Dept. Mines Tasm.*

RAE, K. A. 1941. Report on Asbestos Point. *Rep. Dept. Mines Tasm.*

ROOTS, W. D. 1971. *Report on Macquarie Harbour, West Coast Tasmania, E.L. 37/70. Including some information relative to areas: E.L.47/70 and S.P.L. 96.* Fimiston Minerals N.L. [TCR 71-751]

SCOTT, B. 1957. *Report on examination of three prospects on the western shore, Macquarie Harbour between Double Cove and Birch's Inlet.* Lyell E.Z. Explorations. [TCR 57-152]

SCOTT, B. 1960*a*. *Investigation of Pelias Cove Prospect.* Lyell E.Z. Explorations. [TCR 60-313]

SCOTT, B. 1960*b*. *Airborne anomaly 10/8; Report No. 2.* Lyell E.Z. Exploration. [TCR 60-314.]

SCOTT, B.; PALTRIDGE, I. M.; BONIWELL, J. B. 1959. *Report on Anomaly 10/8.* Lyell E.Z. Exploration. [TCR 59-277]

TAYLOR, B. L. 1955. Asbestos in Tasmania. *Miner. Resour Tasm.* 9.

VOLKMAN, J. K.; O'LEARY, T.; SUMMONS, R.E.; BENDALL, M. R. 1992. Biomarker composition of some asphaltic coastal bitumens from Tasmania, Australia. *Organic Chem.* 8(3):669–682.

WALLER, G. A. 1902. Report on some discoveries of copper ore in the vicinity of Point Hibbs. *Rep. Secr. Mines Tasm.* 1901–1902:281–287.

GEOLOGICAL SURVEY 1:50 000 EXPLANATORY REPORT • 64 (7913S) • MACQUARIE HARBOUR • 1993 • ISBN 0 7246 4008 8